MONASH University

A functional exploration as to how antibiotic resistance mutations occurring in daptomycin resistant isolates of *Staphylococcus aureus* impede dendritic cell activation

Timothy Phillip Patton

BSc. hons (Immunology)

A thesis submitted for the degree of Doctor of Philosophy at
Monash University in 2019
Faculty of Medicine, Nursing and Health Sciences,
Department of Biochemistry and Molecular Biology

Copyright notice

Contents

Figures

Tables

Abstract

Methicillin-resistant Staphylococcus aureus (MRSA) represents an endemic public health threat. Resistance to last-line antibiotics is on the rise, correlating with increased morbidity and mortality in both the hospital and community setting. The mutations conferring resistance to the last-line antibiotic daptomycin affect the composition of the bacterial cell membrane and wall, with recent findings showing that mutations in the cardiolipin synthesis gene, *cls2*, lead to thickening of the cell membrane and an increased ratio of cardiolipin:phosphotidylglycerol. Importantly, these changes reduce neutrophil trafficking to the site of infection, and prolong bacterial survival.

Here we investigate how daptomycin resistance affects innate sensing by dendritic cells (DC). Using paired clinical isolates of MRSA, we show that the acquisitions of daptomycin resistance is associated with a significant decrease in production of pro-inflammatory cytokines and chemokines by responding DC; as well as a reduced expression of co-stimulatory markers CD40 and CD80. These differences are almost entirely dependent on the acquisition of a point mutation in the bacterial membrane cardiolipin synthase gene, *cls2*, with recreation of the wild-type gene restoring DC activation.

Moreover, we demonstrate that these same point mutations modulate phagocytosis of these clinical isolates by DC, with potential implications for the presentation of antigen from these bacteria. We further elucidate the molecular mechanisms regulating the recognition of these MRSA isolates by DC, showing that both DC surface activation and cytokine secretion in response to these bacteria is dependent on MyD88 signalling. Importantly, we further show that the recognition of MRSA by cDC1, but not cDC2 or pDC, is partially dependent on endosomal TLR9. Finally, we provide preliminary evidence suggesting that the differential recognition of a particular daptomycin exposed clinical pair, by cDC1, is regulated via the cytosolic cGAS/STING signalling pathway.

These findings highlight a novel aspect of antibiotic resistance- showing for the first time that point mutations associated with antibiotic resistance can concomitantly impede innate immunological recognition by DC. Such findings

have important implications for the current understanding of bacterial immunopathogenesis, and therefore the design of future vaccines and immunotherapies.

Declaration

This thesis is an original work of my research and contains no material which has been accepted for the award of any other degree or diploma at any university or equivalent institution and that, to the best of my knowledge and belief, this thesis contains no material previously published or written by another person, except where due reference is made in the text of the thesis. This thesis contains fewer than 80,000 words in accordance with Monash University guidelines.

The relative contributions of other contributing authors are described below.

Signed

Timothy Patton

25th November 2019

Contributions

The work presented in this thesis was performed at Monash University in the laboratory of **Meredith O'Keeffe**. As my primary supervisor Meredith O'Keeffe provided academic advice, with dedication, throughout this project. Approximately 90% of the work described in this thesis was performed by **Timothy Patton**, and I gratefully acknowledge the contributions of the individuals who provided their time and expertise as described below.

Jhih-Hang Jiang generously provided his time in the culture and labelling (where indicated) of clinical *S. aureus* isolates for every experiment described in this thesis. Jiang-Hang worked tirelessly to plate and enumerate each strain for each experiment to deliver consistency, while further labelling strains with pHrodo or inducing GFP expression where indicated. Occasionally, **Xenia Kostolious** provided her assistance when Jhih-Hang was unavailable. All of this work was performed in the laboratory of **Anton Y Peleg**, whom provided access to the clinical bacterial isolates used in this study.

Rachel Lundie provided her time and technical expertise in several aspects of experimental work, especially in rare instances when I was otherwise occupied and unable to perform aspects of various experiments myself. Rachel's assistance related to occasional isolation and purification of murine DC, stimulation of DC cultures or subsequent flow cytometry analysis of these samples. Her contributions to these experiments are greatly valued, and Rachel's hands on assistance is estimated to be provided in up to 5% of the experiments described in this thesis.

Jo Pooley provided her time and support in the day to day running of the laboratory. While not directly assisting with any of the experiments published in this thesis, the massive support role played by Jo in the managing administrative and practical operations of the lab merit acknowledgement as indirect contribution- as these experiments would not have ran smoothly without her tireless dedication.

Acknowledgements

It's been almost five long years, with ups, downs and in-betweens. But I have no regrets, and I wouldn't trade any of it away for anything. In considering the achievements over these years, my passion and love of science; the best part of the whole thing has still been coming in each day to the fantastic people I 'work' with. I say 'work' because these people make it feel like anything but. I can confidently say that Rachel Lundie is the most positive person I have ever met. With her persistent optimism, undeservingly kind words, and always welcoming smile it is impossible to be blue around her. Perhaps restoring cosmic balance are Ee Shan Pang and Xi Zen Yap; whom with their collective ironic pessimism (or is it sarcastic realism?) are always fun to be around. Sharing the PhD experience with two other PhD candidates made everything seem okay, even when it felt disastrously not. Jo Pooley, the manager of our lab, and also our lives. In running the lab Jo always managed to be both the carrot and the stick; not just keeping you on the straight and narrow, but also making you want to keep the path. Jo has been a blast to work with, and will continue to be a riot to party with. Christophe Macri, I think we spent the first two years trying to understand each other, and even now we still don't get it 100% right. But please know that all the French I can speak, I learned it from you. *C'est la vie.*

Most importantly, I want to thank my supervisor **Meredith O'Keeffe**. To this day I consider myself lucky to have landed in your lab. You are a true mentor, an excellent scientist, a friend, and an inspiration to me. Your source of perpetual optimism remains a mystery to me, but has helped provide a supportive and nurturing environment for me and the entire lab. I greatly value the time I have had with you, as you have been an enthusiastic supporter of all my pursuits- both scientific and personal. From the bottom of my heart, thank you.

To all my friends who have helped keep me sane over the years, both pre- and during my PhD. One of my closest friends Xavier, whom has been both an emotional support and friend for a laugh throughout most of my life. To my friends Liriye and Katherine, whom have been with me since the beginning of my research career at the Burnet Institute- I value your down to earth

perspectives, advice, support but most importantly your friendship. I also want to thank the entire club at Melbourne Surge Water Polo, my time with the club has been as meaningful as it has exhausting. The club has not only provided an outlet for the fury of an enraged PhD candidate, but also a home away from home, here in Melbourne.

Finally, I would like to acknowledge my family, who have been a constant source of support, an escape, and a reminder that there is still a whole world spinning outside of my own study. My parents Narelle and Tony, have provided emotional, academic and financial support throughout all my tertiary education. I also wish to thank my brother and sister - Jenny and Andrew - for their immense kindness, generosity, patience and even tolerance throughout my study (and life). Last of all, my partner Tom- despite being on the receiving end of my science jargon, rants and frustrations; you have still always been there to make the day a bit better with a smile, a hug and a pinot grigio.

Funding

This project was supported by an Australian Postgraduate Research Training Program (RTP) Scholarship. This project was supported by an Australian Postgraduate Research Training Program Stipend and a CASS foundation medicine and science project grant. Additional support was provided through a Monash University postgraduate research travel grant, an Australian and New Zealand Society for Immunology (ASI) postgraduate travel grant, and a Cell Signalling Technologies postgraduate research travel grant.

Publications during enrolment

2019 | Primary Research Article

Patton T., Jiang J-H., Lundie R., Bafit M., Gao W., Peleg A. & O'Keeffe M. **(2019)** Daptomycin-resistant *Staphylococcus aureus* clinical isolates are poorly sensed by dendritic cells*. Immunol & Cell Biol.* doi 10.1111/imcb.12295

2018 | Review Paper

Macri C., Pang E., **Patton T**., O'Keeffe M. **(2018)** Dendritic cell subsets. *Sem Cell Dev Biol.* **84**, p11-21.

Abbreviations and Nomenclature

ABTS: 2,2'-azinobis(3-ethylbenzothiazoline-6sulfonic acid

AIM2: Absent in melanoma 2

APC: Antigen presenting cell

ASI: Australian and New Zealand Society for Immunology

ATP: Adenosine triphosphate

BHI: Brain heart infusion

BSA: Bovine serum albumin

cDC: Convention dendritic cell

cDC1: Convention dendritic cell 1

cDC2: Convention dendritic cell 2

CDN: Cyclic dinucleotide

cGAMP: Cyclic guanine adenosine monophosphate

cGAS: Cyclic GAMP synthase

CL: Cardiolipin

Cls2: Cardiolipin synthase 2

Clec: C-type lectin domain containing

CLR: C-type lectin receptors

CpG: CpG ODN

DAI: DNA-dependent activation of IFN regulatory factors

Dap: Daptomycin

DapR: Daptomycin resistant

DapS: Daptomycin sensitive

DC: Dendritic cell

DNA: Deoxyribonucleic acid

dsDNA: Double stranded DNA

dsRNA: Double stranded RNA

EDTA: Ethylenediamine tetra-acetic acid

FACS: Fluorescence activated cell sorting

FcR: Fc receptor

FCS: Foetal calf serum

FL: Flt3-Ligand

FLDC: FL induced dendritic cell

GFP: Green fluorescent protein

gMFI: Geometric mean fluorescence intensity

IFN: Interferon

IL: Interleukin

iNOS: Inducible nitric oxide synthase

ITAM: Intracellular tyrosine activation motif

ITIM: Intracellular tyrosine inhibition motif

Ig: Immunoglobulin

LC: Langerhans cell

L-PG: Lysyl-phosphatidylglycerol

LPS: Lipopolysaccharide

mAB: Monoclonal antibody

MAVS: Mitochondrial antiviral signalling protein

MDA5: Melanoma differentiation associated gene 5

MIC: Minimum inhibitory concentration

MIP: Macrophage inflammatory protein

MOI: Multiplicity of infection

MprF: Multiple-peptide resistance factor

MR: Mannose receptor

mRNA: Messenger RNA

MRSA: Methicillin resistant *Staphylococcus aureus*

MSSA: Methicillin sensitive *Staphylococcus aureus*

mutuDC: Murine tumour DC (cell line)

MyD88: Myeloid differentiation primary response 88

NLR: Nod-like receptor

NO: Nitric oxide

ODN: Oligo deoxynucleotide

pAB: Polyclonal antibody

PAMP: Pathogen associated molecular pattern

pDC: Plasmacytoid dendritic cell

PGN: Peptidoglycan

PI: Propidium iodide

pIC: Polyinosinic:polycytidylic acid

PRR: Pattern recognition receptor

PSM: Phenol soluble modulin

RANTES: Regulated on activation, normal T-cell expressed and secreted

RIG-I: Retinoic inducible gene I

RLR: Rig-like helicases

ROS: Reactive oxygen species

rRNA: Ribosomal RNA

SE: Staphylococcal enterotoxin

SEL: Staphylococcal enterotoxin like toxin

SLAN DC: 6-Sulfo N-acetyllactosamine positive dendritic cell

SpA: Protein A

ssDNA: Single stranded DNA

ssRNA: Single stranded RNA

STING: Stimulator of IFN genes

TEM: Transmission electron microscopy

Tip DC: TNF and iNOS producing DC

TLR: Toll-like receptor

TNF-α: Tumour necrosis factor α

TSST-1: Toxic shock syndrome toxin-1

V_H3: Variable heavy type 3

Chapter 1 – Literature Review

1.1 Dendritic Cells: Classification and Immunological Function

Dendritic cells (DC) act as sentinels of the immune system, scouring the periphery for potential pathogens and antigenic material. DC sample their surroundings for antigen, in order to provide a continuous snapshot of their local microenvironment to T-cells. Under steady state mature DC maintain a tolerogenic phenotype acting as a checkpoint to prevent immune responses against 'self'. However, under inflammatory conditions such as infection, the mature DC phenotype is immunogenic serving to initiate the adaptive responses requisite for immunity.

Ralph Steinman completely redefined DC in the 1970's, characterising their potent abilities in the priming of T-cell responses[1]. These DC had been mistakenly described as a neural cell in the late 1800's by Paul Langerhans, and currently retains the historical name of the Langerhans cell (LC). Steinman's re-classification of DC as the most potent antigen presenting cells represents a fundamental paradigm shift in immunology, as these cells gradually took the prominent position in antigen presentation, substituting the previously assumed role of macrophages and B-cells[2,3]. The LC paradigm encapsulates the quintessential DC life cycle; explaining the fundamental concepts of antigen capture in the periphery, subsequent migration towards the lymphoid tissues and the maturation process required for T-cell stimulation.

1.1.1 Functional Dendritic Cell Categorisation

Today, there are a diverse array of well characterised DC subpopulations exhibiting a variety of distinct functional and phenotypic characteristics. However, as new subpopulations and novel functions of existing populations continue to be described, it is becoming increasingly clear that DC represent a heterogeneous population of cells with both distinct and overlapping properties. The boundaries between these subpopulations are blurred by subtle differences in both the phenotype and function in both human and murine DC subsets, which have been

well reviewed[3]. The old LC paradigm has therefore become somewhat antiquated, despite serving as a useful model of the quintessential DC over the years.

Until recently there has been no consistent nomenclature for specific subsets of DC, with terminology tending to be based on surface marker expression; which varies between both the tissue and species under investigation[4]. Recently, broad groupings of DC subsets have become widely accepted, whereby both migratory and lymphoid resident subsets of similar function and phenotype are categorised into the same grouping. Throughout this section both human and murine DC subsets will be considered and discussed in terms of these functional and phenotypic properties. These groupings are structured around the DC paradigm proposed by Heath and Carbone in 2009[2]; categorising dendritic cells into four broad functional groups based on their phenotype and function (figure 1.1).

The first two subsets are of the myeloid lineage, comprising conventional DC (cDC) subsets, including the cross presenting cDC1, and helper T-cell priming cDC2, which are able to potently prime cytotoxic and helper T-cell responses respectively, despite some functional overlap[2,5]. Importantly, the cDC1 and cDC2 can be separated based on a differential dependence on the transcription factor Batf3, Irf8 (cDC1) and Irf4 (cDC2), a topic which has been well reviewed[6]. In 2015 Gurka and colleagues[7] proposed a universal classification system for cDC in mice, separating the cDC1 ($XCR1^+$) from the cDC2 ($SIRP\alpha^+$)[7], and while these markers can separate the two subsets- other markers include Clec9A, CD36, CADM1 (cDC1) and CD1c and CD26 (cDC2) (figure 1.1)[5].

However, given phenotypic differences within each cDC subset, due in part to both maturation state and physiological localisation (such as lymphatic versus peripheral organs and blood), no currently identified markers are entirely universal, nor are the ascribed functions of these subsets entirely distinct- a subject which we have recently reviewed[5]. It has therefore been suggested that DC nomenclature should include both primary and secondary specificity; having ontogeny (cDC1, cDC2 or pDC) as the primary layer of specificity, and secondary specificity based on localisation and phenotype (ie splenic $CD4^+$, dermal $CD141^+$ etc)[8].

The third functional group includes the inflammatory monocyte derived DC subsets, being primarily involved in driving inflammation during infection and presenting antigen to T-cells alongside the other myeloid subsets[9].

Finally, plasmacytoid DC (pDC) form the fourth functional group being primarily involved in anti-viral cytokine secretion and promoting innate immune responses (figure 1.1). The current section does not seek to define each of the currently described DC subsets and their function in detail, but focuses on the subsets and functions thought to be relevant to the development of immunity and clearance of infection.

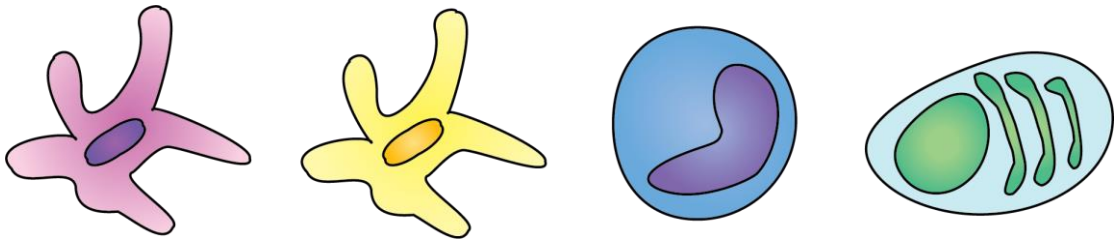

cDC1	***cDC2***	***moDC***	***pDC***
Cross-Presenting cDC	***Classical cDC***	***Inflammatory DC***	***Plasmacytoid DC***
CLEC9A	*SIRPα*	*CD11b*	*CD45RA*
CD24	*CD11b*	*CCR2*	*CD303 (CLEC4C)*
XCR1	*CD26*	*FcεRI*	*CD123*
CADM1	*CD1c*	*CD14*	*CD45R*
CD36	*Dectin-1 (CLEC7A)*	*Ly6C*	*CD317*
CD141	*CD4 (lymphoid)*	*GR1*	*Siglec H*
CD103 (periphery)			
CD8α (lymphoid)			

Figure 1.1 Morphology and phenotype of four distinct dendritic cell functional groups. *Surface markers listed are common but not necessarily ubiquitous across each all types of DC grouped in each subset. Figure shows markers conserved across both human and murine subsets (black), surface marker expression unique to humans (blue), and surface marker expression unique to mice (green)*[3,5,10-19]*. Particular surface markers expressed only in lymphoid or peripheral tissues are indicated in parenthesis. Made with Adobe Illustrator, Creative Cloud 2019.*

cDC1 are efficient in antigen cross-presentation

The subset of DC specifically equipped to shunt exogenous antigen into the endogenous MHC I antigen processing pathway (a process referred to as cross-presentation), are referred to as cDC1, as these subsets share a functional capacity in stimulating $CD8^+$ T-cell responses against extracellular pathogens. These subsets are often characterised in the mouse by the expression of the chemokine receptor XCR1, which is thought to exhibit conserved expression across both lymphoid and peripheral subsets[3], although our labs own unpublished data suggest that XCR1 expression does not fully capture cDC1 at all stages of maturation. The function of XCR1 has recently been elucidated *in vivo,* serving as a chemokine receptor homing towards the CD8+ T-cell secreted ligand known as XCL1[20]. Collectively these findings provide a model for the subsets ability to stimulate cytotoxic CD8+ T-cells; whilst highlighting inadequacies as a phenotypic marker being only transiently expressed by DC subsets following activation. In humans cross-presenting DC are characterised by high expression of CD141, although this marker is not fully correlated with a capacity for cross-presentation-especially in the blood[21,22]. While a large proportion of CD141 DC express XCR1 it is not yet clear whether all XCR1+ DC in humans are capable of cross-presentation[7].

The murine cDC1 can be further divided into lymphoid resident (CD8α+) and migratory (CD103+) populations. The cross-presenting lymphoid resident CD8α+ subset of DC are specifically equipped to process antigen from dead or dying cells[7,23,24], with experimental data showing preferential uptake and cross-presentation of antigens from other late apoptotic DC[25]. These findings provide a model for lymphoid resident DC to prime cytotoxic T-cells against viral infections of the periphery (figure 1.2); a phenomena observed during herpes simplex virus infection of the dermis[26] and other epithelial sites[27].

The migratory DC populations of the dermis had been well characterised prior to the identification of XCR1, characterised by high expression of the integrin CD103[28-31]. Likely functional correlates have also been characterised at other peripheral sites including the lung[32] and liver[28]. Ablation of the migratory CD103+ cross-presenting DC subset in influenza infection models shows an increase in

clinical severity, and delayed development of virus specific cytotoxic T-cells[33]. This suggests distinct roles for the two subsets of cross-presenting DC; the CD103+ subset functioning as a conventional migratory sentinel, and the CD8α+ lymphoid resident subset functioning to detect and process antigen from virally infected or otherwise stressed cells (figure 1.2).

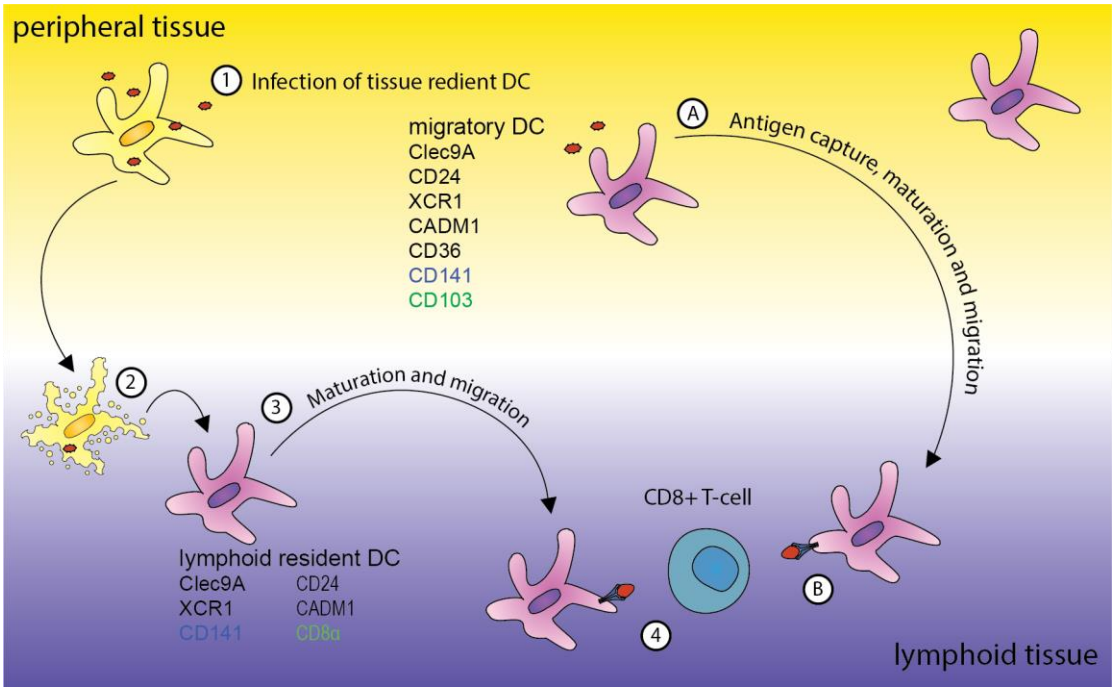

Figure 1.2 Functional subdivision of cross-presenting cDC1 into peripheral and lymphoid subsets.

Cross-presenting migratory cDC1 exist at a low abundance in peripheral tissues including the skin, lungs and intestinal mucosa. During infection these cells capture exogenous antigen, mature and begin migration to the lymph nodes ***(A)****, where they cross-present the exogenous derived antigen to CD8+ T-cells in association with MHC-I* ***(B).*** *Tissue resident DC (either cDC1 or cDC2; cDC2 shown) that succumb to infection become active and migrate towards the lymph nodes* ***(1).*** *As migratory DC become apoptotic, they are detected and taken up by lymphoid resident cDC1* ***(2).*** *The lymphoid resident DC than mature and begin migration towards the T-cell zone* ***(3)*** *where they are able to stimulate activation of CD8+ T-cells* ***(4).*** *Cross-presentation of antigen from apoptotic cells has also been demonstrated in the periphery by the CD103⁺ DC (not shown). Markers common to both human and murine cross-presenting DC subsets are shown in black, whereas those specific to murine DC are shown in green and those specific to human DC are shown in blue. Image created on Adobe Illustrator, Creative Cloud, 2019.*

cDC2 and the LC

Throughout this thesis, DC primarily restricted to stimulating $CD4^+$ T-helper cells are referred to as cDC2. The cDC2 can be further sub-divided into two groups based on function, the first group including all SIRPα+ migratory DC of peripheral tissues and the second including all the SIRPα+ non-migratory DC of the lymph nodes and spleen[2,11]. This functional separation is well correlated with surface marker phenotype in mice (figure 1.3), although not well defined in humans. With all cDC2 subsets in humans and mice being $SIRP\alpha^+$, murine migratory DC of the periphery can be further distinguished based on the expression of traditional marker CD11b[3], whereas the non-migratory lymphoid resident cDC2 are both $CD11b^+$ and $CD4^+$[3].

In the context of infection and immunity, the primary role of the cDC2 is to capture exogenous antigen for presentation to $CD4^+$ T-helper cells, with migratory subsets scouring peripheral tissue and non-migratory subsets filtering the lymphatics (figure 1.3). Whilst several studies have demonstrated the presentation of MHC I restricted antigens to CD8 T-cells by cDC2[32-35]; it has been long argued that these instances probably reflect direct infection of the DC and presentation via the cytosolic antigen processing pathway, and not cross-presentation of exogenous antigen[2]. More recent evidence from Desch and colleagues[36] has resolved this issue demonstrating; (i) the cross-presentation of ovalbumin by pulmonary $CD11b^+$ migratory cDC2, and (ii) the subsequent activation of $CD8^+$ CTLs in the draining lymph node of mice deficient for migratory cDC1 ($CD103^+$)[36]. In these experiments cDC2 required specific adjuvants to achieve full $CD8^+$ T-cell stimulatory capacity[36], illustrating the functional plasticity of the subset dependent on the local micro-environment.

The LC are arguably the most well-known DC subset, although cannot be classified as *bona fide* DC based on their development from the monocyte lineage, independently of flt3-l[5]. Moreover, their contributions to immunity during infection and inflammation has recently come under question. The controversies regarding LC function remain unresolved but have been well reviewed[37], with suggestions that they primarily function in tolerance by regulating immune responses against commensals in the skin[3].

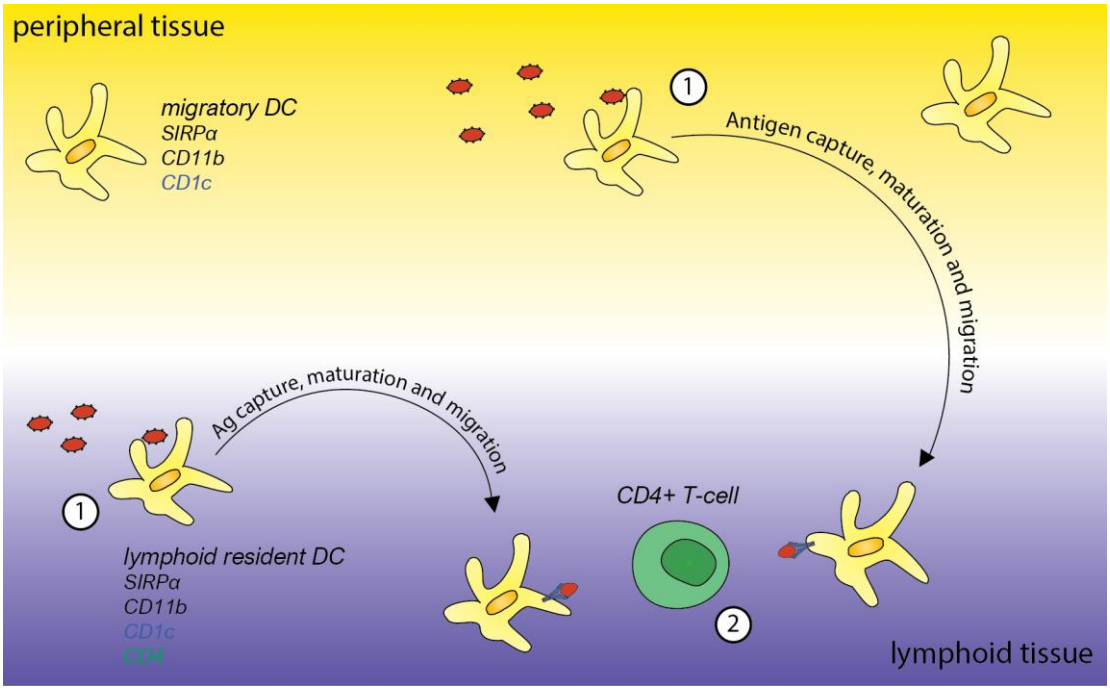

Figure 1.3 Subdivision of cDC2 into peripheral and lymphoid subsets. cDC2 exist in low abundance in peripheral tissues including the skin, lungs and intestinal mucosa.

Lymphoid resident cDC2 filter the lymphoid tissue including the lymph nodes and spleen, and can be distinguished from murine migratory subsets based on expression of CD4. During active infection both cDC subsets capture exogenous antigen, mature and migrate to the T-cell zone of lymph nodes ***(1),*** *where they present antigen to CD4+ T-cells* ***(2).*** *Markers common to both human and murine DC subsets are shown in black, those specific to murine DC are shown in green and those specific to human species are shown in blue. Image created with Adobe Illustrator, Creative Cloud, 2019.*

pDC are potent interferon producers and critical in antiviral defence

The pDC are an atypical subset of DC sharing a common developmental pathway with the cDC, but unlike cDC subsets pDC fully mature in the bone marrow[38], subsequently migrating to the thymus and secondary lymph via the blood stream[38]. The pDC are functionally unique with their primary role being the potent secretion of anti-viral type I interferon (IFNα/β) following activation[39]. Unlike all other DC subsets the pDC exhibit poor antigen presentation abilities, ascribed to a low expression of MHC II and co-stimulatory molecules[39]. Human and murine pDC are phenotypically distinguished based on the expression of BDCA-2 and SiglecH respectively[39]. While there are several other surface markers that can be used to identify pDC, BDCA-2 and SiglecH for human and mice respectively exclude most other cell types[40].

The potent and rapid secretion of type I interferon unique to pDC is likely due to a combination of molecular factors. pDC constitutively express the transcription factor IRF-7[41], priming them for type I IFN secretion upon activation of the transcription factor. Secondly, relative to cDC the pDC exhibit altered endosomal trafficking increasing the duration of nucleic acid exposure to TLR9[42] – a critical receptor involved in inducing expression of type I interferon via activation of IRF-7.

Aside from a potent secretion of IFN-I upon stimulation, pDC can be functionally distinguished from the cDC by an inefficient capacity for T-cell stimulation. While pDC express lower levels of co-stimulatory molecules than the conventional DC, their expression of HLA/MHC indicates a restricted potential for antigen presentation. Studies have demonstrated that pDC are able to present endogenous peptides on both MHC I and MHC II, including those derived from either self[43,44] or viral agents infecting the pDC[44-47]. By contrast, the abilities of pDC to capture and present exogenous antigen are somewhat restricted. This is likely due to the relatively low expression of MHC-II and co-stimulatory markers required for efficient T-cell priming[5].

Inflammatory monocyte derived DC

The classification of inflammatory DC is ambiguous in the literature, with some of these populations also described as monocyte-like or monocyte related

cells[10,48,49]. Throughout this thesis the term inflammatory DC will be used to describe both monocyte related subset commonly referred to as TipDC and a second subset known as SLAN DC. The latter are characterised by their unique carbohydrate modification 6-sulfo N-acetyllactosamine (SLAN) of the adhesion molecule PSGL-1[50]. While SLAN DC are well reviewed for their role in driving autoimmunity[51], there is relatively little known about their role in infection and immunity and therefore will not be further discussed.

The Tip-DC were first characterised in 2003 for their unique production of both TNF-α and nitric oxide (NO); and so called TNF and inducible nitric oxide synthase (iNOS) producing DC (TipDC)[52]. This novel DC subset is not detectable at steady state transiently increasing in abundance during infection and inflammation, dependent on CCR2 signalling for migration to the site of infection and subsequent differentiation[52]. The TipDC precursor is a bone marrow derived monocyte characterised by $Ly6C^{+}$ and $Gr1^{+}$ phenotype in mice[52], or a $CD14^{hi}$ $CD16^{lo}$ phenotype in humans[10]. TipDC share many features typical of the myeloid DC including the classical dendritic morphological characteristics, migratory properties and the ability to prime naïve T-cell responses[9]. However, their unique production of both TNF-α and iNOS distinguishes them from other subsets, playing an important role in the clearance of parasites[53] and intracellular bacteria such as *Listeria monocytogenes*[52].

1.1.2 DC Function in Infection and Immunity

In the context of infection, the foremost role of the DC is to promote the expansion of adaptive immune responses, providing a crucial link between the adaptive and innate immune responses. DC provide the necessary signals for not only the activation of T-cells, but also the subsequent direction of their responses. This section will consider the essential immunological functions of the DC, characterising the contributions played by the various subsets in the context of infection and immunity.

Dendritic Cell Maturation and T-cell Activation

The pathways surrounding the activation of DC following recognition of a pathogen are both complex and intricate, estimated to involve the regulation of

several thousand genes[54-56]. Furthermore, the phenotype of a mature DC is dynamically regulated dependent upon both the type of stimulus received and the local inflammatory micro-environment. The LC paradigm describes the most basic function of conventional DC, categorising them as being in either one of two states: mature and immature. While this model is admittedly simplistic, it provides a basic understanding of DC biology.

In order to capture antigen, immature cDC are highly phagocytic and express high levels of pattern recognition receptors (PRRs). In this state these DC have low level expression of co-stimulatory molecules and MHC required for T-cell stimulation[57], but a rapid turnover of MHC increasing the rate of 'antigen sampling'. Upon stimulation of a PRR DC undergo maturation associated with short burst in endocytic capacity[58], alongside an increase in expression of MHC but a reduction in turnover enhancing the chances of 'pathogenic' antigen presentation[57]. Maturation stimuli also induce increased expression of the co-stimulatory molecules required for T-cell activation and the lymphoid homing chemokine receptor CCR7, as well as inducing a dendritic morphology increasing surface area and chance of contact with T-cells[57].

Under the LC paradigm the primary consequence of DC maturation is lymphatic migration and subsequent T-cell activation. Therefore, the extent of DC maturation and their ability to prime T-cells are tightly linked. The activation and functional differentiation of T-cell by DC is widely regarded as a three-signal process: (i) recognition of cognate antigen in association with MHC, (ii) affirmation of activation by recognition of co-stimulatory molecules and (iii) functional programming and terminal differentiation triggered by cytokine signalling. These three signals must be provided by an antigen presenting cell, such as an activated DC (figure 1.4).

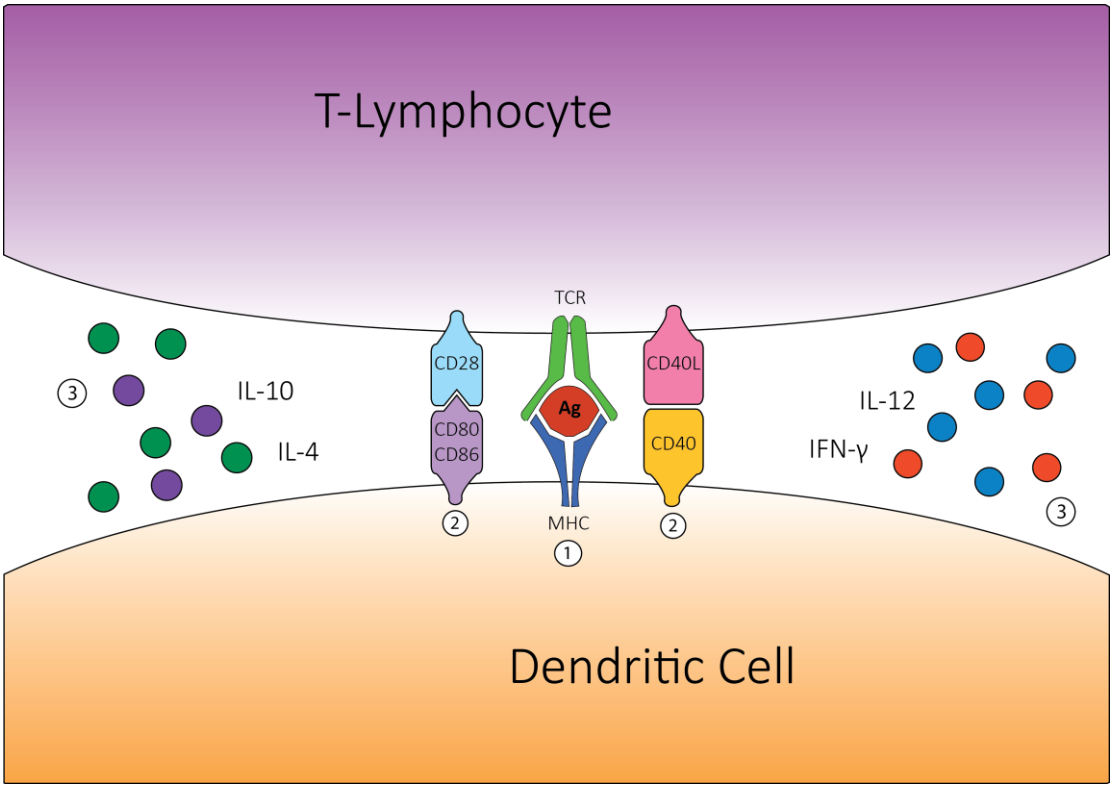

Figure 1.4 Three signal process for T-cell activation.

Antigen specific T-cells are provided the first signal for activation through the T-cell receptor (TCR), recognising peptide in the context of MHC ***(1).*** *The second signal for activation is provided by the recognition of co-stimulatory markers on the surface of an activated DC including the recognition of CD40 by CD40L and CD80 or CD86 by CD28* ***(2).*** *The final activation signal is the detection of cytokines produced in paracrine by the DC providing instruction for differentiation. Secretion of IL-12 and IL-10 by DC induce Th1 and Th2 differentiation respectively* ***(3).*** *Amplification of the signal is provided in both autocrine and paracrine with positive feedback provided by T-cells, via the secretion and recognition of IFN-γ and IL-4 for* Th_1 *and* Th_2 *respectively* ***(3).***

1.2 Pattern Recognition and Innate DC Activation

In the context of infection DC activation is initially triggered by the detection of foreign matter, mediated by a diverse array of PRRs. During the later course of infection subsequent DC maturation is triggered by pro-inflammatory cytokines signalling both in autocrine and paracrine[54]. This section focuses on the activation of DC in terms of infection, providing an overview of the pathways signalling maturation in response to danger signals, and how these pathways are regulated.

The pathways surrounding the maturation of DC upon encounter of danger signals are both complex and intricate, estimated to involve the regulation of several thousand genes[54-56]. The signalling pathways described in this section will therefore describe specific examples of DC subsets in infection, as the outcome of signalling is dependent on a complex combination of factors including the type and duration of stimulus, cytokine milieu[54], and the DC subset stimulated[59].

1.2.1 Toll Like Receptors

Toll-like receptors (TLRs) represent the most diverse and well characterised family of pattern recognition receptors; sensing a variety of pathogen derived molecular species including proteins, carbohydrates, lipids, nucleic acids, and combinations thereof[60]. TLRs are innate immune receptors expressed ubiquitously by all cell types as membrane associated receptors localised either to the plasma membrane or internal endosomes (figure 1.5). This diverse expression pattern allows a cell to scan both the extracellular environment and recently internalised material for pathogens. To date there are 10 and 12 functional TLRs characterised in human and murine species respectively, of which TLR 1-9 are functionally synonymous[60]. TLR10 is non-functional in mice, whereas TLRs 11-13 are exclusive to the mouse genome.

Each of the 13 TLRs recognise distinct pathogen associated molecular patterns (PAMPs; table 1.1), and while all TLRs are expressed by DC- the expression patterns vary between each of the DC subsets (table 1.1). Most notably, expression of TLR3 is largely restricted to cDC1 in both mouse and humans[5], facilitating recognition of viral ligands and stimulating cross-presentation of antigen[61]. By contrast, cDC2 are geared towards the recognition of bacteria, tending to express

the highest levels of TLR2, 4, 5 and 6[5]- although the expression of these TLR are not restricted to cDC2 (table 1.1). Lastly, the pDC are largely restricted in their expression of TLR, but express very high levels of TLR7 and 9, facilitating their potent and rapid secretion of type I IFN during viral infection[59].

TLR signalling is highly conserved between the species, with the intricacies of these signalling mechanisms being well characterised (figure 1.5)[59,60,62]. Depending on the stimulus, the fundamental consequence of TLR stimulation is the secretion of pro-inflammatory cytokine, chemokine and IFN. These cytokines vary between cell type and play a critical role during early infection inducing inflammation and recruiting cells of immune system. Aside from these essential innate functions, TLRs play a critical role in inducing the maturation of DC and therefore linking the innate and adaptive responses.

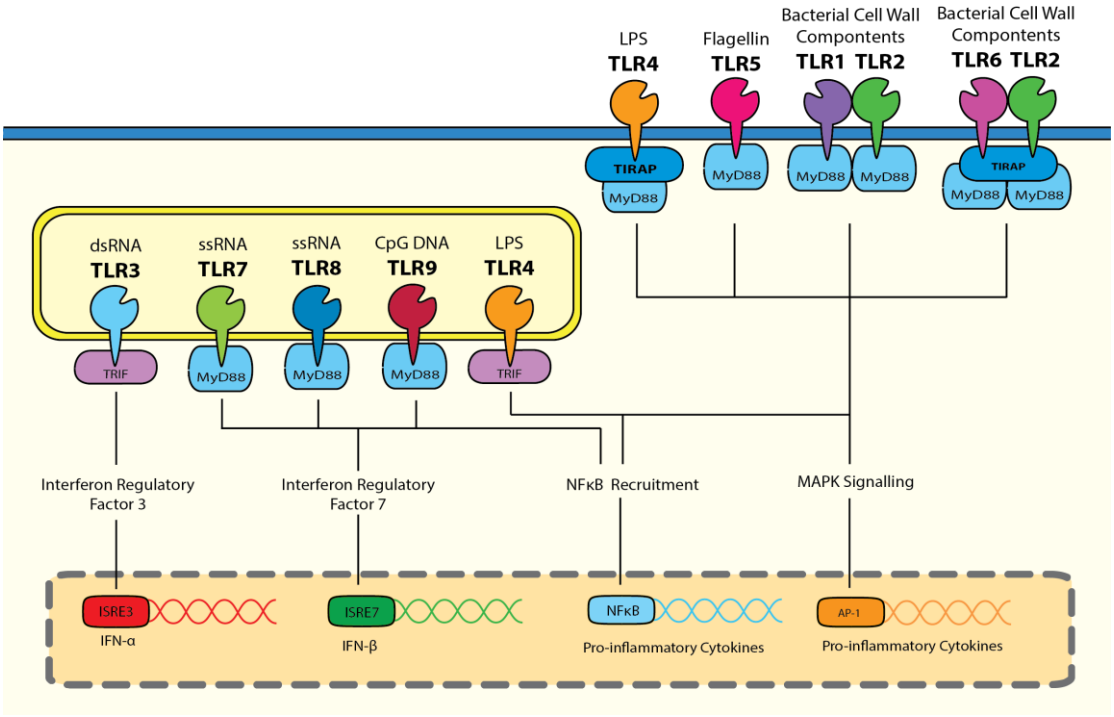

Figure 1.5 Membrane localisation of human toll like receptors and schematic representation of general signalling mechanisms.

TLR signalling is initiated by recognition of a PAMP, triggering dimerization of the receptor. For simplicity, only TLRs forming heterodimers are depicted as dimeric. Dimerisation stimulates downstream signalling mediated by the exclusive use of an adaptor molecule (MyD88 or TRIF), with the exception of TLR4 recruiting either MyD88 or TRIF adaptor molecules at the plasma membrane and endosome respectively[63]. All signalling pathways result in either recruitment of NFκB, AP-1 or IFN regulatory factors resulting in the secretion of either pro-inflammatory cytokines or Type I IFN.

Table 1.1 TLR Expression across primary human and murine dendritic cell subsets.

Toll Like Receptors[5,37,41,62,64-71]							
	Known Ligands	**cDC1**		**cDC2**		**pDC**	
		Hu	**Mu**	**Hu**	**Mu**	**Hu**	**Mu**
TLR1	Triacyl lipopeptides	++	++	++	++	+	+
TLR2	Lipoprotein, lipoteichoic acid, zymosan	++	++	+++	++	-	+
TLR3	dsRNA	+++	+++	+	+/-	-	-
TLR4	Lipopolysaccharide	-	++	+	++	-	-
TLR5	Flagellin	-	-	++	++*	-	-
TLR6	Lipoteichoic acid, diacyl lipopeptides, zymosan	++	++	++	+++	+	++
TLR7	ssRNA	-	-	++	++	+	+++
TLR8	ssRNA	++	++	++	++	-	++
TLR9	CpG DNA	-	++	-	++	++	+++
TLR10	Lipoproteins, peptidoglycans	++		++		+	
TLR11	Profilin (*Toxoplasma gondii)*		+++		-		-
TLR12	Profilin (*Toxoplasma gondii)*		++		-		+
TLR13	Bacterial rRNA		+		+		-

+++ High receptor expression
++ Moderate receptor expression
+ Low receptor expression
- No detectable expression
* Only expressed on a subset of ESAM^{lo}, Clec12A^{hi} cDC2

1.2.2 C-Type Lectin Receptors

C-Type Lectin Receptors (CLRs) represent a diverse family of PRRs well known for their role in responding to fungal pathogens. However, the role of CLRs in bacterial, viral and parasitic immunity has become of growing interest[72]. Indeed it is now known that CLR ligands encompass a broad range of PAMPs and self-DAMPs; with common examples including mannose, fucose, glucan carbohydrates and signals from dead or dying cells (table 1.2)[73].

The differential expression of CLRs across the DC subsets closely correlates with their ascribed functions. For example, both human and murine cDC1 exhibit high surface expression of C-type lectin domain containing (Clec)9A, which is responsible for binding filamentous actin exposed in apoptotic or damaged cells[74,75]. Importantly, the expression of Clec9A by cDC1 has been shown to facilitate cross-presentation of dead and necrotic cell antigen to $CD8^+$ T-cells *in vitro*[64]. Clec9A is expressed on the plasma membrane and in endosomal compartments of the XCR1 DC, and its ligand mediated signalling has been demonstrated to slow endosomal maturation thus increasing the longevity of its captured antigens[76,77]. While it has been well established that the targeting of Clec9A ultimately leads to enhanced cross-presentation of antigen[17,76], the mechanisms inducing cross-presentation following Clec9A signalling are yet to be fully elucidated[76].

The signal transduction mechanisms employed by CLRs are diverse and not fully characterised, with the signalling mechanisms of Dec-205 and the Mannose Receptor (MR) yet to be elucidated[72]. However most CLRs are known to signal via the recruitment of the tyrosine kinase Syk[72], although exception include DC-SIGN and Dectin-1, which are able to signal via the serine/threonine kinase Raf-1[72,78]. Dectin-1 exhibits dual signalling capacity able to recruit either Syk or Raf-1[78], whereas DC-SIGN is restricted to signalling via Raf-1. Both signalling pathways ultimately result in downstream modulation of NFκB and the MAPK signalling cascade[72].

A common theme of CLR stimulation is the modulation of other PRR signalling mechanisms to shape the immune response. For example, Co-stimulation of

Dectin-1 with TLR2 synergistically enhances the Dectin-1 dependant production of reactive oxygen species (ROS)[68], which are not typically induced with the stimulation of TLRs alone. Dectin-1 is also able to synergistically enhance the secretion of pro-inflammatory cytokines when stimulated in combination with either TLR2[68]or TLR4[78]. In both instances the signalling pathways converge on NF-κB signalling, with Dectin-1 simultaneously modulating the activity of NF-κB subunit p65 and inducing expression of subunits c-rel and RelB[68]. In terms of infection and immunity the co-stimulation of Dectin-1 not only enhances TLR2 signalling, but modulates it to bias the secretion Th_1 and Th_{17} cytokines for an anti-fungal response[68]. This is an important consideration given the promiscuity of TLR2 in recognising bacterial and fungal ligands.

The signalling mechanisms of CLRs require either the direct recruitment of an adaptor molecule to an Immunoreceptor Tyrosine-based Activation Motif (ITAM) domain located within the cytoplasmic tail[72], or indirect recruitment through association with other ITAM containing receptors[72]. Several CLRs such as Clec4a (DCIR) instead recruit the tyrosine phosphatase SHP-1 via an Immunoreceptor Tyrosine-based Inhibition Motif (ITIM) domain[73]. SHP-1 is known to modulate signalling by RIG-I and several TLRs, inhibiting the production of pro-inflammatory cytokines whilst increasing the production of IFN-I[73,79]. This inhibition occurs through a negative regulation of NFκB activation[80]

Table 1.2 Expression of well characterised CLR across the DC subsets.

C-type lectin receptors[17,74-76,81-89]				
	Known Ligands	**cDC1**	**cDC2**	**pDC**
Clec9A	Filamentous actin	++	-	+
Clec12A	Plasmodial hemozoin, Monosodium urate crystals	++	+	++
Dec-205	Keratins, CpG DNA	+	-	-
Dectin-1	β-1,3- and β-1,6- glucans (fungal glucans)	+	+	-
DC-SIGN	Mannose carbohydrates (HIV)	+	+	-
Mannose Receptor	Ligands bearing mannose, fucose, N-acetyl glucosamine or sulphated sugars	+ (migratory only)	-	-

\+ Receptor is expressed
\- Receptor is not expressed

1.2.3 Cytosolic Sensors

The PRRs discussed thus far provide comprehensive surveillance for detection of PAMPS both at the cell surface and in the endosome. However there remain a variety of cytosolic PRRs available for the detection of pathogens which may directly infect and replicate inside of the cell. These include major receptor families such as Rig-Like Receptors (RLRs) and Nod-Like Receptors (NLRs) as well as other signalling molecules such as cGAS/STING[60,90,91].

The Nod-Like Receptors which encompass a family of proteins able to recognise a diverse number of both pathogen and danger associated molecular patterns[92]. The NLRs share a similar structural composition, comprising a C-terminal leucine rich repeat which plays a critical role in pattern recognition, and an N-terminal nucleotide-binding oligomerisation domain which facilitates the oligomerisation of activated receptor proteins[92,93]. The NLRs are well characterised for their capacity to oligomerise into large multimeric complexes referred to as inflammasomes, which play a critical role in the proteolytic cleavage of IL-1 and IL-18 into their bioactive forms[92]. Perhaps the most well characterised of the inflammasomes is the NLRP3 and NLRC4 inflammasomes which have been well reviewed for their capacity to sense a diverse array of bacterial moieties, including cell wall components, secretion systems, toxins and flagellin[92,94]. While not all of the activating ligands are fully elucidated, it is known that the inflammasome plays an important role in sensing bacterial infection. Indeed, the production of IL-1β in response to the bacteria *Francisella tularensis* is dependent on the inflammasome, and moreover AIM2 inflammasome deficient mice are more susceptible to lethal challenge with *F. tularensis* than are controls[95,96].

The RLRs include retinoic inducible gene I (RIG-I), melanoma differentiation-associated gene 5 (MDA5) and RIG-I-like receptor 3 (RLR-3). These RLRs are RNA helicases well characterised for their capacity to sense discrete structures of cytoplasmic RNA, subsequently inducing anti-viral signalling through mitochondrial antiviral signalling protein (MAVS)[97,98]. Recognition of cytoplasmic DNA has more recently been described to occur through signalling via the cGAS/STING pathway, whereby DNA is initially detected via cyclic GAMP Synthase (cGAS), facilitating the conversion of ATP and GTP into cGAMP, which subsequently elicit IFN production via the stimulator of IFN genes (STING)[91,99] (figure 1.6). While activation of this pathway was initially determined for the

detection of DNA viruses, this pathway has shown to also be involved in the detection of bacterial DNA in the cytoplasm[100], including that of *Neisseria gonorrhoeae*[101], *Listeria monocytogenes*[102], Group B Streptococcus[103], *Mycobacterium Tuberculosis*[104], and *S. aureus*[105]. Moreover, it has further been established that bacterial derived cyclic dinucleotides are able to directly act upon STING to induce IFN production, circumventing the cGAS pathway[106] (figure 1.6). The identification of other DNA recognition molecules has been controversial[107,108], however several other molecules have been proposed as DNA receptors including DNA-dependent activation of IFN regulatory factors (DAI)[107], and absent in melanoma-2 (AIM2)[108].

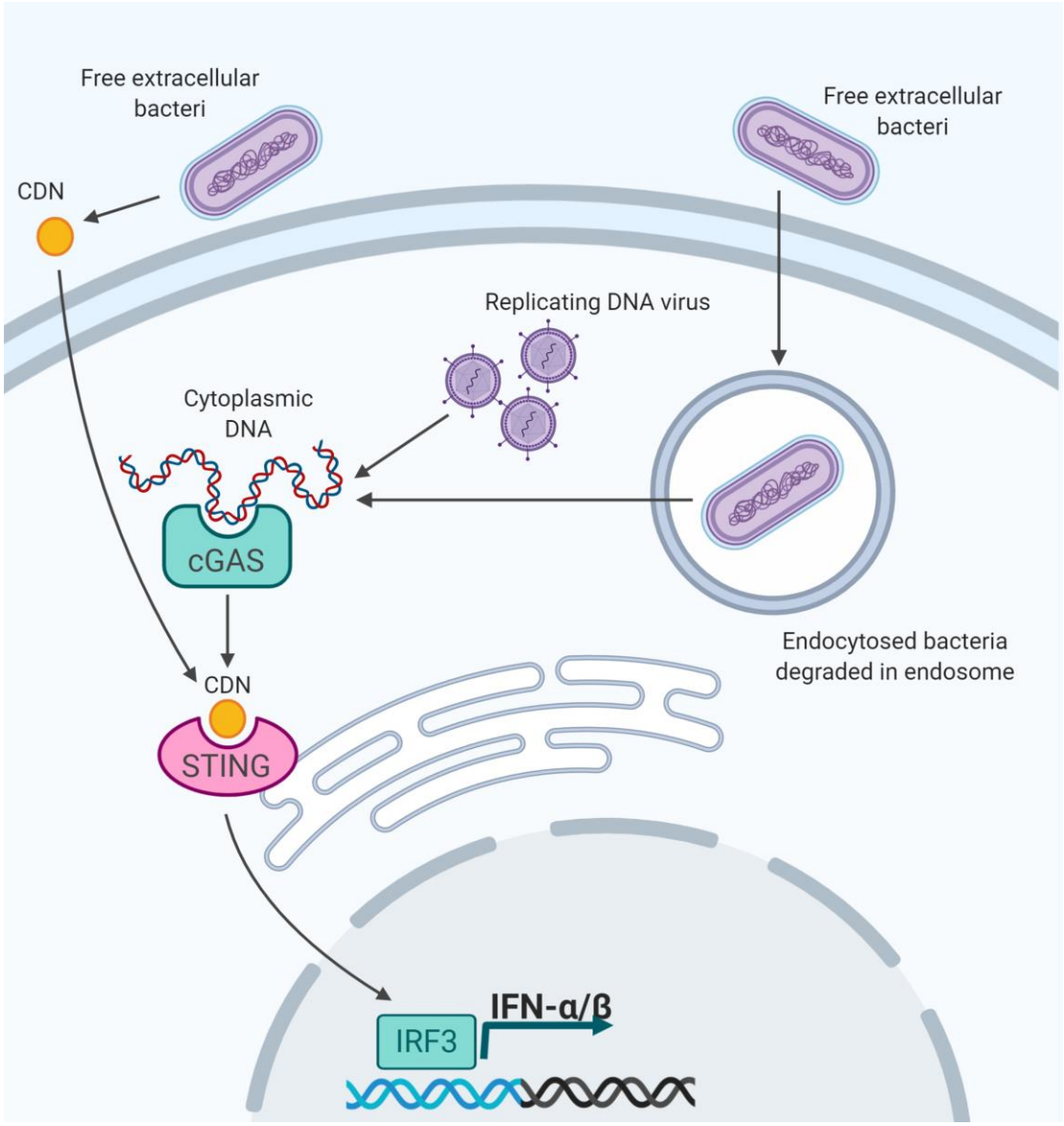

Figure 1.6 Cytosolic sensing of viral and bacterial nucleic acid via the cGAS/STING pathway.

Actively replicating nucleic acids from DNA viruses, and bacterial DNA released during endosomal breakdown are sensed by cGAS. Stimulation of cGAS with DNA induces production of cyclic dinucleotides (CDN) which activate STING[91]. STING activation leads to a signalling cascade resulting in recruitment of IRF3 and early phase production of IFN-β. Importantly, STING can be activated directly by bacterial CDN independently of the cGAS pathway[106]. This figure was created with BioRender at 'www.biorender.com'.

1.2.4 Antigen Capture and Processing

The capture, processing and presentation of antigen represents a core function of the conventional DC subsets, allowing for both regulation of immunological tolerance under steady state and the induction or expansion of adaptive immune responses during infection. As such DC subsets are equipped with a dynamic array of surface and internal receptors facilitating the capture of antigen, including PRRs, endocytic receptors and scavenger receptors.

The PRRs include several diverse families of receptors involved in the regulation of DC activation. It should be noted that these receptors also play an important role in the internalisation of antigen, therefore linking the capture of antigen with the activation of the DC. This provides a model for the processing and presentation of antigen following DC activation. For example, the stimulation of TLRs has been demonstrated to transiently stimulate endocytosis, induce expression of essential antigen processing components and upregulate surface MHC[58]. The increased rate of endocytosis is inversely correlated with the motility of the DC, and has been estimated to peak 30 minutes post-stimulus[58]. This is immediately followed by a long-term downregulation in endocytic capacity and a restoration in cell motility[58], allowing for the preservation of presented antigen during lymphatic migration and T-cell stimulation.

pDC are poorly endocytic and are more well known for their potent capacity to secrete anti-viral cytokines following activation. A study published in 2008 demonstrated that human pDC exhibit a poor receptor mediated endocytic capacity compared to cDC[109]. This study demonstrated more than a 20-fold increase in particle uptake by cDC, when particles were conjugated to either TLR2, TLR4 or Fc receptor ligands[109]. However particle uptake by pDC was not increased when conjugated to TLR2 or TLR4 ligands, and only marginally increased when conjugated to high doses of Fc receptor (FcR) ligand (IgG)[109]. While neither TLR2 or TLR4 are expressed by pDC[37], they express at least 3-fold more high affinity FcγRI transcripts than do the cDC[19]- suggesting that the nuances in the regulation of endocytosis are not due to differences in protein expression, but rather regulated at the cellular level.

1.2.5 Cytokine Secretion

The cytokine profile of a DC shapes the downstream immune response, dictating the differentiation of stimulated T-cells. The differential capacity of DC to produce cytokine are intrinsically linked to their differential expression of TLR (table 1.1) and other PRR. For example, TLR3 is predominantly expressed by both human and murine cDC1, facilitating their capacity to produce abundant IFN-λ[61]. Similarly, high expression of TLR3 on murine CD8α⁺ cDC1 induces secretion of type I IFN, playing an important role in stimulating cross-presentation of antigen and the induction of CD8+ T-cells[59,110,111]. cDC1 are also able to produce bioactive IL-12[112], (which is critical for the induction of Th_1 and cytotoxic CD8 T-cell response), therefore complementing their capacity for cross-presentation.

The cDC2 are able to produce a broad panel of pro-inflammatory cytokines including IL-1β, IL-6, IL-10, IL-12, IL-23, TNF-α and TGF-β[113-115]. The subset has also been shown to play an important role inducing Th_1 responses via potent production of bioactive IL-12[112], but can also play a role in Th_{17} differentiation at mucousal sites with the production of polarising cytokines IL-6 and IL-23[116]. Of particular note, IFN-λ not produced to appreciable levels by cDC2[112,117], with abundant secretion restricted to cDC1[61]. Nonetheless, the cDC2 are well equipped to produce IFN-α in response to recognition of cytoplasmic viral RNA via RIG-I and other RLRs[118]. In contrast, the pDC are able to rapidly produce abundant type I and III IFN following the ligation of TLR9 with CpG ODNs, producing relatively low levels of other inflammatory cytokines and chemokines with the exception of the macrophage inflammatory proteins (MIPs) and RANTES[119].

For the remainder of this chapter, we will focus on a specific pathogen, *Staphylococcus aureus*, discussing epidemiology, clinical significance and interactions with the host immune system. Specifically, we will end this chapter reviewing what is currently known about innate sensing of *S. aureus* by DC, leading into our project aims and hypothesis.

1.3 Methicillin Resistant *Staphylococcus aureus*

1.3.1 MRSA Epidemiology and Clinical Significance

Staphylococcus aureus is an extracellular, gram positive bacterium colonising the epidermis of approximately one third of the population[120-122]. Under normal conditions colonisation of the epidermis by *S. aureus* represents a commensal relationship with no detriment to the host. However, with spread to the blood stream or deeper tissue sites the bacterium is able to establish persistent infection, causing significant morbidity and mortality rates estimated from 20-50% around the world[123-125]. These infections tend to be characterised as either hospital acquired or community associated dependent on the mode of acquisition. In this thesis we focus on the former, and therefore community associated *S. aureus* will not be further reviewed here.

Hospital Acquired *S. aureus*

Hospital acquired *S. aureus* infections comprise 60% of all *S. aureus* infections in Australia[124]. The overall 30-day mortality rate of these infections is 22%, increasing to 33% when the infection is with methicillin resistant *S. aureus* (MRSA)[124]. Approximately one quarter of all *S. aureus* infections in Australia are methicillin resistant *S. aureus* (MRSA), of which more than half (60%) are multi-resistant to three or more classes of antibiotics[124].

Hospital-acquired infections comprise a diverse range of clinical manifestations, including blood-stream infection (bacteraemia), infection of the bone (vertebral osteomyelitis) and/or infection of the heart valve (endocarditis)[126]. These infections are largely attributed to the insertion of medical devices, with estimates suggesting approximately 80% of hospital acquired *S. aureus* infections being of an endogenous source, meaning the infection is sourced from the carrier[121]. Of particular note non-carriers experience significantly higher mortality rates than persistent carriers[121,127]; suggesting a partial protective role from symbiotic *S. aureus.* Nonetheless neither colonisation with *S. aureus* nor frequent or chronic infections has demonstrated protection against subsequent infections[128,129].

Community-acquired *S. aureus*

The earliest documented cases of community associated MRSA were reported in remote indigenous Australian populations in 1993[130]. These isolates were noteworthy being found to be genetically distinct from the major circulating strains of hospital acquired MRSA at the time[130]. Unlike hospital acquired infections, community acquired MRSA tends cause skin and soft tissue infections[131,132]; and is therefore readily transmissible via direct contact with an infected or colonised individual[133].

While the mode of transmission represents an important distinction between community and hospital acquired infections, there is substantial overlap between the isolates which cause these infections. Indeed, over the past two decades in Australia community associated MRSA lineages have progressively replaced clone of hospital acquired MRSA[134]. These findings highlight the diverse pathogenic potential of MRSA isolates, suggesting that the mode of transmission – rather than infecting strain – is a critical determinant for the type of infection.

Laboratory strains of *S. aureus*

Most published studies of bacterial immunopathogenesis tend to utilise such references strains, with some of the most common including USA300[135-138], Cowan Strain I[138-140], and SH1000[141-143]. However, concerns have been raised over the use of laboratory reference strains for pathogenicity studies as they do not recapitulate the species level diversity observed amongst distinct clinical isolates. Moreover, with some reference strains having been sub-cultured for decades, substantial genomic and phenotypic differences have been further documented between labs culturing identical reference strains[144]. For these reasons we agree that immunopathogenesis studies should examine low-passage clinical isolates to maintain optimal biological significance, a key objective of the current thesis. However due to the scarcity of such published studies, the remainder of this section will provide a comprehensive review of the literature pertaining to both laboratory reference strains and clinical isolates.

1.3.2 Innate sensing of *S. aureus* by DC

While there is a body of literature focussing on the molecular mechanisms regulating innate recognition of *S. aureus* by DC, much of it is either assumed from DC receptor expression and their known ligands, or findings of *S. aureus* interactions with other phagocytes[145]. The latter tends to be obtained from either monocyte inducible DC or macrophage models which do not recapitulate primary DC subsets. Especially lacking is literature pertaining to the role of primary cDC subsets in response to *S. aureus*, with few direct experiments investigating cDC subsets and their function either *in vitro* or *ex vivo*.

Jin and colleagues[141] were the first group to extensively phenotype human blood DC in response to stimulation with the S. aureus model strain SH100[141]. Their study indicated that conventional BDCA1+ DC (cDC2) are the sole blood DC subset able to efficiently phagocytose S. aureus, consequently upregulating surface activation markers and secreting IL-12p70[141]. However, conflicting studies have demonstrated human pDC are able to phagocytose S. aureus, consequently upregulating CD86 and secreting IL-6, TNF-α and IFN-α[21,139,146]. The discrepancies between cDC2 and pDC activation in these studies highlight the intricacies of DC function, but may also be indicative of a broader issue in using laboratory bacterial strains for functional studies of primary infection.

Parcina and colleagues[146] have examined the molecular mechanisms regulating the innate recognition of *S. aureus* by human pDC, demonstrating that activation is dependent on sensing of endosomal nucleic acids via TLR7/9[146]. In a later study the same group further demonstrated that pDC stimulate a short lived, IFN dependent, IL-10 producing B-cell population in response to Protein A expressing strains of *S. aureus*[139]. This population is hypothesised to facilitate immunosuppression during *S. aureus* infection, with IL-10 previously being demonstrated to interfere with antigen presentation and T-cell activation in a model of *Salmonella typhimurium* infection[147]. Collectively, these observations have important implications for the immunoregulation and suppression of the host during clinical infection, the studies of Parcina and colleagues[139] are limited in their analysis of several high-passage laboratory strains.

cDC function during *S. aureus* infection

While there is little experimental data pertaining to mechanisms of cDC recognition of *S. aureus,* it is nonetheless clear that they play an important role during infection[143]. In a

murine infection model, cDC deficient mice (CD11c-DTR transgenic mice) exhibit increased bacterial loads, accelerated mortality and more severe pathology than do controls[143]. Furthermore, *S. aureus* stimulation is able to elicit cDC dependent IL-12p70[143], suggesting a possible role for cDC1 in Th1 induction. Nonetheless, the former findings relating to the CD11c-DTR transgenic model should be treated with caution due to the potential for non-specific ablation of other CD11c expressing cells-including monocytes, macrophages, NK and B-cells[148].

Earlier this year, Darkwah and colleagues[149] have further shown that cDC differentially stimulate CD4+ T-cell proliferation based on the DC anatomical location during sepsis[149]. In this study, murine mucosal cDC of the mesenteric lymph node exhibited higher surface expression of MHC-II and CD40 than did cDC of spleen during sepsis. Importantly, the cDC of the mesenteric lymph node were also superior to splenic cDC in the induction of CD4 T-cell proliferation *ex vivo*. While novel, key limitations of this study include not distinguishing between the capacity of cDC subsets to induce T-cell proliferation, or the subsequent Th polarisation.

More recently, Richardson and colleagues[150] have demonstrated a role for phenol soluble modulins (PSM), a *S. aureus* virulence factor, in altering the Th balance in a murine infection model[150]. This study demonstrated a reduction in both Th1 and Th17 numbers in response to *S. aureus* strains expressing PSM, when compared to knockout strains[150]. Importantly, the PSM expressing strains induced an increase in abundance of Tregs[150], suggesting a potential role for cDC2 in the differentiation of T-cells in favour of infection. While PSM was able to alter the Th balance in this study[150], it is admittingly limited in only examining the USA300 laboratory strain of *S. aureus,* and further work should examine clinical isolates of bacteria.

In terms of DC pathogenesis, *S. aureus* is established to induce DC toxicity, with decreased numbers of murine splenic cDC1 and cDC2 during infection[150]. Recently, it has been shown that the toxicity of *S. aureus* leucocidins in monocyte derived DC are primarily induced through the action of pore forming leucocidin, leucocidin AB[151]. However, given the choice of monocyte derived DC for this research, these findings may not necessarily be reflective of primary DC subsets. Of note, *S. aureus* has also been shown to survive and replicate following internalisation by cDC *in vitro*[143]; however, this finding is limited by the use of bulk CD11c+ splenocytes, which contain a complex mixture of cDC,

macrophages and their precursors[5]. It is therefore clear, that further work is required to understand the nuances of *S. aureus* immunopathogenesis, especially so with regard to the distinct primary DC subsets.

1.3.3 Immune Evasion Mechanisms

Staphylococcus aureus enterotoxin induced T-cell activation

Staphylococcal enterotoxins (SEs) are a type of superantigen able to directly bind MHC-II and broadly stimulate both a large and diverse population of T-cells (an estimated 20-30% of the total pool)[152], subsequently inducing production of IL-1, IL-2, IL-6, TNF-α, IFN-γ, MCP-1 and MIP-1α[153,154]. To date there are at least 24 serologically distinct SEs described to date encompassing 12 SEs (SEA-E, SEG-J and SER-T), 11 SE-like toxins (SELs; SELK-Q, SELU, V, X and SELZ) and Toxic Shock Syndrome Toxin-1 (TSST-1)[152,155]. While these represent a diverse set of toxins from several phylogenetically distinct protein families, they have been shown to induce activation of extensive but overlapping and partially redundant human Vβ T-cell repertoires[156]. Recently, superantigen producing isolates of *S. aureus* have been identified in cattle suffering bovine mastitis, with these isolates demonstrating the capacity to stimulate the total bovine Vβ repertoire[155]. Given that a majority of MRSA strains are known to produce some form of superantigen, these results highlight the importance of superantigens in *S. aureus* pathogenesis not only in humans but indeed across the species barrier.

Paradoxically, the super antigenic capacity of SEs and SELs are inconsistent with the slow clinical progression of chronic antibiotic resistant MRSA infection[125,157]. Rather these super antigens are reported to result in fatalities due to related complications[125,157,158] rather than sepsis induced cytokine storms. These observations are potentially explained by the functional effects of SEs *in vivo,* whereby T-cell activation is thought to lead to either anergy or apoptosis[159]. Indeed, it has been shown that the hyperactivation of T-cells is transient in murine models, with injection of SEB leading to a reduction in expression of surface L-selectin[160], CD3 and TCR[161] within 1 hour of exposure. Moreover, the SEB induced activation of T-cells has been shown to be transient with a majority of activated T-cells being eliminated via activation induced apoptosis by 48 hour post exposure[162]. It therefore remains unclear as to the precise mechanisms by which SEs facilitate the pathogenesis of *S. aureus* infections, however it seems likely that the

modulation of the T-cell compartment involves active suppression of potentially MRSA specific T-cells *in vivo.*

Cell-wall immunomodulation through PRRs

Immunity to *S. aureus* has been linked to the induction of a Th1/Th17 response[163-165], and in the case of cutaneous infections, Th17 and γδ T cell clearance[166]. It has been reported that the staphylococcal cell wall contains TLR2 ligands within peptidoglycan that induce potent secretion of the immunosuppressive cytokine IL-10 by human PBMCs[167]. In this study IL-10 was seen to induce apoptosis of T-cells, thus impeding the T-cell response to *S. aureus*[167]. Moreover, Li and colleagues[168] have shown that the cell wall of *S. aureus* is able to further downregulate the production of the Th1 chemoattractant IP-10, independent of IL-10 activity[168]. In this work Li et. al., demonstrated a complete abrogation of IP-10 secretion by PBMCs responding to Staphylococcal Enterotoxin-E (SEE), in the presence of either heat inactivated *S. aureus* or peptidoglycan[168]. These findings provide a model of immune distraction linking the non-specific and pan-activation of T-cells by superantigens with an ablated recruitment of potentially pathogen-specific T-cells to the site of infection in the host.

Host antibody interference through Protein A

Protein A (SpA) is a virulence factor found on most clinical isolates of *S. aureus,* interfering with the humoral immune response[169,170]. SpA is a 45kDa secreted and membrane bound protein containing five immunoglobulin binding domains with affinity for the Fcγ region of IgG and the Fab region of IgM and IgG Variable Heavy Type 3 (V_H3) antibodies[169,171-173] – the largest subset of the V_H3 family[174]. The Fcγ binding activity of SpA has been demonstrated to protect *S. aureus* from opsonisation induced phagocytosis[170,175], while the V_H3 Fab binding activity induces super antigenicity via cross linking of V_H3 type B-cell receptors inducing B-cell activation[176].

SpA super antigenicity is estimated to facilitate the binding of up to 30% of the human B-cells during an immune response; compared to the binding capacity of a 'conventional antigen' typically binding 0.01% of the total B-cell pool[177-179]. It has therefore been proposed that SpA hampers the germinal centre response through a mechanism of immune distraction- whereby the non-specific activation and expansion of B-cells impedes the formation of a pathogen specific antibody response[169]. This hypothesis is supported by the observation that immunised mice producing SpA neutralising

antibodies are able to mount antibody responses against other staphylococcal antigens during infection[180].

1.3.4 Antibiotic Resistance

S. aureus has a well-documented history of rapidly acquiring resistance to antibiotics. Penicillin resistance was first documented in 1948, 2 years after its initial discovery[181], and methicillin resistance was reported two years after its introduction as a therapeutic for penicillin resistant *S. aureus*[182-184]. Rapid acquisition of resistance to novel antibiotics has proven a constant and significant hindrance in the treatment of *S. aureus* infections, with as little as a single nucleotide change in the 2.8 Mbp genome being sufficient to provide broad resistance to a wide range of antibiotics[185].

Today, treatment of MRSA infection often relies on the use of last-line antibiotics including linezolid, daptomycin and vancomycin[158]. These antibiotics represent the last line of antimicrobial defence with no other available antibiotics should treatment fail. Over recent years, resistance to these last-line antibiotics has been on the rise[186,187], representing a new era of complete antibiotic resistance. Importantly, cross-resistance to the last line antibiotic daptomycin has been observed in clinical isolates following vancomycin therapy- notably in the absence of daptomycin exposure[188-190]. With last line antibiotics currently failing and methicillin resistant *S. aureus* (MRSA) endemic in the hospital systems of most developed countries[133,191], MRSA represents a significant global health burden and threat to public health.

Mechanisms of resistance to daptomycin

S. aureus resistance to daptomycin is most closely associated with gain-of-function point mutations in the *mprF*[158,192,193], coding for multiple peptide resistance factor, a lysyl-phosphatidylglycerol (L-PG) synthetase[192]. This leads to an increased expression of cationic L-PG on the outer surface of the cell membrane, thereby increasing its overall positive charge of the membrane (figure 1.7)[192]. It has been postulated that these changes in membrane phospholipid composition electrostatically repel positively charged complexes of daptomycin and calcium[158,192]. However, mutations in *cardiolipin synthase 2* (*Cls2*) have also been associated with daptomycin resistance[158], and contrary to this hypothesis these mutations have recently been demonstrated to significantly increase the expression of anionic cardiolipin on the bacterial membrane[194]. Importantly, these changes have been demonstrated to impair both daptomycin penetration and disruption of the cell membrane (figure 1.7)[194]. It therefore seems likely that the mechanism of resistance is complex and multi-factorial, dependent on various factors including not only

electrostatic interactions, but also other established factors affecting the composition and thickness of both the bacterial cell membrane and wall[158,194] (figure 1.7). Moreover, the impacts of these changes on the sensing of bacterial isolate by the innate immune system currently remains unclear.

Interestingly, daptomycin resistant clinical isolates of *S. aureus h*ave been shown to be significantly less virulent than susceptible parent strains following daptomycin therapy and clinical failure[192]. Cameron and colleagues[192] demonstrated that these resistant clinical isolates are not only less virulent lending an increased rate of survival in murine challenge models, but that these strains also persist for longer *in vivo* than their daptomycin susceptible parent strains[192]. Given their development of complete resistance to available antibiotics, and their capacity to persist *in vivo* causing ongoing chronic infections, these strains are therefore of clinical significance.

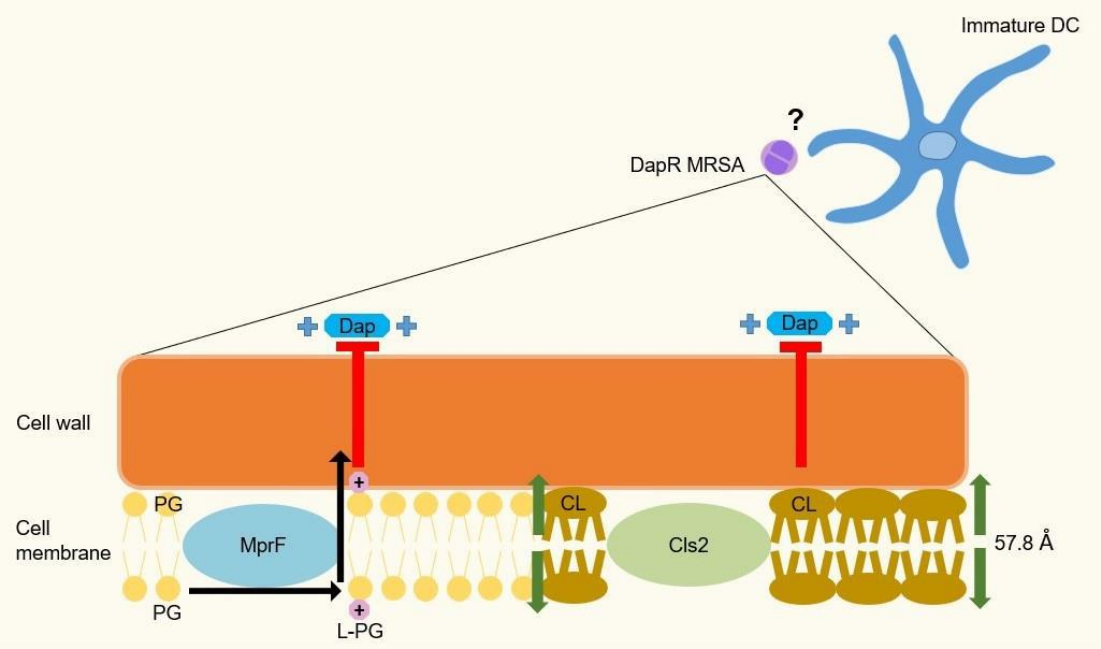

Figure 1.7 Proposed models for the disruption of daptomycin activity on the staphylococcal membrane. *Daptomycin (Dap) resistance frequently arises from mutations in phospholipid biosynthesis genes, mprF and cls2. MprF point mutations lead to enhanced synthesis of cationic L-PG from PG shuttling, which is then transported to the outer membrane[192]. Several previously described Cls2 point mutations increase cardiolipin (CL) content in the membrane, resulting in a thickened cell membrane. Cls2 point mutations reduce lipid extraction from MRSA cell membranes by Dap, preventing the membrane permeabilization activity of Daptomycin[24]. Image property of the O'Keeffe laboratory, provided courtesy of Sharifah Askary.*

Interplay between antibiotic resistance and innate immunity

With the mutations conferring antibiotic resistance being well characterised, growing evidence is emerging regarding a duality in function; whereby resistance mutations further modulate immune effector mechanisms. Perhaps most well characterised is that of the multi-peptide resistance factor (MprF), which is an evolutionarily conserved protein expressed by various bacterial species including *S. aureus*[195-197]. The MprF protein attenuates the negative charge of anionic phospholipids in the bacterial cell membrane[197], serving to protect bacteria from the action of several host antimicrobial peptides including defensins, kinocidins, cathelicidins and other cationic antimicrobial peptides[195 198,199]. As previously discussed, gain of function mutations in MprF are associated with reduced daptomycin susceptibility. Importantly, daptomycin resistant strains containing such point mutations have further demonstrated cross-resistance to three host cationic anti-microbial peptides[200]. While it remains unclear if these mutations are driven by host or antibiotic selective pressures (or some combination thereof); it is clear that antibiotic resistance mutations are able to simultaneously confer resistance to innate immune effectors.

Aside from directly interfering with innate effectors, *S. aureus* has the remarkable capacity to also accumulate antibiotic resistance mutations that simultaneously mask ligands of critical innate sensors. Indeed, it has been shown that specific mutations in the 23*S* rRNA of *S. aureus* confer resistance to macrolide, lincosamide and streptogramin group antibiotics, whilst ***simultaneously*** preventing detection through TLR13[71]. The notion that bacteria can change throughout the course of infection to evade innate immune detection is indeed novel, and these findings set an important precedent for further investigation.

Acquisition of resistance to the last line antibiotic daptomycin is associated with dramatic remodelling of the bacterial cell wall and membrane[158,194], and with the exception of the work presented in this thesis (some of which we have recently published[201]), there is no literature pertaining to how these alterations affect innate immune recognition of these isolates. This thesis therefore seeks to provide a novel perspective as to how changes occurring in the bacterial cell wall and membrane – occurring under both host and antibiotic selective pressures – modulate innate immune recognition. In doing so we will examine paired clinical isolates of daptomycin exposed MRSA, seeking to determine their

immunogenicity towards DC. This will address the hypothesis that the remodelling of the bacterial cell wall and membrane – occurring under both host immune and antibiotic selective pressures – impairs innate immune recognition of these isolates.

Specifically, this thesis will address how, these changes to the bacterial membrane and wall occurring with the acquisition of antibiotic resistance will modulate innate immune recognition by primary DC subsets, and evaluatethe impact on their subsequent activation. This thesis will therefore examine the role of pattern recognition receptors in recognising various staphylococcal isolates, seeking to validate the hypothesis that these changes – occurring at the bacterial cell surface throughout infection and antibiotic therapy – will impede detection by these innate sensors.

We contend that in the face of rising levels of broad antibiotic resistance, vaccines and immunotherapies should be considered as a new approach to overcome these infections. It is therefore critical to develop a deeper understanding of the immunopathogenesis of *S. aureus* infections, specifically as to how such infections persist in the absence of strong innate immune activation.

Chapter 2 – Materials and Methods

2.1 Lists of common lab reagents, buffers and media

All common laboratory buffers and media used for this research are described in table 2.1. A further comprehensive list of all laboratory reagents and suppliers are described in table 2.2.

Table 2.1 List of common buffers and media used for work with murine dendritic cells

Name of buffer or media (abbreviation)	**Composition**
Citric acid	0.1 M citric acid stock solution in MilliQ water, adjusted to pH 4.2
EDTA	Made up as a 0.1 or 0.5 M stock solution in MilliQ water and adjusted to mouse osmolarity (308 mOsmo) and physiological pH (pH = 7.2).
Roswell Park Memorial Institute 1640 medium with GlutaMAX™ (RPMI)	As provided by manufacturer (Gibco, ThermoFisher Scientific; Massachusetts, USA) For full recipe see Appendix E1
Murine RPMI/FBS (mu-RPMI)	RPMI 1640 medium with GlutaMAX™ (ThermoFisher Scientific), supplemented with 2% foetal bovine serum; Adjusted to 308 mOsmo/kg
Murine complete media (mu-CM)	Mu-RPMI as above, supplemented with 10% (v/v) foetal bovine serum, 33.6 mM HEPES, 14.3 µM β-mercaptoethanol, 10 U/ml penicillin and 10 µg/ml streptomycin; adjusted to 308 mOsmo/kg
Murine PBS (mu-PBS)	Phosphate buffered saline; pH 7.2 (Gibco, ThermoFisher Scientific), 2.67 mM potassium chloride (KCl), 1.47 mM potassium phosphate monobasic (KH_2PO_4), 137.93 mM sodium chloride (NaCl), 8.06 mM sodium phosphate dibasic (Na_2HPO_4-$7H_2O$) Adjusted to 308 mOsmo/kg
Murine PBS + 2% FBS (mu-PBS/FBS)	Mu-PBS as above, supplemented with 2% foetal bovine serum; Adjusted to 308 mOsmo/kg
Murine MACS buffer (mu-MACS)	Mu-PBS/FBS as above, supplemented with 2 mM EDTA; Adjusted to 308 mOsmo/kg

Table 2.2 List of common lab reagents

Reagent	Storage and Makeup	Supplier	Catalogue Number
2,2'-azinobis (3-ethylbenzothiazoline-6sulfonic acid) diammonium salt (ABTS)	Stored at RT as a lyophilised power. Made up at 50 X working concentration (27.4 mg/ml stock) in MilliQ water, and aliquots stored at -20°C.	Sigma Aldrich (Part of Merck) [New Jersey, USA]	A1888
Bovine serum albumin (BSA), heat shock fraction, pH 7; ≥ 98% pure	Stored at 4°C and a lyophilised powder. Reconstituted in appropriate buffer or medium as required.	Sigma Aldrich (Merck)	A7906
Collagenase, Type III	Stored with desiccant at -20°C as a lyophilised power. Made up to 7 X working concentration (7 mg/ml stock) in mu-RPMI, with grade II bovine pancreatic DNase as above, and aliquots stored at -20°C.	Worthington Chemical Company (New Jersey, USA)	LS004182
DNase, Grade II	Stored at 4°C as a lyophilised powder. Made up to 7 X working concentration (1 mg/ml stock) in murine RPMI (mu-RPMI), with type III collagenase as below, and aliquots stored at -20°C.	Roche diagnostics (Zug, Switzerland)	10104159001
Dulbecco's Phosphate Buffered Saline (PBS)	Stored at RT.	ThermoFisher Scientific	20012-027
Ethylenediaminetetraacetic-acetic acid (EDTA)	Made up as either a 0.1 or 0.5 M stock solution with MilliQ water, adjusted to murine osmolarity (308 mOsmo) and a physiological pH (pH of 7.2), and stored at room temperature.	Ajax Finchem (ThermoFisher Scientific) [Massachusetts, USA]	E5391
Eosin	Made up to working concertation at 0.5%	Sigma Aldrich (Merck)	E-4383

Reagent	Storage and Makeup	Supplier	Catalogue Number
	[$^{w}/_{v}$] in murine PBS (mu-PBS), and stored at 4°C.		
Foetal Bovine Serum (FBS), Gamma Irradiated, Australian Source	Stored at –80°C prior to use. Heat inactivated at 56°C for 30 minutes, and aliquots stored at -20°C.	In Vitro Technologies (Noble Park, Australia)	IVTA11582
4-(2-hydroxyethyl)-1-piperazineethanesulfonic acid (HEPES)	Stored in solution as provided at 4°C.	ThermoFisher Scientific	1563-080
Nycoprep 1.077 g/ml	Stored as provided at 4°C, supplemented with 2.5 mM EDTA (from 0.5 M stock) upon opening.	Axis-Shield	1114741
Penicillin-Streptomycin Liquid		Invitrogen (ThermoFisher Scientific)	15140-122
Propidium Iodide	Made as a 200 X stock solution at 100 µg/ml in murine (mu)-PBS, and stored at 4°C.	Calbiochem (Merck)	537 059
Phosphate buffered saline (PBS)	Stored at provided at 4°C, adjusted to 308 mOsmo/kg for murine tonicity	Gibco, Life Technologies (Thermofisher Scientific)	14190250
Red Blood Cell Lysing Buffer	Stored at RT.	Sigma Aldrich (Merck)	R7757
Roswell Park Memorial Institute Medium-1640 Glutamax (RPMI)	Stored at 4°C.	Gibco, Life Technologies (ThermoFisher Scientific)	61870
Sodium Chloride	Stored at RT.	Sigma Aldrich (Merck)	S7653
Tween-20	Stored at RT.	Sigma Aldrich (Part of Merck)	P7949

2.2 Ex vivo isolation of dendritic cells and culture systems

Dendritic cells exist in low abundance constituting less than 1% of peripheral organ cellularity, and representing approximately 0.01% of peripheral blood. Therefore, this research will rather focus on murine DC and cultures systems, utilising both DC and their precursors, obtained from primary and secondary lymphoid organs.

There are two major, and one minor, sources of DC used for this research. The is the culture of DC induced by Flt3-ligand (FL) from murine bone marrow precursors. These FLDC are heterogeneous, correlating neatly with the three functional subsets of the spleen. This culture system is well characterised and accepted in the literature[5,202].

As the spleen is the most DC enriched organ and contains resident sub-populations of all three functional DC subsets, primary splenic DC will be used as a model to characterise the activation processes of the DC. The use of *ex vivo* splenic DC serves to validate the integrity of the research findings in a model based on primary cells, however it is worth noting that the abundance of these cells is at least 10-fold lower than the FLDC on a per mouse basis.

Finally, the murine tumour (mutu) DC line recapitulating cDC1 are used for a single experiment, outlined in figure 6.13. This experiment was performed by Nazneen Jahan, a PhD student in our laboratory whom has kindly provided the pilot data for inclusion in this thesis.

2.2.1 Animal strains and housing

All strains of mice used for the current research were housed at the Monash Research Animal Platform (MARP) animal facility. Wild-type C57BL/6J mice were obtained under ethics number MARP/2016/027. All mice used for experiments were culled between 6-12 weeks of age.

MyD88 knockout (*MyD88*$^{-/-}$), TLR9 knockout (TLR9$^{-/-}$) and cGAS knockout (cGAS-$^{/-}$) mice were of C57BL/6J background, and organs from these mice were obtained from the laboratories of Profs Mikael Martino, Irina Caminschi and Nicole La Gruta respectively). Organs were scavenged from mice used for other purposes contributing to the principles of Reduction, Replacement and Refinement in the Australian code for the care and use of animals for scientific purposes (8th Edition, 2013).

MyD88$^{-/-}$ mice

MyD88$^{-/-}$ mice were generated as previously described[203]. MyD88$^{-/-}$ mice were backcrossed onto a C57BL/6 background at least eight times and maintained at the Monash Animal Research Platform by Prof Martino, as previously described[204].

Tlr9$^{-/-}$ mice

TLR9$^{-/-}$ mice were generated on a C57BL6 background as previously described[205]. TLR9$^{-/-}$ mice were maintained at the Monash Animal Research Platform by Assoc Prof Caminschi, as previously described[74]. Homozygote wild-type littermate controls, bred from heterozygotes, were used for all experiments with these mice.

cGAS$^{-/-}$ mice

cGAS$^{-/-}$ mice were generated as previously described[206]. cGAS$^{-/-}$ mice were maintained at the Monash Animal Research Platform by Prof La Gruta, and homozygote wild-type littermate controls, bred from heterozygotes, were used for all experiments with these mice.

2.2.2 Culture of Flt3-L induced dendritic cells from murine bone marrow

FLDC were cultured from murine bone marrow (BM) as previously described by *Naik* et. al.[202]. Briefly, to isolate BM, a small incision was made in the lower abdomen with surgical scissors, and the skin gently removed from the waist down. The hind legs were completely removed from the carcass, carefully trimming the flesh and dislocating at the hip with the blade of the scissors. The heads of both the femur and tibia were removed and bone marrow flushed with mu-RPMI using a 23-gauge needle until the bones appeared a clear whitish colour.

Cells were resuspended in mu-RPMI and pelleted at 400 *g* for 7 minutes at 4°C and the supernatant completely aspirated, resuspended in 1 ml of red cell lysis buffer and gently agitated for 1 minute. The marrow was washed twice in 50 ml of murine RPMI as described above, and ran through a 70 µm cell strainer. Strained cells were incubated for 8 days at 37°C and 10% CO_2, at a density of 1.5 X 10^6 cells per ml in mu-CM supplemented with FL (BioXCell; West Lebanon, USA) at 100 ng/ml to induce DC differentiation.

2.2.3 Isolation of splenic dendritic cells

Primary murine DC were isolated from the spleen as previously described[207,208]. In brief, murine spleens were removed from the carcass and minced into a fine paste for 5-10 minutes with surgical scissors, adding 1-2 drops of murine RPMI as necessary to prevent the preparation from drying out.

Minced cell suspensions were digested with gentle mixing for 30 minutes at room temperature in mu-RPMI supplemented with DNase and collagenase mixture (grade II bovine pancreatic DNase at 143 µg/ml and collagenase type III at 1 mg/ml). The digest was rinsed through a 70 µm cell strainer and washed twice in mu-RPMI at 700 *g* and 4°C for 7 minutes. Splenocytes were resuspended in 5 ml of cold Nycoprep per 4 spleens, and gently layered above 5 ml of cold Nycoprep. Density gradients were topped with 1 ml of FBS, and given a brief single swirl with a transfer pipette to gently disturb the interface of each layer. Gradients were spun for 15 minutes at 1850 *g*, 4°C with minimum acceleration and brake.

The top 5mls corresponding to the splenic light density fraction was aspirated with a transfer pipette, washed twice in mu-MACS at 700 *g* for 7 minutes at 4°C. The fraction was resuspended in 10 µl of antibody depletion cocktail (table 2.3) per million cells and incubated on ice for 30 minutes. Cells were washed once as described above and incubated on a roller for 20 minutes at 4˚C with goat anti-rat Ig magnetic beads (Qiagen; Hilden, Germany). Beads were prepared to a concentration of 8 beads per cell and washed on a magnet, at least three times with mu-RPMI, in order to fully remove the preservatives.

The bead-cell suspension was brought up in 1 ml per spleen (minimum and maximal volume 3 and 7 ml respectively) and placed in a magnetic field for 2-3 minutes allowing beads to attach. The supernatant containing DC aspirated, placing in front of a magnet and repeating above to increase purity. Purified DC were washed twice as described above in the buffer or medium required for their intended use.

Table 2.3 Antibody depletion cocktail for purification of splenic dendritic cells

Target	Clone	Host
CD3	KT3-1.1	Rat
Thy-1	T24/31.7	Rat
Gr-1	RB68C5	Rat
CD19	ID3	Rat
Erythrocyte	TER119	Rat

2.2.4 Culture of mutuDC

MutuDC (line 2114; passage number 28) were provided courtesy of Dr Brodnicki at St. Vincent's Hospital Melbourne. MutuDC were cultured as previously described[209]. Briefly, mutuDC were seeded at 1.5 X 10^5 cells per mL, in 10 mL of Iscove's Modified Dulbecco's Medium (IMDM; ThermoFisher Scientific), supplemented with 10% ($^v/_v$) FBS, 100 µM 2-mercaptoethanol, 10 units/mL penicillin and 10 µg/mL streptomycin, adjusted to 308 mOsmo/L. MutuDC were incubated at 37°C with 10% CO_2 in humidified conditions until 80-90% confluent, and either reseeded at 1.5 X 10^5 cells per mL as described above. Passaging of mutuDC, and all experimental methods pertaining to mutuDC, including the analysis of the data presented in figure 6.13, were carried out by Nazneen Jahan.

2.3 Stimulation of dendritic cells with *Staphylococcus aureus*

2.3.1 Bacterial strains used to stimulate dendritic cells

This research utilised primary and lab strains of *S.* aureus, including both methicillin sensitive and resistant strains of bacteria (MSSA and MRSA respectively). Primary isolates of MRSA correspond to paired clinical isolates obtained from patients prior to the initiation of therapy with last line antibiotics daptomycin and vancomycin, and after the acquisition of resistance to the treatment (table 2.4 and 2.5). Lab modified strains included daptomycin susceptible clinical isolates mutated to carry daptomycin resistance point mutations occurring in the resistant daughter strain (table 2.6). Primary isolates of MSSA corresponded to two distinct clinical isolates, included as a reference antibiotic susceptible *S. aureus* (table 2.7). All the bacterial strains mentioned above were kindly provided courtesy of Anton Peleg at Monash University.

2.3.2 Culture of bacterial strains

Bacterial strains were grown in Brain Heart Infusion (BHI) broth overnight and the bacterial density was adjusted to 4 x 10^9 CFU/ml. The required bacterial density was estimated by an optical density of 600nm (OD_{600}) equal to 8. The bacterial cell suspension was serially diluted and plated on BHI agar to confirm the desired bacterial cell density was achieved. All work relating to bacterial culture and density estimation were performed by Jhih-Hang Jiang or Xenia Kostoulias in the laboratory of Anton Peleg at Monash University.

2.3.3 Heat inactivation of bacterial strains

In instances where heat inactivation was required prior to stimulation of DC, bacteria were treated on a heat block for a minimum of 30 minutes at 95°C.

2.3.4 Bacterial stimulation of dendritic cells

Unless otherwise indicated, the standard conditions for the stimulation of DC with bacteria were as follows. DC preparations and cultures were stimulated in complete media at a final concentration of 1 X 10^6 cells per ml in 96-well U-bottom plates (bulk DC cultures and preparations), and 0.5 X 10^6 cells per ml in 96-well V-bottom plates (FACS sorted DC cultures and preparations). DC were stimulated with live bacteria at a

multiplicity of infection (MOI) of 10, for 18 hours, in a humidified incubator at 37°C with 10% CO_2. For stimulation of DC with heat inactivated bacteria, a dosage equivalent to an MOI of 10 prior to heat inactivation was used. For the stimulation of DC with reconstituted commercial strains of bacteria (table 2.7), the equivalent MOI was derived from the provided count of 'cells per ml' enumerated by *Invivogen* using proprietary methods not disclosed by the manufacturer.

2.3.4 STING inhibition of mutuDC with H-151

Four parts of STING inhibitor H-151 (Invivogen), a synthetic indole derivative, was mixed gently with LyoVec™ transfection reagent (Invivogen), at RT, and left overnight at 4°C to equilibrate. 1 X 10^6 mutuDC were incubated with H-151 (500 ng/ml) in LyoVec™ (10% [$^v/_v$] final concentration) for 1 hour at 37°C with 10% CO_2. Cells were than stimulated as required per the protocols above. The experiments relating to H-151 inhibition of mutuDC presented in figure 6.13, as well as all associated titration of the H-151 inhibitor on these cells, were performed by Nazneen Jahan.

Table 2.4 Clinical and genomic characteristics of daptomycin exposed MRSA isolates

Adapted from Patton et. al., (2019)[201]

Strain	Clinical diagnosis	Dp MIC ug/ml[a]	Genomic Mutations[b]	Mutated genes affecting cell wall or membrane	Ref
A8796	Bacteraemia	0.5	2	*mprF* *citz*	Peleg *et. al* (2012)[158]
A8799	Vertebral osteomyelitis	2			
A9719	Bacteraemia	0.25	6	*mprF* *cls2* *atl*	Peleg *et. al* (2012)[158]
A9744	Endocarditis	2			
A9754	Bacteraemia	0.5	9	*mprF*	Peleg *et. al* (2012)[158]
A9757	Endocarditis	4			
A9763	Bacteraemia	0.25	3	*mprF* *cls2*	Peleg *et. al* (2012)[158]
A9764	Osteomyelitis, Prosthetic joint infection	4			
A8819	Bacteraemia	0.25	5	*mprF* *cls2*	Peleg *et. al* (2012)[158]
A8817	Osteomyelitis, septic arthritis	2			

[a] Daptomycin resistance is defined as a minimum inhibitory concentration (MIC) > 1 μg/ml

[b] Total number of point mutations observed in the clinical daptomycin resistant daughter isolate with reference to the susceptible parent strain

Table 2.5 Clinical and genomic characteristics of vancomycin exposed MRSA isolates

Strain	Clinical diagnosis	Vn MIC ug/ml[a]	Genomic Mutations[a]	Mutated genes affecting cell wall or membrane[b]	Ref
A8090 (JH1)	Endocarditis	1	33 - 35	*nagB* *agrC* yych *prsa* SA1249 & SA1702	Mwangi *et. al.,* (2007)[210]
A8094 (JH9)	Bacteraemia	8			

[a] Total number of point mutations observed in the clinical vancomycin intermediate daughter isolate with reference to the susceptible parent strain

[b] Genes listed with a known or putative function affecting cell wall or membrane structure. Genetic mutations described in full in the supporting information of Mwangi *et. al.,* (2007)[210]

Table 2.6 Genomic characteristics of clinically derived mutant lab strains of MRSA

Strain	Dp MIC ug/ml[a]	Mutated genes affecting cell wall or membrane	Strain of origin for genomic mutation	Ref
$A8819_{Cls2\text{-}T33N}$	2	*cls2*	A8817	Jiang *et. al.,* (2019)[194]
$A8819_{Cls2\text{-}T33NN33T}$	0.5	*cls2*	A8819	Jiang *et. al.,* (2019)[194]
$A8819_{MprF\text{-}T345I}$	2	*mprF*	A8817	Patton *et. al.,* (2019)[201]
$A8819_{Cls2\text{-}L52F}$	1	*cls2*	A9764	Jiang *et. al.,* (2019)[194]

[a] Daptomycin resistance is defined as a minimum inhibitory concentration (MIC) > 1 μg/ml

Table 2.7 Commercially available heat inactivated bacterial species used to model DC activation in this thesis

Binomial name (genus and species)	**Manufacturer**	**Catalogue number**
Listeria monocytogenes	Invivogen	tlrl-hklm
Streptococcus pneumoniae	Invivogen	tlrl-hksp
Lactobacillus rhamnosus	Invivogen	tlrl-hklr
Staphylococcus aureus	Invivogen	tlrl-hksa
Staphylococcus epidermis	Invivogen	tlrl-hkse
Escherichia coli Strain 0111:B4	Invivogen	tlrl-hkeb
Helicobacter pylori	Invivogen	tlrl-hkhp

2.4 Functional quantitation of dendritic cell activation and maturation

2.4.1. General staining protocol for flow cytometry

Cells were harvested by pelleting at 400 *g* for 7 minutes at 4°C and washed in murine MACS buffer (PBS supplemented with 2% foetal bovine serum, 2 mM EDTA; adjusted to 308 mOsmo/kg). Samples were incubated for 10 minutes with Fc block (α-CD16/32, clone 2.4G2; 40 μg/ml) in murine MACS buffer (15 μl per 10^6 cells), and subsequently incubated in the applicable antibody or antibody cocktail (15 μl per 10^6 cells) for 30 mins on ice (achieving 1X concentration for all antibodies and Fc block). Where applicable, cells were washed as above and stained for 20 minutes on ice with a secondary streptavidin conjugate. Samples were washed as described above, resuspending in at least 50 μl of murine MACS buffer with PI (1:200) for flow analysis. Samples were acquired on the BD Fortessa using FACSDiva software.

2.4.2 General staining protocol for cell sorting

Cells for sorting were washed in murine MACS buffer, pelleting at 400 *g* for 7 minutes at 4°C. Staining was performed for 30 minutes at 4°C, using the relevant antibody cocktail (10 μl per million cells). Where applicable, cells were washed as above and stained for 20 minutes on ice with a secondary streptavidin conjugate. Cells were then washed 3 times as described above, and sorted by technical staff at Monash FlowCore on a BD Influx cell sorter. Re-analysis was performed after each sort to confirm purity of each DC subset. Appropriate single stains and unstained controls were included for all sorts.

2.4.3 Antibody panels for surface phenotyping and FACS sorting

For population analysis and/or FACS sorting, antibody panels were designed with multiple colour options for staining and separating both FLDC and primary splenic DC (table 2.8 and 2.9 respectively). All antibodies used for FACS were routinely titrated for optimal saturation and staining of activated DC, thus accounting for batch to batch variation. Where required, a secondary streptavidin conjugated fluorophore was selected from one of several colour options (table 2.10). The availability of multiple fluorophore options provided the flexibility for co-staining unsorted DC for analysis, or re-staining FACS sorted DC with sub-panels for the analysis of classical DC activation markers (table 2.11), checkpoint inhibitors (table 2.12), other markers associated with DC activation

(table 2.13) and relevant isotype controls (as described in appendix B). All antibody cocktails were diluted in muMACS buffer to the appropriate concentration.

Table 2.8 Antibody panel for FACS sorting and population analysis of murine FLDC

Antibody Target	Clone	Conjugate[a]	Manufacturer (catalogue number)	Dilution factor[c]
CD24	M1/69	eFluor605 NC	BioLegend (93-0242)	1 : 100
		BV711	BD (564 450)	1 : 300
		APC/Fire 750	BioLegend (101 840)	1 :100
CD11c	N418	BV421	BioLegend (117 330)	1 : 100
		PE-Cy7	TONBO (60-0114-U100)	1 : 1,000
	HL3	FITC	BD (553 801)	1 : 200
CD45R[b]	RA3-6B2	PE-Cy7	BioLegend (103 222)	1 : 400
		APC	BioLegend (103 212)	1 : 400
		APC-Cy7	BioLegend (103 224)	1 : 100
CD45RA[b]	14.8	Biotin	n/a	1 : 100
CD172α (SIRPα)	P84	BUV395	BD (740 282)	1 : 50
		PE	BD (560 107)	1 : 200
		APC	eBioscience (17-1721-82)	1 : 50

[a] One conjugate per marker was selected for each experiment, in order to reduce spectral overlap based on other staining panels to be used in combination with, or subsequent to this panel

[b] Either of CD45R or CD45RA was selected as required for each experiment to minimise spectral overlap based on other staining panels

[c] Dilutions predetermined in titration of primary DC to give opt saturation

Table 2.9 Antibody panel for FACS sorting and population analysis of murine splenic DC

Antibody Target	Clone	Conjugate[a]	Manufacturer (catalogue number)	Dilution
CD8α	53-6.7	BV650	BioLegend (100 741)	1 : 400
CD11c	N418	BV421	BioLegend (117 330)	1 : 100
		PE-Cy7	TONBO (60-0114-U100)	1 : 1,000
CD317	120G.8	Biotin	n/a	1 : 500
CD172α (SIRPα)	P84	BUV395	BD (740 282)	1 : 50
		PE	BD (560 107)	1 : 200
		APC	eBioscience (17-1721-82)	1 : 50
CD3[b]	17A2	AlexaFluor 488	BioLegend (100 210)	1 : 400
CD49b[b]	FITC	FITC	BD (553 57)	1 : 100
CD161c[b]	PK136	FITC	BioLegend (108 733)	1 : 400

[a] One conjugate per marker was selected for each experiment, in order to reduce spectral overlap based on other staining panels to be used in combination with, or subsequent to this panel

[b] CD3, CD49b and CD161c are all used as either FITC/AlexaFluor488 conjugates for the purpose creating a junk gate

Table 2.10 Streptavidin conjugated fluorophores for secondary stains

Fluorochrome	Manufacturer (catalogue number)	Dilution
BUV395	BD (564 176)	1 : 400
FITC	Invitrogen (S11223)	1 : 2,000
BV785	BioLegend (405 249)	1 : 200
APC/FIRE 750	BioLegend (405 250)	1 : 200

Table 2.11 List of antibodies against murine DC activation markers for phenotyping

Antibody Target	Clone	Conjugate[a]	Manufacturer (catalogue #)	Dilution
CD40	3/23	FITC	BD (553 790)	1 : 100
		APC	BD (558 695)	1 : 100
CD69	H1.2F3	FITC	BD (553 236)	1 : 100
		PE	BioLegend (104 508)	1 : 100
CD80	16-10A1	PE	BD (553 769)	1 : 100
	1G10	APC	Molecular Probes (A14 724)	1 : 100
CD86	GL1	PE-Cy7	BioLegend (105 014)	1 : 1,500
		AlexaFluor700	BD (560 581)	1 : 500
		APC	BD (558 703)	1 : 1,000
H-2K (MHC-I)	M1/42	PE	BioLegend (125 506)	1 : 500
I-A b, d, q / I-E (MHC-II)	M5/114.15.2	V500	BD (562 366)	1 : 100 **(2 : 1)**[b]
		PE-Cy7	BioLegend (107 630)	1 : 300 **(1 : 17.5)**[b]
		APC-Cy7	BioLegend (107 628)	1 : 500 **(1 : 2.5)**[b]

[a] Due to the available fluorophore conjugates these markers we routinely split over two stain panels, and/or combined with markers from other staining panels (tables 2.12 and 2.13).

[b] Due to the high expression of MHC-II and bright staining of these fluorophores, antibody stocks were spiked with unlabelled MHC-II (M5/114.15.2) in order to keep staining from going off-scale. Ratio's indicate labelled:unlabelled antibody.

Table 2.12 List of antibodies against murine checkpoint inhibitors for DC phenotyping

Antibody Target	Clone	Conjugate[a]	Manufacturer	Dilution
PD-1 (CD279)	29F.1A12	BV421	BioLegend (135 217)	1 : 100
	RMPI-30	PE-Cy7	BioLegend (109 110)	1 : 100
PD-L1 (CD274)	10F.9G2	BV605	BioLegend (124 321)	1 : 25
		APC	BioLegend (124 312)	1 : 50
PD-L2 (CD273)	TY25	APC	BD (560 086)	1:200
GITR (CD357)	DTA-1	BV421	BD (563 391)	1 : 400
		PE-Cy7	e Bioscience (28-5874)	1 : 3,000
CTLA-4 (CD152)	UC10-4B9	BV421	BioLegend (106 312)	1 : 25
		APC	BioLegend (106 310)	1 : 25

[a] Due to the available fluorophore conjugates these markers we routinely split over two stain panels, and/or combined with markers from other staining panels (tables 2.11 and 2.13).

Table 2.13 List of antibodies against murine surface markers associated with DC activation

Antibody Target	Clone	Conjugate[a]	Manufacturer	Dilution
CD25 (IL-2Rα)	PC61	AlexaFluor488	BioLegend (102 017)	1 : 200
CD62-L (L-selectin)	MEL-14	BV570	BioLegend (104 433)	1 : 200
		FITC	BD (553 150)	1 : 1,000
CD197	4B12	PE-Cy7	BioLegend (120 123)	1 : 50
CD199	eBioCW-1.2	PE	eBioscience (12-1991-82)	1 : 100

[a] Due to the available fluorophore conjugates these markers we routinely split over two stain panels

2.4.4 Bead assays for detection of cytokine and chemokines from culture supernatant

A custom LEGENDplex kit (BioLegend) was used to quantify secretion of cytokine panels (table 2.14) in fresh or freeze-thawed murine DC culture supernatants, per the manufacturer's instructions. This panel was selected based from cytokines secreted by DC following MRSA stimuli during preliminary screens of the available murine inflammation and murine inflammatory chemokine panels. Supernatants were diluted as required for accurate quantitation in the linear range of the standard curve for each cytokine. Samples were acquired for each bead panel on a BD Fortessa X20 flow cytometer with FACS Diva software, then standard curves fitted and samples interpolated using LEGENDplex software version 7.0.

2.4.5 ELISA assays for detection of cytokine and chemokine from culture supernatant

Capture sandwich ELISA was also used to quantify secretion of cytokine sub-panels as required, based on the results of the broader custom cytokine multiplex bead array. Paired antibodies and standards were obtained from various suppliers and the concentrations of each antibody were optimised for detection with Amdex™ streptavidin-horse radish peroxidase conjugate (SA-HRP, Merck) at 1:8,000 (table 2.15).

General ELISA protocol

Plates were coated with capture antibody in PBS for 2 hours at room temperature, or overnight at 4˚C. Plates were washed 5 times in PBS-Tween (0.05% [$^{v}/_{v}$] Tween) and incubated with either sample supernatants or standards in mu-CM overnight at 4˚C. Plates were washed as above and blocked with detection antibody in PBS-BSA (1% [$^{w}/_{v}$) BSA) for 1-3 hours at room temperature. Plates were washed 5 times and probed with streptavidin-HRP (provider and dilution) for 1-2 hours at room temperature**.** Plates were washed 5 times and detected with substrate solution (548 µg/ml ABTS; and 0.03% [$^{v}/_{v}$] H_2O_2 in 0.1 M citric acid) for 5-30 minutes at room temperature. Optical density was measured at 405 nm with path-length correction at 490 nm, using a Versa Max microtitre plate reader and SoftMax Pro version 6.4.2**.** Standard curves were fitted and samples interpolated using an asymmetric sigmoidal 5-paramter logistic regression on Graph Pad Prism version 6.07.

Table 2.14 List of cytokines and chemokines quantified in murine DC culture supernatants using the BioLegend custom 11-plex

Cytokine	Alternate Names	Manufacturer	Kit
IFN-β		BioLegend	Custom cytokine and chemokine panel
IFN-γ			
IL-6			
IL-10			
IL-12p70			
TNF-α			
MIP-1α	CCL3		
MIP-1β	CCL4		
RANTES	CCL5		
MDC	CCL22		
IP-10	CXCL10		

Table 2.15 List of cytokines and chemokines and the optimised concentrations of paired antibodies used for detection of cytokines and chemokines in tissue culture supernatants by ELISA

Cytokine (Alternate Names)	**Clone, kit name or Cat. #[a]**	**Manufacturer**	**Primary Antibody (µg/ml)**	**Secondary Antibody (µg/ml)**
IFN-λ2/3 (IL-28a, IL-28b)	1' (MAB17892) 2' (MAB17891)	R&D Biosystems	1	0.25
IFN-α	LumiKine™ mIFN-α kit (Cat # lumi-mifna)	Invivogen	1	0.03
IL-6	1' (MP5-20F3) 2' (MP5-32C11)	BD	1	0.25
MDC	1' (Cat # 500-P176) 2' (Cat # 500-P176BT)	Peprotech	0.25	0.25
MIP-1α (CCL22)	1' (Cat # 500-P121) 2' (Cat # 500-P121BT)	Peprotech	0.25	1
MIP-1β (CCL3)	1' (Cat # 500-P213) 2' (Cat # 500-P213BT)	Peprotech	0.25	1
TNF-α	1' (Cat # 500-P64) 2' (Cat # 500-P64BT)	Peprotech	1	0.5

[a] Catalogue numbers and kit names (where applicable) are listed for polyclonal (pAb) antibody products, and where clones are not provided with the commercial products

2.5 Hamster polyclonal non-specific binding experiments

2.5.1 Titration of hamster IgG for blocking in flow cytometry

Mature murine FLDC (outlined in section 2.2.1) stimulated for 18 hours with daptomycin exposed MRSA paired clinical isolates (outlined in section 2.3), were stained for flow cytometry using a deviation of the standard staining protocol (section 2.4.1). In place of Fc block, this modified protocol instead blocked DC for 10 minutes at on ice with a commercial preparation of healthy Syrian hamster IgG (Alpha Diagnostics; Texas, USA). This preparation was provided as ammonium sulphate, sephadex and DEAE-ion exchange chromatography purified IgG sample, and used to block at a final concentration ranging from 500 – 1 µg/ml. All subsequent staining steps were as per the standard protocol.

2.5.2 SDS-PAGE

Samples of cells and MRSA were pelleted for 7 minutes at 700 and 7,000 *g* respectively, then resuspended and heated at 95°C in Lameli's buffer (ThermoFisher Scientific) for 5 minutes. Where samples were to be prepared under reducing conditions dithiothreitol (DDT; ThermoFisher Scientific) was included at a final concentration of 0.1 M. Samples were loaded into 4-15% Mini-PROTEAN TGX precast protein gels (Bio-Rad Laboratories Pty., Ltd.; California, USA), alongside Precision Plus Dual Xtra Protein Standards™ (Bio-Rad Laboratories Pty., Ltd.) as molecular weight markers. Where Western Immunoblotting was to follow, these markers were spiked at a ratio of 1:9 with streptactin conjugated Precision Plus Protein Western C Standards™ (Bio-Rad Laboratories Pty., Ltd.). SDS-PAGE was ran in Tris-Glycine running buffer (Bio-Rad Laboratories Pty., Ltd.) at 50 V for 2 hours, or as required for optimal band resolution. Gels were immediately rinsed in sterile MilliQ water, and equilibrated in western transfer buffer while assembling blotting sandwich.

2.5.3 Western Immunoblotting

Standard Protocol for Western Immunoblotting

Immobilon-P polyvinylidene fluoride (PVDF) membranes (Merck) were wetted in 100% ($^{v}/_{v}$) methanol for 15 seconds and equilibrated in transfer buffer. Proteins were transferred from SDS-PAGE gels to PVDF membranes with Tris-CAPS transfer buffer (Bio-

Rad Laboratories Pty., Ltd.) in a sandwich blot at 100 V for 3 hours at 4°C. Following visual confirmation of protein transfer, PVDF membranes were blocked overnight in rolling tubes with 10% ($^{w}/_{v}$) BSA in PBS. Membranes were washed 5 times in western buffer (TBS with BSA 1% ($^{w}/_{v}$); and Tween-20 0.05% [$^{w}/_{v}$]). Membranes were probed with primary antibody in western buffer for 2 hours at room temperature, in rolling tubes, and washed as above. Where applicable membranes were stained with a secondary HRP conjugated antibody and Precision Protein StrepTactin-HRP (Bio-Rad Laboratories Pty., Ltd.; 1:10,000), with gentle agitation and washed as above. Membranes were developed with SuperSignal Pico™ (ThermoFisher Scientific) per manufactures instructions, and imaged using a ChemiDoc Touch Imaging System (Bio-Rad Laboratories Pty., Ltd.).

Antibody pairs for western immunoblotting

Antibody pairs for western blot were optimised for the detection of the protein non-specifically bound by hamster α-murine CD69 (table 2.16).

Table 2.16 Antibody pairs used for the detection of S. aureus Protein A, and other antibody binding factors

	Species	Specificity	Manufacturer (Clone)	Conjugate	Dilution factor (concentration)
Primary antibody	Hamster	CD69	BioLegend (H12.F3)	None	1 : 3,000 (0.33 μg/ml)
Secondary antibody	Goat	Hamster Ig	Jackson ImmunoResearch (Polyclonal)	Horse Radish Peroxidase	1 : 100,000 (16 ng/ml)
Primary antibody	Hamster	CD69	(H1.2F3)	Biotin	1 : 2,000 (0.25 μg/ml)
Streptavidin	N/A	Biotin	N/A	Horse Radish Peroxidase	1 : 5,000

2.6 Analysis of DC phagocytosis of *S. aureus*

2.6.1 Preparation of GFP bacteria for live cell imaging and flow cytometry

Clinical bacterial isolates (table 2.4) and single nucleotide point mutant lab strains (table and 2.6) were previously modified to express anhydrotetracycline (Atc) inducible recombinant enhanced green fluorescent protein (GFP) under the xyl/tetO promoter[211], and provided courtesy of Anton Peleg. Bacteria were cultured as described in section 2.2.2, inducing GFP expression in the presence of 1 μg/ml Atc (Sigma) for 5 hours prior to enumeration. DC were stimulated with these GFP recombinant strains as indicated, with the addition of Atc to the culture medium at a concentration of 1 μg/ml, as previously described[194].

2.6.2 Live cell imaging of *S. aureus* stimulated DC

Labelling of DC cytoplasm for live cell imaging

Samples of DC for live cell imaging were washed twice in 10 mL in muPBS, to remove protein from suspension. Briefly, samples were centrifuged at 700 *g,* for 7 minutes at 4°C, and the supernatant completely aspirated following each wash. DC were then resuspended in Cell Trace Orange (ThermoFisher Scientific) diluted 1:1,000 with muPBS, staining for 30 minutes at 37°C in a volume of 10 μL per 1 X 10^6 cells. DC were immediately resuspended into muCM supplemented with 300 nM Draq7 viability dye (BioLegend), and prepared for imaging.

Live cell imaging of *S. aureus* stimulated DC

Live samples of DC stimulated with MRSA were imaged using a Leica LX Inverted microscope, whilst maintained in a humidified chamber at 37°C with 10% CO_2. Images were acquired with LAS software, using find and focus to track cell vertical displacement in the media, and acquisition of z-stacks to quantify the maximum projection. Samples were maintained in the chamber for up to 12 hours post stimuli during live cell analysis.

2.6.3 Flow cytometric quantitation of MRSA uptake

Preparation of fluorescently labelled bacterial isolates

Clinical bacterial isolates (table 2.4) and single nucleotide point mutant lab strains (table and 2.6) expressing recombinant enhanced green fluorescent protein (GFP) were provided courtesy of Anton Peleg. Where indicated, both GFP recombinants and their respective wild-type parental strains, were stained with the pH sensitive and amine reactive dye, pHrodo™ Red succinimidyl ester (Life Technologies, Company of ThermoFisher Scientific), per manufacturer's instructions. All work relating to bacterial culture, bacterial density enumeration and pHrodo labelling was carried out by Jhih-Hang Jiang, as described previously (section 2.2.2) and above.

Stimulation of DC with labelled MRSA for quantitation of uptake

Bulk DC were stained with population markers (table 2.8), as described in section 2.4.1. DC were resuspended in muCM at a density of 2 X 10^6 cells per mL. For time course assays investigating very early time points (less than 1 hour) DC were pre-incubated for 90 minutes at 37°C, 10% ($^v/_v$) CO_2. Bacterial stimuli were resuspended to a density of 2 X 10^7 cfu per mL in pre-warmed muCM, and added to achieve a 1:1 final volume of bacteria to DC (MOI = 10). At indicated time points DC were resuspended in ice cold muMACS buffer and immediately ran on the BD LSR Fortessa flow cytometer using BD FACS Diva software (BD).

2.6.4 Cryo Transmission Electron Microscopy (TEM) of DC and *S. aureus*

All sample preparation from fixation through to sectioning of embedded samples for imaging, was kindly performed by Viola Oorschot with assistance from Joan Clarke. This assistance was provided through the Monash Ramaciotti Centre for Cryo EM under the supervision of Georg Ramm.

Normal preparation of samples for cryo EM

Samples were prepared in eppendorf tubes and fixed for 2 hours at room temperature, or overnight at 4°C in fixative (2% [$^v/_v$] glutaraldehyde in 0.1M sodium cacodylate buffer). Samples were washed in 0.1 M sodium cacodylate buffer, and post-fixed for 30 minutes in the dark at room temperature in post-fixation buffer (1% [$^w/_v$] OsO4, 1.5%

[$^{w}/_{v}$] K3Fe(III)(CN)6 in 65 mM cacodylate buffer). Cells were embedded in 4% ($^{w}/_{v}$) low melting point agarose for support. Dehydration was performed with ethanol and propylene oxide. Blocks of cells in agarose were embedded in Epon 812. Ultrathin sections of 70 nm were cut using a diamond knife (Ultra 45˚ Diatome) on a Leica Ultracut UCT7, placed on 50 mesh copper grids with carbon coated formvar support film and stained with uranyl acetate and Waltons lead citrate.

Preparation of ruthenium red stained samples for cryo EM

Samples were prepared as above, fixing instead with ruthenium red fixative (500 µg/ml ruthenium red, 1.2% [$^{v}/_{v}$] glutaraldehyde in 67 mM cacodylate buffer), and post-fixing in ruthenium red post-fixative (500 µg/ml ruthenium red, 0.67% [$^{w}/_{v}$] OsO4, in 67 mM cacodylate buffer).

High resolution cryo EM

High resolution EM imaging was performed on a Jeol1400Flash TEM at 80 KeV. All electron microscopy imaging was completed at the Ramaciotti Centre for Cryo Electron Microscopy (Monash University, Melbourne).

Analysis of MRSA internalisation by DC through electron microscopy

Entire grids from sections of embedded samples were imaged in sequence, and both the number of live DC and MRSA visible per each DC were independently counted by a lab member, enumerated by eye in blinded sections. For cDC, both dead cells (fully necrotised or apoptosed) and cells smaller than 3 µm were excluded from analysis. For pDC, both dead cells and cells smaller than 2 µm were excluded from analysis. MRSA were enumerated on the basis of having clear contrast from the cytoplasm of the DC, and the presence of a visible cell wall.

Chapter 3 – Daptomycin resistance modulates the DC response to *S. aureus*

DC act as orchestrators, playing a key role in linking and directing both the innate and adaptive immune responses, mediated through the secretion of a complex variety of pro-inflammatory cytokines and the differential expression of a diverse array of surface receptors. Therefore, DC play a pivotal role in host immune surveillance; being tasked with distinguishing pathogenic from non-pathogenic stimuli in order to balance essential inflammatory immune responses with the maintenance of tolerance. As such, the phenotype correlating both the activatory and the inhibitory functions of the DC have been extensively characterised. With reference to the steady state conventional DC (cDC), canonical activation has been defined to include each of (i) the upregulation of MHC, (ii) the upregulation of co-stimulatory molecules such as CD80 or CD86 and (iii) the secretion of inflammatory cytokines directing activated T-cell differentiation, such as IL-4, IL-12p70 and IFN-γ[5,212,213]. The upregulation of peptide:MHC complexes increases the capacity for recognition by the cognate T-cell receptor (TCR), initiating the early signals for naïve T-cell activation. Importantly, co-stimulation and cytokine secretion by DC is required to achieve full activation and subsequent effector differentiation; with the absence of the phenotypes leading to either T-cell anergy or deletion[214].

In order to maintain the delicate balance between inducing T-cell activation and anergy, DC are equipped to express both co-stimulatory molecules including CD40, CD80 and CD86 alongside inhibitory type molecules such as PD-L1 and PD-L2[215]. While initially thought to act on T-cells directly through PD-1 signalling, Kuipers and colleagues[216] have demonstrated that T-cell proliferation is independent to the recognition of DC expressed PD-1 ligands –proposing that these ligands rather reduce DC maturation through self-signalling following binding of the T-cell PD-1 receptor[216]. Moreover, it has been shown that DC are able to express the PD-1 receptor itself, and the expression of PD-1 dictates the activatory capacity of DC activation during infection[217]. Therefore, in order to dissect the immune response to any pathogen it is critical to evaluate and characterise the inhibitory and activatory phenotype of DC, which act as critical conductors of both innate and adaptive immune responses.

In this chapter we describe a comprehensive phenotype of both primary and cultured murine dendritic cell subsets following stimulation with live and heat inactivated bacterial isolates, focussing on *S. aureus.* We have used the flt3-l murine bone marrow derived DC (FLDC) culture system described by Naik *et. al.*[202], which recapitulate the three primary splenic cDC and pDC subsets[202]. This system was selected for the capacity to provide a high yield of *bona fide* DC counterparts to primary DC subsets; a significant limitation of other common DC differentiation protocols involving GM-CSF and IL-4[202]. Furthermore, this chapter further provides a validation of the novel research findings from the FLDC system via replication in primary murine *ex vivo* splenic DC.

While there is an abundance of literature characterising the response of DC to bacteria, many of these studies rely on monocyte or BM derived models using GM-CSF and IL-4, and or laboratory strains of bacteria[139,146,218,219]. There are little work phenotyping primary DC subsets following bacterial stimulus, and even less using primary clinical isolates of infectious bacteria. To our knowledge this chapter contains the first published research to extensively phenotype DC subsets stimulated with primary clinical isolates of MRSA. Further, the findings of this chapter are the first of their kind in demonstrating a differential activation of DC following stimulation with primary clinical isolates of *S. aureus*, whilst further highlighting that the activation of DC is directly affected by antibiotic resistance mutations arising within these strains during primary infection and therapy with the antibiotic daptomycin.

3.1 FLDC are potently activated by heat inactivated bacterial stimuli

3.1.1 Bacterial stimuli elicit broad cytokine, chemokine and interferon production by FLDC

We initially established the response of FLDC to a panel of both pathogenic and non-pathogenic strains of Gram-negative and Gram-positive heat-killed bacteria (table 3.1). At day 8, these cultures clearly recapitulated *ex vivo* murine primary splenic DC subsets (figure 3.1), producing abundant cDC1, lesser cDC2, and modest pDC (figure 3.1); consistent with FLDC routinely cultured in our, and other laboratories[201,202,220,221]. Stimulation of total FLDC with these bacterial stimuli induced secretion of a range of inflammatory mediators, including RANTES (CCL5), MDC (CCL22), MIP-1α (CCL3), MIP-1β (CCL4), IL-6, TNF-α and IFN-β (figure 3.2a). Whilst there were differences in the level of inflammatory cytokines secreted by DC amongst bacterial stimuli, overall the cytokine profile was largely consistent between each of the strains (figure 3.2a). The main exception to this trend was the cytokine production following stimulation with heat-killed *Streptococcus pneumoniae*, which stood out as a poor all-round inducer of most of the examined cytokines and chemokines, yet notably inducing potent secretion of both MDC and IFN-β, equivalent to the other strains (figure 3.2a). Similarly, while *Helicobacter pylori* was able to elicit most inflammatory mediators in abundance, however was a poor induced of RANTES, TNF-α and IL-6 (figure 3.2a).

Of interest, bacterial stimulation of FLDC triggered secretion of IFN-β, but not IFN-α (figure 3.2a), despite the ability of FLDC to produce both of these type I IFNs in equivalence following stimulation with CpG ODN 2216 (a synthetic analogue of bacterial DNA, figure 3.2a). Further, we observed dose dependent production of the type III interferon, IFN-λ, in response to stimulation with higher concentrations of *S. aureus, Escherichia coli* and *Listeria monocytogenes* at an MOI greater than 25 (figure 3.2b), but IFN-α was still not detected (data not shown). Nonetheless, while we observed a binary differential in the ability of bacterial strains to induce secretion of IFN-λ (figure 3.2b), secretion of type I IFN did not correlate, as there was an approximately equivalent secretion of IFN-β by DC in response to the entire bacterial panel (figure 3.2a), with the exception of *L. rhamnosus,* which was a poor inducer of IFN globally (figure 3.2a and 3.2b).

3.1.2 Bacterial stimuli differentially upregulate CD40 and CD86 expression by FL-cDC

We next considered the surface phenotype of FL-cDC and found differential upregulation of the canonical surface activation markers by cDC dependent on bacterial stimuli (figure 3.3). Unfortunately, given the relatively low abundance of pDC in these cultures (figure 3.9), and an upregulation of both the CD11c and CD45R lineage markers upon activation, we were unable to clearly distinguish pDC from the cDC population (data not shown), and therefore favoured FACS sorting for comparisons of this subset in future analysis

Indeed, each of CD40, CD80, CD86, MHC-I and MHC-II were upregulated relative to complete media by both cDC1 (figure 3.3a) and cDC2 (figure 3.3b); however most of the differences in expression amongst bacterial strains were observed for CD40 and CD86. Of the entire bacterial panel, the commensal bacteria *L. rhamnosus* was the least efficient inducer of CD40 and CD86 expression by both cDC1 and cDC2 (figure 3.3), despite efficiently inducing secretion of most cytokines, but not IFNS, equivalent to the other bacteria examined (figure 3.1a). By contrast, *L. monocytogenes* was the most potent inducer of CD40 and CD86 by both cDC1 and cDC2 (figure 3.3), correlating with its potent induction of all the examined cytokines (figure 3.1a).

We next examined the expression of checkpoint inhibitory ligands PD-L1 (CD274) and PD-L2 (CD273), negative regulators of activated and mature DC and PD-1 expressing lymphocytes[215,216]. Both cDC1 and cDC2 upregulated PD-L1 in response to bacteria stimuli (figure 3.4a and c), with cDC2 expressing higher levels than cDC1. By contrast, only cDC1 upregulated PD-L2 following bacterial stimuli, with cDC2 levels not changing from the media control baseline (figure 3.4a and c). Both PD-L1 and PD-L2 were differentially expressed depending on the bacterial stimuli, with the most potent expression induced by the pathogenic commensal bacterial strains *S. aureus, S. epidermis* and pathogenic non-commensal strain of *L. monocytogenes.* We further examined the checkpoint inhibitory molecule GITR (CD357), but found no changes in expression relative to media for any of the bacterial stimuli (figure 3.4a and c).

Lastly, we investigated expression of CD25, a marker previously associated with DC activation[222], and the adhesion molecule CD62-L (L-selectin). CD25 upregulation was

more prominent for cDC2 than cDC1, but nonetheless followed the same trends as CD40, CD86, PD-L1 and PD-L2 with more potent expression induced by *L. monocytogenes, S. aureus,* and *S. epidermis* (figure 3.4b and d). Not surprisingly, expression of CD62-L did not correlate with cDC activation (figure 3.4b and d). CD62-L was included as a marker for pDC activation, as it is known to be downregulated upon activation[223], although we were unable to phenotype pDC in this experiment.

Table 3.1 Panel of heat inactivated bacteria used for FLDC stimulation

	Gram-stain	**Pathogenicity**	**Common infections**
Listeria monocytogenes	Gram-positive	Pathogenic, non-commensal	Listeriosis
Streptococcus pneumoniae	Gram-positive	Pathogenic, non-commensal	Pneumonia
Lactobacillus rhamnosus	Gram-positive	Non-pathogenic, commensal	n/a
Staphylococcus aureus	Gram-positive	Pathogenic and commensal	Bacteraemia
Staphylococcus epidermis	Gram-positive	Non-pathogenic, commensal	n/a
Escherichia coli Strain 0111:B4	Gram-negative	Pathogenic, non-commensal	Intestinal infection
Helicobacter pylori	Gram-negative	Pathogenic, non-commensal	Gastric ulcers, gastritis

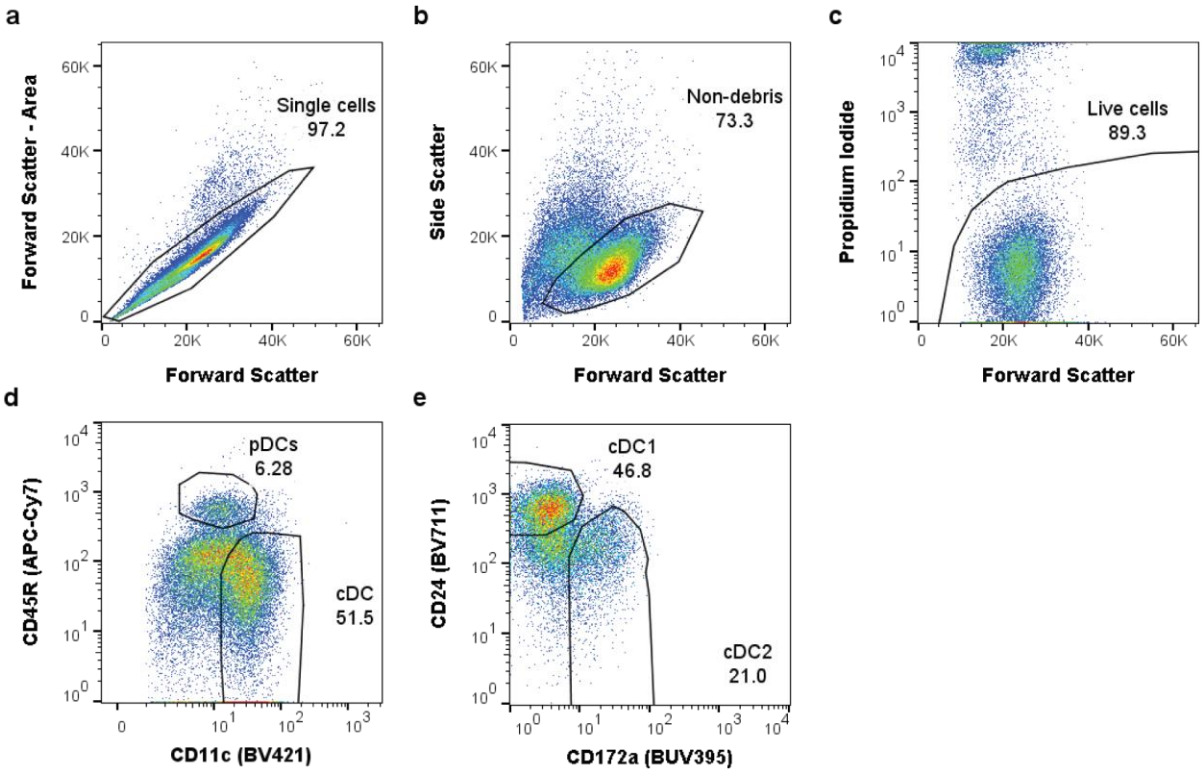

Figure 3.1 Gating strategy used to characterise FLDC subsets for flow cytometry and FACS sorting. ***(a)*** *Doublet exclusion performed on FSC-A and FSC-H, and subsequently SSS-A and SSC-H (not shown).* ***(b)*** *Cell sized events are selected excluding debris from cultures based of FSC-A and SSC-A.* ***(c)*** *Live cells are gated based on differential staining in PI.* ***(d)*** *Separation of cDC (CD11c high, CD45R intermediate) and pDC (C45R high, CD11c intermediate).* ***(e)*** *Separation of cDC1 (CD24 high, SIRPα low) and cDC2 (SIRPα high and CD24 low).*

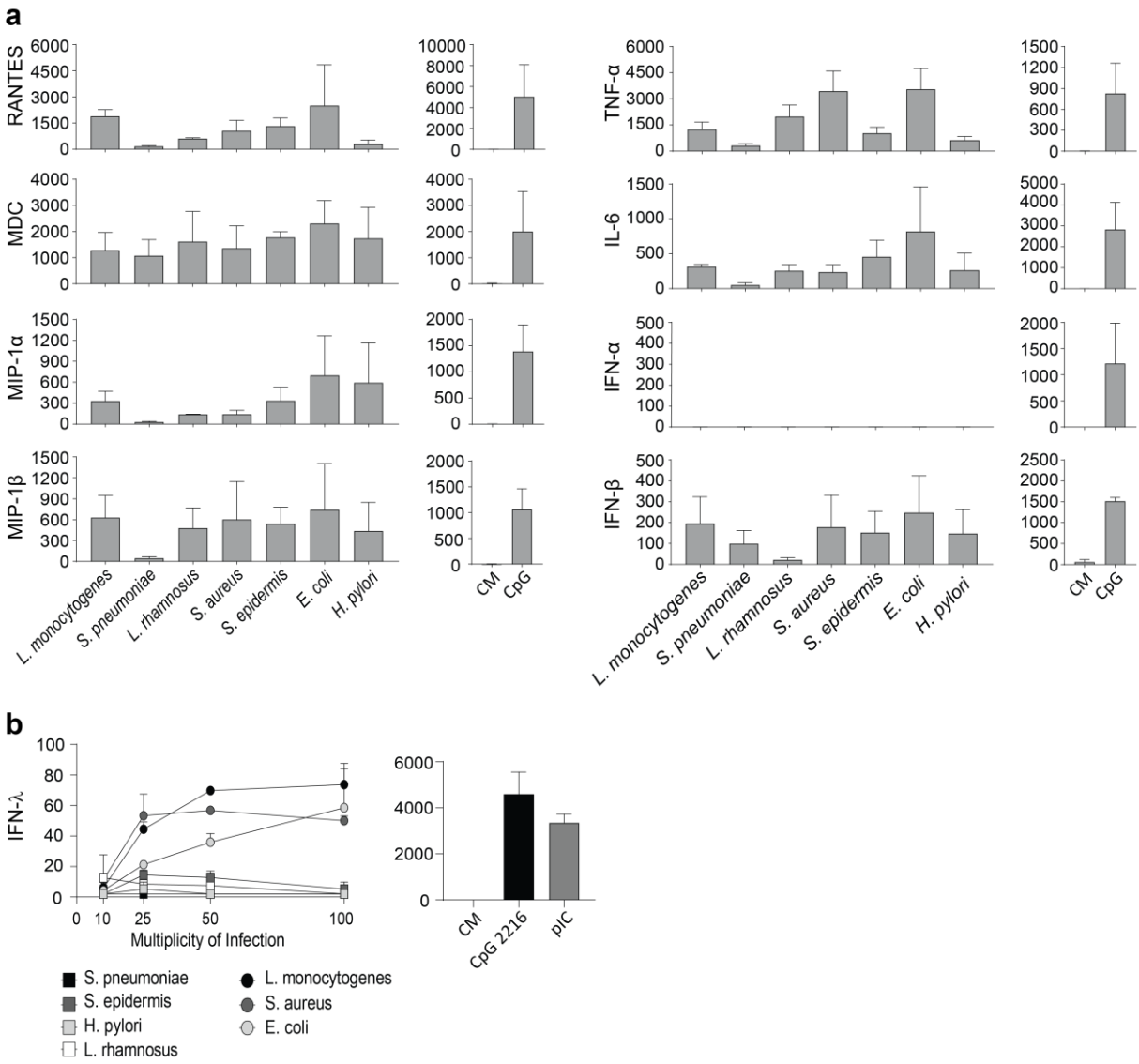

Figure 3.2 Cytokine, chemokine and IFN secretion by FLDC following stimulation with heat inactivated bacteria.

(a) *Cytokine production (pg/ml) by FLDC preparations (pooled from four mice) after 18-hour stimulus with heat inactivated bacteria, equivalent to MOI = 10. Mean and range of two independent experiments are shown for each stimuli (n = 2).* ***(b)*** *IFN-λ production (pg/ml) by FLDC following 18 hours stimulus with heat inactivated bacteria from an MOI of 10 - 100, CpG 2216 (0.5 µM), polyIC (100 µg/ml) or CM. Bars show the mean and range of biological duplicates from one experiment (n = 1).*

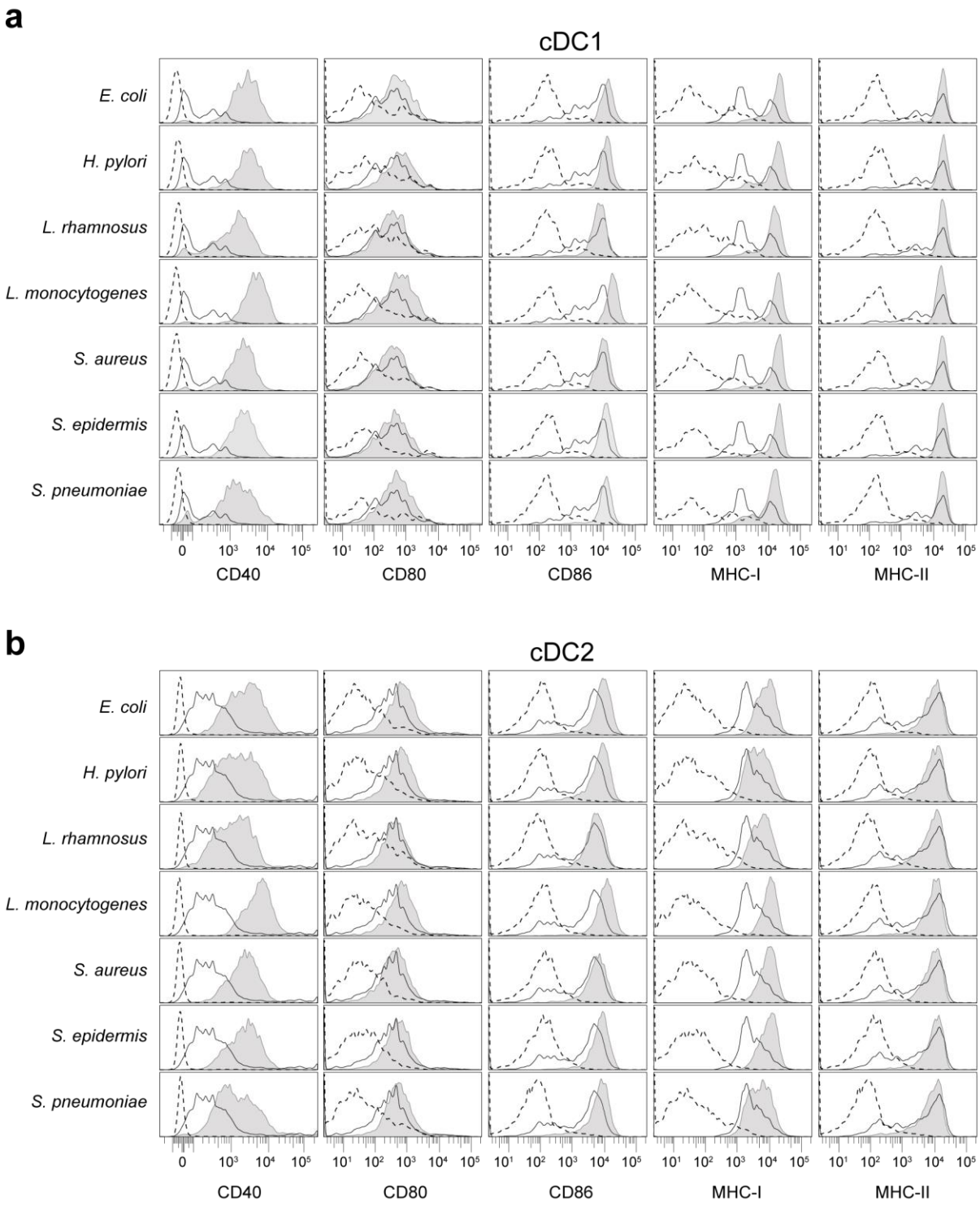

Figure 3.3 FLDC surface phenotype for co-stimulatory molecules & MHC following stimulus with heat inactivated bacteria.

CD40, CD80, CD86, MHC-I and MHC-II expression by cDC1 (a) and cDC2 (b) FLDC subsets following stimulation with heat inactivated bacteria. Histograms show surface marker expression quantified via flow cytometry for bacterial stimulations (shaded grey) complete media (solid black line). and pooled FMO control (dotted black line). Data shown from one experiment and representative of two independent experiments (n = 2).

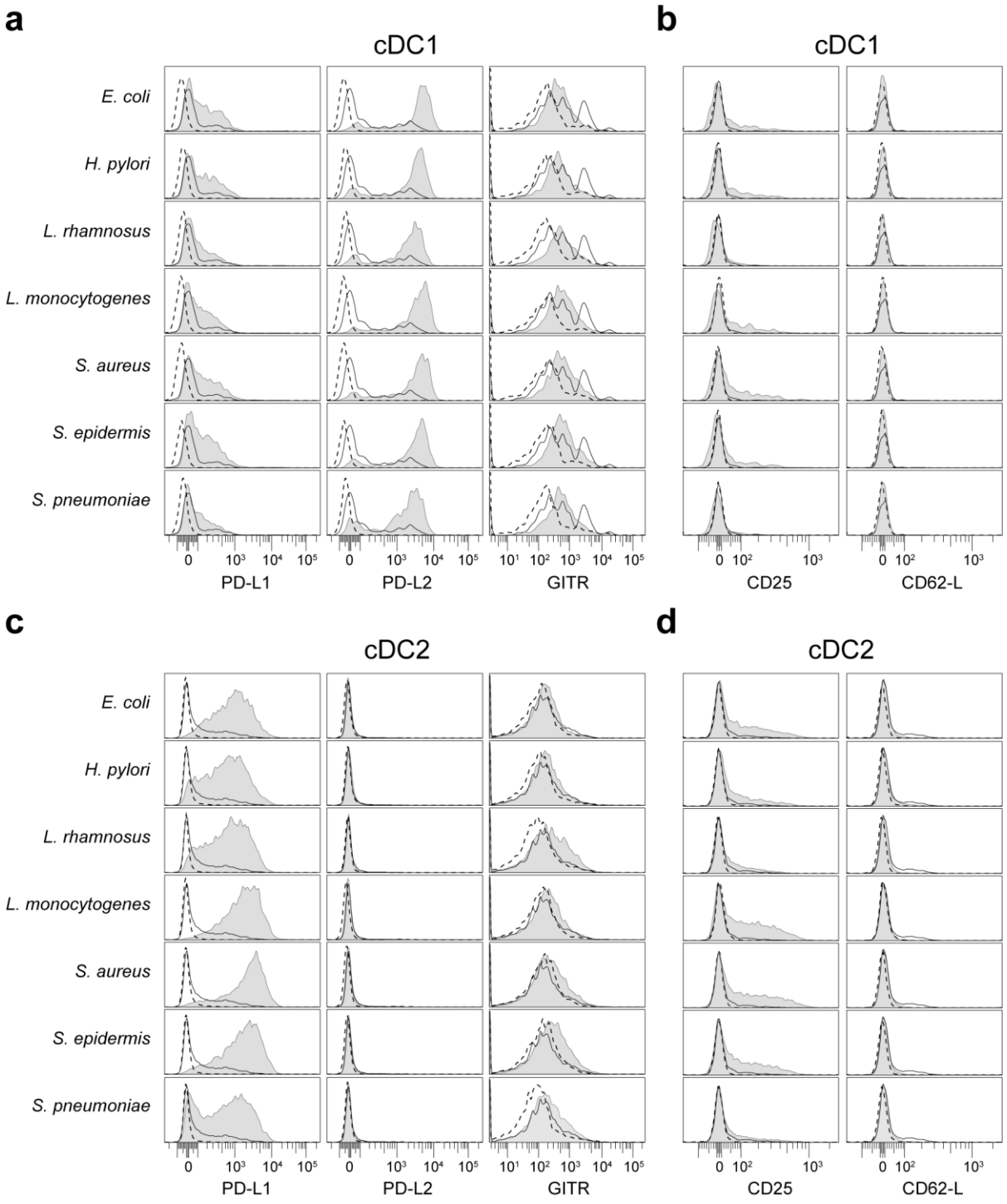

Figure 3.4 FLDC surface phenotype for inhibitory type molecules and other non co-stimulatory molecules associated with DC activation following stimulus with heat inactivated bacteria.

PD-L1, PD-L2, GITR, CD25 and CD62-L expression by cDC1 (a,b) and cDC2 (c,d) FLDC subsets following stimuli heat inactivated bacteria. Histograms show surface marker expression quantified via flow cytometry for bacterial stimulations (shaded grey) complete media (solid black line). and FMO control (dotted black line). Data shown from one experiment and representative of two independent experiments for all markers (n = 2), except for CD25 and CD62-L representative of one experiment (n = 1).

3.2 Optimisation of dendritic cell stimulation with clinical isolates of MRSA

3.2.1 Live stimulation of DC with *S. aureus* is most potent at an MOI of 10

Having established a panel of cytokines, IFNs and cell surface markers to test the response of DC to heat inactivated bacterial stimuli (figures 3.1, 3.3 and 3.4), we next analysed responses to live clinical isolates of methicillin resistant *S. aureus* (MRSA), to determine whether they similarly induced production of inflammatory cytokines and IFN by DC. The MRSA strains were paired clinical isolates corresponding to a daptomycin susceptible (DapS) and a daptomycin resistant (DapR) strain isolated from a patient during daptomycin therapy. The DapS strain (A8819), was isolated from a patient with bloodstream infection before treatment with daptomycin[158]. While on daptomycin therapy, resistance emerged leading to the DapR daughter strain (A8817)[158].

We initially found that IFN-λ production was higher from live MRSA than the HI strains (not shown) and used IFN-λ as a surrogate for FLDC activation. We initially performed a dose response titration and found IFN-λ secretion was optimal at a multiplicity of infection (MOI) of 10 (figure 3.5a). Interestingly, we found that the DapS strain of MRSA induced IFN-λ more potently than the DapR daughter strain at all concentrations between an MOI of 1 and 10 (figure 3.5a), yet there was no substantive difference in viability at any of these concentrations (figure 3.5b). Further, the DapR MRSA strain was unable to induce appreciable IFN-λ at any of the tested concentrations, therefore suggesting a differential between the two strains in their ability to activate DC.

Given optimal secretion of IFN-λ at an MOI of 10, and no appreciable differences in viability, we selected this concentration for future stimulations with these strains. To confirm this concentration was appropriate to model DC activation we further considered other inflammatory mediators and two unrelated clinical isolates of methicillin sensitive *S. aureus* (MSSA) at this concentration. We found that while all strains were capable of efficiently inducing the production of both IFN-β and IL-6, the two MSSA strains (D57 and D85) were far superior and potently induced the secretion of these inflammatory mediators (Figure 3.5c). Furthermore, we observed diversity in the response to these MSSA clinical isolates, with the D57 strain inducing significantly more IL-6 production by FLDC than the unrelated D85 MSSA isolate (figure 3.5c) – despite an

approximately equivalent viability of DC following stimuli with each of these strains (data not shown).

We next sought to address the potential impact of penicillin and streptomycin on bacterial viability and immunogenicity in our DC culture medium (appendix A1). In summary, bacteria remained viable for the first 4-hour post-stimulus in the presence of penicillin and streptomycin- yet these antibiotics were critical to prevent the overgrowth of bacteria in overnight culture (appendix A1). While we considered shorter incubation times, it was clear that overnight incubation was optimal for phenotyping complete activation of DC. A full description of these optimisation steps and associated results are described in appendix A1.

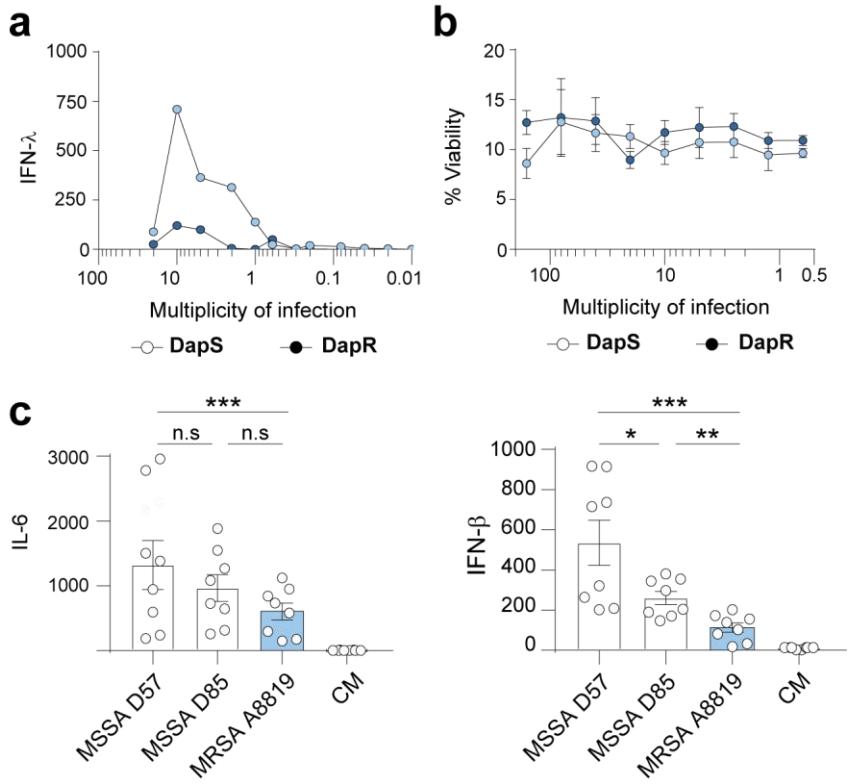

Figure 3.5 FLDC dose response to exposure with live clinical isolates of MRSA.

(a) *IFN-λ production (pg/ml) by FLDC after 18-hour stimulus with paired daptomycin sensitive (DapS) and resistant (DapR) clinical isolates of MRSA (2-fold serial dilutions from MOI of 20).* ***(b)*** *FLDC viability following 18-hour stimulus with paired DapS and DapR clinical isolates of MRSA from an MOI of 160. Data showing the mean and range of technical replicates from one experiment, representative of at least three independent experiments.* ***(c)*** *IFN-β and IL-6 production (pg/ml) by FLDC after 18-hour stimulus with A8819 (DapS) MRSA and two unrelated MSSA clinical isolates at an MOI of 10. Data showing the mean and SEM of 8 independent biological replicates pooled from several experiments (n = 8). Significance shown as * p < 0.05, ** p < 0.005, *** p < 0.001 from a one-way ANOVA using Tukey's test to correct for multiple comparisons.*

3.3 Clinical isolates of daptomycin exposed *S. aureus* differentially stimulate DC activation

3.3.1 Acquisition of daptomycin resistance in *S. aureus* significantly reduces dendritic cell activation

Having observed a differential and dose dependent secretion of IFN-λ by bulk FLDC stimulated with paired daptomycin exposed clinical isolates (figure 3.4a), we next examined a broader panel of inflammatory chemokines and cytokines. In line with the lower IFN-λ secretion in response to the DapR strain compared to the DapS parent strain, we further found that the DapR stimuli resulted in significantly less secretion of RANTES, MIP-1α, MIP-1β, IL-6 and TNF-α (figure 3.6). The observed decrease in inflammatory chemokine secretion was up to five-fold in the case of MIP-1β and four-fold for RANTES, which we found especially striking considering the genomic differences between these strains consist of five point mutations in the coding region of the genone[158].

The trend of reduced cytokine secretion in response to DapR compared with DapS MRSA were not shared by either IL-10 or IFN-β (figure 3.6), which were produced in equivalence between the two strains, in spite of the previous observation that MSSA strains induce significantly more IFN-β secretion than these MRSA isolates (figure 3.5c). Moreover, the chemokine MDC showed inverse kinetics to that of the other cytokines and chemokines, with the DapR strain inducing *significantly more* secretion by FLDC than the DapS strain (figure 3.6). Collectively these findings show that the trend of reduced inflammation following stimulation with the DapR MRSA isolate is not an artefact of decreased replication and bacterial load, but rather a poorer inflammatory capacity of the isolate itself.

We also examined the cytokine response of FLDC stimulated with these MRSA strains following heat inactivation, and found a global reduction in the secretion of each of cytokines and chemokines with the exception of RANTES (figure 3.6). These results highlight the importance of using live and intact bacteria for immunogenicity studies, as heat inactivation substantially alters the innate recognition of these bacterial strains. Nonetheless, there was again less overall secretion of almost all cytokines examined following DapR stimuli (figure 3.6). However, with the heat inactivated isolates these differences were ablated and only statistically significant for IFN-β (figure 3.6).

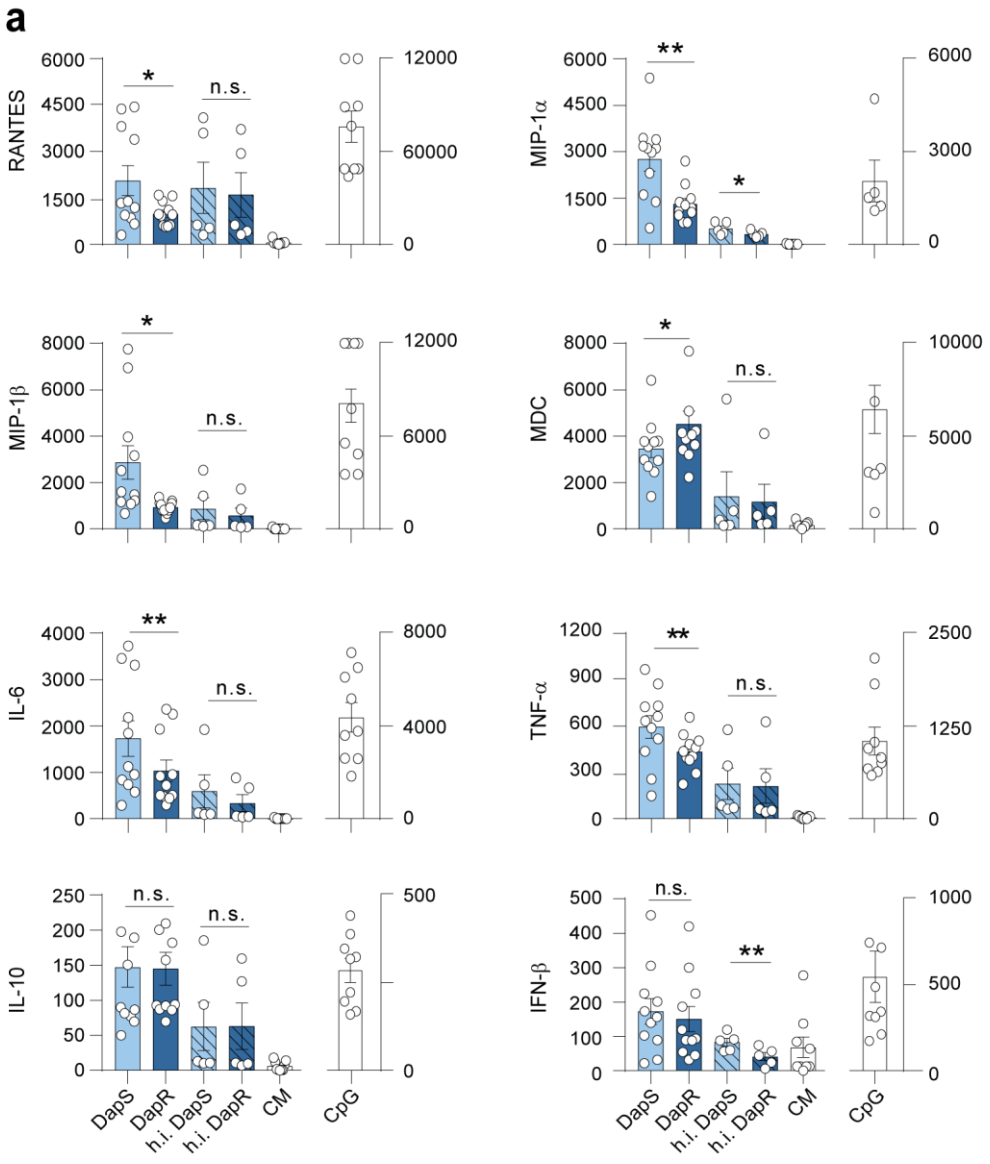

Figure 3.6 Cytokine secretion by bulk FLDC exposed to paired clinical isolates of MRSA.

(a) *Cytokine production (pg/ml) by FLDC following 18 hour stimulus with live (filled bars) and heat inactivated (filled patterned bars) of A8819 (DapS) and A8817 (DapR) MRSA (MOI = 10), equivalent to MOI = 10. Bars show the mean and SEM of stimuli for eight individual FLDC preparations (hollow circles) pooled from five independent experiments (n = 8). Significance shown as * p < 0.05, ** p < 0.005, *** p < 0.001 in paired two-tailed t-tests.*

3.3.2 The FLDC inflammatory response to MRSA is dominated by the CD24+ cDC1 subset

To understand the differential response to the DapS/DapR clinical isolates we first sought to phenotype FACS sorted FLDC subsets challenged with these stimuli. We found that the CD24+ DC subset corresponding to cDC1 were the broadest and most potent producers of the inflammatory cytokines, chemokines and IFN tested (figure 3.7). Of the three subsets, cDC1 were the main producers of RANTES, IL-6, MDC, and IFN-β following MRSA stimuli, and the only producers of IL-12p70 and IFN-λ (figure 3.7). The cDC1 subset also produced MIP-1α, MIP-1β and TNF-α in abundance, although the pDC produced these chemokines in equivalence (figure 3.7). Despite being potent producers of MIP-1α, MIP-1β and TNF-α, the pDC made the least contribution to production of IFN-β, a role instead dominated by the cDC- especially cDC1 (figure 3.7). Similarly, neither the pDC, nor any other DC subset were capable of producing appreciable IFN-α in response to live MRSA (figure 3.7), consistent with our findings for the heat inactivated bacterial panel (figure 3.2). Importantly, our IFN-a ELISA detects only IFN-a2, while being cross-reactive with IFN-α1, α4, α5 and α6 (product TDS; appendix C). We therefore next investigated other IFN-a subtypes and confirmed that the absence of IFN-α in these cultures (appendix A2),

The differential response to the DapS/DapR pair, observed for bulk FLDC (figure 3.6), was further recapitulated by FACS sorted cDC1 (figure 3.7). Comparing cDC1 stimulation with DapS MRSA, the DapR daughter strain resulted in up to four-fold lower secretion of each inflammatory mediator tested, except for MDC (figure 3.7). MDC secretion was instead higher following stimulation with DapR MRSA than DapS MRSA (figure 3.7), an observation consistent with that seen for bulk FLDC (figure 3.6). The trends observed for the DapS/DapR pair were not carried across all subsets, with the SIRPα+ cDC2 and the pDC showing no substantial differences for most cytokines (figure 3.7). This data therefore demonstrates that the cDC1 mediate most of the differences in cytokine secretion observed following stimuli of FLDC with the DapS/DapR pair.

To further confirm that these findings are not an artefact of MRSA toxicity and cell death, we examined the viability of these DC subsets following stimulus, and indeed found

greater survival of each subset following stimuli with DapR MRSA (figure 3.bc). These data confirm that the DapS MRSA does indeed induce more potent production of inflammatory mediators than DapR MRSA, and that this difference is not an artefact of viability- rather the difference is greater when considered on a cytokine per cell basis (indirectly shown in figure 3.7).

Given the differences observed in the secretion of inflammatory cytokines by FLDC in response to the DapS/DapR MRSA isolates we next examined surface phenotype. We found that the surface phenotype of FLDC following stimulus with DapR MRSA was similar to that following stimulation with DapS MRSA (figure 3.8). The upregulation of activation markers CD40, CD86 and MHC-II by following stimulus with DapS and DapR MRSA were equivalent for the cDC1, cDC2 and the pDC subsets (figure 3.8a). Consistent with their potent cytokine secretion, the cDC1 reached the highest peak expression of all activation markers examined in response to MRSA (figure 3.8a). Importantly, the cDC1 also exhibited by far the largest differential between mock and MRSA stimulation for these markers (figure 3.8a).

Despite the similarities in most activation markers following stimulus with the DapS/DapR MRSA pair, these strains induced differential expression of CD80 by all three DC subsets (figure 3.8a). Stimulation of cDC1 and cDC2 with DapS MRSA resulted in approximately 2-fold higher CD80 expression than did DapR MRSA (figure 3.8a), furthermore, very few pDC upregulated CD80 in response DapR MRSA compared to the DapS parent strain (figure 3.8a). Of particular interest, the DapS MRSA isolate was able to elicit expression of CD69 by cDC subsets to levels at least four fold higher than those induced by the DapR isolate (figure 3.8b). While CD69 was upregulated by pDC in response to both strains, there was a less clear differential between the two (figure 3.8b).

These finding of differential expression of CD69 by cDC in response to the Dap exposed MRSA clinical pair was of substantial interest to us. However, in subsequent experiments we determined that the interaction represented a non-specific binding interaction specific to hamster IgG λ-light chain (appendix B). While we have to date, been unable to verify the molecular identify of the factor causing this non-specific binding, we currently hypothesise it is some staphylococcal antibody binding protein. The experiments supporting this hypothesis are extensively described in appendix B.

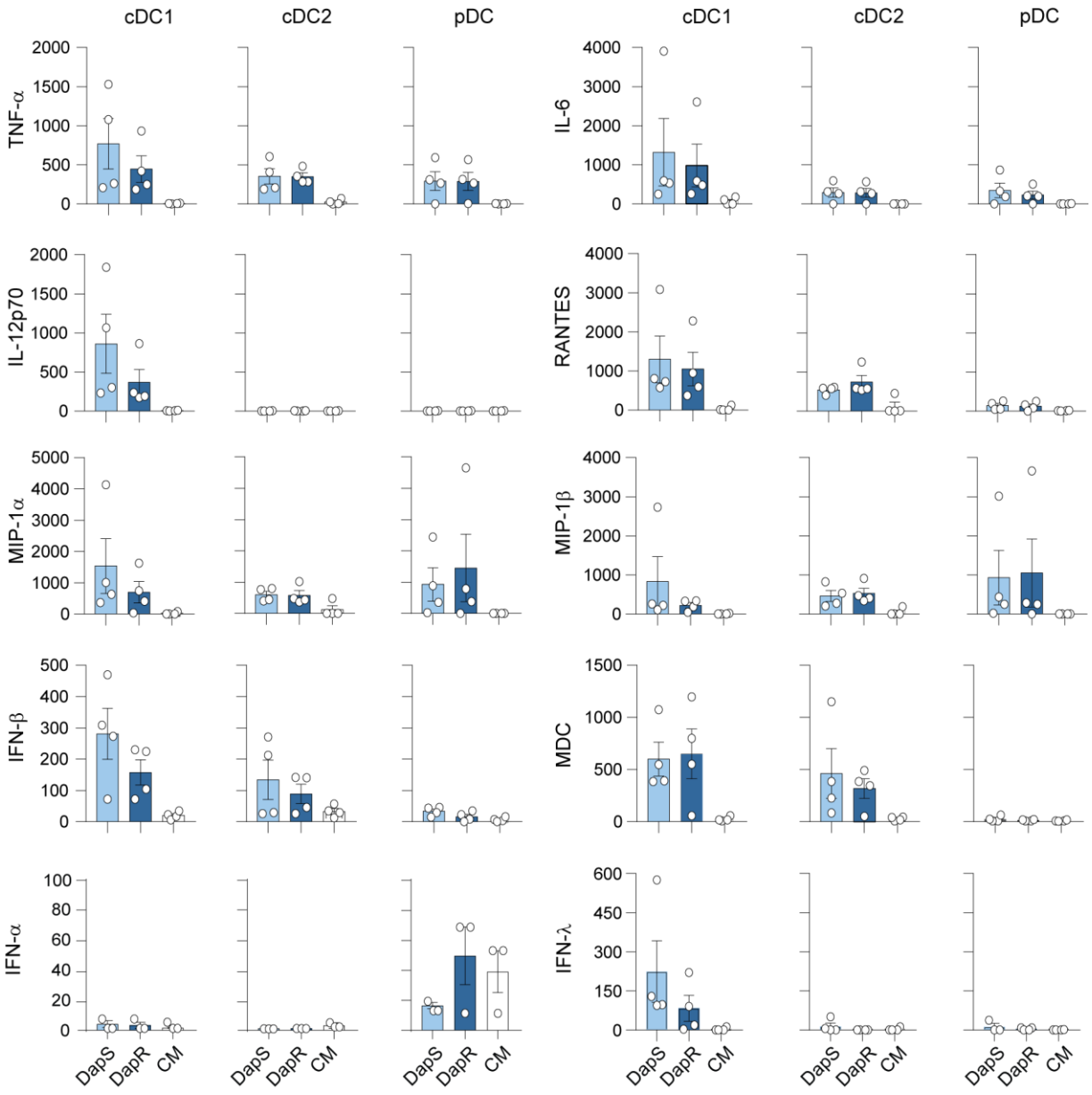

Figure 3.7 Cytokine secretion by FACS sorted FLDC exposed to paired clinical isolates of MRSA.

(a) *Cytokine production (pg/ml) by FACS sorted FLDC at 18 hour stimulus with A8819 (DapS) and A8817 (DapR) MRSA or complete media alone. Bars show the mean and standard error of the mean of biological replicates from 4 independent experiments (n = 4).*

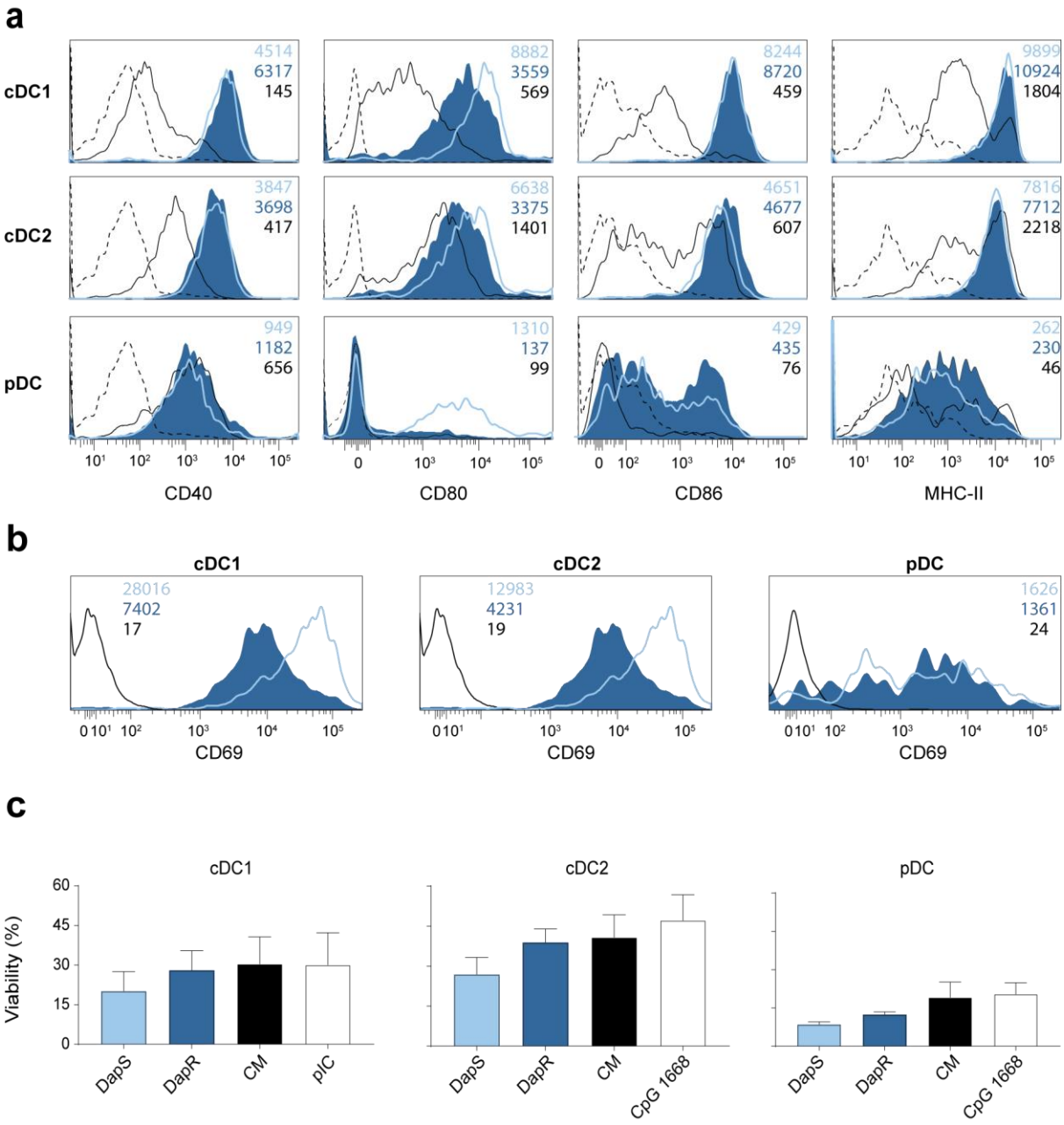

Figure 3.8 Surface marker expression by FACS sorted FLDC exposed to paired clinical isolates of MRSA. ***(a)*** *Activation marker expression by FLDC stimulated with A8819 DapS MRSA (light blue line), A8817 DapR MRSA (dark blue shaded), or complete media (black solid line). Histograms showing CD40, CD80, CD86 and MHC-II expression by cDC1, cDC2 and pDC in pooled sample FMO controls (dotted black line). Data shown from one experiment and representative of three independent experiments for CD40 and MHC-II (n = 3), and four independent experiments for CD80 and CD86 (n = 4).* ***(b)*** *CD69 expression by bulk FLDC subsets at 6 hours post stimulus with DapS and DapR MRSA as in 'a'. Data shown from one experiment (n = 1).* ***(c)*** *Viability of FACS sorted FLDC at 18 hour stimulus with A8819 (DapS) and A8817 (DapR) MRSA, media alone, CpG 1668 (0.5 µM) or pIC (100 µg/ml). Bars show the mean and standard error of the mean of replicates from 3 independent experiments (n = 3).*

3.3.2 Both splenic cDC subsets dominate the cytokine response to MRSA

Having established a novel phenotype of DC activation to the DapS/DapR MRSA pair using FLDC, we next sought to validate these findings using *ex vivo* murine splenic DC. Similar to our findings in FLDC (figure 3.7), splenic cDC1 differentially expressed TNF-α, IL-6, IL-12p70, RANTES, MIP-1α and MIP-1β following stimuli with the A8819/A8817 clinical MRSA pair (figure 3.9). The same trend was apparent for the chemokine GROα (figure 3.9), although this response was not tested on FLDC. Importantly, we saw no difference in secretion of IFN-β and IL-10 by splenic cDC1 following stimulation with the A8819/A8817 clinical pair (figure 3.9), a finding again consistent with the FL-cDC1 (figure 3.7 and data not shown). These trends confirmed that the DapS A8819 isolates induces an overall greater inflammatory response by cDC1 than does its DapR daughter isolate A8817.

In contrast to the FLDC system both splenic cDC subsets were found to dominate the inflammatory response (figure 3.9), with each subset abundantly producing a different set of cytokines and chemokines (figure 3.9). Similar to FL-cDC1, the splenic cDC1 were found to secrete RANTES, IL-6 and IL-12p70 to higher levels than the other DC subsets (figure 3.9). The cDC1 also dominated the secretion of GROα (figure 3.9), although this was not tested in the FLDC system. By contrast the cDC2 were found to be the most potent producers of TNF-α (figure 3.9), and further, were able to produce both MIP-1α and MIP-1β to levels at least equivalent that of the cDC1 (figure 3.9).

Despite the shared contribution towards the inflammatory response by both cDC subsets, the differential response to the A8819/A8817 clinical pair was not entirely conserved between the cDC1 and cDC2. Indeed, the cDC2 exhibited inverse kinetics to cDC1 for both production of TNF-α, IL-6 and RANTES following stimulation with the A8819/A8817 clinical pair; producing these mediators to higher levels in response to the DapR A8817 isolate (figure 3.9). However, the kinetics of MIP-1α and MIP-1β production were conserved between the cDC subsets, with both cDC1 and cDC2 secreting more in response to the DapS A8819 isolate than the DapR A8817 isolate (figure 3.9). Overall, these data suggest that while the cDC subsets play a dominate role in the inflammatory response to MRSA clinical isolates, the mechanisms regulating recognition and activation of these subsets are distinct.

Of all the splenic DC subsets, pDC were the weakest responders to MRSA stimuli (figure 3.9); a finding consistent with their FLDC counterparts (figure 3.7). However, in stark contrast to FL-pDC their splenic pDC were unable to produce substantial quantities of MIP-1α or MIP-1β (figure 3.9). Rather the splenic pDC were more active in the production of IFN-β, which they produced in equivalence with the cDC1 (figure 3.9). While in our early experiments were able to detect IFN-λ by splenic cDC1 (data not shown), these experiments were plagued by issues with poor viability and low cytokine secretion following FACS sorting (appendix A3). To resolve these issues, we supplemented sorted cultures with GM-CSF, reflected in all figures shown in the body of this thesis. While we found the addition of GM-CSF improved sorted DC viability at 18 hours post stimulus and enhanced the capacity to secrete cytokine (as shown in figure 3.9), we were unable to detect IFN-λ in the supernatants of sorted splenic cDC1 stimulated with MRSA in the presence of GM-CSF (data not shown). Of note, aside from enhancing viability of DC and leading to greater inflammatory capacity, we noted that sorted splenic and FLDC stimulated with *S. aureus* we able to secrete IL-12p70 in the presence of GM-CSF (figure 3.7 and 3.9), while it was not detectable in the DC supernatants when stimulated with MRSA in the absence of GM-CSF (Appendix A3).

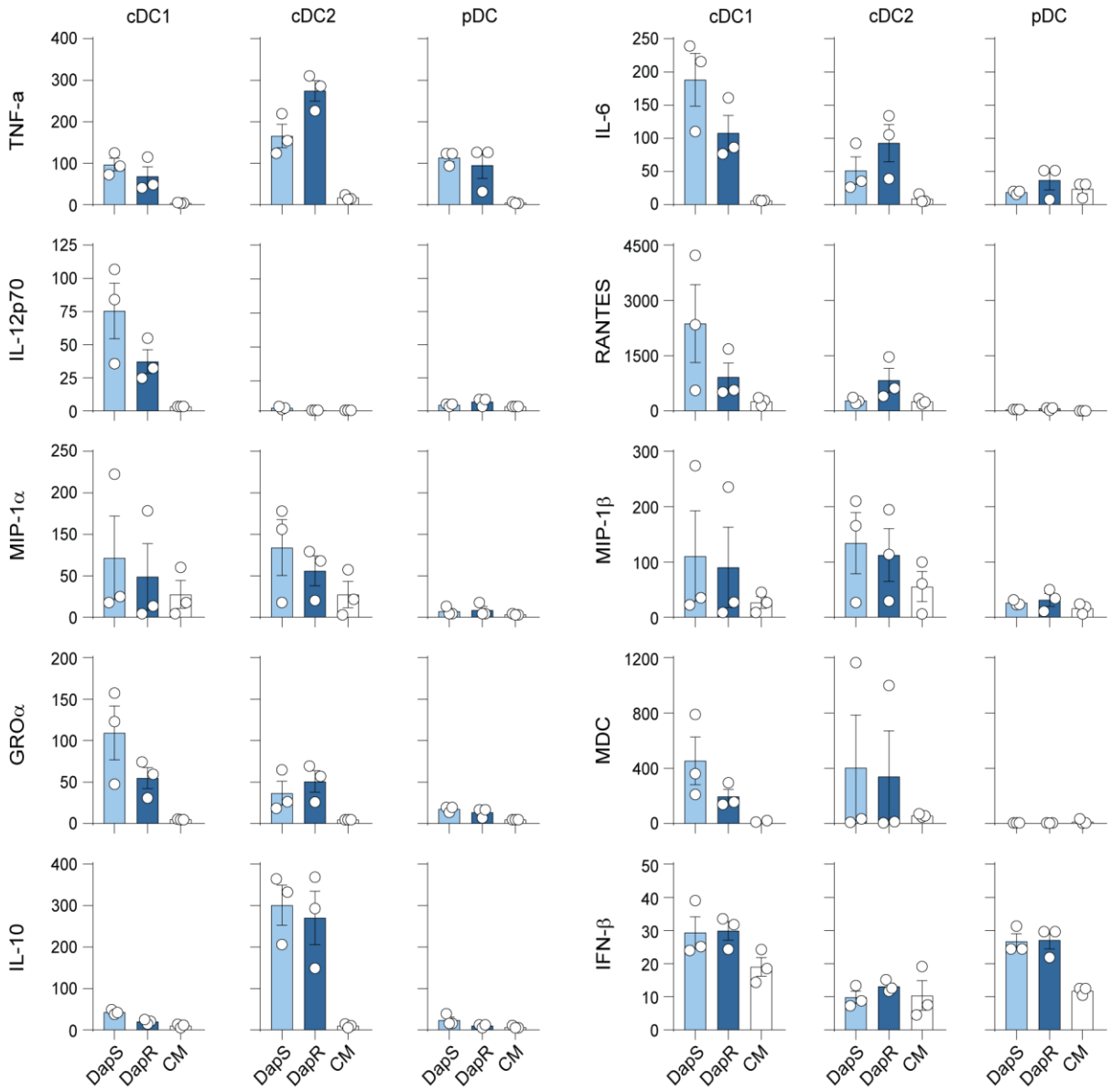

Figure 3.9 Cytokine secretion by FACS sorted splenic DC exposed to paired clinical isolates of MRSA. *Cytokine production (pg/ml) by FACS sorted splenic DC at 18 hour stimulus with A8819 (DapS) and A8817 (DapR) MRSA at an MOI of 10, or mock stimulated with media alone. Bars show the mean and standard error of the mean of biological replicates pooled from 3 independent experiments (n = 3).*

3.3.3 All splenic DC subsets strongly upregulate surface activation markers in response to MRSA stimuli

We next investigated the surface activation phenotype of sorted splenic DC following stimuli with the MRSA pair. Despite the splenic cDC2 dominating the inflammatory response, we found that both the splenic cDC1 and cDC2 exhibit potent upregulation of the conventional activation markers CD40, CD80, CD86 and MHC-II (figure 3.10a). Despite the cDC1 expression more of each marker per cell on average than cDC2, most of these markers were strongly upregulated by cDC1 with overnight culture in media alone (figure 3.10a). Despite not reaching peak expression to cDC1, the cDC2 differentially expressed both CD40 and CD80 in response to culture with media alone, DapS and DapR MRSA- with DapS MRSA inducing higher levels of both activation markers (figure 3.10a). Similarly, pDC shared this phenotype with DapR MRSA stimuli inducing less expression of CD40 and CD80 than DapS stimuli (figure 3.10a). Overall, the pDC exhibited the least surface activation of the splenic DC subsets following MRSA stimuli (figure 3.10a and b), a finding consistent with their poor capacity to efficiently present antigen to T-cells[5].

We included CD69 in our panel of surface activation markers for splenic DC, finding DapS MRSA could induce expression up to 1,000 fold higher than DapR MRSA (figure 3.10a). Further, we found that all cDC and pDC subsets expressed CD69 at very high levels following MRSA stimuli relative to culture with CM alone (figure 3.10a), a finding which was surprising to us given CD69 upregulation is associated with the early activation of pDC and typically expressed at lower levels by cDC subsets[224-226]. As previously mentioned, these findings warranted further investigation into the molecular basis of this phenomena, which was later determined to be a non-specific binding interaction restricted to hamster IgG λ-light chain (appendix B).

Having observed differential expression of both CD40 and CD80 by splenic and FLDC (figure 3.8a and 3.10a), we further examined the expression of checkpoint inhibitory receptor PD-1 (CD279) and its ligands PD-L1 (CD274) and PD-L2 (CD273). Like CD40 and CD80 we found that PD-1 and PD-L1 were differentially expressed by splenic DC following stimuli with the daptomycin exposed MRSA pair (figure 3.10b). Both the cDC2 and pDC expressed more PD-1 following stimulation with DapS MRSA than the DapR daughter strain (figure 3.10b), whilst each of cDC1, cDC2 and pDC expressed more PD-L1 following stimuli with DapS than DapR MRSA (figure 3.10b). By contrast, PD-L2

expression was equivalent irrespective of DapS or DapR stimuli in each of splenic cDC1 and cDC2 (figure 3.10b). This trend appeared consistent for the pDC, although these observations were limited by a degradation of the APC-Cy7 tandem fluorophore used to sort pDC based on their high expression of CD317; subsequently causing substantive bleeding into the APC channel used to detect PD-L2, and thus increased background for pDC (figure 3.10b).

We further considered expression of CD25 (IL-2R) and CD62-L (L-selectin) as markers of activation on sorted DC subsets following MRSA stimuli (figure 3.10c). Both strains of MRSA induced higher expression of CD25 than did incubation with media alone, but in contrast we were unable to detect any quantifiable increase in expression of CD62-L by splenic cDC or pDC following stimulus with MRSA (figure 3.10c). In regard to CD25, both cDC2 and pDC expressed more per cell on average following stimulation with DapR MRSA compared to the DapS parent strain (figure 3.10c)- an inverse trend to that observed for CD40, CD80, PD-1 and PD-L1 (figure 3.10a and b).

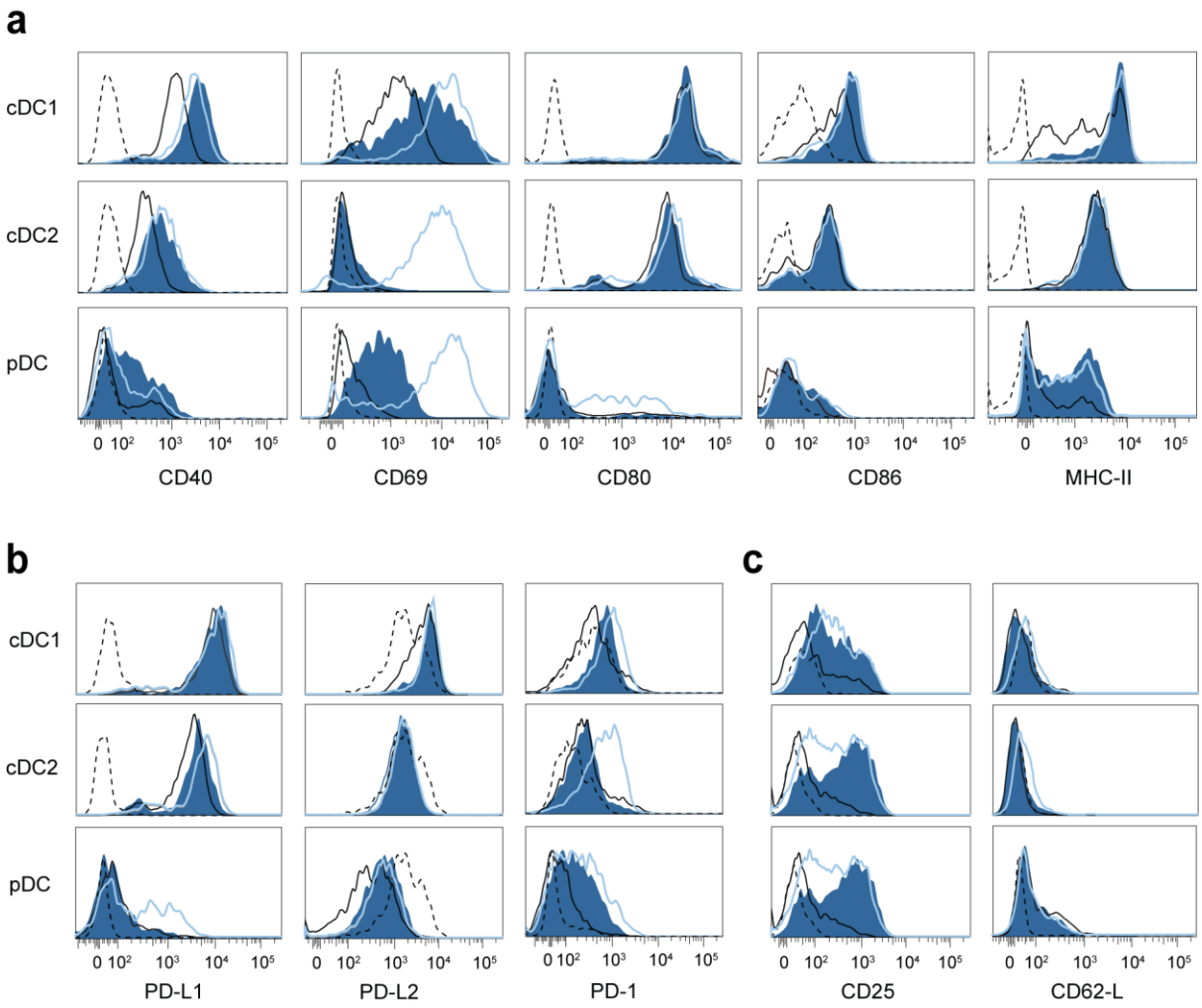

Figure 3.10 Surface marker expression by FACS sorted splenic DC exposed to paired clinical isolates of MRSA.

(a) *Activation marker expression by splenic DC stimulated with A8819 DapS MRSA (light grey line), A8817 DapR MRSA (dark grey shaded), or complete media (black solid line). Histograms showing CD40, CD80, CD86 and MHC-II expression by cDC1, cDC2 and pDC with pooled FMO controls (dotted black line). Data shown from one experiment and representative of between three and seven independent experiments for each marker (n ≥ 3).* ***(b)*** *Inhibitory type marker expression by splenic DC stimulated as in (a). Histograms showing PD-L1, PD-L2 and PD-1 expression by DC subsets. Data shown from one experiment and representative of two to five independent experiments (n ≥ 2).* ***(c)*** *Non-canonical activation marker expression by splenic DC stimulated as in (a). Histograms showing CD25 and CD62-L expression by DC subsets. Data shown from one experiment (n = 1).*

3.4 Discussion

3.4.1 Live bacteria should be considered the gold standard for immunogenicity studies

In this chapter we have optimised the culture conditions for the stimuli and subsequent phenotyping of both murine FLDC and *ex vivo* splenic DC with live clinical isolates of MRSA. Most of the currently published research on the DC response to *S. aureus* has utilised the IL-4 and GM-CSF inducible DC culture system[138,142,218,227] and/or laboratory strains of MRSA[139,146,218]. A problem with the former approach is that these DC culture systems do not recapitulate primary DC subsets, and as such the use of these systems to model DC function is contentious[228-230]. We have therefore addressed this knowledge gap in the literature, in phenotyping the response of *bona fide* murine DC to clinically derived, antibiotic-resistant *S. aureus*. In doing so, we have demonstrated a clear differential in DC activation when comparing live and heat inactivated samples of MRSA (figure 3.6), highlighting the necessity for utilising live bacterial samples in immunogenicity studies.

These observations are consistent with the earlier findings of Haller and colleagues[231], whereby the maximal production of TNF-α by monocytes following stimulation with *L. monocytogenes* was recorded almost 3-log lower for live stimuli than heat inactivated[231]. Similarly, it has been observed that both TNF-α and IL-6 production by human peripheral blood mononuclear cells (PBMCs) are impeded in response to bacteria following fixation[232]. It is therefore clear, that the inactivation of bacteria by means of chemical and heat treatment alter their biochemical composition in such a way as to alter their immunogenicity, and thus live bacterial isolates should be preferred to preserve the PAMPs in their native form as recognised by the innate immune system.

3.4.2 Acquisition of daptomycin resistance by MRSA impedes DC activation

Critically, in this chapter we have uncovered novel differences between paired primary clinical isolates of MRSA in their ability to activate both FLDC and *ex vivo* splenic DC; in terms of both cytokine secretion and co-stimulatory marker expression. Specifically, we demonstrated that a DapS MRSA isolate (A8819), induced secretion of pro-inflammatory cytokines and chemokines to significantly higher levels than the paired DapR (A8817) daughter strain (figure 3.6). Recently, Nguyen and colleagues have demonstrated

differential immunogenicity between staphylococci species, whereby the inflammatory response following stimulation with commensal species including *Staphylococcus epidermis* and *S. aureus* were reported to be more than 10-fold below that of the non-commensal species *Staphylococcus carnosus*[219]. While novel, these findings are derived from the stimulation of a monocytic cell line (MM6), with various laboratory strains of streptococci. However, the recently published work described in this chapter[201], is distinct in the evaluation of the immunogenicity of ***primary*** clinical isolates of *S. aureus,* as opposed to the general comparison of strains on the species level. Furthermore, this chapter presents the first extensive characterisation of primary DC subset activation in response to clinical isolates of *S. aureus*, highlighting novel differences in immunogenicity between paired *S. aureus* isolates obtained throughout the duration of a single clinical infection- despite these strains differing by only 5 single amino acid point mutations in the coding region of the genome[158].

Importantly, the diversity observed in immunogenicity of clinical isolates was by in large restricted to their capacity to induce differential cytokine secretion by DC (figures 3.5, 3.6, 3.7 and 3.9), with only subtle variations in the cell surface phenotype of DC stimulated with these isolates (figures 3.8 and 3.10). These findings suggest that while clinical isolates, induce a DC activation state sufficient to provide both a strong signal 1 and signal 2 for T-cell activation (upregulation of MHC and co-stimulatory molecules respectively); the differences between these clinical isolates rather regulate signal 3 (cytokine secretion), which rather affects T-cell ***differentiation***. Despite a substantive lack of published literature on this topic, there is precedent for these findings. Indeed Braat and colleagues[233] have previously demonstrated that despite a potent differential in the induction of inflammatory cytokine by DC stimulated with *Klebsiella pneumoniae* and *L. rhamnosus,* the expression of co-stimulatory markers CD40, CD83 and CD86 by DC differ only slightly between these stimuli[233]. Importantly, the stimuli of DC with *K. pneumoniae* but not *L. rhamnosus,* induced secretion of IL-12p70 and induced a Th1 bias in mixed leukocyte reactions[233]. Indeed, our observations highlight that the capacity of cDC1 to secrete IL-12p70 is compromised following stimuli with the DapR (A8817) clinical isolate, compared to the parent strain (figure 3.9). It is therefore possible that this differential in secretion of the bioactive IL-12p70 would similarly impede the capacity of cDC1 to polarize Th1 responses against DapR MRSA.

Despite a largely consistent surface phenotype for both cDC following various bacterial stimuli, there is clear differential in expression of CD80 following stimulation with the A8819/A8817 clinical pair, whereby both FL-cDC subsets exhibit greater expression of CD80 following stimulation with the DapS (A8819) isolate (figure 3.8). While these observations were not fully replicated in the spleen; all three splenic DC subsets expressed higher PD-1 following stimulation DapS A8819 than the DapR daughter strain (figure 3.10b). The expression of PD-1 by the DC subsets following stimuli with *S. aureus* may provide a model for the poor cytokine secretion, given the previous work of Yao and colleagues demonstrating that PD-1 expression by DC *in vivo* correlates with inferior protection against bacterial infection and reduced secretion of both IL-12p70 and TNF-α[217].

3.4.3 Differential in IFN-α and IFN-β production by DC in response to *S. aureus*

In our initial stimulation of DC with heat inactivated bacteria we observed production of both IFN-λ and IFN-β in the absence of IFN-α (figure 3.2 and 3.12). These findings were surprising given that we have previously demonstrated that murine pDC are able to produce IFN-α in response to pansorbin[207] (heat killed *S. aureus*). Pansorbin is a preparation of heat-killed formalin fixed *S. aureus* Cowan strain I. By contrast, the heat killed strains utilised in this study are not formalin fixed, but rather autoclaved to inhibit stimulation through TLR9 (personal communication with *Invivogen*; Appendix D). It is therefore likely that the tertiary structure of the CpG DNA required for stimulation of TLR9 is lost; and that the remaining cyclic dinucleotides (CDNs), which are potent inducers of IFN-β by DC[106], account for this response.

Regarding live stimuli, Kaplan and colleagues[234] have previously noted trace production of IFN-β, but IFN-α, in response to *S. aureus*[234]. While this work considers both laboratory strains of bacteria and the GM-CSF induced model of BMDC, these results closely match our own observations of splenic DC stimulated with clinical *S. aureus* isolates (figure 3.9), which unlike the FLDC (figure 3.7), were very poor producers of IFN-β. Moreover, Warnking and colleagues have recently demonstrated that *S. aureus* inhibits the production of IFN-α during influenza virus superinfection, inhibiting dimerization of STAT1/STAT2[140]; which are critical signaling molecules of the IFNα/β receptor. This therefore provides a basic model for our findings of IFN-β secretion by DC in the absence

of IFN-α (figure 3.11). While this model does not explain the poor contribution from pDC, are geared to readily produce IFN-α through constitutive expression of IRF-7[5,39,41,235,236]; we content that these differences may be a result of less antigenic load as evidenced through their modest contribution to inflammation more generally. This hypothesis is investigated in further detail throughout chapter 6.

3.4.5 Concluding remarks

The notion of reduced immunogenicity for a given bacterial isolate broadly correlating with resistance to antibiotics inhibiting cell wall synthesis would have far reaching consequences; substantially altering the way in which we consider the development of novel therapeutics and indeed the prescription of existing therapeutics. With a progressing understanding as to how the A8819/A8817 clinical pair of MRSA mutates to alter the cell wall and membrane during daptomycin therapy[158,194], future work should also focus on the extent to which these changes occur during antibiotic therapy more broadly. Understanding whether similar changes occurring during antibiotic therapy affect immunogenicity of other *S. aureus* isolates, and indeed those of other bacterial species of bacteria, should be of key interest to future research- informing the design of novel therapeutics, vaccines and other potential treatment strategies.

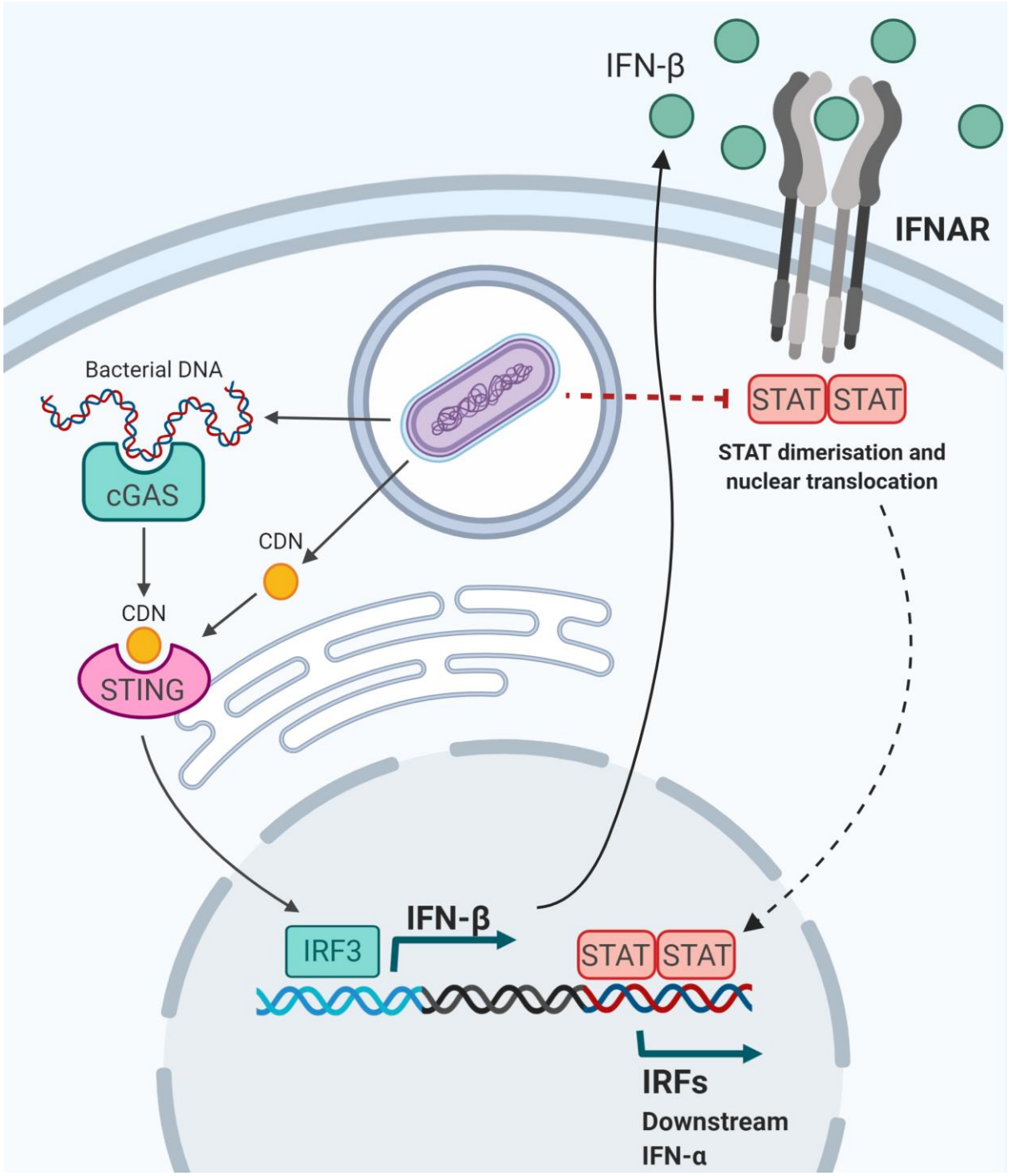

Figure 3.11 Hypothesised mechanism for regulation of type I IFN by DC in response to S. aureus.
Internalised bacteria stimulate the cytosolic sensor cyclic GAMP synthase (cGAS), which produces cyclic dinucleotides (CDNs) acting on STING to activate interferon regulatory factor 3 (IRF-3). Activation of IRF-3 stimulates early type I IFN, including trace IFN-α (not shown) and IFN-β[237,238].Production of early type I IFN stimulates the IFN-α/β receptor (IFNAR), normally triggering STAT dimerization and late phase IFN-α production mediated by other IRFs; however staphylococcal mediated inhibition of STAT dimerisation[140] subsequently prevents nuclear translocation, subsequent IRF transcription and therefore late phase IFN-a production.

Chapter 4 – Defining the genetic determinants of *S. aureus* facilitating innate recognition by DC

Chapter three has provided an extensive phenotype of both culture-derived and primary DC in response to live paired clinical isolates of MRSA. Importantly, this work revealed a novel trend in the DC response between a pair of clinical isolates, A8819 DapS and A8817 DapR, whereby the latter induced significantly poorer activation of DC than did its parent strain. The diversity in DC responses between clinical strains highlights the requirement for the use of primary isolates for immunogenicity studies, in place of the more popular tendency to use laboratory strains and heat inactivated bacterial samples.

This chapter investigates the genetic determinants of *S. aureus* regulating the innate immune recognition of such isolates by DC, seeking to further explore and validate our hypothesis that there is a broader correlation between antibiotic resistance and innate immune recognition by DC. Initially, the activation and phenotype of DC are compared following stimulation with broadly antibiotic susceptible strains (MSSA) and broadly antibiotic resistant strains (MRSA). Further, using multiple clinical pairs of daptomycin exposed MRSA, this chapter further demonstrates that the acquisition of daptomycin resistance results in reduced activation more generally, while highlighting that it is clearly only one of several factors regulating innate immune recognition by DC.

Nguyen and colleagues have previously demonstrated that there is a differential in the inflammatory response of a human monocytic cell line following stimuli with lab strains of diverse Staphylococcal species[219]; and that indeed these differences are due to differential expression of various lipid moieties of lipoproteins on the outer membrane leaflet[219]. Furthermore, Jiang and colleagues have recently shown that the mutations occurring in the A8819/A8817 clinical pair result in significant alterations in lipid metabolism and dramatic remodelling of the plasma membrane[194]. Taken together these findings provide precedent for altered immunogenicity between bacterial isolates based upon the composition of the cell membrane. Using the A8819/A8817 clinical pair as a model, this chapter concludes with a brief characterisation of the genetic determinants which facilitate the reduced capacity to induce activation of DC.

4.1 Antibiotic resistance is correlated with poorer immune recognition of *S. aureus* by DC

4.1.1 Clinical MSSA isolates induce superior cytokine secretion by all DC subsets

Considering the novel differential in DC activation following stimulation with the A8819/A8817 MRSA clinical pair, we next sought to elucidate whether the activation of DC in response to clinical isolates correlated more broadly with that isolates level of antibiotic resistance. Preliminary data from our initial titration experiments suggested that indeed the secretion of both RANTES and IFN-β was far superior in response to broadly antibiotic susceptible isolates of *S. aureus* (MSSA), in comparison with the broadly resistant MRSA isolates previously characterised (figure 3.4). We therefore sought to obtain a more detailed DC phenotype, comparing activation in response to these MSSA clinical isolates (D57 and D85) with reference to the A8819 DapS MRSA clinical isolate.

In stimulating bulk unsorted FLDC populations with clinical isolates of MSSA, D57 and D85, it became clear that these isolates were able to induce a broad production of inflammatory cytokines and chemokines, far superior to that of the A8819 DapS MRSA isolate (figure 4.1a). Indeed, the MSSA isolate D85 induced more than 4-fold higher inflammatory cytokine and chemokine production by FLDC, than did the A8819 DapS MRSA isolates (figure 4.1a). While these trends were conserved for RANTES, MIP-1α, MIP-1β, IL-6, TNF-α and IFN-β, the trends were only statistically significant for RANTES, IL-6 and IFN-β (figure 4.1a). Furthermore, there was a clear differential in the secretion of the aforementioned cytokines between both the MSSA isolates, which were obtained from distinct clinical infections, highlighting the diversity in immunogenic capacity among clinical isolates- although these trends were only statistically significant for IFN-β (figure 4.1a).

We next considered the immunostimulatory capacity of these strains on sorted *ex vivo* splenic DC subsets. In contrast to the findings that only the cDC1 differentially respond to the A8819/A8817 MRSA clinical pair, we found that all three DC subsets were able to produce substantially more MIP-1α, MIP-1β, TNF-α and MDC in response to MSSA stimuli than they were MRSA stimuli (figure 4.2). Indeed, the amount of inflammatory cytokine produced by these DC subsets in response to the MSSA strains D85 and D57 ranged

between 2 and 10-fold higher that observed for the DapS A8819 MRSA isolate (figure 4.2). Importantly, both cDC1 and cDC2 secreted abundant cytokine and chemokine in response to MSSA isolates, while the contribution of pDC remained relatively poor (figure 4.2), findings which are consistent with the previous observations described for the *ex vivo* splenic DC throughout chapter three.

Given the magnitude of cytokine secretion in response to the MSSA isolates D85 and D57, both by bulk FLDC (figure 4.1) and sorted *ex vivo* splenic DC (figure 4.2), we next considered whether the MSSA isolates were able to induce greater surface activation of DC than the MRSA clinical isolates. Despite the differences in cytokine secretion, upregulation of the surface activation markers (CD80 and MHC-II) and checkpoint inhibitory molecules (PD-1 and PD-L2) was only subtly different between the MRSA and MSSA stimuli (figure 4.3). Indeed, the MSSA isolate D57 was able to induce only equivalent expression of CD80, MHC-II, PD-L1 and PD-1 than the MRSA isolate A8819 on average (figure 4.3b). Intriguingly, the D85 MSSA isolate was not able to elicit DC surface activation equivalent to the D57 isolate, on average or in experimental replicates (figure 4.3a and b), despite its capacity to elicit more potent cytokine secretion by FLDC (figure 4.2).

Of particular surprise, the pDC consistently upregulated CD80, PD-1 and PD-L1 to higher levels following stimulation with the MRSA isolate A8819 than they did following stimulation with either of the two MSSA clinical isolates (figure 4.3a and b). Indeed, the MSSA isolate D85, which induced the highest secretion of MIP-1α, MIP-1β and TNF-α by pDC (figure 4.2), conversely induced the lowest expression of CD80, PD-L1 and PD-1 markers (figure 4.3a and b). Furthermore, the MSSA isolate D57 induced lesser expression of these surface markers by pDC than did the MRSA isolate A8819; although surface marker expression following stimulation with D57 was not equivalent to that induced with D85 (figure 4.3 a and b).

Importantly, the survival of each DC subset in response to MSSA D85 was approximately 2-fold higher than in response to the D57 MSSA and A8819 MRSA isolates in these experiments (data not shown). These findings therefore suggest an inverse correlation between surface activation and viability. Moreover, these findings likely explain the differential in DC cytokine secretion elicited by the MSSA isolates. Yet considering survival in response to the MSSA D57 and MRSA A8819 isolates were approximately

equivalent (data not shown), it is therefore clear that the differences in cytokine secretion between MSSA and MRSA isolates are due to factors other than DC survival.

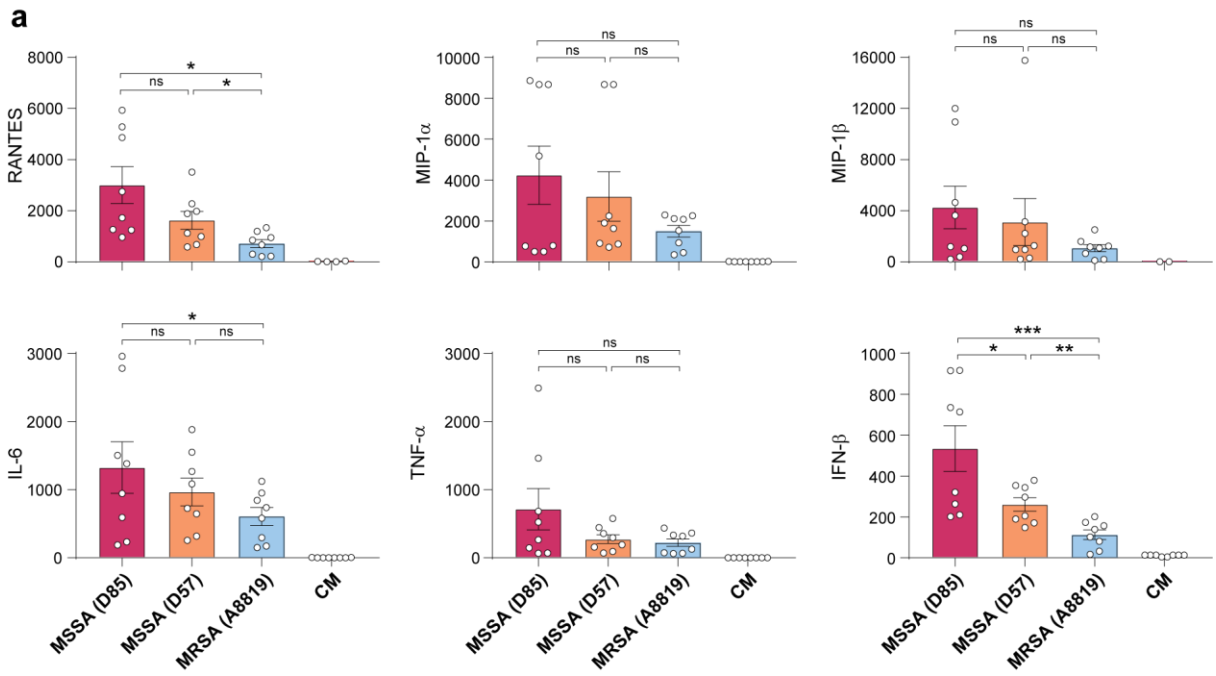

Figure 4.1 MSSA clinical isolates induce potent secretion of pro-inflammatory cytokines, chemokines and interferon by bulk FLDC.

(a) Cytokine production (pg/ml) by bulk FLDC at 18 hour post stimulus with unrelated MSSA clinical isolates (D57 and D85), daptomycin susceptible MRSA (A8819) at an MOI of 10, or complete media (CM). Bars show the mean and SEM of eight individual FLDC preparations (biological replicates; hollow circles), pooled from three independent experiments (n = 8). Significance reflects the results of a one-way ANOVA using Tukey's test to correct for multiple comparisons; whereby degree of significance is defined by $p \leq 0.05$ (*), $p \leq 0.01$ (**) and $p \leq 0.001$ (***); whilst non-significance (ns) is defined by $p > 0.05$.

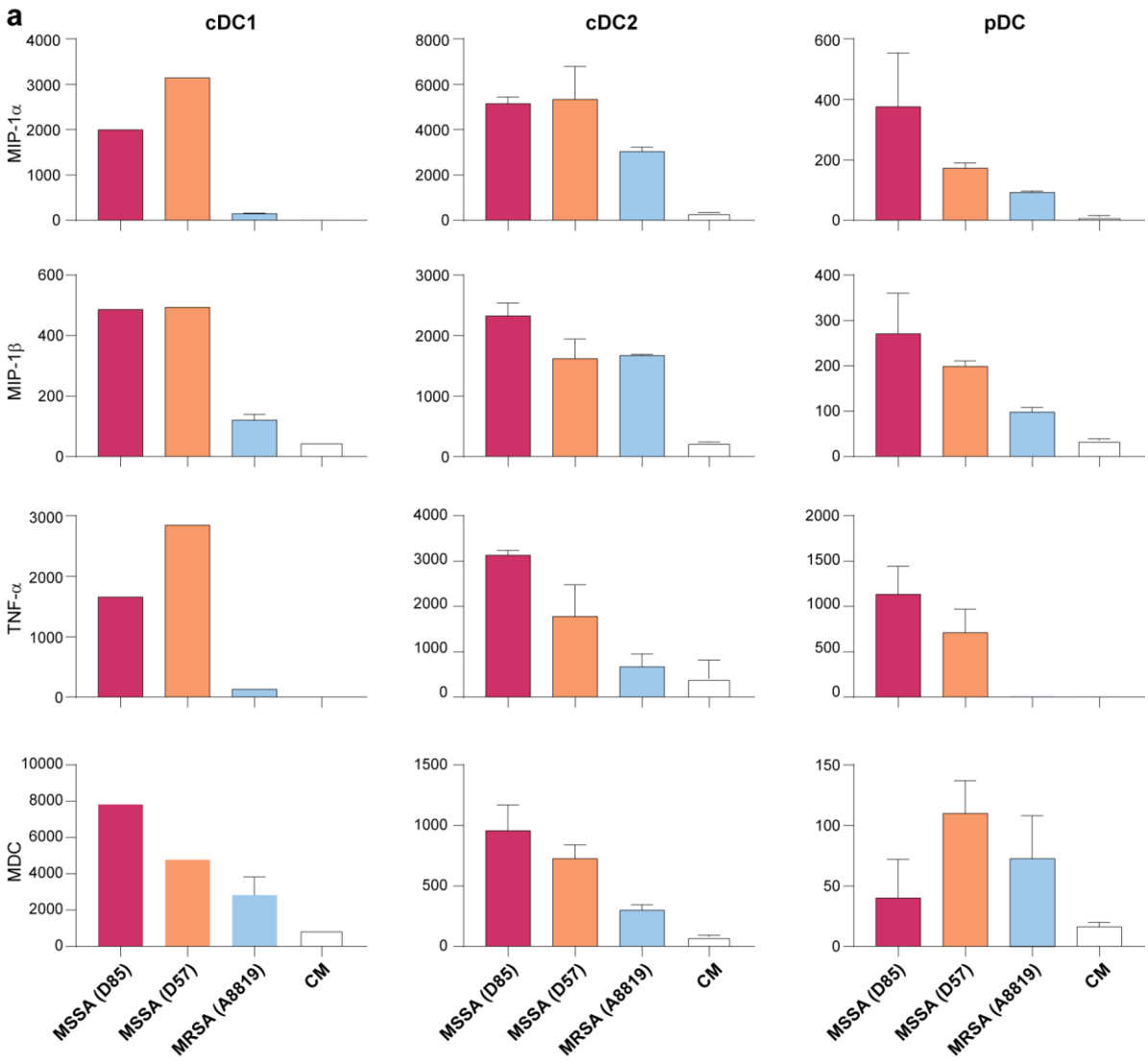

Figure 4.2 MSSA clinical isolates induce potent secretion of pro-inflammatory cytokines and chemokines by sorted splenic DC.

(a) Cytokine production (pg/ml) by FACS sorted splenic cDC1, cDC2 and pDC at 18 hour post stimulus with unrelated MSSA clinical isolates (D57 and D85), daptomycin susceptible MRSA (A8819) at an MOI of 10, or complete media (CM). Error bars (where indicated) show the mean and range of two technical replicates from one experiment (n = 1). Error bars not shown for cDC1 stimulations with MSSA isolate whereby there were no technical replicates. Trends representative of two independent experiments (n = 2).

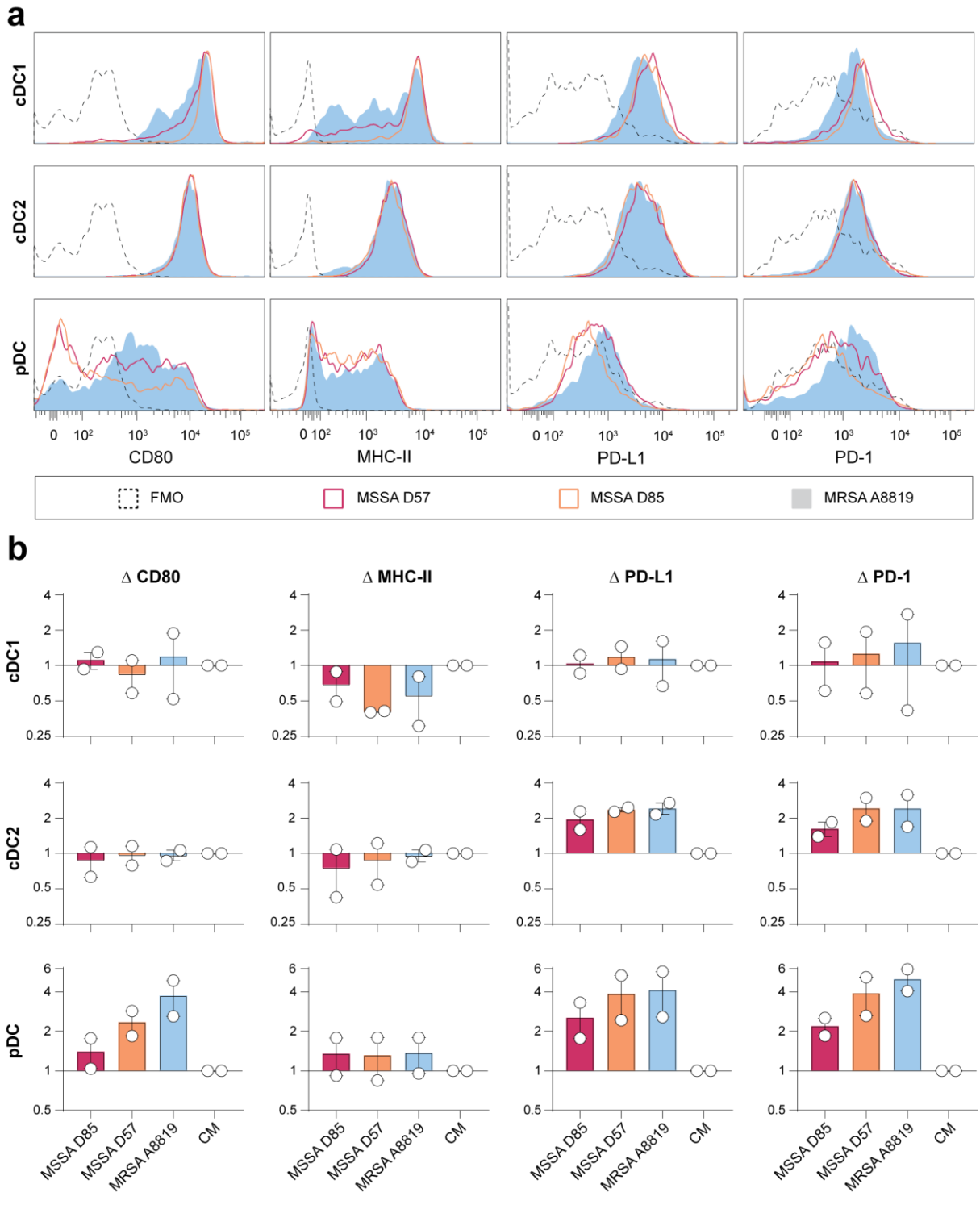

Figure 4.3 Both MRSA and MSSA clinical isolates induce similar surface activation of FACS sorted splenic DC.

(a) *Expression of surface activation markers CD80 and MHC-II, and checkpoint inhibitor molecules PD-1 and PD-L1 by FACS sorted splenic cDC1, cDC2 and pDC at 18 hours post stimulus unrelated MSSA clinical isolates (D57, red histogram; and D85, blue histogram) and daptomycin susceptible MRSA (A8819, light grey shaded) at an MOI of 10. FMO controls represent pooled samples consisting of all DC subsets with each stimuli (dotted black histogram).* ***(b)*** *Fold change from CM in expression of activation and*

checkpoint inhibitory markers by splenic DC stimulated as in 'a'. Fold change in expression quantified as difference in geometric mean fluorescence intensity (gMFI) from 18 hour stimuli in CM for each of the described stimuli, as in 'a'. Bars show the mean and range of two biological replicates (hollow circles), pooled from two independent experiments (n = 2).

4.2 Mutations affecting *S. aureus* phospholipid biosynthesis are associated with altered immune recognition by DC

It is clear from the results in section 5.1, that there is substantial diversity in immunogenicity of MRSA and MSSA clinical isolates. Importantly, the observed trends indicate more potent immunogenic potency of MSSA isolates when compared to MRSA isolates. Moreover, the trend of resistance to the last line antibiotic daptomycin leading to inferior immunogenicity, as described in chapter 3, was largely recapitulated with the vancomycin exposed clinical pair A8090/A8094.

While it is therefore clear that the innate recognition of these vancomycin exposed clinical isolates are differentially regulated; the accumulation of 35 point mutations required to achieve intermediate resistance make it difficult to model the mechanisms regulating the innate recognition of this pair. Therefore, the remainder of this chapter will instead continue to focus on the mutations regulating the innate recognition of the daptomycin exposed clinical pair A8819/A8817, alongside four other clinically distinct daptomycin exposed pairs. In the acquisition of resistance, each of these clinical pairs accumulates between two and nine point mutations, making them a more useful model for the mechanisms regulating immunogenicity (table 2.4).

The clinical characteristics of these strains, and the mutations accumulating in the resistant isolates have previously been described (table 2.4). Critically, in the acquisition of resistance each of these pairs acquire a unique mutation in *mprF*; and three of these five pairs further acquire a unique mutation in *cls2.* We are therefore able to organise these clinical pairs into two useful subgroups: those with mutations in *mprF* alone, and those with mutations in both *mprF* and *cls2.* As it has previously been shown that each of these mutations are associated with an increase in resistance to daptomycin[158]; and given their respective roles in phospholipid metabolism these genes are likely candidates to be involved in the regulation of innate recognition.

4.2.1 Mutation of the *cls2* and *mprF* genes in DapR MRSA isolates are associated with reduced DC activation

Given the differential immunogenicity of the A8817/A8819 clinical pair (chapter 3), we first sought to investigate the broader relationship between the acquisition of

daptomycin resistance mutations occurring in clinical isolates and their inflammatory potential. Having previously identified differential expression of surface activation markers in response to MRSA isolates is largely restricted to CD80 (chapter 3 and figure 4.16), we first compared expression of CD80 on FACS sorted FL-cDC1 populations stimulated with the panel of 5 daptomycin exposed clinical pairs (figure 4.4).

Of interest, the differential expression of CD80 by FLDC subsets observed in response to the A8819/A8817 clinical pair (chapter 3 and figure 4.4), were not fully recapitulated in response to stimulation with the A9719/A9744 or A9763/A9764 clinical pairs (figure 4.4a), which were similarly grouped based on acquisition of mutations in both *cls2* and *mprF.* Nonetheless, these pairs exhibited subtle differential in the induction of CD80 by FLDC, with a slight peak shift and increase in gMFI, most obvious for cDC1 and pDC, following stimuli with the DapS parent strain (figure 4.4). By contrast, the pairs grouped with mutations in *mprF* alone, A8796/A8799 and A9753/A9754, showed either no change in CD80 expression or an increase in CD80 expression following stimulation with the DapR daughter strain (Figure 4.4a). Collectively, these data suggest, that *cls2* plays a role in the regulation of DC activation as measured through CD80 expression following bacterial stimulation.

Having previously established that FL-cDC1 dominate the inflammatory response to MRSA (chapter 3, figure 3.8a), we next considered their capacity to secrete cytokine chemokine and IFN in response to the panel of Dap exposed clinical pairs. Importantly, despite the subtle differences in the expression of CD80 by cDC1 following stimulation (figure 4.4), there was substantial diversity in the secretion of inflammatory cytokines and chemokines by following stimulation with each of these isolates (figure 4.5). Indeed, three of the five clinical pairs corresponding A9719/A9744, A897/A8799 and A9754/A9757 were poorly immunogenic inducing negligible secretion of almost all pro-inflammatory cytokines and chemokines by cDC1 (figure 4.5); while the two remaining pairs, corresponding A8819/A8817 and A9763/A9764, induced more potent secretion of these inflammatory mediators (figure 4.5). Importantly, both MDC and IFN-β were produced in approximate equivalence in response to all five of the daptomycin exposed clinical pairs (figure 4.5). This trend is consistent with the previous findings of chapter three; whereby reduced MDC and IFN-β induction by MRSA did not correlate with the acquisition of daptomycin resistance. Collectively, these findings suggest that the

regulation of MDC and IFN-β secretion by cDC1 share a similar pathway independent of the other pro-inflammatory cytokines and chemokines.

The poor immunogenicity of select clinical pairs prior to the acquisition of daptomycin resistance (figure 4.5), suggests that isolates of *S. aureus* may lose immunogenicity under selective pressures of the host in the absence of antibiotics. Nonetheless, the finding that the acquisition of daptomycin resistance can reduce immunogenicity of clinical isolates was clearly demonstrated with the A8819/A8817 clinical pair (chapter 3 and figure 4.5), and is further recapitulated with the A9763/A9764 clinical pair (figure 4.5). In both instances the DapS parent isolate was moderately immunogenic compared to MSSA, and lost immunogenicity with the acquisition of daptomycin resistance (figure 4.5). Importantly, in the instance of both of these clinical pairs, the DapR isolates with reduced immunogenic potential contain single amino acid point mutations in the *cls2* and *mprF* genes (figure 4.4 and 4.5).

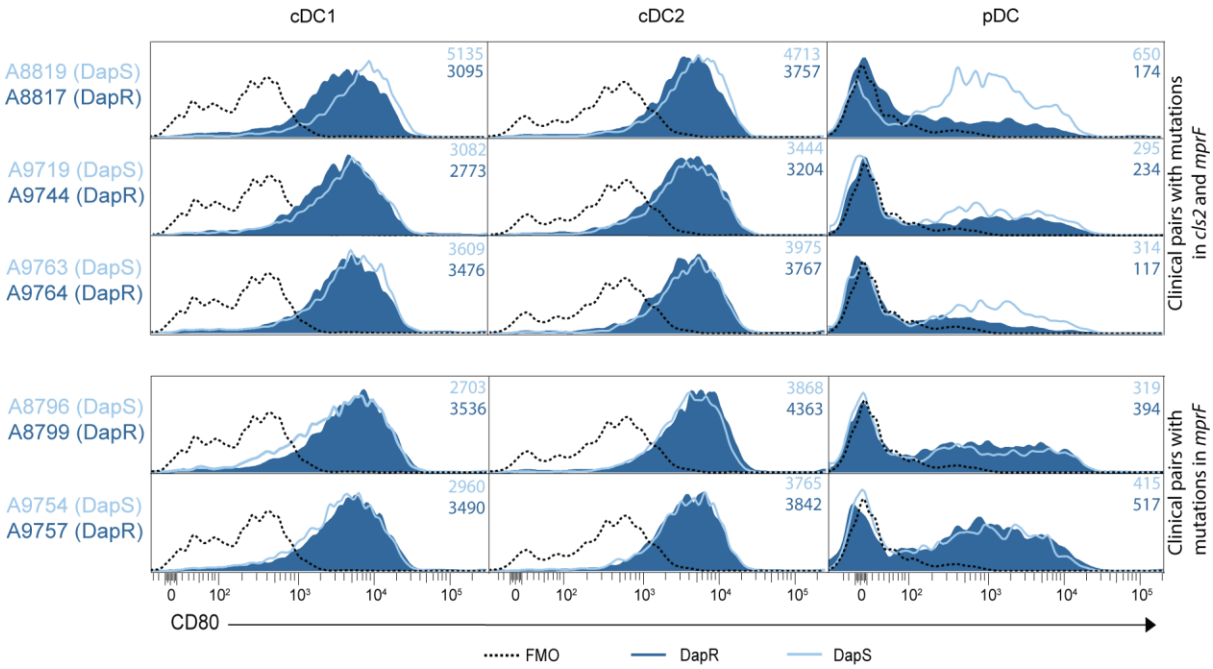

Figure 4.4 CD80 expression by FLDC following stimulation with five paired daptomycin exposed MRSA clinical isolates.

CD80 staining of sorted FLDC subsets following 18 hours stimuli of DC with DapS (green trace) and DapR (dark grey shaded) MRSA clinical isolates at an MOI of 10 (dark grey shaded), media alone (black trace) and FMO control (dashed black trace). MRSA isolates correspond A8819/A8817, A9719/A9744, A9763/A9764, A8796/A8799, A9754/A9757 clinical pairs. Data shown from one experiment for cDC2 and pDC (n = 1), and representative of two independent experiments for cDC1 (n = 2).

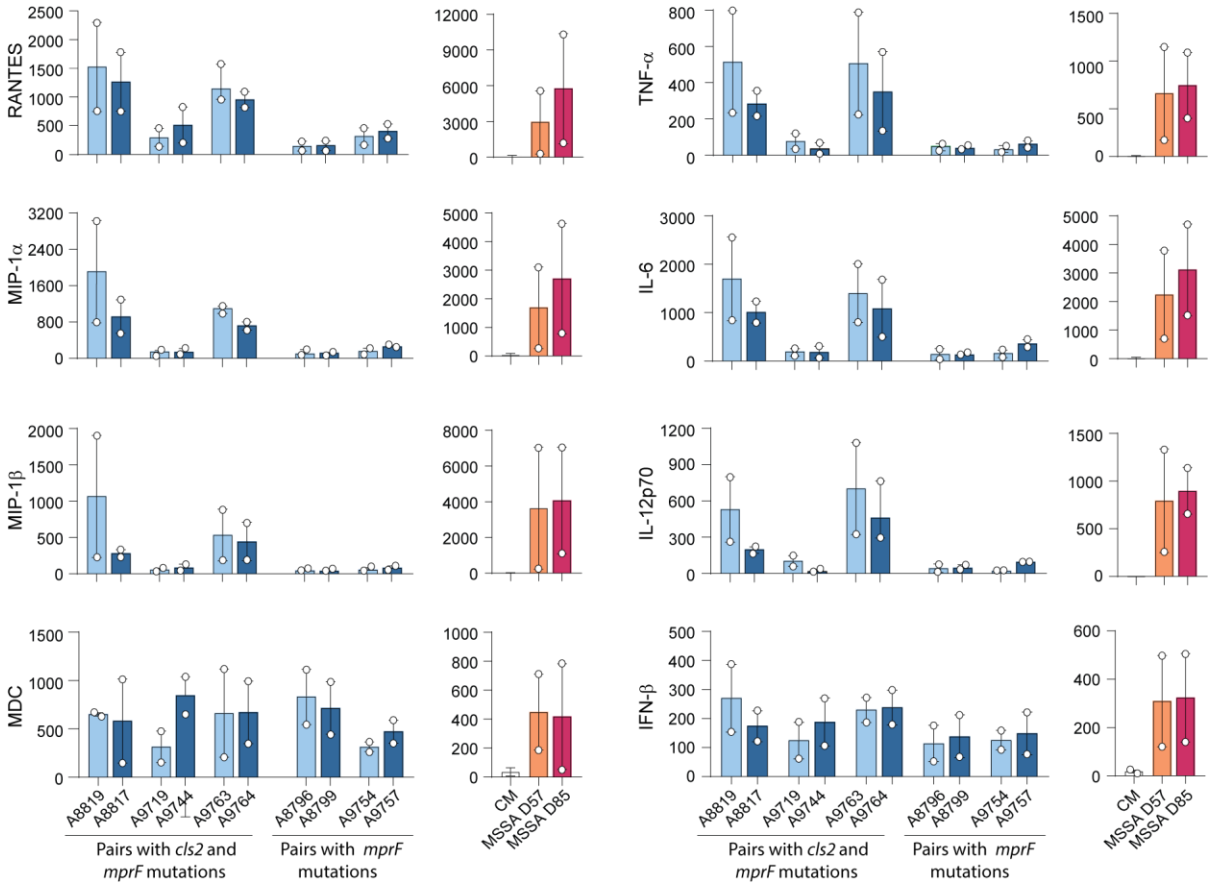

Figure 4.5 FLDC activation following stimulation with five pairs of daptomycin exposed MRSA clinical isolates.

Cytokine, chemokine and IFN secretion (pg/ml) by FACS sorted FL-cDC1 at 18 hours post stimuli with paired clinical isolates of daptomycin exposed MRSA (MOI = 10), distinct clinical isolates of MSSA (MOI = 10), and media alone. Bars show the mean and range of cytokine secretion quantified from two independent experiments (n = 2).

4.2.2 Daptomycin resistance significantly affects surface activation of DC in response to both the A8819/A8817 and A9763/A9764 clinical pairs

Having shown that A9763/A9764 clinical pair differentially induces activation of FLDC (figure 4.4 and 4.5), we next sought to validate these findings in primary splenic DC. In analysing the surface phenotype of FACS sorted splenic cDC1 responding to this pair, we observed no differential in the expression of CD40, CD80, MHC-II, PD-1 or PD-L1 (figure 4.6 and 4.7). These findings are consistent with the preliminary data shown for FL-cDC1, whereby the A9763/A9764 did not induce differential expression of CD80, unlike the A8819/A8817 clinical pair (figure 4.4). Of note, the expression of both PD-1 by splenic cDC1 was subtly increased in response to the A9763 parent strain when compared to the DapR A9764 daughter strain (figure 4.6), although these differences were not statistically significant (figure 4.6).

In contrast to splenic cDC1, the cDC2 exhibited lower overall expression of all analysed markers (figure 4.6 and 4.7). Importantly, the cDC2 upregulated the checkpoint inhibitory molecule PD-1 to significantly higher levels following stimulation with the DapS A9763 isolate than following stimulation with the DapR A9764 isolate (figure 4.7). These trends were clearly recapitulated for PD-L1, although not found to be statistically significant with a notable lower *n* (figure 4.7). Moreover, a subtle increase of CD80 expression in response to DapS A9763 (Figure 4.6), but this again was not statistically significant through repetition (figure 4.7).

Unlike the cDC subsets, splenic pDC exhibited a clear differential expression of CD80, PD-1 and PD-L1 in response to both the A8819/A8817 and A9763/A9764 clinical pairs (figure 4.6). In all instances these differences were statistically significant (figure 4.7), except for PD-L1 upregulation in response to the A9763/A9764 pair; whereby the trend was consistently observable across independent experiments, but not found to be statistically significant (figure 4.7). It therefore clear, that while the surface activation of DC is relatively consistent following stimuli with clinically distinct isolates of MRSA (figure 4.7), the expression of PD-1 and CD80 by pDC, and to a certain extent cDC2, are differentially regulated in response to these pairs (figure 4.6 and 4.7).

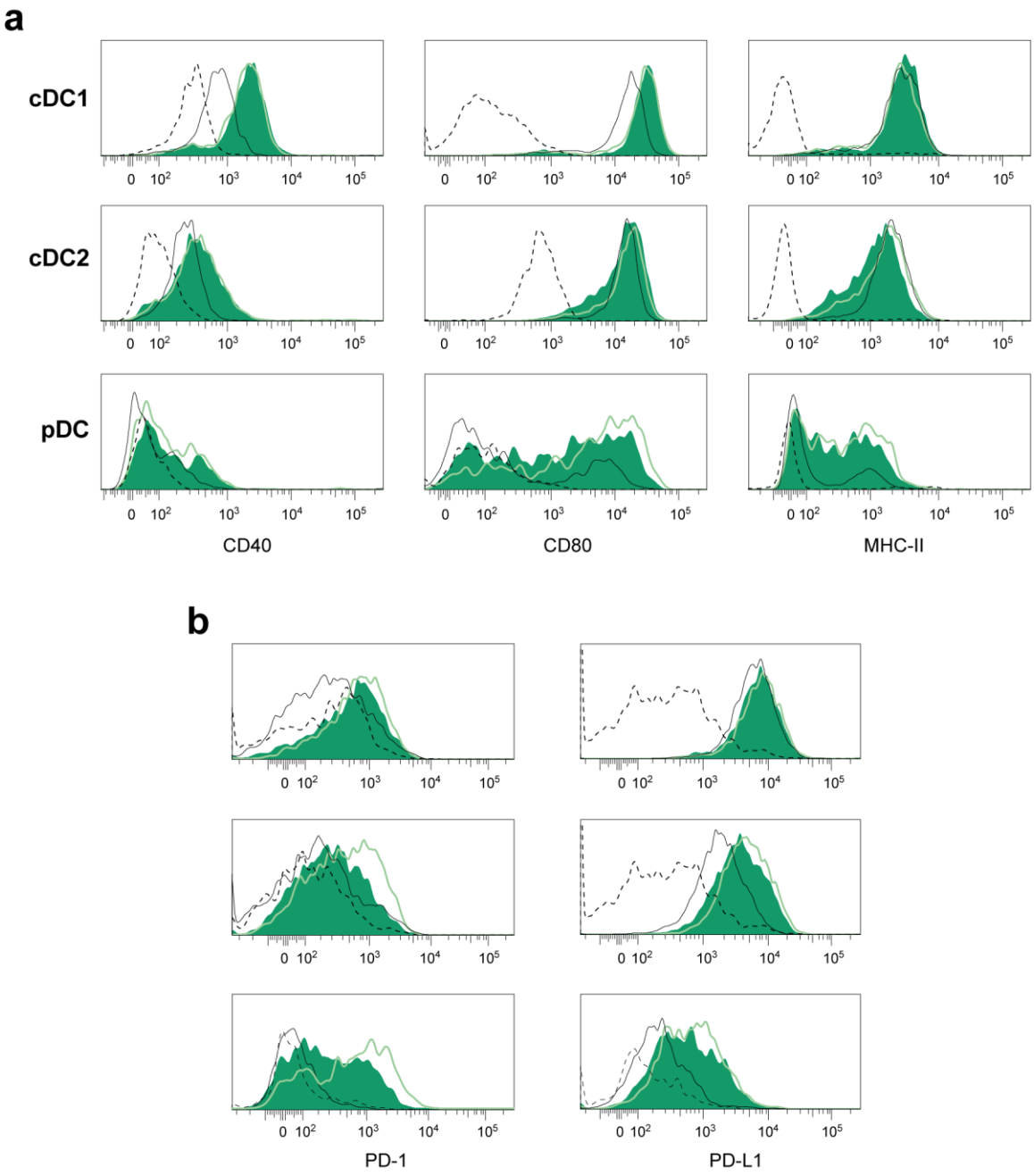

Figure 4.6 Acquisition of daptomycin resistance in the A9763/A9764 clinical pairs differentially regulates surface activation of pDC.

(a)*Expression of surface activation markers CD40, CD80 and MHC-II (gMFI) by FACS sorted splenic DC at 18 hours post stimulus with live daptomycin exposed paired clinical MRSA isolates, at an MOI of 10, or media alone (CM; black trace). MRSA isolates correspond daptomycin sensitive (A9763; light green trace) and resistant (A9764; dark green shaded) strains. FMO controls (dotted black trace) representative of pooled stimuli stain for each sorted DC subset. Data shown from one experiment representative of up to seven independent experiments (CD40; n = 3), (CD80; n = 7), (MHC-II n = 4).* ***(b)*** *Expression of surface checkpoint inhibitory molecules PD-1 and PD-L1 (gMFI) by FACS sorted splenic DC stimulated for 18 hours, as in 'a'. FMO are representative of pooled stimuli stain for each sorted DC subset, with the exception of PD-L1 FMO for cDC which are representative of pooled stimuli from cDC1*

and cDC2. Data shown from 1 experiment, representative of up to seven independent experiments (PD-1; n = 7), (PD-L1; n = 3).

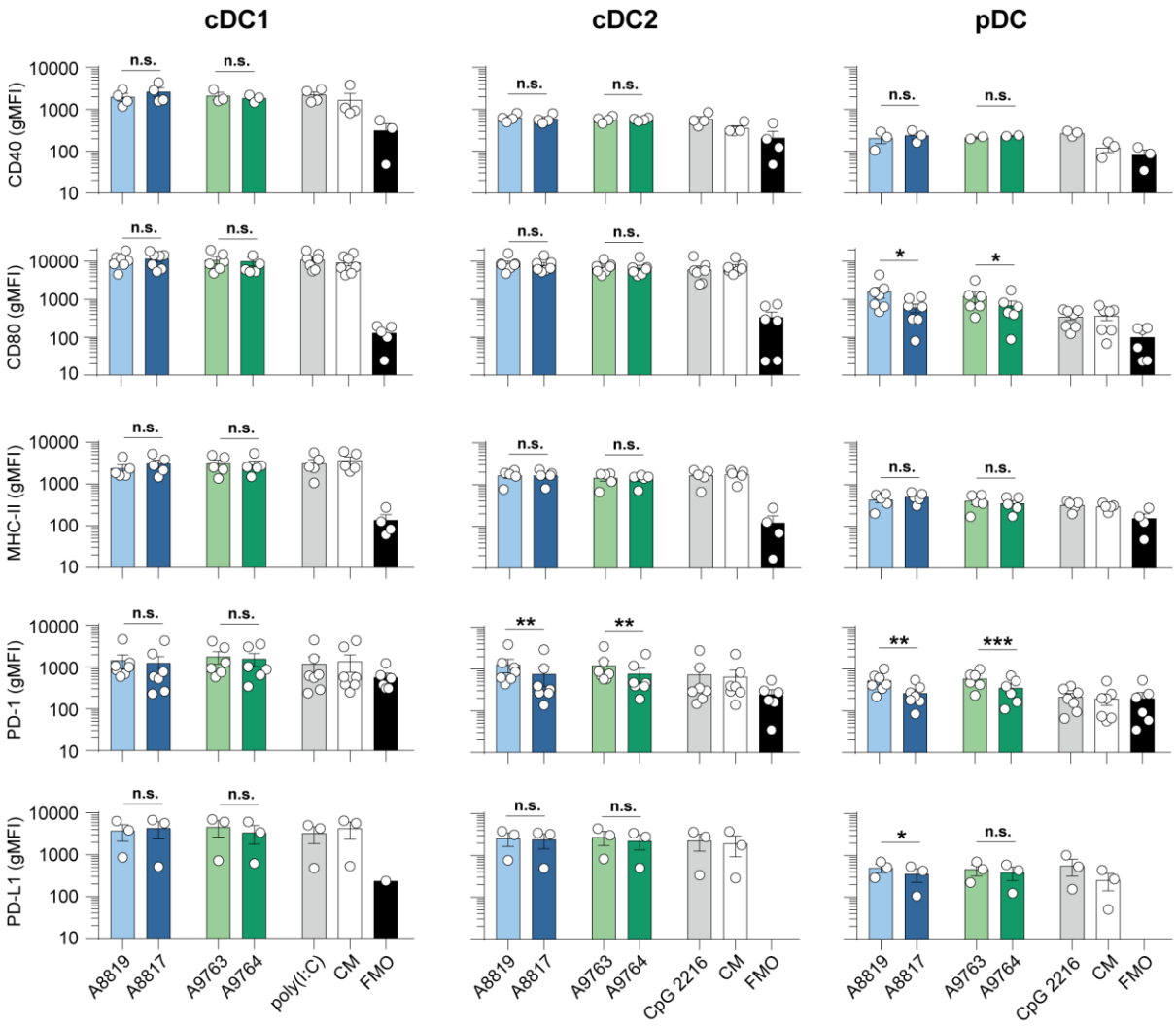

Figure 4.7 Acquisition of daptomycin resistance in the A8819/A8817 and A9763/A9764 clinical pairs differentially regulates surface activation of pDC.

Expression of surface CD40, CD80, MHC-II, PD-1 and PD-L1 (gMFI) by FACS sorted splenic DC at 18 hours post stimulus with live daptomycin exposed paired clinical MRSA isolates, at an MOI of 10, poly(I:C) (100 µg/ml), CpG ODN 2216 (0.5 µM) or media alone (CM). MRSA isolates correspond daptomycin sensitive (A8819 and A9763) and resistant (A8817 and A9764) strains. FMO controls representative of pooled stimuli for each sorted DC subset, and not shown for clarity on cDC2 and pDC charts for PD-L1 having a gMFI of less than 10. Significance representative of a paired two-tailed t-test, whereby $p < 0.05$ (*), $p < 0.01$ (**), $p < 0.01$ (***), or $p > 0.05$ (n.s.). Bars show the mean and SEM of between biological replicates (hollow circles) pooled from between 3 and seven independent experiments as indicated.

4.2.3 Daptomycin resistance significantly reduces cytokine secretion by DC in response to the A8819/A8817 and A9763/A9764 clinical pairs

We have previously shown that of the five daptomycin exposed clinical pairs tested, only the A8819/A8817 and A9763/A9764 clinical pairs are strong stimulators of cytokine secretion by FL-cDC1 (Figure 4.5). We therefore next sought to phenotype these strains relative capacity to induce cytokine secretion by primary splenic DC (figure 4.8). Consistent with the cytokine secretion observed by FL-cDC1 (Figure 4.5), it became clear that the 9763/A9764 clinical pair induced superior secretion of cytokine by splenic cDC1 when compared to the A8819/A8817 pair (figure 4.8).

Critically, the A9763/A9764 clinical pair further induced a differential secretion of cytokines by all three splenic DC subsets (figure 4.8). These findings are in stark contrast to the cytokine secretion by both splenic and FLDC subsets following stimulation with the A8819/A8817 clinical pair; whereby differential secretion was largely mediated by the cDC1 subset (figures 3.8a, 3.10, and 4.8). While not always statistically significant, these trends were most clear for TNF-α, IL-6, MIP-1a and IFN-β, whereby stimulation with the DapS A9763 strain tended to induce more abundant secretion by each DC subset than did the DapR A9764 isolate (figure 4.8).

Strikingly, the production of IL-6 and TNF-a by cDC1 following stimulation with the DapS A9763 isolate was often double that produced following stimulation with the DapR A9764 isolate in experimental replicates (figure 4.8). These trends were recapitulated, although to a lesser extent for MIP-1α, MIP-1β and IFN-β (figure 4.8). Similar to cDC1, the splenic cDC2 produced more TNF-α, IL-6, MIP-1α and IFN-β in response to the DapS A9763 isolate than the DapR A9764 isolate (figure 4.8), and these findings proved statistically significant for both TNF-α and IL-6 (figure 4.8). Yet, in contrast to the other cytokines, production of MIP-1β by cDC2 was equivalent in response to both A9763/A9764 across all experimental replicates (figure 4.8).

Similar to both cDC subsets, secretion of TNF-α, MIP-1α and IFN-β by pDC tended to be lower following stimulation with the DapR A9764 isolate when compared to the DapS parent strain (figure 4.8). However, unlike the cDC subsets this trend was not recapitulated for IL-6 (figure 4.8). Of particular interest, the secretion of MDC was significantly lower in response to the DapR A9764 clinical isolate when compared to the

DapS parent strain (figure 4.8). This finding is especially noteworthy given that we have not previously observed any correlation between MDC secretion and daptomycin resistance in bulk or FACS sorted, splenic or FLDC subsets in our analysis of the A8819/A8817 clinical pair (figures 3.7, 3.8, 3.10 and 5.8). Cumulatively, these data suggest distinct mechanisms regulating the innate recognition of distinct clinical isolates of daptomycin exposed pairs.

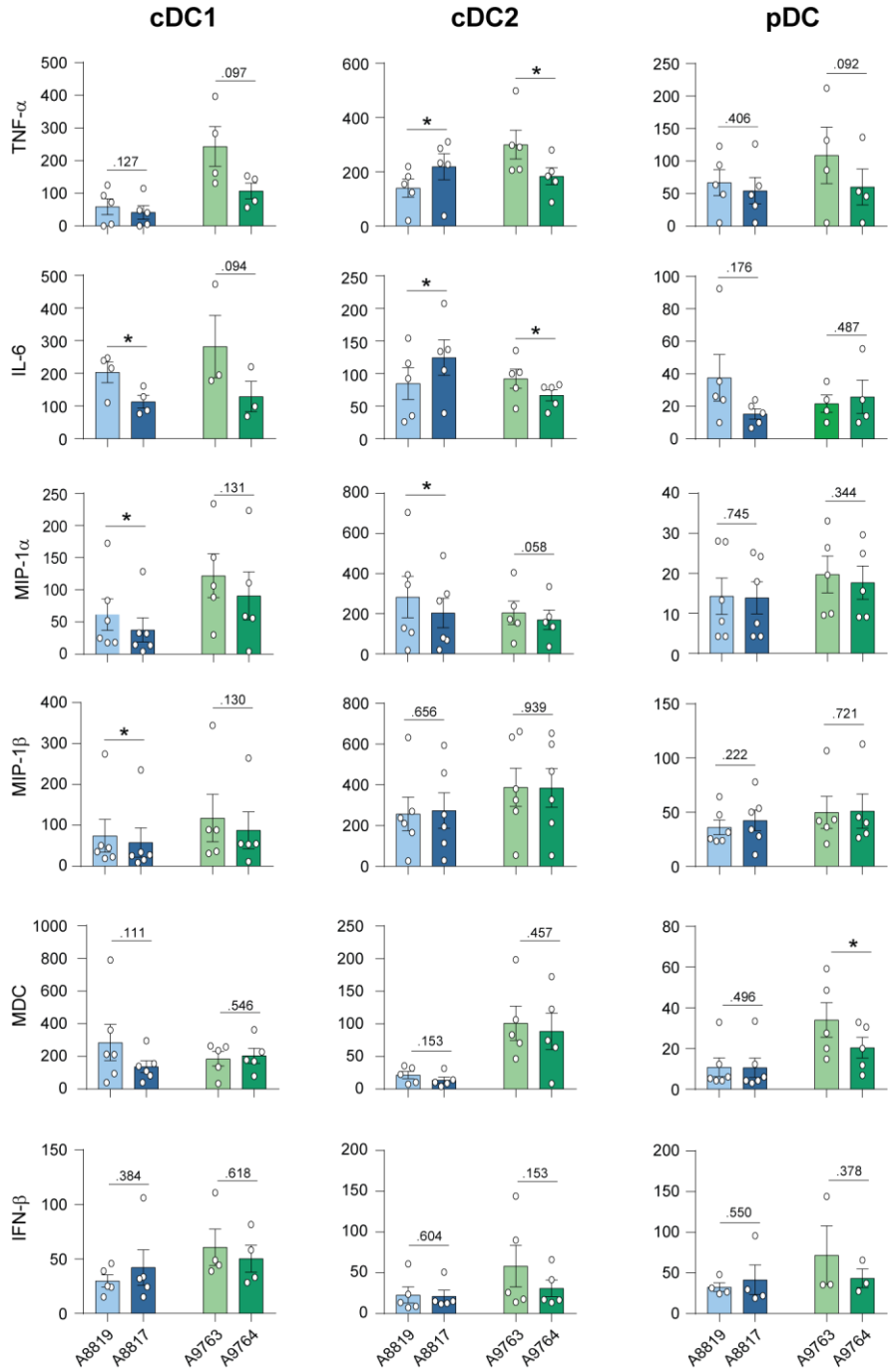

Figure 4.8 Acquisition of daptomycin resistance in the A8819/A8817 and A9763/A9764 clinical pairs differentially impedes cytokine secretion by splenic DC.

Cytokine secretion (pg/mL) by FACS sorted splenic DC at 18 hours post stimulus with live daptomycin exposed paired clinical MRSA isolates, at an MOI of 10. MRSA isolates correspond daptomycin sensitive (A8819 and A9763; green) and resistant (A8817 and A9764) strains. Significance representative of a paired two-tailed t-test, whereby p < 0.05 (*), and p-values reported to three significant figures for non-significant findings. Bars show the mean and SEM of between 3 and 6 biological replicates (hollow circles) from independent experiments (n = 3-6).

4.3 Point mutations in both *cls2* and *mprF* genes are responsible for differential activation by DC

4.3.1 Individual recreation of DapR point mutations in the A8819 DapS isolates impairs innate recognition by FLDC

Having found that the acquisition of daptomycin resistance impedes the immunogenicity of DapR MRSA isolates A8817 and A9764 (figures 3.7, 3.8, 3.10, and figures 4.5, 4.6, and 4.8 respectively), we next sought to investigate the mutations regulating the differential recognition of these bacterial isolates by DC. Both the A8817 and A9764 DapR clinical isolates contain genetic mutations in *cls2* and *mprF,* which have been previously shown to confer daptomycin resistance[158].

We first sought to quantify the isolated effects of each of *cls2* and *mprF* mutations, which arise in both the DapR strains A8817 and A9764. The independent role of these mutations in causing daptomycin resistance was confirmed by recreating specific DapR resistance mutations in the DapS parental strain A8819, creating $A8819_{Cls2\text{-}T33N}$ and $A8819_{MprF\text{-}T345I}$ as previously published[194,201]. We therefore stimulated bulk unsorted FLDC populations with the A8819/A8817 clinical pair, as well as the $A8819_{Cls2\text{-}T33N}$ and $A8819_{MprF\text{-}T345I}$ lab strains. Importantly, both the mutation in *cls2* and *mprF* tended to result in a significantly lesser secretion of MIP-1α, MIP-1β, RANTES, TNF-α and IL-6 by FLDC (figure 4.9). Despite the lesser secretion of inflammatory cytokines by FLDC following stimulation with each of the two point mutants when compared to DapS A8819, neither mutation in isolation was able to fully recapitulate the phenotype observed following stimulation with DapR A8817 (figure 4.9).

Having compared the capacity of these point mutants to stimulate cytokine secretion by bulk FLDC, it was apparent that $A8819_{Cls2\text{-}T33N}$ induced subtly less production of inflammatory mediators than did $A8819_{MprF\text{-}T345I}$ (figure 4.9). Importantly, $A8819_{Cls2\text{-}T33N}$ induced significantly less IFN-β production by DC than did either of the A8819/A8817 isolates (figure 4.9), which we have previously shown do not differentially induce IFN-β production by DC (chapter 3). These findings suggest that the mutation of *cls2* in isolation, but not in combination with *mprF*, reduces the capacity of *S. aureus* isolates to induce type I IFN secretion by DC. Of note, these findings were further recapitulated in experiments on sorted FL-cDC1 (appendix A4-1), which we have previously shown to be the dominant

inflammatory mediators in this system (figure 3.8). Indeed, we found that A8819$_{Cls2\text{-}T33N}$ tended to induce lesser secretion of MIP-1α, MIP-1β, TNF-α, IL-6, IL-12p70 and IFN-β, than did A8819$_{MprF\text{-}T345I}$, both on average and in most independent replicates (Appendix A4-1). Collectively, these data support a dominant role for the mutation of *cls2* in altering the immunogenicity of the A8819/A8817 clinical pair, whilst highlighting that the mechanism by which the *cls2* and *mprF* point mutations regulate immunogenicity of these isolates are likely distinct.

In order to confirm that the differential cytokine secretion induced by the *cls2*-T33N and *mprF*-T345I point mutants are genuine, and not a result of reduced DC survival, we next compared the viability of the sorted FLDC subsets in response to these stimuli. Critically, the survival of all FLDC subsets in response to stimulation to the poorly immunogenic A8819$_{Cls2\text{-}T33N}$ strain was greater than following stimuli with both the DapS A8819 parent and the DapR A8819$_{MprF\text{-}T345I}$ lab strain (appendix A4-1). It is therefore clear, that the differential in cytokine secretion in response to these point mutants is not an artefact of DC viability, but would rather be increased when considered on a per cell basis. Of note, the survival of FLDC subsets following stimulation with A8819$_{Cls2\text{-}T33N}$ was similar to that of A8817; whilst the survival following stimuli with A8819$_{MprF\text{-}T33N}$ was similar to that of A8819 (appendix A4-1). Therefore, these trends suggest that the viability of FLDC following stimuli with these isolates is inversely correlated with their inflammatory capacity.

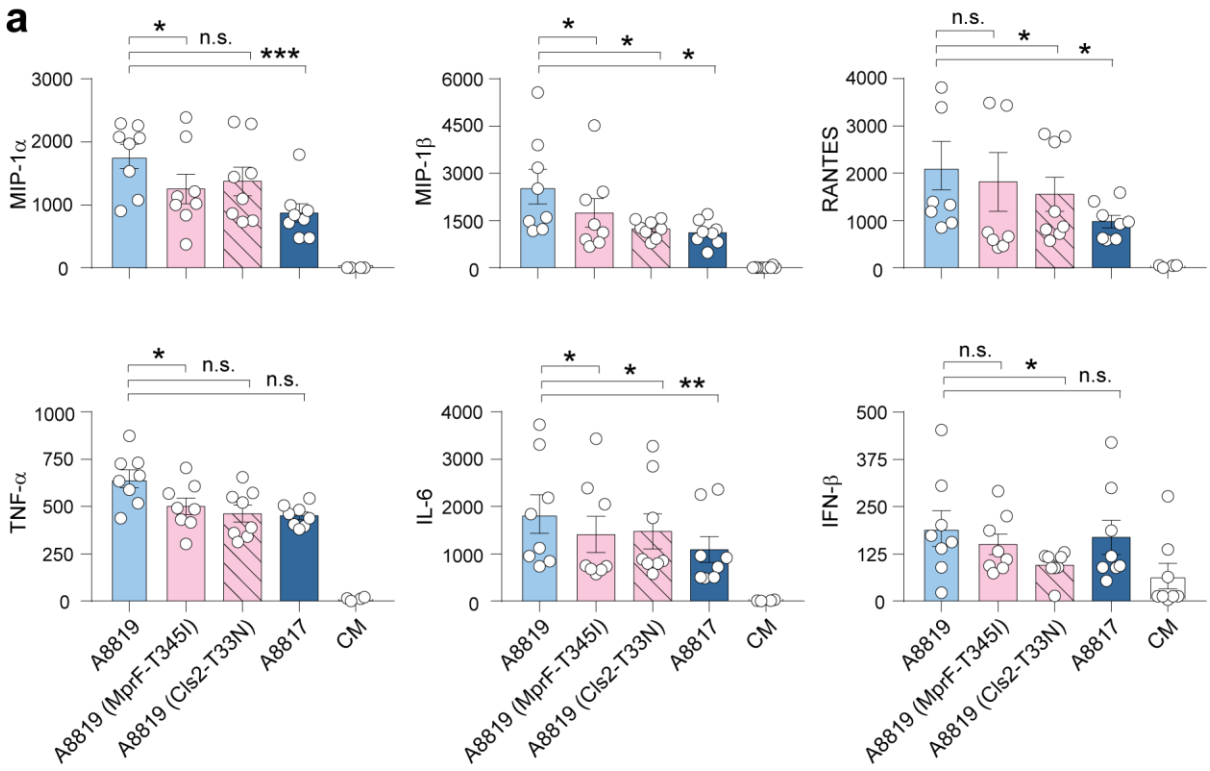

Figure 4.9 Recreation of daptomycin resistance mutations Cls2-T33N and MprF-T345I in the DapS parent strain reduces cytokine secretion by FLDC

(a) *Cytokine secretion by bulk FLDC following 18 hour stimulus with A8819 and A8817 MRSA clinical isolates, A8819$_{Cl2\text{-}T33N}$ and A8819$_{MprF\text{-}T345I}$ strains (MOI=10). Data show the mean and SEM of replicates from 8 individual mouse FLDC preparations (n = 8), pooled from three independent experiments. Significance shown as * P < 0.05, ** P < 0.005, *** P < 0.001 from a paired two-tailed t-test.*

Having established that both *cls2*-T33N and *mprF*-T345I point mutations influence the capacity of *S. aureus* isolates to elicit cytokine responses from DC (figure 4.9 and Appendix A4-1), we next considered the role of the mutations in regulating the expression of the co-stimulatory marker CD80. The recreation of the *cls2* mutation in $A8819_{Cls2\text{-}T33N}$, but not the *mprF* mutation in $A8819_{MprF\text{-}T345I}$, resulted in lesser upregulation of CD80 by cDC1, cDC2 and pDC, than did stimulus with the DapS A8819 isolate (figure 4.10a, 4.10b and 4.10c). Importantly, the recreation of the mutation of *mprF* alone did not result in a visible peak shift in CD80 expression by any DC subsets (figure 4.10a), whereas by contrast the mutation in *cls2* alone induced a peak shift in CD80 expression for all DC subsets, most discernible for cDC1 (figure 4.10b). While these trends were replicated for each FL-cDC subset in each independent experiment with a ~20% decrease in gMFI (figure 4.10c), statistical significance was only achieved for the pDC with more than a 50% decrease in CD80 gMFI (figure 4.10c).

While we observed a clear decrease expression of CD80 by each FLDC subset following stimulation with the $A8819_{Cls2\text{-}T33N}$ point mutant compared to the DapS A8819 isolate, the resultant phenotype did not fully recapitulate that produced in response to the DapR A8817 isolate for any DC subset (figure 4.10b and 4.10c). It is therefore clear that while the mutation in *cls2* has the most dominant impact on CD80 expression by FLDC, it is on its own insufficient to fully recapitulate the phenotype observed in response to the DapR A8817 isolate. Given that the *mprF*-T345I mutation has no discernible impact on CD80 expression by FLDC, it seems likely that the DapR phenotype is likely resultant either from the combination of these two mutations acting in synergy, or a combination of other factors not investigated here.

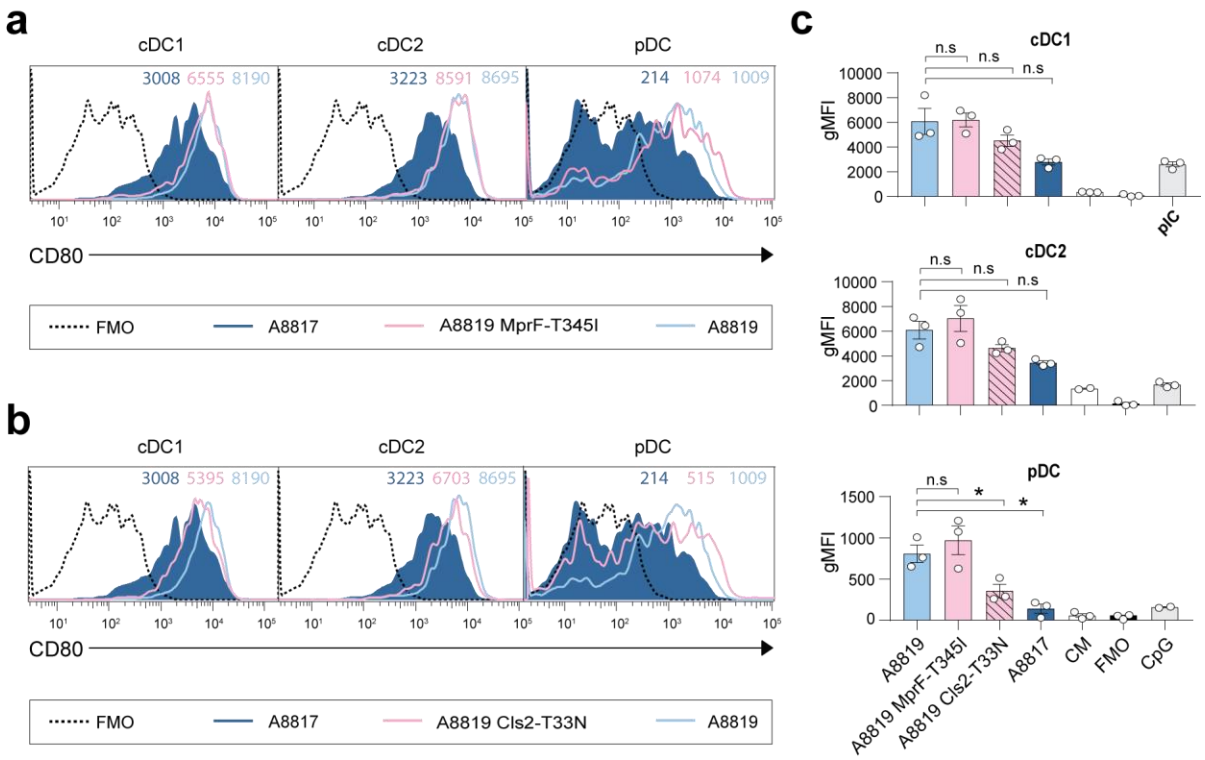

Figure 4.10 Figure 4.10 Cls2-T33N but not MprF-T345I mutations reduce impede CD80 upregulation by FLDC subsets

(a,b) *Histogram overlays showing CD80 expression by FACS sorted FL-cDC1, cDC2 and pDC after 18 hours stimulus with paired daptomycin exposed MRSA isolates A8819 (DapS; light blue trace) and A8817 (DapR; dark blue shaded), a lab strain of DapS A8819 MRSA recreated for the cls2 point mutation T33N (panel a; light pink trace) and the mprF point mutation T345I (panel b; light pink trace). FMO controls represent pooled DC subsets taken from each experimental stimulation (dotted black trace). Data representative of three independent experiments (n = 3).* ***(c)*** *Geometric mean fluorescence intensity (gMFI) of CD80 expression by DC subsets as shown in 'a', showing the mean and SEM of expression pooled from three independent experiments. Significance shown as * p < 0.05, ** p < 0.01, *** p < 0.001 from a one-way ANOVA using Tukey's test to correct for multiple comparisons.*

4.3.2 Distinct mutations of the Cls2 transmembrane domain regulate the immunogenic potential of *S. aureus* clinical isolates

The previous results demonstrate that mutations in *cls2* and *mprF* are both able to modulate innate detection of clinical bacterial isolates by DC, the mechanisms by which this occurs remain unclear. However, it is clear that the *cls2*-T33N more prominently affects DC activation than does the *mprF*-T345I point mutation (figures 4.9, 4.10 and Appendix A4-1). While A8819$_{\text{MprF-T345I}}$ expresses the mutation derived from the DapR daughter strain of the A8819/A8817 pair[194,201]; our attempts to recreate the *cls2* point mutation occurring in A8817 (*cls2*-F60S), have so far been unsuccessful[194]. The *cls2*-T33N point mutation expressed in A8819$_{\text{Cls2-T33N}}$ is derived from an unrelated MRSA clinical isolate following *in vitro* exposure to daptomycin[158,194].

This *cls2*-T33N mutation is of clinical relevance as it was found to arise independently in two distinct reference strains of MRSA exposed to daptomycin *in vitro*[158]. Moreover, both *cls2*-T33N and a distinct mutation arising in the A9719/A9744 pair during clinical exposure to daptomycin, *cls2*-A23V, are mapped to the same transmembrane domain (TMD), TMD-1, of the Cls2 protein (figure 4.11). Critically, the *cls2*-T33N, *cls2*-A23V alongside a third *cls2*-L52F mutation arising from the A9763/A9764 clinical pair, have been shown to similarly increase membrane cardiolipin content in the membrane of DapR isolates[194]. These findings demonstrate a highly conserved gain-of-function mechanism by which these mutations reduce daptomycin susceptibility, and therefore very likely perturb innate recognition by DC.

Despite the lack of success recreating the A8817 *cls2*-F60S mutation in the A8819 parent strain; the *cls2* point mutation arising A9764, *cls2*-L52F, has been successfully recreated in the A8819 isolate, creating A8819$_{\text{Cls2-L52F}}$[194]. Given that both the L52F and F60S mutation both arise in TMD-2, unlike T33N in TMD-1 (figure 4.11), we next considered whether the recreation of L52F mutation would similarly impede DC activation in comparison the A8819 DapS strain. Indeed, splenic cDC1 produced lesser overall TNF-α, IL-6, MIP-1α and MIP-1β in response to A8819Cls2-L52F than they did the DapS A8819 isolate (figure 4.12), both on average and in all biological replicates except for one replicate for MIP-1a (figure 4.12) – although these findings were not statistically significant. Nonetheless, these findings therefore demonstrate that distinct mutations

arising in different transmembrane domains of Cls2, can similarly impede the immunostimulatory potential of clinical *S. aureus* isolates.

In addition to the capacity of the L52F point mutation to modulate cytokine secretion by cDC1 when recreated in A8819 (figure 4.12), this mutation subtly reduced surface expression of PD-1, but not CD80 (figure 4.13). These results are consistent with our previous data showing that unlike FL-cDC1, splenic cDC1 surface activation is largely unaffected in response to the A8819/A8817 and A9763/A9764 daptomycin exposed clinical isolates. By contrast, both cDC2 and pDC exhibited a lesser expression of PD-1 in response to $A8819_{Cls2\text{-}L52F}$ than they did the A8819 parent, both on average and in each biological replicate (figure 4.13). Of no surprise to us, we further found that the expression of PD-1 by pDC and cDC2 in response to $A8819_{Cls2\text{-}L52F}$ was significantly increased compared to that observed in response to A9764 (figure 4.13). These results highlight that the differences in immunogenicity between unrelated clinical isolates cannot be fully accounted for by mutations in Cls2.

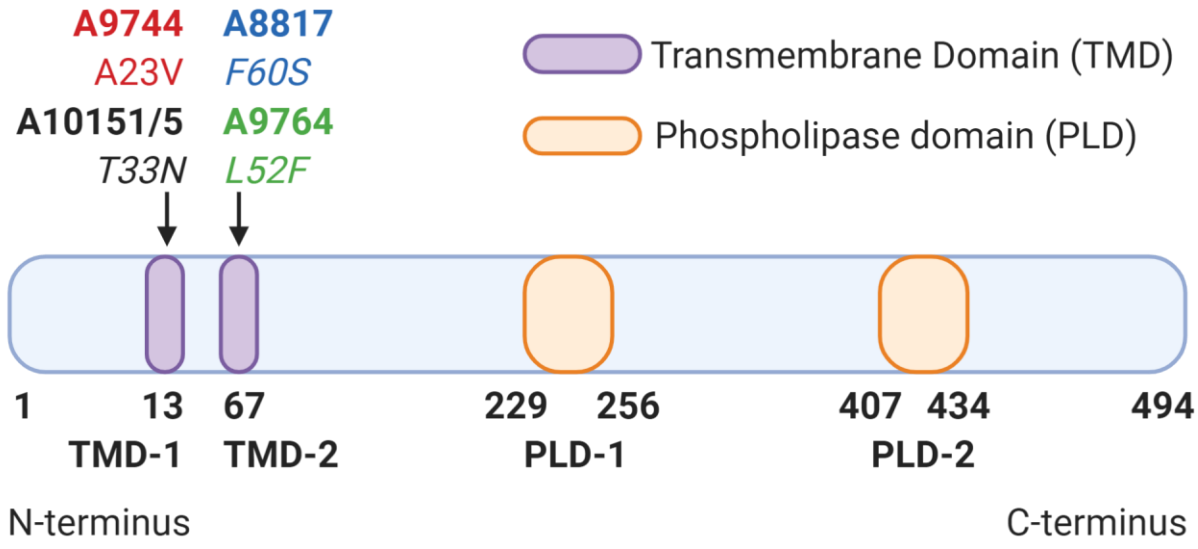

Figure 4.11 Daptomycin resistance point mutations in cls2 arise in regions coding transmembrane domains of protein.

Structure of the Cls2 protein highlighting the five point mutations previously described by Peleg et. al., (2012)[158]. Each of the identified point mutations were mapped to one of the two predicted transmembrane domains (TMD; purple). The A23V (red), F60S (blue) and L52F (green) point mutations arose in clinical isolates exposed to daptomycin in vivo, and are shown below each of the bolded DapR strain from which they were sequenced; being A9744, A8817 and A9764 respectively[158]. The T33N mutation (black) arose in two independent reference strains of exposed to daptomycin in vitro, and is shown below the name of the strains from which it was sequenced; A10151 and A10155 respectively. This figure was created with BioRender at 'www.biorender.com'. Adapted from Peleg et. al., (2012)[158].

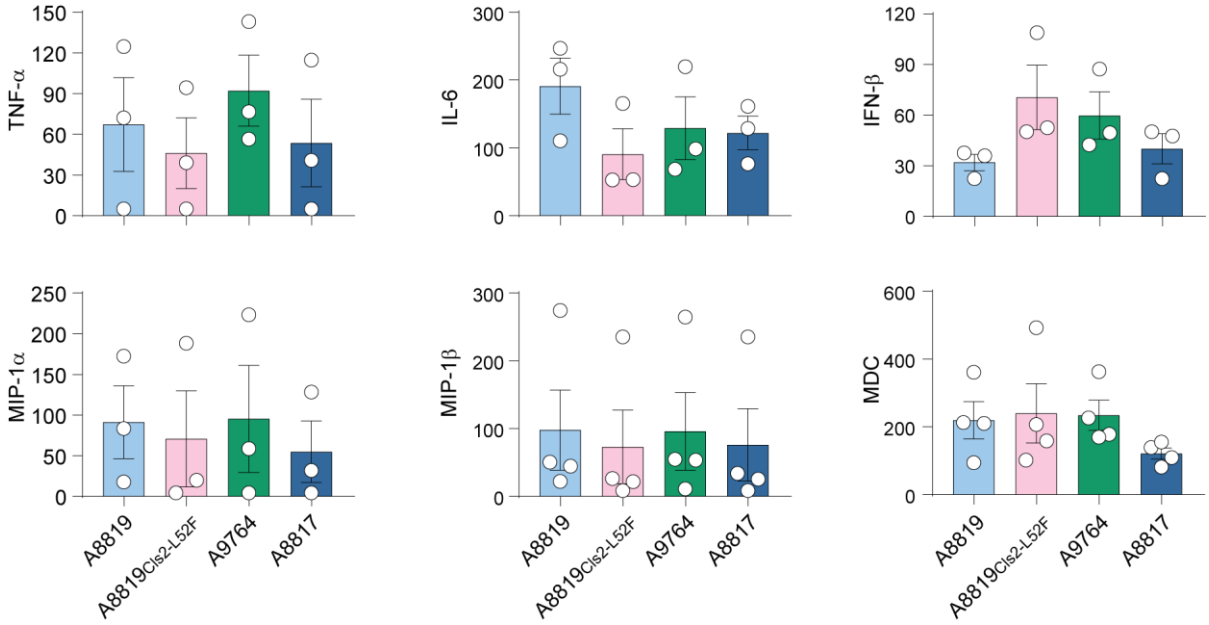

Figure 4.12 Cytokine secretion by splenic cDC1 is impaired following stimulation with A8819 strain recreated for Cls2-L52F point mutations, respective to both A8819 and A9764 isolates.

Cytokine secretion (pg/mL) by splenic cDC1 following 18 hour stimulus with A8819 and A8817 MRSA clinical isolates, laboratory strains of A8819 recreated for the T33N point mutation in cls2 (A8819$_{Cls2\text{-}T33N}$), and the A8819$_{Cls2\text{-}T33N}$ mutant strain restored to wild-type (A8819$_{Cls2\text{-}T33NN33T}$) at an MOI of 10. Data show the mean and SEM of biological replicates (hollow circles) pooled from between three and four independent experiments (n = 3-4).

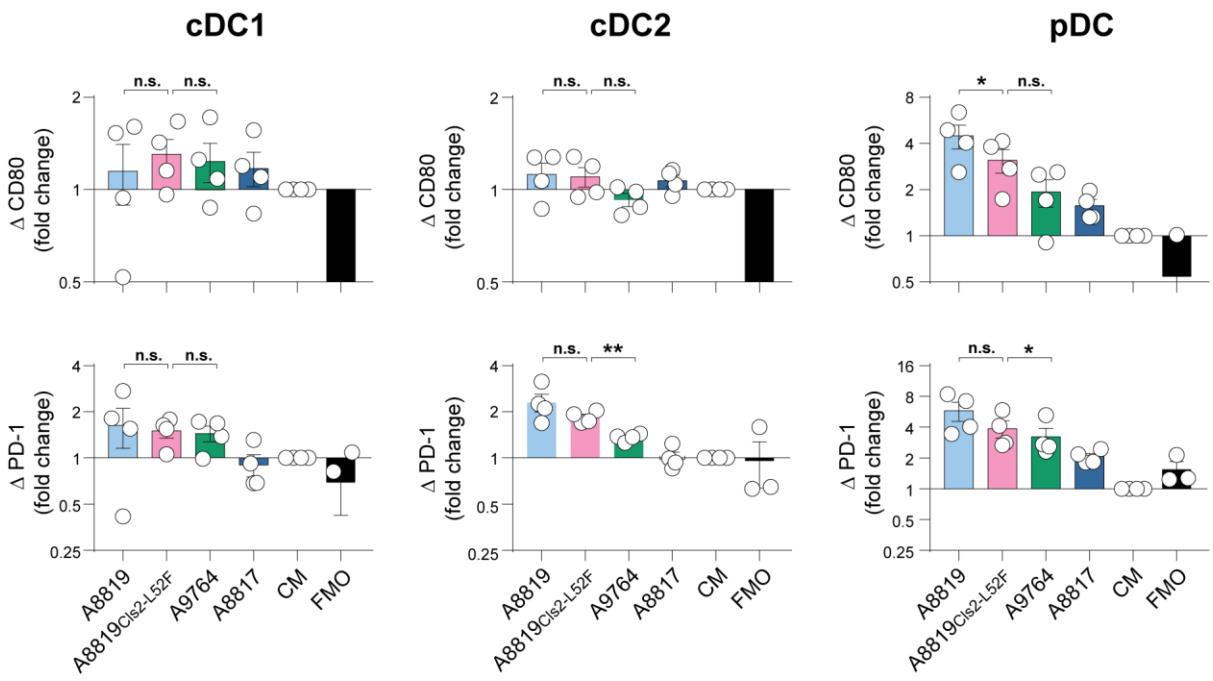

Figure 4.13 Surface expression of CD80 and PD-1 by pDC is impaired following recreation of the Cls2-L52F point mutation in A8819.

*Fold change in geometric mean fluorescence intensity (gMFI), of CD80 and PD-1 surface expression by sorted splenic DC following 18 hour stimulus with A8819 and A9764 clinical isolates, the laboratory strains of A8819 recreated for the L52F point mutation in cls2 occurring in A9764 ($A8819_{Cls2\text{-}L42F}$), or media alone (CM). Fold change calculated as fold difference in gMFI between each sample stimuli and stimulus with CM at 18 hours. Fluorescence minus one (FMO) controls are representative of pooled stimuli for each DC subset. Data show the mean and SEM of biological replicates (hollow circles) pooled four independent experiments as indicated (n = 4). Statistical significance represents the results of a paired two-tailed t-test; whereby * $p < 0.05$, ** $p < 0.001$, and *** $p < 0.001$.*

4.3.3 Reversion of the DapR *cls2* point mutation restores the capacity for innate recognition by DC

Having shown that the A8819$_{Cls2\text{-}T33N}$ strain exhibits a reduced capacity to stimulate cytokine secretion and CD80 upregulation by FLDC, in comparison to the A8819 parent strain (figure 4.10 and Appendix A4-1); we next sought to validate that the *cls2*-T33N point mutation regulates this phenotype, and not some other genetic difference transferred during the allelic replacement. We therefore further stimulated FLDC with both A8819, A8819$_{Cls2\text{-}T33N}$ and a reversion of this *cls2*-T33N point mutant strain, A8819$_{Cls2T33NN33T}$ (figure 4.14). Indeed, the reversion of the *cls2*-T33N point mutant to its wild-type form rescued cytokine secretion by bulk FLDC, with no significant differences between stimulation with the DapS A8819 strain and the A8819$_{Cls2\text{-}T33NN33T}$ rescue (figure 4.14a). We further considered the capacity of the *cls2* rescue strain to elicit upregulation of CD80 by FLDC subsets, and found that the rescue strain was capable of inducing CD80 expression by each subset equivalent to that of the DapS A8819 isolates (figure 4.14b).

We therefore next sought to confirm that these mutations similarly impeded recognition and activation of splenic DC. Indeed, the recreation of the *cls*-T33N, but not *mprF*-T345I point mutation, in the DapS A8819 strain, resulted in lower overall secretion of pro-inflammatory cytokine and chemokine by splenic cDC1 (Appendix A4-2). Moreover, the reversion of the *cls2* gene to wild-type was similarly able to rescue cytokine and chemokine production of splenic DC (Appendix A4-2).

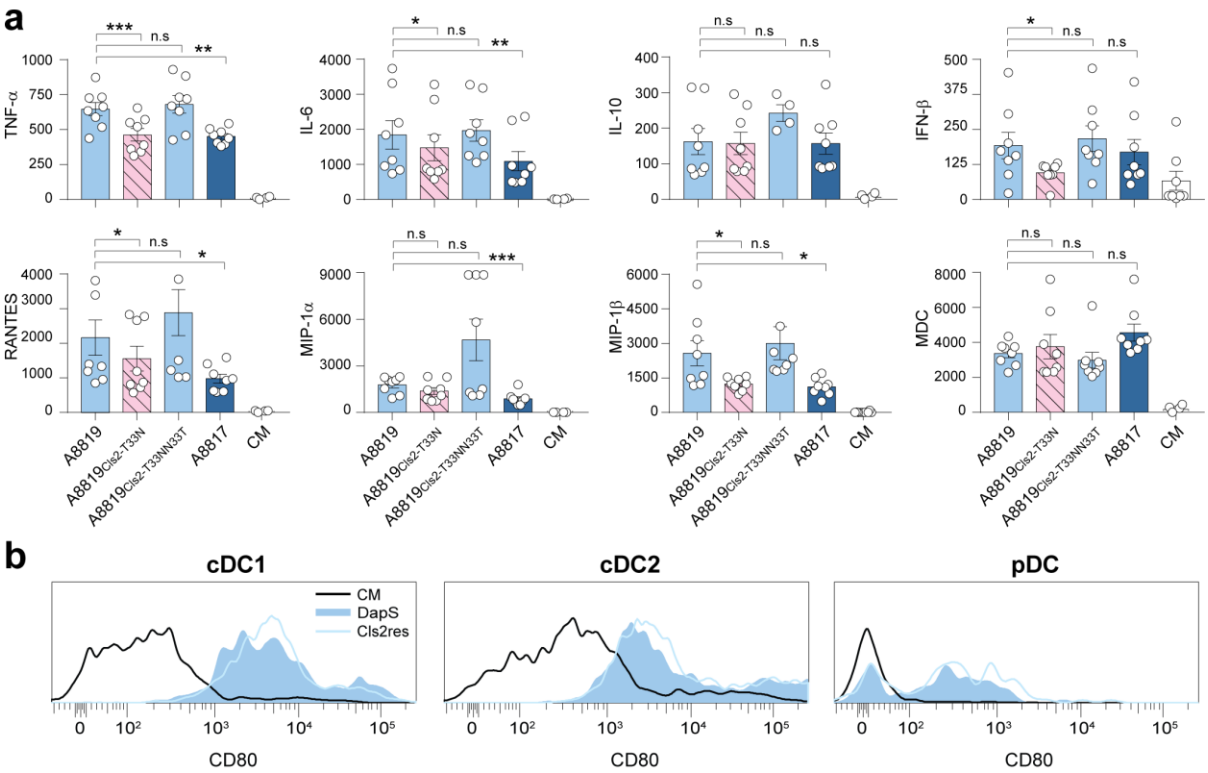

Figure 4.14 Reversion of A8819Cls2-T33N to A8819Cls2-T33NN33T restores capacity to induce potent cytokine secretion by bulk FLDC, and CD80 expression by FLDC subsets.

(a) *Cytokine secretion (pg/mL) by FLDC following 18 hour stimulus with A8819 and A8817 MRSA clinical isolates, a laboratory strain of A8819 recreated for the T33N point mutation in cls2 ($A8819_{Cls2\text{-}T33N}$) and the same strain subsequently restored to wild-type ($A8819_{Cls2\text{-}T33NN33T}$) at an MOI of 10. Data show the mean and SEM of eight biological replicates pooled from five independent experiments (n = 8). Statistical significance reflects the results of a paired two-tailed t-test, whereby; * p < 0.05, ** p < 0.01, *** p < 0.001.* ***(b)*** *Histogram overlays showing CD80 expression by FLDC subsets at 18 hour post stimulus with DapS A8819 (blue shaded histogram), the cls2 reversion strain $A8819_{Cls2\text{-}T33NN33T}$ (light blue trace) and media alone (black trace). Data shown from 1 experiment, representative of three independent experiments (n = 3).*

4.4 Resistance to the last line antibiotic vancomycin also modulates the immunogenic potential of MRSA

4.4.1 Acquisition of vancomycin resistance alters cytokine secretion by DC

Having established that broadly antibiotic susceptible isolates of *S. aureus* (MSSA) have the capacity to induce substantially greater cytokine secretion by DC than MRSA isolates, we sought to further explore the mechanisms by which the acquisition of resistance to a single antibiotic can affect the immunogenicity of clinical isolates. Given the findings of chapter 3 describing differential immunogenicity between the daptomycin exposed clinical pair A8819/A8817, we considered the immunogenicity of a distinct clinical MRSA series exposed to the last line antibiotic vancomycin. This clinical series comprises a fully vancomycin susceptible *S. aureus* (VSSA) isolate, JH1 (A8090), isolated from the blood-stream of a patient suffering congenital heart disease; and a vancomycin intermediate *S. aureus* (VISA) isolate, JH9 (A8094), isolated from the bloodstream following extensive therapy with daptomycin[239].

Given the diversity demonstrated thus far in immunogenicity between clinical isolates, we first sought to titrate these strains to confirm that the MOI of 10 is appropriate for both the daptomycin and vancomycin exposed MRSA pairs. Indeed, with stimulations of bulk FLDC with the vancomycin exposed isolates, it is clear that optimal secretion of IFN-λ occurs at an MOI of 10, with lower bacterial doses inefficiently stimulating the production of IFN-λ (Figure 4.15a). Moreover, at doses higher than an MOI of 20, both secretion of IFN-and the overall viability of the cultures was impeded (data not shown). In one experiment, cytokine and chemokine secretion by FLDC further revealed that the MOI of 10 induced superior secretion of TNF-α, IL-6, MIP-1α and MIP-1β in comparison to lower doses of both 2.5 and 0.625 bacteria per DC (Figure 4.15b).

We previously demonstrated that heat inactivation of the A8819/A8817 clinical pair impeded secretion of all examined pro-inflammatory cytokines and chemokines, with the exception of RANTES when compared to live stimuli (figure 3.7). Similarly, heat treatment of the vancomycin exposed clinical pairs seemingly inhibited secretion of IFN-λ and MIP-1α at high doses (Figure 4.15a and b), yet in contrast enhanced secretion of IL-6 and TNF-α by FLDC (Figure 4.15b).

Importantly, the acquisition of resistance to vancomycin resulted in an increased capacity of the A8094 isolate to induce secretion of TNF-a, IL-6 and MIP-1α compared to its vancomycin sensitive parent strain (Figure 4.15a), despite an impeded capacity to induce secretion of both MIP-1β and IFN-λ (Figure 4.15a and b). These trends were maintained from an MOI of 10 through to less than 1 (Figure 4.15a and b), indicating that the factors regulating the innate recognition of this A8090/A8094 clinical pair are distinct to those regulating the recognition of the A8819/A8817 clinical pair described in chapter three. These differences in innate recognition are however not surprising, given distinct clinical infections and progression of disease. Indeed, it is known that the A8817/A8819 clinical pair differ by 5 point mutations in the coding region of the genome[158], whereas, the A8090/A8094 vancomycin exposed pair differ by 35 point mutations across 31 coding loci[210]. These mutations include a combination of non-synonymous point mutations, frame-shift mutations, truncations and mutations in intergenic gene sequences[210], collectively demonstrating the potential for substantial alterations in the cell wall an membranes between these two isolates.

4.4.2 Acquisition of vancomycin resistance disrupts DC surface activation

Considering the differences in the cytokine secretion by FLDC stimulated with the 8090/A8094 vancomycin exposed clinical pair, we next sought to elucidate the effect of vancomycin on the surface activation phenotype. Similar to our previous findings showing differential expression of CD80 in response to the daptomycin exposed A8819/A8817 clinical pair, we also found that the vancomycin susceptible parent strain induced greater expression of CD80 by all DC subsets than did the vancomycin resistant daughter strain (Figure 4.16). Moreover, it was clear that cDC expression of other co-stimulatory markers CD40 and CD86, alongside MHC-II, were also subtly elevated on cDC following stimuli with the A8090 susceptible strain (Figure 4.16). Importantly, while pDC were not seen to substantially upregulate co-stimulatory markers CD40 and CD86, the expression of MHC-II was seen to be subtly upregulated following stimulus with the vancomycin susceptible parent isolate A8090, in comparison to the intermediate daughter strain (Figure 4.16).

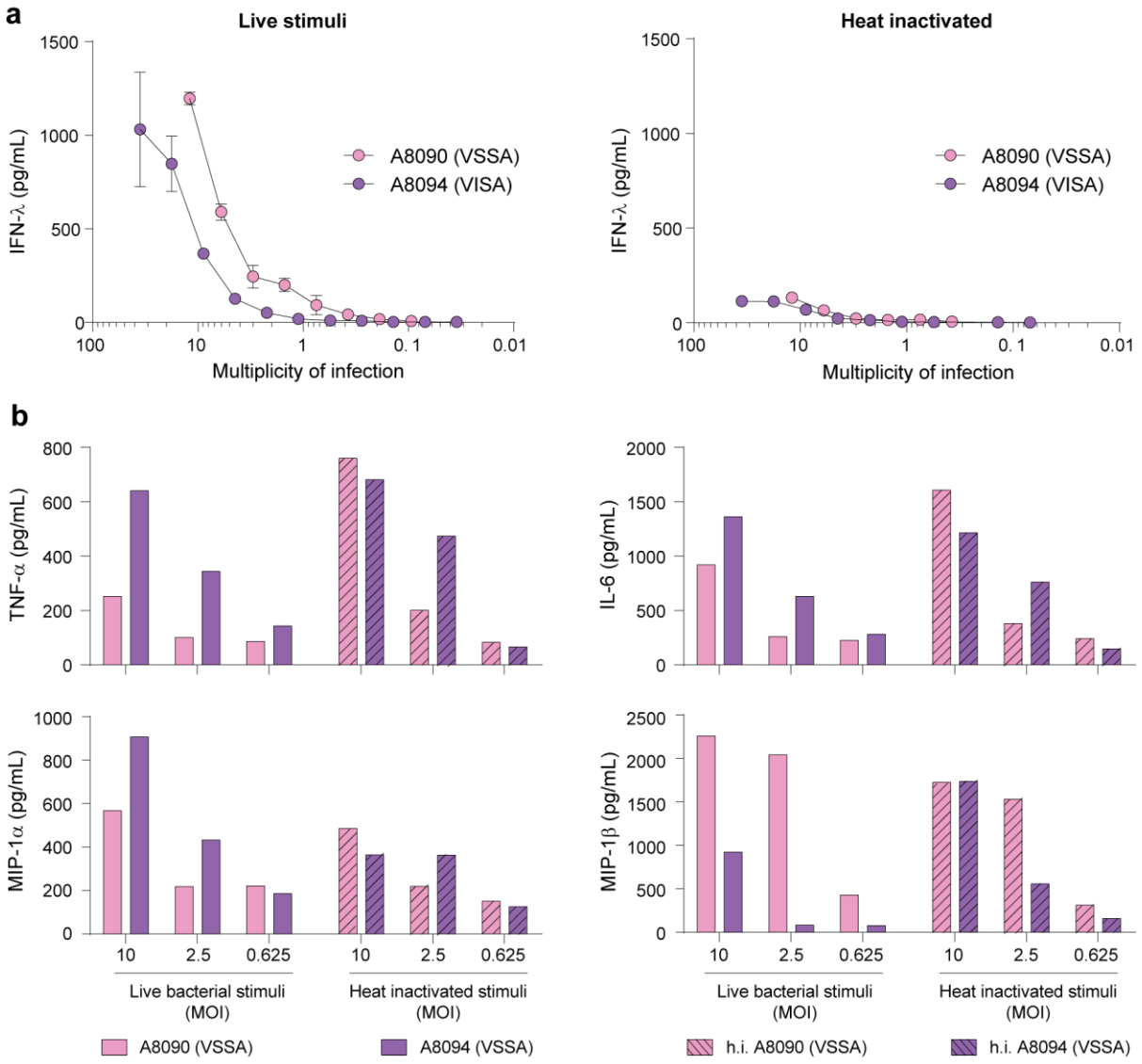

Figure 4.15 Vancomycin susceptible and intermediate clinical isolates differentially stimulate inflammatory cytokine and chemokine secretion by FLDC

(a) *Dose response showing IFN-λ secretion (pg/ml) by bulk unsorted FLDC following 18 hour stimulation with live and heat inactivated clinical isolates of vancomycin susceptible (A8090) and intermediate (A8094) MRSA. Heat inactivation of bacterial isolates was performed at 95°C for 30 minutes. Data points show the mean and range of technical replicates from 1 experiment, representative of two independent experiments (n=2). (b) Secretion of TNF-α, IL-6, MIP-1α and MIP-1β (pg/ml) by bulk unsorted FLDC following 18 hour stimulation with live and heat inactivated clinical isolates of vancomycin susceptible (A8090) and intermediate (A8094) MRSA as in 'a'. Bacterial stimuli were performed at an MOI (or equivalent for h.i. stimuli) of 10, 2.5 and 0.625. Bars show individual data points from a single experiment (n = 1).*

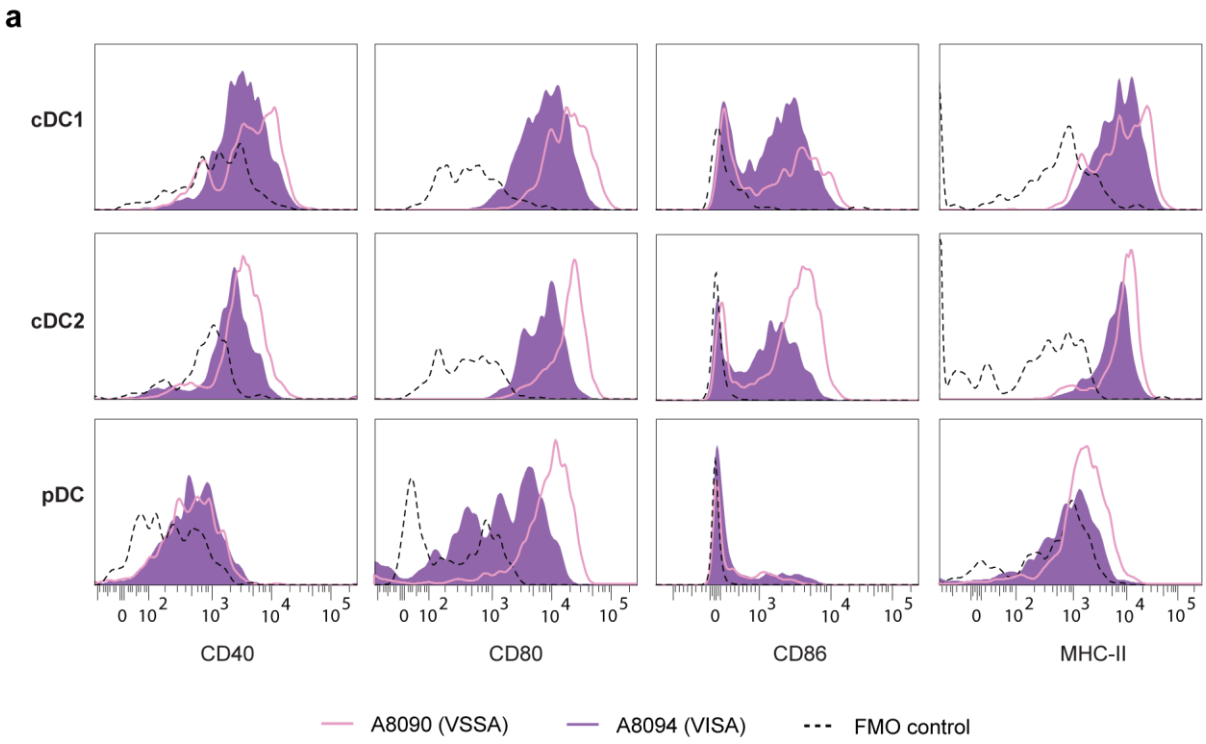

Figure 4.16 Vancomycin intermediate clinical isolate A8094 induces weaker splenic DC surface activation than does the susceptible parent strain

(a) *Surface expression of MHC-II and co-stimulatory markers CD40, CD80 and CD86 by bulk stimulated splenic DC subsets, at 18 hour post stimuli with vancomycin susceptible (A8090; light pink trace) and vancomycin intermediate MRSA (A8094; purple filled histogram) at an MOI of 10. Pooled stimuli FMO control shown for each DC subset (dotted trace). Data shown from one experiment, but representative of 3 independent experiments on bulk and sorted splenic DC (n = 3).*

4.5 Discussion

4.5.1 Staphylococcal antibiotic resistance correlates reduced immunogenicity

The findings of this chapter build upon those of chapter three; indicating a broader trend whereby the acquisition of antibiotic resistance by *S. aureus* isolates impedes the innate recognition of these strains by DC. We began this chapter with a comparison the immunostimulatory capacity of two distinct clinical isolates of MSSA with that of the previously examined DapS A8819 MRSA isolate. Previous Australian estimates indicate that mortality rates for nosocomial infections with MRSA are 50% higher than those recorded for infections with MSSA[124]. Given MSSA isolates are broadly more susceptible to antibiotics than MRSA, and further considering the substantial remodelling of the bacterial wall and associated with antibiotic resistance; we theorised that MSSA isolates were also be more immunogenic than isolates of broadly antibiotic resistant MRSA. Importantly, we have shown that MSSA isolates tend to exhibit more potent immunogenicity than do clinically distinct, broadly resistant MRSA isolates (figures 4.1 and 4.2). Indeed, we have found, and recently published, that of five examined daptomycin exposed clinical pairs, three were unable to elicit appreciable cytokine secretion by DC- even prior to daptomycin exposure[201] (figure 4.5). These findings highlight the inferior immunostimulatory capacity of these multi-drug resistant isolates, even prior to the acquisition of daptomycin resistance.

Nonetheless, in addition to the A8819/A8817 pair discussed in chapter three, we have further identified both a second clinically distinct daptomycin exposed pair (A9763/A9764) and a vancomycin exposed pair (A8090/A8094), which differentially stimulate DC activation (figures 4.6-8, 4.15 and 4.16). Importantly, while the acquisition of resistance similarly impedes DC activation in both of daptomycin exposed clinical pairs; the differential in the activation phenotype of DC stimulated with the vancomycin exposed isolates exhibited distinct trends (figures 4.15 and 4.16). Most notably, the vancomycin exposed pair is able to modulate CD80, CD86 and MHC-II expression by DC (figure 4.16), while CD80 is the only one of these markers modulated in response to daptomycin exposed pairs (figure 4.4). Daptomycin and vancomycin are both last line antibiotics used to treat infections with multi-drug resistant strains of MRSA[240], each acting through unique mechanisms disrupting the bacterial cell wall, and thus leading to ionic depolarisation[241-245]. It is therefore clear that despite a similar mechanism of action

in the regulation of antibiotic resistance, the mechanisms by which these mutations regulate innate recognition remain distinct.

4.5.2 Regulation of innate recognition in daptomycin exposed clinical isolates

In our analysis of the A9763/A9764 daptomycin exposed clinical pair, it was clear that the trend of reduced immunogenicity upon the acquisition of resistance were similar to those of the A8819/A8817 clinical pair described in chapter three. Indeed, the capacity to induce CD80 expression by cDC2 and pDC was impaired following the acquisition of resistance in the A9764 isolate (Figure 4.6), as was the capacity to induce PD-1 expression by all DC subsets (figures 4.6 and 4.7). Of particular interest, the A9763/A9764 pair tended to induce superior cytokine secretion to the A8819/A9917 clinical pair (figure 4.8), and indeed all three splenic DC subsets were seen to differentially respond to the A9763/A9764 clinical pair (figure 4.8); a contrast to the A8819/A8817 pair whereby only cDC1 exhibited this trend (figures 3.8, 3.10 and 4.8).

Importantly, each of the A8819/A8817 and A9763/A9764 pairs accumulate similar mutations in cardiolipin synthase (*cls2)* and multiple peptide resistance factor (*mprF)* genes upon the acquisition of daptomycin resistance[158], and therefore likely share a similar mechanism to regulate innate immune recognition. MprF and Cls2 are essential in the maintenance of the staphylococcal cell membrane, regulating the conversion of Phosphatidylglycerol (PG) into lysyl-PG (L-PG) and cardiolipin respectively[246-248]. Of note, we demonstrated that the individual recreation of *cls2* but not *mprF* point mutations in the A8819 DapS isolate led to impaired upregulation of CD80 by DC (figure 4.10), although was this mutation alone was not sufficient to reduce CD80 expression to levels similar to that elicited by the A8817 DapR isolate (figure 4.10).

Consistent with CD80 regulation we found that pro-inflammatory cytokine, chemokine and IFN is reduced following the recreation of either mutation; although more substantially following the recreation of distinct *cls2* point mutations (figures 4.9, 4.14, Appendix A4-1 and A4-2). Of note, the recreation of *cls2* point mutations in isolation are insufficient to recreate the activation phenotype induced by DapR isolates (figure 4.9, 5.14, appendix A4-1 and A4-2). Collectively, these findings suggest that both mutations are act synergistically in regulating the production of cytokines by DC, although the expression of CD80 may be further regulated by other factors not identified in this study.

Further experimental evidence will be needed to confirm this hypothesis through the creation of an A8819 *cls2* and *mprF* double point mutant.

4.5.3 Concluding remarks

In this chapter we have identified key genetic determinants associated with impaired innate recognition of daptomycin resistant *S. aureus* by DC. We have clearly demonstrated that common mutations in *cls2* and *mprF*, both regulating membrane phospholipid biosynthesis, are individually sufficient to modulate surface activation and cytokine secretion by responding DC. The role of membrane phospholipids in the regulation of staphylococcal pathogenicity has recently been described by Nguyen and colleagues, demonstrating that membrane lipoproteins from commensal staphylococci dampen immune activation; whereas membrane lipoproteins from pathogenic staphylococci are potently inflammatory[219]. This differential in immunogenicity at the species level was shown to be a result of structural modifications to staphylococcal lipoproteins; triggering stimulation of suppressive signalling through TLR1:2 and stimulatory signalling through TL1:6 heterodimers respectively[219]. Nonetheless, the findings of our study provide a further layer of complexity to this system, given that neither the mutation of *cls2* nor *mprF* are capable of modulating membrane lipoproteins in this manner. Indeed, our findings further highlight additional diversity at the *strain* or *isolate* level as sufficient to modulate innate recognition. Of clinical relevance, the *cls2* and *mprF* mutations regulating this recognition occur commonly during therapeutic exposure to daptomycin[158,201], and therefore likely occur under the combination of host and antibiotic selective pressures.

In considering the capacity of these various isolates to stimulate activation of DC, the broader implications on the innate and adaptive immune responses were largely ignored. Indeed, given the enormous complexity of the immune response to bacteria, such an endeavour was truly beyond the scope of this thesis, and certainly merits further investigation.

Nonetheless, our collaborators have very recently published in PNAS, demonstrating that the recreation these same *Cls2* point mutations in the A8819 DapS strain impair neutrophil recruitment *in vivo*, in soft tissue infection models of zebrafish[194]. Critically, these strains were also found to impair human neutrophil migration in *ex vivo* models,

and were subsequently found to impede bacterial clearance in both the human and zebrafish models[194]. Collectively, these findings suggest a model whereby these mutations impede the early detection of *S. aureus* by DC, and other innate cells, subsequently impairing recruitment of other immune cells and the amplification of the immune response required for bacterial clearance. Further research towards understanding the impact on the recruitment and engagement of the adaptive immune system should be prioritised, as these findings may have significant implications towards the development of potential vaccines and immunotherapies.

Chapter 5 – Daptomycin resistant isolates of MRSA are inefficiently internalised by DC

Throughout chapters three and five we have provided an extensive phenotype of DC activation following stimulation with live *S. aureus*, including a variety of both MSSA and MRSA isolates. Importantly, in addition to demonstrating a differential capacity to induce activation of DC, chapter five further demonstrates that these differences are due to changes in the cell membrane occurring as a result of non-synonymous single nucleotide polymorphisms (SNPs)- an important finding which we have recently published[201]. Given the substantial changes occurring in the bacterial cell wall and membrane in the DapR daughter strain of the A8819/A8817 clinical pair, we theorised that the differential activation of DC in response to pair was due to a reduction in bacterial internalisation and therefore impaired innate recognition.

In this chapter we discuss the adaption of a flow based assay to quantify the relative uptake of fluorescently labelled bacterial isolates, similar in principal to that previously described by Fabbrini *et. al.*[249] for the quantitation of opsonophagocytic antibodies against group A streptococcus. Importantly, we demonstrate that the poorly immunogenic DapR clinical isolates are inefficiently internalised by DC in comparison to their DapS strains, and we validate these findings through transmission electron microscopy (TEM). Importantly, we demonstrate that this differential internalisation of bacterial isolates is regulated exclusively by point mutations in the cardiolipin synthase gene, *cls2*.

5.1 Development, optimisation and validation of a flow cytometric assay to quantify MRSA internalisation by DC

In order to quantify differences in uptake between clinical strains of MRSA we utilised enhanced green fluorescent protein (GFP) expressing lab strains of the primary A8819 (DapS) and A8817 (DapR) isolates. We first sought to visualise MRSA uptake by splenic DC via time lapse imaging of live cells stimulated with GFP recombinant MRSA (figure 5.1a). Unfortunately, this approach was limited by the non-adherent characteristics of primary DC; becoming a technical challenge to automate the tracking of multiple cells over a time in the correct focal plane (figure 5.1a). While other laboratories have previously obtained excellent results in using a-MHC-II to adhere *ex vivo* DC in live cell microscopy[250], we were concerned by the potential for this to interfere with the function of DC in the situation of quantifying uptake and first sought to investigate other experimental systems. Nonetheless, the data gathered in our optimisation of time lapse microscopy indicated that DC efficiently phagocytose MRSA

To overcome the limitations of imaging live DC in real time, we considered coating wells with α-MHC-II as previously described to immobilise the DC[250]. However, without knowing the functional impact this may have on DC, we first considered using flow cytometry as an alternative method with the added potential benefit of being able to directly quantify uptake.

5.1.1 A flow cytometric assay to quantify *S. aureus* internalisation by DC

Using GFP recombinant MRSA strains as before, we utilised flow cytometry to quantify uptake of these strains by splenic DC. By staining bulk splenic DC with population markers prior to MRSA stimuli, we were able to efficiently process multiple samples over a flexible time course- whilst being able to clearly separate cDC1, cDC2 and pDC for up to 12 hours (data not shown). Using GFP fluorescence on DC subsets as a surrogate marker for uptake, we were then able to quantify the relative uptake of MRSA by each DC subset (figure 5.1b). Using this information, we were then able to generate two data outputs, the first being the percentage of each DC subset positive for GFP- estimating the amount of DC containing phagocytosed MRSA (figure 5.1c), and the second being the gMFI- estimating the average amount of MRSA taken up by each DC subset relative to each other (data not shown).

The results of this assay showed uptake of MRSA by both cDC1 and cDC2 as early as 30 minutes, and subsequently peaking by 1 hour post stimuli (figure 5.1c). By contrast, pDC exhibited a gradual but nonetheless constant uptake kinetic of MRSA over 12 hours, peaking with ~15% of the population positive for GFP (figure 5.1c). Importantly, we found that uptake of DapS MRSA strain A8819 by both cDC1 and cDC2 was more than 2-fold higher than that recorded for the DapR A8817 daughter strain over the first 8 hours (figure 5.1c). This trend was not recapitulated by pDC (figure 5.1c), with only slight differences apparent between the two strains over the first four hours (figure 5.1c and d). Using GFP+ as a surrogate marker for uptake, we found significantly more splenic cDC2 internalised MRSA than cDC1 or pDC in the first four hours of stimulation with GFP recombinant A8819 and A8817 MRSA (figure 5.1d), however of the cDC1 reached higher overall GFP expression (figure 5.1c)- indicating a higher number of bacteria per cell.

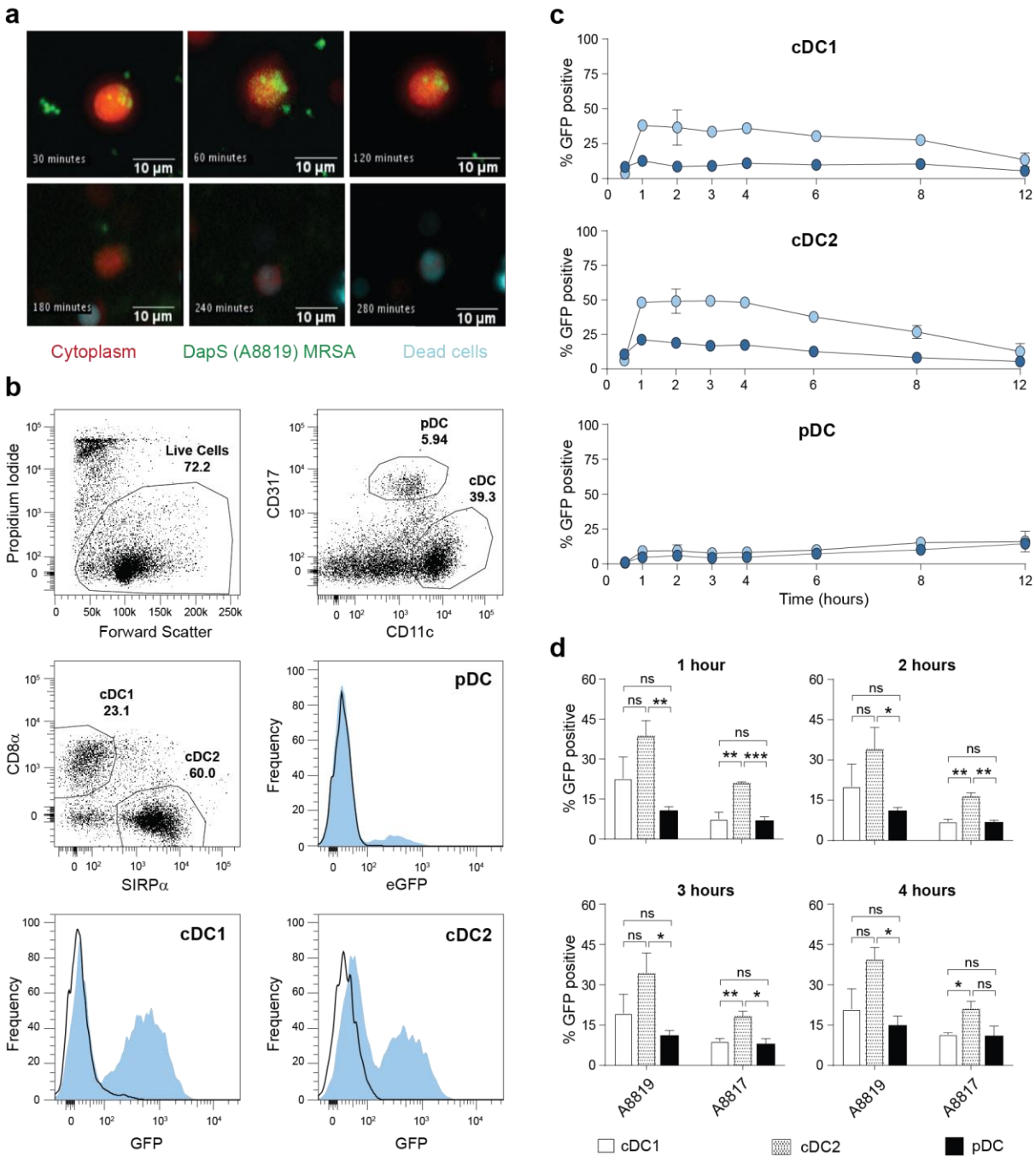

Figure 5.1 Quantitation of splenic cDC1, cDC2 and pDC phagocytic activity using recombinant GFP MRSA clinical isolates.

(a) *Fluorescence microscopy time series showing incubation of splenic DC co-incubated with GFP recombinant DapS MRSA (A8819, MOI=10) over five hours. DC were pre-stained with cytosolic dye Cell Trace Orange (orange), and co-incubated with dye Draq7 viability dye (300 nM, cyan) and GFP recombinant DapS MRSA (green). Cells were maintained at 37°C in a humidified chamber (10% CO_2), for the duration of imaging with a Leica AF6000 LX microscope. (b) Gating strategy for flow cytometric analysis of GFP acquisition by cDC1, cDC2 and pDC following stimuli of purified splenic DC with GFP recombinant MRSA. Live cells gated by differential staining in propidium iodide, and cDC subsequently separated from pDC based on differential expression of lineage markers CD11c and CD317. cDC1 and*

cDC2 are separated based on respective positive expression of CD8α and SIRPα. Histograms show GFP fluorescence acquisition by each of the cDC and pDC subsets following stimulus with GFP recombinant DapS MRSA A8819 at an MOI of 10 (grey shaded), and complete media alone (black trace). Data shown are representative of two independent experiments (n=2). (c) Percent of live DC positive for GFP (as in b), over 12 hours following stimulus with paired Dap exposed clinical isolates of MRSA (A8819 light blue; and A8817 dark blue) recombinant for GFP. Data show mean and range of biological duplicates from one experiment (n = 1). (d) Percent of live DC positive for GFP (as in c), showing cDC1 (hollow bars), cDC2 (dotted bars) and pDC (filled bars) from bulk culture with GFP recombinant A8819 (DapS) and A8817 (DapR) MRSA over four hours. Bars show the mean and SEM of biological replicates pooled from three independent experiments (n = 3). Significance reflects the results of a two-tailed t-test whereby the degree of significance is defined by $p \leq 0.05$ (*), $p \leq 0.01$ (**) and $p \leq 0.001$ (***); whilst non-significance (ns) is defined by $p > 0.05$.

5.1.2 *S. aureus* strained with pHrodo offers superior detection and more accurate quantitation than GFP via flow cytometry

Despite the apparent differences in the uptake of GFP recombinant MRSA by splenic DC subsets, and further differences in uptake between the A8819 and A8817 strain (figure 5.1); there are two key limitations of using the GFP recombinant MRSA in a flow assay. The first being that detection of a GFP+ DC is not a *bona fide* indicator of uptake, as it may potentially reflect extracellular MRSA bound to the surface of the cell. Secondly, while GFP is relatively stable between a pH 6 and 9; its considerably less stable at pH below 7, performing poorly at the endosomal pH between 4 and 6[251]. Given both the low pH and the abundance of protease in the phagocytic compartments of DC, we therefore sought an alternative marker of uptake to validate our findings.

We next considered the use of pHrodo red, a fluorescent dye with poor fluorescent properties at a neutral pH, but brightly fluorescent at the acidic pH endolysosomes[249]. This dye can be readily conjugated to bacteria, and has previously been used to quantify antibody induced internalisation of group A streptococcus by the myeloma cell line HL-60, using a flow based assay[249]. Here, we adapt this assay to differentiate between surface localised and internalised MRSA, through the staining of GFP recombinant strains of MRSA with the pHrodo red dye.

We therefore stimulated DC as with GFP recombinant MRSA pre-stained with the endosomal activated dye pHrodo, and were able to gate DC positive for pHrodo (figure 5.2a). When comparing the two fluorescent dyes, we found that GFP underestimated the number of DC taking up MRSA within each DC subset (figure 5.2b). Indeed, the use of GFP indicated that at least 2-fold less cDC1 had phagocytosed MRSA than did pHrodo over the 12 hour time course (figure 5.2b). Further, the kinetics of GFP over the time course showed rapid decrease in fluorescence from 4 hours onwards in both cDC subsets (figure 5.2c), yet the number of cDC positive for pHrodo was sustained from 4 hours onwards (figure 5.2b). These findings are consistent with our hypothesis of GFP degradation during endosomal acidification. Of note, we observed a population of SIRPa and CD8 double positive cells following stimuli with MRSA (figure 5.2a), which was not present following stimuli with media alone (data not shown). These cells were found to be a result of CD11c upregulation by an unknown cell population in these bulk cultures following stimulation with MRSA, and could be gated out with tighter CD11c gating (data

not shown). However, considering the ease of excluding these cells with conventional cDC1 and cDC2 gates, we continued chose not to alter our gating strategy for consistency.

As opposed to quantifying the total number of DC taking up MRSA, the gMFI of the positive population provides an estimate of relative MRSA phagocytosis by each DC subset. Overall, the pHrodo gave superior separation between positive and negative populations, being at least one log higher the GFP for each subset at each time point (figure 5.2b). However, in contrast to the measurement of total DC positive for MRSA, the gMFI of pHrodo was not sustained over the time course from the 30 minute peak for cDC subsets (figure 5.2c), but rather decreased throughout the time course. This likely reflects endosomal degradation of both fluorophores over the time course, with the maintenance of GFP fluorescence likely reflecting bacterial accumulation at the cell surface. Importantly, the pHrodo dye kinetics exhibited an initial burst in fluorescence detectable at 30 minutes post stimulation, and subsequently decreasing over the time course (figure 5.2c). This trend was not replicated with GFP expressing strains (figure 5.2c), and we concluded that this fluorophore was not accurately modelling the kinetics of uptake.

Importantly, while GFP did correlate with pHrodo fluorescence (figure 5.3a), it was clear that some cells were pHrodo positive in the absence of GFP fluorescence (figure 5.3a and b). The most likely scenario for this observation is the degradation of GFP following bacterial internalisation and pHrodo activation. Of particular emphasis, while there were clearly $pHrodo^{+}$ GFP^{-} events recorded in this assay (figure 5.3a and b), we were unable to detect substantial GFP^{+} $pHrodo^{-}$ DC. We therefore selected pHrodo for subsequent flow cytometric analysis of MRSA uptake, given a superior brightness and stability making it suitable for long term culture systems.

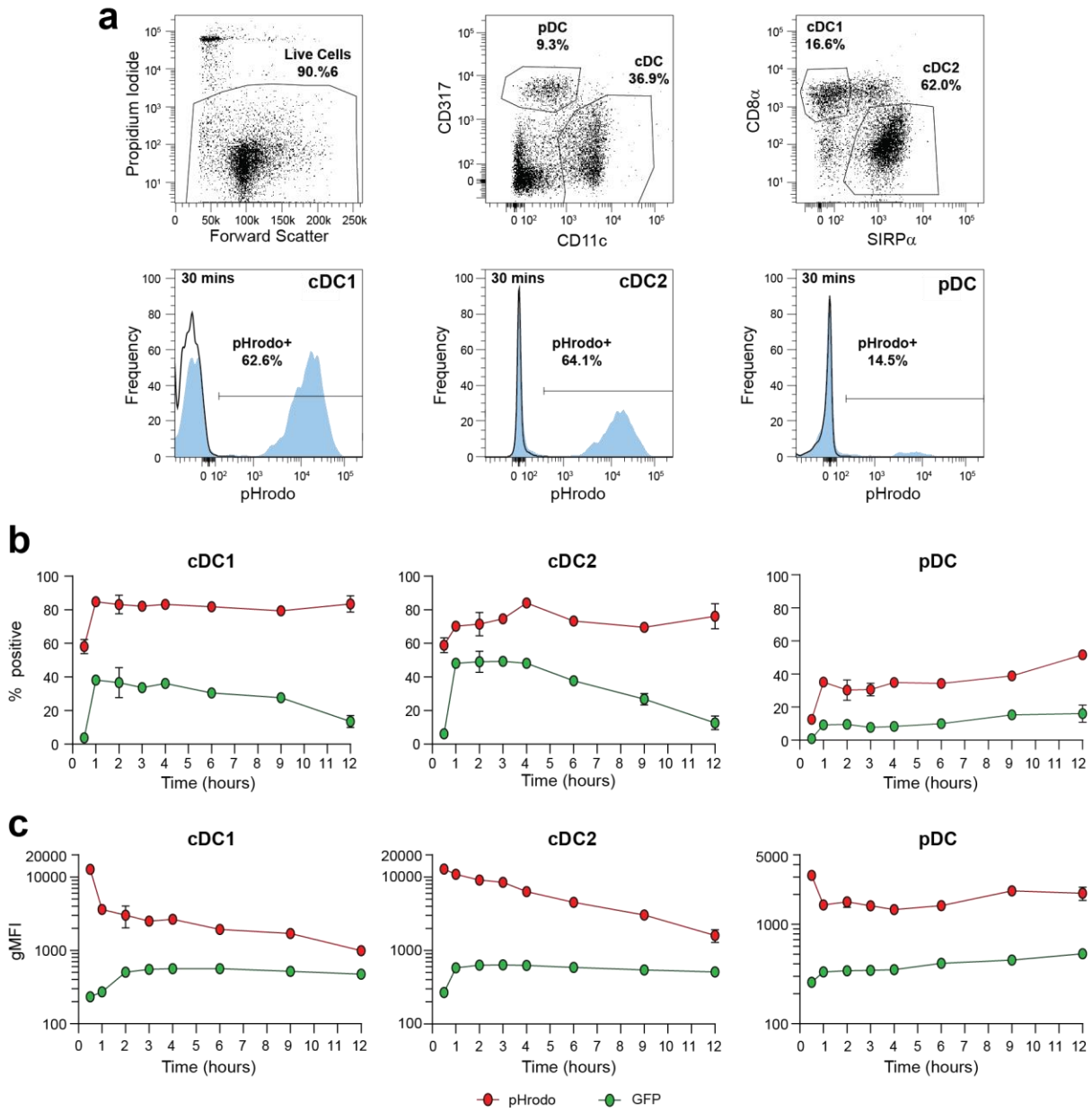

Figure 5.2 Comparison of pHrodo and GFP for flow cytometric quantitation of DC phagocytic activity. ***(a)*** *Gating strategy for flow cytometric analysis of pHrodo fluorescence associated with cDC1, cDC2 and pDC following stimuli of splenic DC with pHrodo labelled MRSA. Live cells gated by differential staining in PI, and cDC subsequently separated from pDC based on differential expression of lineage markers CD11c and CD317. cDC1 and cDC2 are separated based on respective positive expression of CD8α and SIRPα. Histograms show pHrodo fluorescence by each of the cDC and pDC subsets at 30 mins post stimuli with pHrodo labelled DapS MRSA A8819 at an MOI of 10 (blue shaded), and complete media alone (black trace). Data shown are representative of four independent experiments.* ***(b)*** *Percent of live DC subsets in bulk culture positive for either GFP (green; as in 6.1b) or pHrodo (red; as in 6.2a). DC were analysed at intervals over 12 hours following stimuli with GFP recombinant DapS MRSA strain A8819 prestained with pHrodo. Data show the mean and range of biological duplicates from one experiment (n = 1).* ***(c)*** *Geometric mean fluorescence intensity (gMFI) of pHrodo positive DC (pHrodo gMFI; red) and GFP positive DC (GFP gMFI; green) for DC stimulated with MRSA as in 'b'. Data show the mean and range of biological duplicates from one experiment (n = 1).*

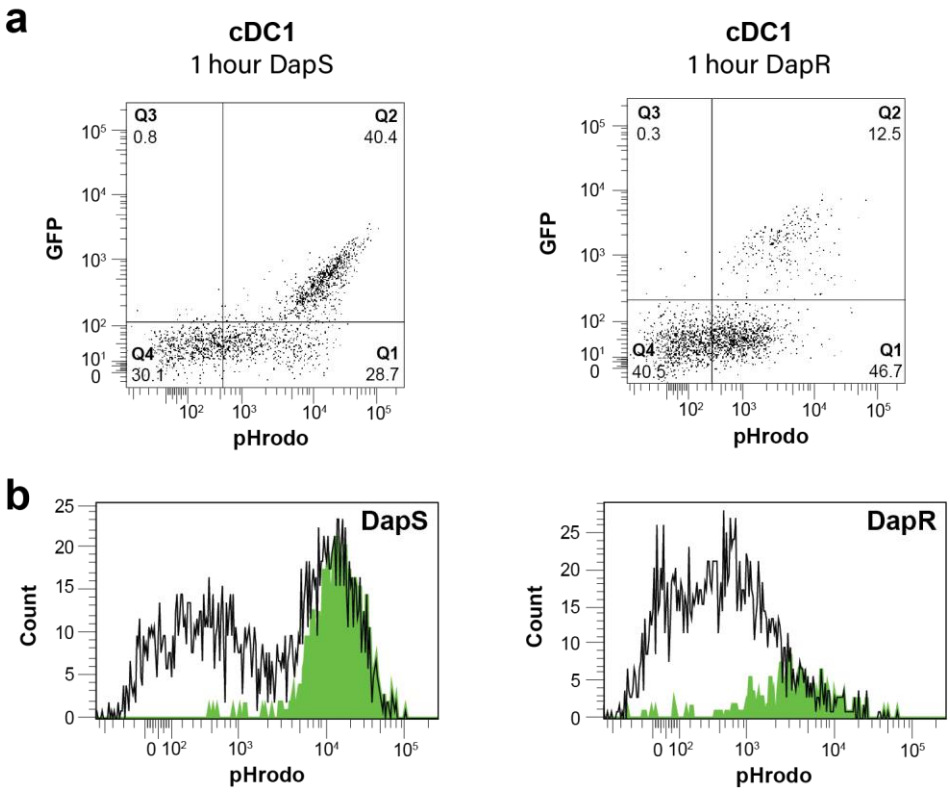

Figure 5.3 pHrodo staining estimates uptake of MRSA more accurately than GFP expression of recombined strain.

(a) *Dot plot showing GFP and pHrodo fluorescence by cDC1 gated as in '6.2a', following 1 hour stimulation with A8819 (DapS) or A8819 (DapR) MRSA at an MOI of 10. Quadrant gates are based off the staining pattern of mock stimulated controls (not shown).* ***(b)*** *Histograms showing pHrodo expression of cDC1 stimulated for 1 hour with A8819 (DapS) and A8817 (DapR) MRSA as in 'a', showing total cDC1 (all quadrants; black line) and the GFP positive DC (quadrants 2 & 3; green shaded). Data shown from 1 experiment (n = 1).*

Overall, we found that splenic cDC1 and pDC reached peak bacterial internalisation by 1 hour post stimuli, whereas the cDC2 did not reach their maximal internalisation until 4 hour post stimuli (figure 5.4a). In contrast, all three subsets peaked maximal fluorescence (gMFI) within the first hour (figure 5.4b), suggesting rapid endosomal acidification following MRSA uptake.

Importantly, we found that both cDC1 and cDC2 phagocytosed the A8819 MRSA isolate (DapS) at a faster rate than they did the A8817 daughter strain (DapR), as indicated by the proportion of the population becoming positive for pHrodo in the first four hours (figure 5.4a). The cDC1 were more efficient in phagocytosing the A8817 (DapR) strain than were the cDC2, with ~70% of cDC1 becoming positive for pHrodo within the first hour of stimulus compared to only 25% of cDC2 (figure 5.4a). In terms of quantifying uptake between the two strains, the relative amount of A8819 (DapS) MRSA internalised by the cDC1 was at least double that recorded for the A8817 (DapR) strain. Similar trends were observed for cDC2 with A8819 (DapS) uptake more than 5-fold higher than that of A8817 (DapR) at 4 hours post stimulus (figure 5.5b). Further pDC exhibited more uptake of A8819 (DapS) than A8817 (DapR) across the entire time course (figure 5.4b).

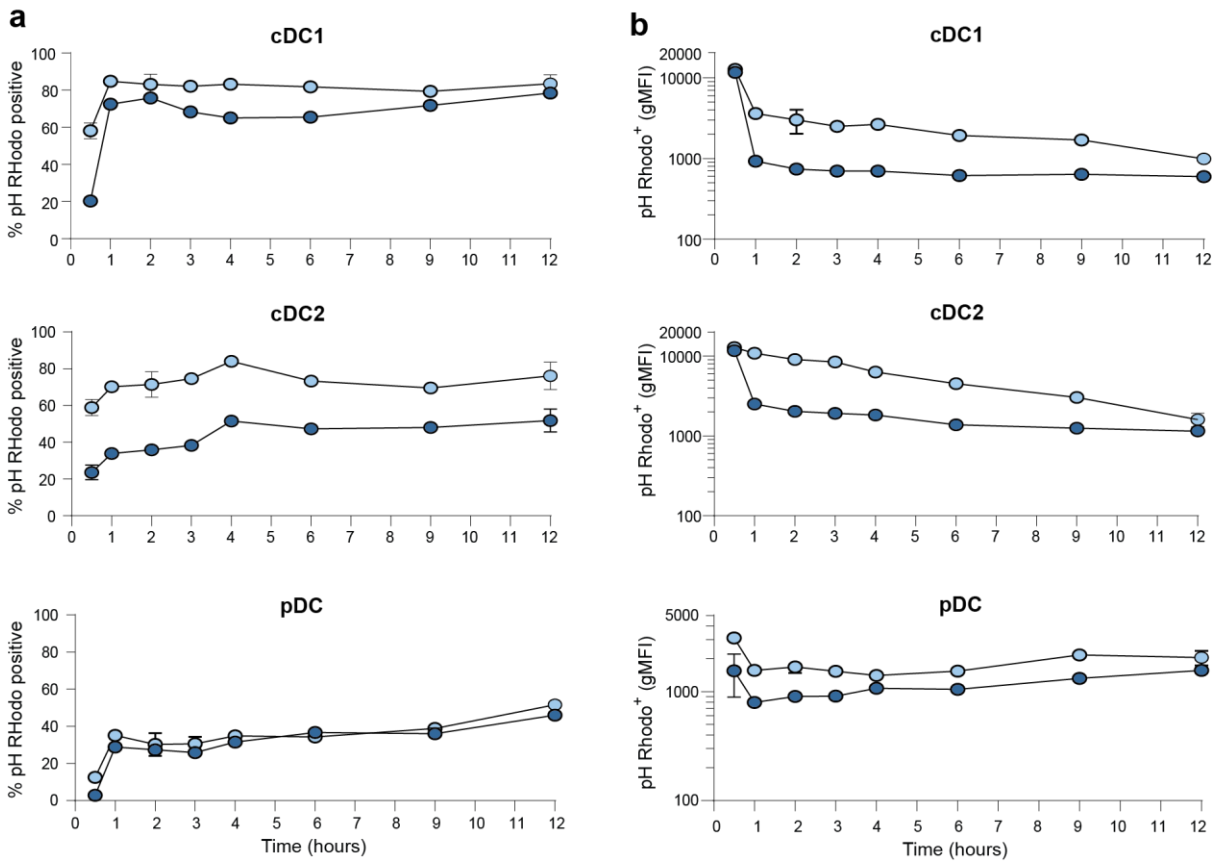

Figure 5.4 Flow analysis shows differential uptake of paired daptomycin exposed clinical isolates of MRSA by splenic DC subsets.

(a) *Percent of live DC positive for pHrodo over 12 hours following stimulus with paired Dap exposed clinical isolates of MRSA recombinant for GFP and prestained with pHrodo, corresponding to A8819 (DapS, light blue) and A8817 (DapR, dark blue). Data show mean and range of biological duplicates from one experiment (n = 1).* ***(b)*** *Geometric mean fluorescence intensity (gMFI) of pHrodo positive DC following stimulation with MRSA as in 'a'. Data show the mean and range of biological duplicates from one experiment (n = 1).*

5.1.3 Transmission electron microscopy validates the flow cytometry assay for internalisation of MRSA

Despite the differential in pHrodo fluorescence following stimulation of each splenic DC subset with the daptomycin exposed clinical pair A8819/A8817 (figure 5.4c), which is indicative of differences in uptake between the strains; the assay is unable to definitively prove a differential in uptake. Given the pHrodo dye is dependent upon acidic pH for its activation, it remained plausible that these data were due to either differential trafficking of the phagocytosed strains or alterations in the endosomal acidification process. Using transmission electron microscopy (TEM), we therefore sought to directly image DC, enumerate visibly internalised bacteria, and therefore directly compare differences in uptake between stimuli with the two strains. Having imaged cultures of bacterial splenic DC stimulated with *S. aureus*, we were unable to distinguish DC subsets through visual analysis (data not shown), and therefore continued in imaging of sorted DC subsets stimulated with MRSA.

Initially, we sought to investigate phagocytosis by cDC1 and at eight hours post stimulus with either the DapS A8819 or DapR A8817 strains. Using a Chi-squared test we found a significant relationship between the observation of phagocytosis and the strain of bacteria (χ^2 (1) = 28.12, $p < 0.0001$); whereby we were significantly more likely to observe phagocytosis for cDC1 stimulated with the A8819 DapS strain than the A8817 DapR strain (figure 5.4).

Having enumerated phagocytosis in every cDC1 visible on each section following stimulus with DapS A8819 (n = 194) and DapR A8817 MRSA (n = 435). We found that the A8819 DapS strain was phagocytosed significantly more efficiently than the A8817 DapR strain by cDC1 (figure 5.6b and c), with the average number of phagocytosed DapS MRSA observed per cell being 3-fold higher than that recorded for the DapR MRSA strain ($\bar{x}$ = 0.87 and 0.29 respectively). Indeed, we were able to enumerate as many as 11 bacteria in a single DC stimulated with DapS A8819 (5.67a, b and c), yet following stimuli with the A8817 DapR strain we did not find DC containing more than 5 bacteria per section (figure 5.6a, b and c). These findings are consistent with the findings of the pHrodo assay, despite the TEM images suggesting approximately 5-fold more DC negative for MRSA internalisation (figure 5.4 and 5.6 respectively). These discrepancies

are likely accounted for by fundamental differences in the techniques, and the two-dimensional imaging of DC cross-sections in the EM experiments.

a

	Observed Uptake	No Observed Uptake
A8819 DapS	68 (35.1%)	126 (64.9%)
A8817 DapS	72 (16.2%)	373 (83.8%)

b

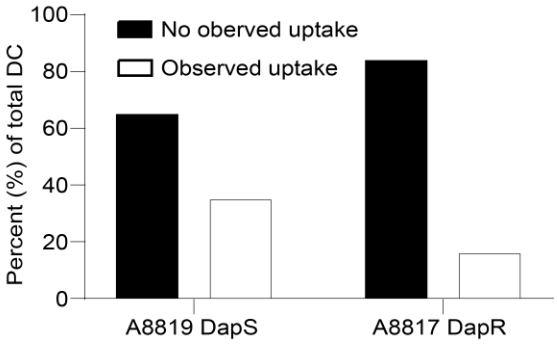

Figure 5.5 Contingency table and bar chart showing observed uptake of A8819/A8817 paired clinical isolates by cDC1.

(a) *Contingency table showing the total number of cDC1 with either observed uptake or no observed uptake of MRSA, as quantified via TEM, following 8 hour stimulus with either DapS A8819 or DapR A8817 MRSA. Integers from contingency table were used to perform a Chi-squared test finding a significant relationship between uptake and strain ($\chi^2 = 28.12$, $df = 1$, $p < 0.0001$). Percentages (%) shown for each count are derived from the row total.* ***(b)*** *Bar chart showing percentage of cDC1 observed to phagocytose A8819 or A8817 MRSA at 8 hours post stimulus, relative to the total number of DC observed for each stimuli. Data show 629 cDC1 imaged and enumerated by TEM in one experiment (n = 1), representative of two independent experiments at 4 or 8 hours (n = 2).*

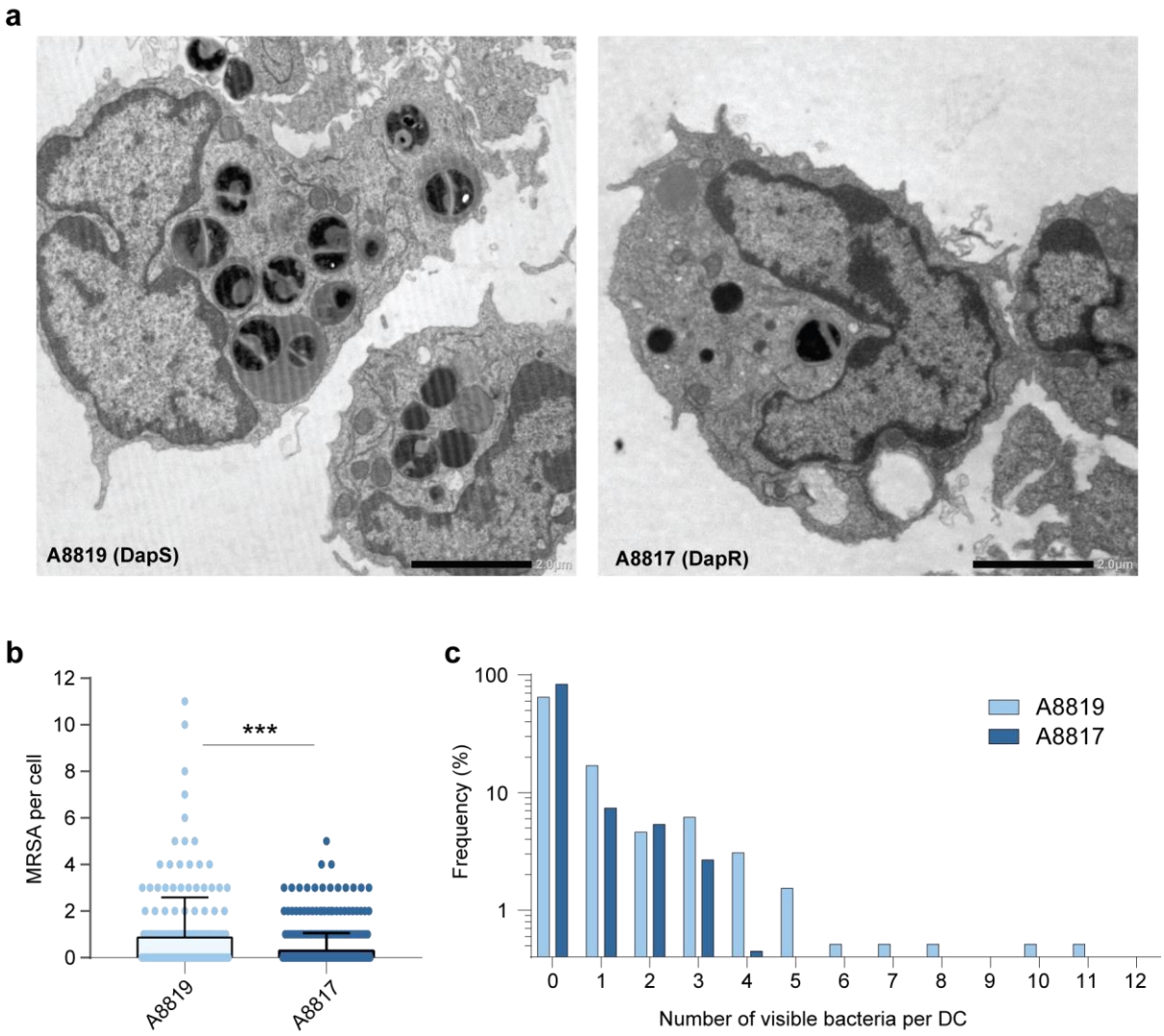

Figure 5.6 TEM images, dot plots and histograms reflecting MRSA uptake by cDC1 at eight hours post stimulus with A8819/A8817 isolates.

(a) *TEM of fixed and Epon embedded DC sections corresponding to FACS sorted cDC1 following 8 hour MRSA stimuli with either A8819 DapS or A8817 DapR (MOI of 10). Images were acquired on a JEOL TEM electron microscope with between 200 and 30,000 X magnification. Images were selected to show a single cell representative of the most highly phagocytic DC containing MRSA in each sample. Scale bars are representative of 2 µm. Data shown from 1 experiment representative of two independent experiments (n = 2).* ***(b)*** *Dot plot showing the number of visible MRSA enumerated per DC imaged as in 'a', in a full dataset of images comprising cDC1 stimulated with DapS A8819 MRSA (n = 194), and DapR A8817 MRSA (n = 435). Significance reflective of an unpaired two-tailed t-test using Welches correction for not assuming equal SD; whereby *p<0.05, **p<0.01, and ***p<0.001.* ***(c)*** *Histogram showing frequency of MRSA in cDC1 with visible internalised bacteria at 8 hours post stimulus with DapS A8819 (light blue bars) and DapR A8817 MRSA (dark blue bars). Data are representative of two independent experiments at 4 and 8 hours (n = 2), and trends representative of an additional experiment on unsorted DC at 4 and 8 hours (n = 1).*

5.2 Daptomycin resistance confers resistance to phagocytosis

The previous section discussed the design of a flow cytometry based assay to detect the and quantify the relative uptake of pHrodo labelled MRSA isolates by DC. Having validated these results via TEM (section 6.1.3), we therefore sought to further examine the impact of daptomycin resistance on phagocytosis by DC. This section will describe the impact of daptomycin resistance on uptake of MRSA, modelling both the A8819/A8817 and the A9763/A9764 clinical pairs. Further, we will characterise several lab derived point mutants of these clinical isolates to further understand the molecular basis for the differential in phagocytosis of these strains by DC.

5.2.1 Daptomycin resistant MRSA are inefficiently phagocytosed by splenic DC

Preliminary data from the pilot pHrodo experiment indicated rapid uptake of DapS MRSA strains within 1 hour of stimulation, exhibiting a sustained differential in internalisation between the A8819/A8817 clinical pair over 12 hours (figure 5.2 and 5.4). We therefore sought to validate these findings, modelling both the A8819/A8817 and A9763/A9764 clinical pairs over a shorter time course. These pairs were selected given that *cls2* and *mprF* point mutations arise in each paired daptomycin resistant isolate; and these daptomycin resistant isolates further exhibit reduced immunogenicity relative to their parent strain – suggesting that the handling of these strains by DC are similarly regulated. The data confirm that all three splenic DC subsets are able to internalise DapS A8819 and A9763 MRSA isolates more efficiently over 6 hours than they are the DapR partners A8817 and A9764 (figure 5.7a and 5.7b respectively). I

Importantly, correlating with the greater inflammatory response induced by the DapS A9763 strain compared to the DapS A8819 strain (see chapter 5), the relative amount of phagocytosis observed for A9763 was superior to that observed for A8819 (figure 5.7a and b). This finding was most evident in examining cDC subsets, particularly at the early time points of both 30 and 60 minutes, where the average induction of pHrodo fluorescence by A9763 was up to double that of A8819 (figure 5.7a and b). Moreover, unlike the kinetics of A8819 uptake by cDC – which exhibited sustained pHrodo fluorescence over 6 hours – stimulus with A9763 resulted in an initial spike in pHrodo fluorescence peaking before 1 hour and gradually declining over 6 hours (figure 5.7b). Cumulatively, these data suggest that the A9763 strain induces a phagocytic shutdown

by cDC within 30 minutes of stimulation, and that by contrast neither the A9764 DapR daughter strain nor the A8819/A8817 clinical pair induce this shutdown with sustained fluorescence over the time course.

Both cDC subsets dominate the uptake of MRSA, although it seemed that the cDC2 internalised MRSA to greater levels than did cDC1 (figure 5.7a and b). However, there was no significant difference in the capacity of cDC to internalise A8819 DapS MRSA (figure 5.8a). Nonetheless, both cDC subsets internalised significantly more A8819 MRSA than pDC over the first three hours of the time course (figure 5.8a). Despite equivalence in internalisation of DapS A8819 MRSA between the splenic cDC subsets, the cDC2 were noticeably poorer at phagocytosing the DapR A8817 strain when compared to cDC1 (figure 5.8a and b). Indeed, the cDC2 phagocytosed approximately 10-fold less DapR A8817 MRSA on average than they did DapS MRSA (figure 5.7a and b), having only slightly higher fluorescence the FMO control (figure 5.7a). We therefore recommend caution in comparing relative internalisation between each of the DC subsets. Nonetheless, while unable to make direct statistical comparisons between the subsets, we were able to demonstrate that the differences in internalisation of the A8819/A8817 clinical pair were indeed significant for each of the three subsets (figure 5.8c).

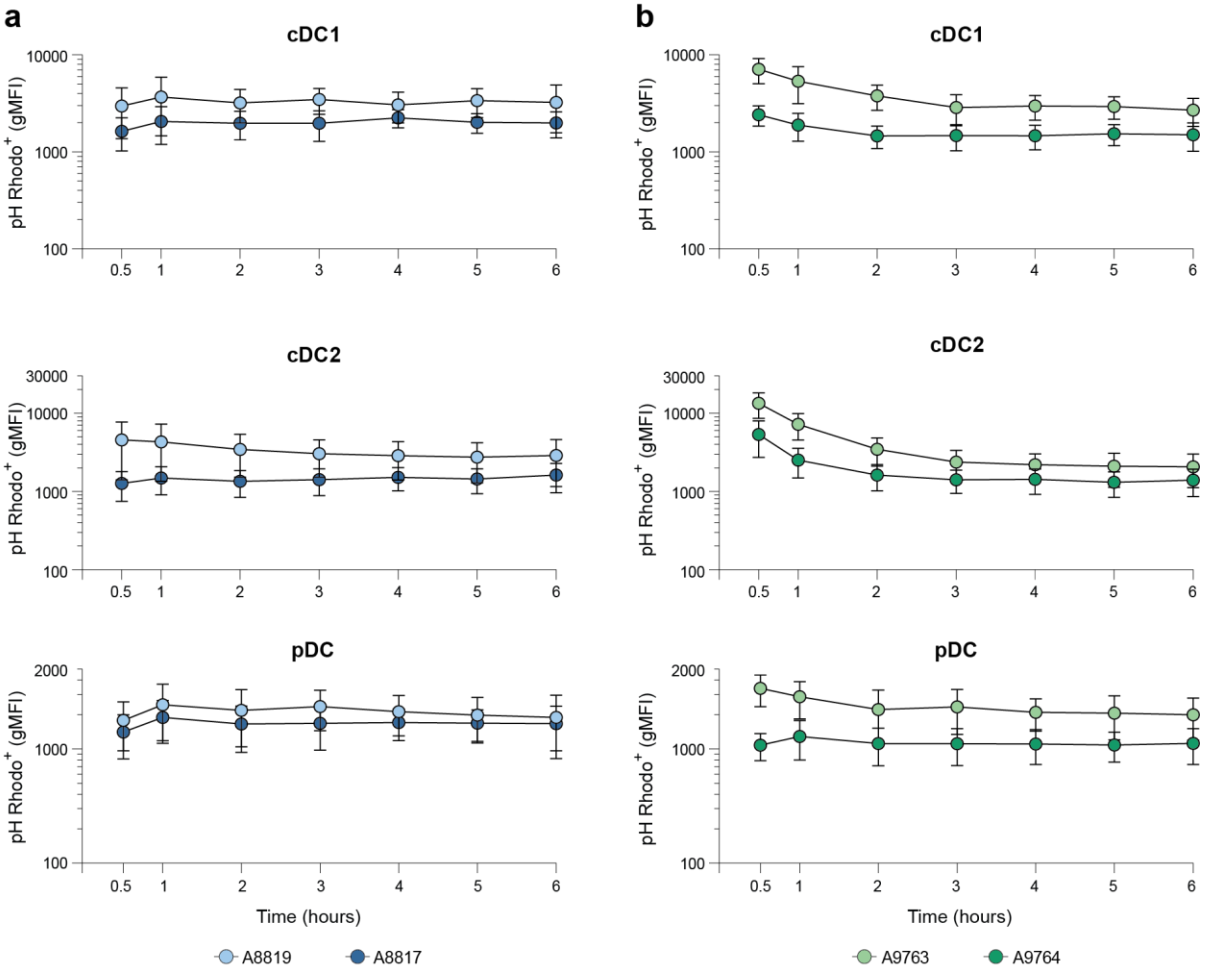

Figure 5.7 Time course showing pHrodo expression by splenic DC subsets following stimulation with two distinct clinical pairs of DapS and DapR MRSA.

(a) *pHrodo geometric mean fluorescence intensity (gMFI) of pHrodo positive cDC1, cDC2 and pDC, stimulated over 6 hours with pHrodo stained A8819 (DapR) and A8817 (DapR) MRSA. Splenic DC subsets were pre-stained with antibodies against key surface markers, and stimulated in bulk culture, allowing for discrimination of distinct DC subsets. Error bars show the mean and SEM of three biological replicates (n = 3).* ***(b)*** *pHrodo geometric mean fluorescence intensity (gMFI) of pHrodo positive cDC1, cDC2 and pDC, stimulated over 6 hours with pHrodo stained A9763 (DapR) and A9764 (DapR) MRSA. Splenic DC subsets were pre-stained with antibodies against key surface markers, and stimulated in bulk culture, allowing for discrimination of distinct DC subsets. Error bars show the mean and SEM of three biological replicates (n = 3).*

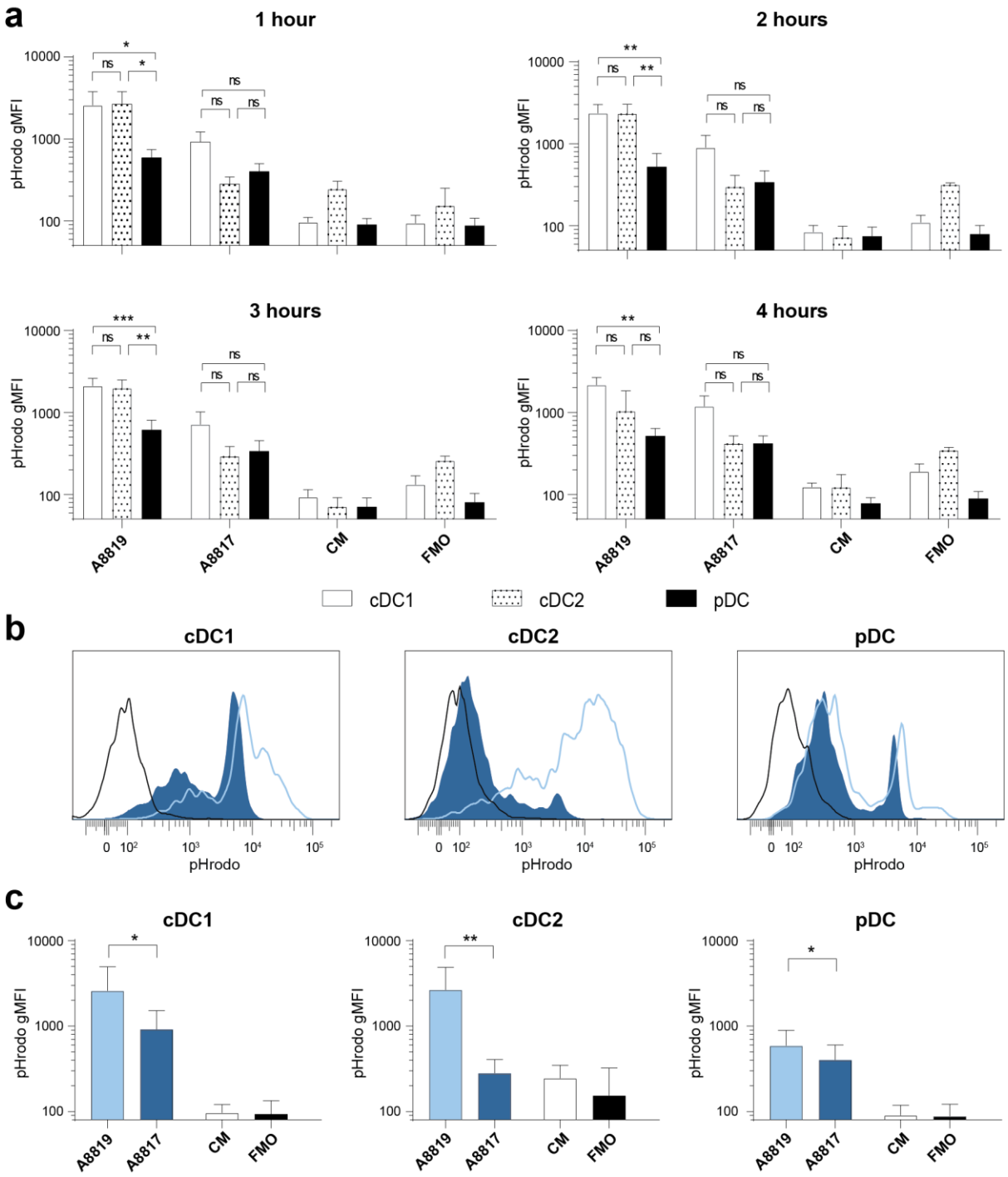

Figure 5.8 cDC internalise significantly more DapS MRSA than do pDC, but DapR MRSA is poorly internalised by all DC subsets.

(a) *pHrodo gMFI for cDC1, cDC2 and pDC, stimulated over 4 hours with pHrodo stained A8819 (DapR) and A8817 (DapR) MRSA. Splenic DC subsets were pre-stained with antibodies against key surface markers, and stimulated in bulk culture, allowing for discrimination of distinct DC subsets. Significance in panels b and c reflect the results of an ordinary two-way ANOVA, using Tukey's test to correct for multiple comparisons; whereby the degree of significance is defined by $p \leq 0.05$ (*), $p \leq 0.01$ (**) and $p \leq 0.001$ (***); whilst non-significance (ns) is defined by $p > 0.05$.* ***(b)*** *pHrodo fluorescence for cDC1, cDC2 and pDC, at 1 hour post stimulus with pHrodo stained A8819 (DapS; light blue trace) and A8817*

(DapR; dark blue shaded) MRSA, and media alone (black trace). Data shown from 1 experiment representative of four independent experiments (n = 4). ***(c) pHrodo geometric mean fluorescence intensity (gMFI) for cDC1, cDC2 and pDC, as in 'a'. Data showing the mean and SEM of biological replicated pooled from four independent experiments (n = 4).***

5.2.2 Phagocytosis of *S. aureus* by DC is impeded by mutations in *cls2*

Having established both differential uptake and activation of DC in response to stimulation with paired isolates of MRSA (section 6.2.1 and chapter 3 respectively), we sought to further investigate the resistance mutations that affect the phagocytosis of MRSA by DC. Given the finding that point mutations occurring in *mprF* and *cls2* genes of *S. aureus* isolates impede DC activation (see chapter 5), we initially considered how mutations in these two genes may regulate uptake of the bacteria by DC.

In using the flow based assay to quantify uptake of pHrodo labelled bacteria, we further stimulated splenic DC with A8819/A8817 clinical pair and the A8819 derived lab strains individually recreated for mutations in *cls2* and *mprF* ($A8819_{Cls2\text{-}T33N}$ and $A8819_{Cls2\text{-}T45I}$ respectively). In contrast to our previous findings showing that both the *cls2* and *mprF* point mutations contribute to the reduced activation of DC observed following stimuli with the DapR strain, it is evident that only the *cls2* mutation affects the ability of DC subsets to phagocytose the bacteria (figure 5.9a and b). Indeed, the kinetics of pHrodo fluorescence by DC subsets stimulated with $A8819_{MprF\text{-}T345I}$ were essentially identical to that of DapS A8819 (figure 5.9a).

By contrast, the uptake observed for the $A8819_{Cls2\text{-}T33N}$ by all DC subsets was lesser than that observed for A8819 at all time points (figure 5.9b), most notably cDC1 and pDC whereby the observed uptake was instead approximately equivalent to that observed for the DapR A8817 strain (figure 5.9b). Furthermore, while the relative uptake of $A8819_{Cls2\text{-}T33N}$ by cDC2 was consistently below that of that of the DapS A8819 strain, the amount of observed uptake was not reduced to the levels observed for the DapR A8817 strain (figure 5.9b). It is therefore clear, that differences in *cls2* are responsible for the reductions observed in phagocytosis by the cDC1 and pDC, but not the cDC2. Given that the $A8819_{MprF\text{-}T345I}$ strain had no discernible impact on phagocytosis by any DC subset, it remains more likely that the phenotype observed for cDC2 responding to DapR A8817 is a result of both the *cls2* and *mprF* mutations acting in synergy to achieve a result neither mutation can induce in isolation.

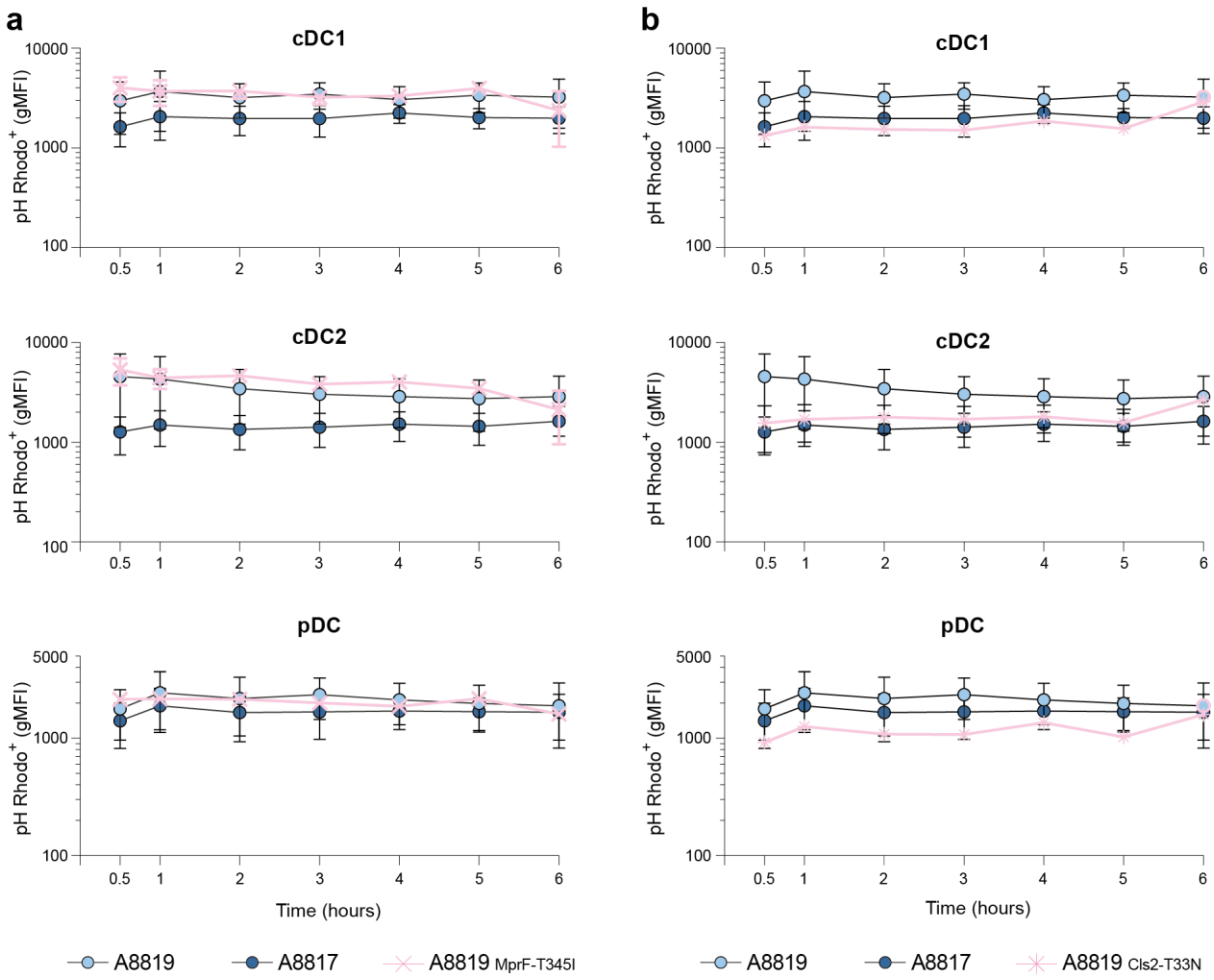

Figure 5.9 Time course showing pHrodo expression by splenic DC subsets following stimulation with MprF and Cls2 point mutants of A8817 recreated in A8819.

(a) *pHrodo geometric mean fluorescence intensity (gMFI) of pHrodo positive cDC1, cDC2 and pDC, stimulated over 6 hours with pHrodo stained A8819 (DapR), A8817 (DapR) and the lab strain A8819$_{MprF\text{-}T345I}$ (DapR) of MRSA. Splenic DC subsets were pre-stained with antibodies against key surface markers, and stimulated in bulk culture, allowing for discrimination of distinct DC subsets. Error bars show the mean and range of technical duplicates. Representative of three biological replicates (n = 3).* ***(b)*** *pHrodo geometric mean fluorescence intensity (gMFI) of pHrodo positive cDC1, cDC2 and pDC, stimulated over 6 hours with pHrodo stained A8819 (DapR), A8817 (DapR) and the lab strain A8819$_{Cls2\text{-}T33N}$ (DapR) of MRSA. Splenic DC subsets were pre-stained with antibodies against key surface markers, and stimulated in bulk culture, allowing for discrimination of distinct DC subsets. Error bars show the mean and range of technical duplicates. Representative of three biological replicates (n = 3).*

Given that the T33N point mutation does not arise in the A8817 DapR daughter strain, and is rather recreated in A8819 from an unrelated daptomycin exposed isolate[194], we next sought to establish that these differences in internalisation were due to the T33N point mutation- and not other factors resultant from the allelic replacement. We therefore next compared the capacity of splenic DC to internalise the repaired A8819$_{Cls2\text{-}T33NN33T}$ strain, in comparison to A8819 and A8819$_{Cls2\text{-}T33N}$ (figure 5.10). Critically, the reversion of cls2-T33N to cls2-N33T enhanced the internalisation of S. aureus by up to 2-fold (figure 5.10). However, the cls2-N33T reversion was not internalised by any splenic DC subset to an equivalent level of A8819 (figure 5.10). Cumulatively, these findings demonstrate that indeed the T33N point mutation acquired in cls2 modulates the capacity of S. aureus to be internalised by DC, although other factors in the wild-type gene lead to differences in internalisation between A8819$_{Cls2\text{-}T33NN33T}$ and A8819 (figure 5.10).

Given that the *cls2*-T33N point mutation has only previously been recorded following daptomycin exposure *in vitro*[158], we next sought to quantify the effect of the L52F point mutation arising in the DapR A9764 isolate following daptomycin exposure *in vivo*[158] (figure 5.11). Similar to the observations for the A8819$_{Cls2\text{-}T33N}$ strain (figure 5.9), the A8819$_{Cls2\text{-}L52F}$ strain was internalised less efficiently than A8819 (figure 5.11a). Importantly, the A9763 isolate, being the parent of the L52F point mutation, is more efficiently internalised by all DC subsets than A8819 (figure 5.7); therefore highlighting the role of the L52F point mutation in the modulation of A8819 internalisation. These findings therefore demonstrate that both T33N and L52F point mutations in *cls2* modulate internalisation of *S. aureus* by DC. In order to determine the role of factors extrinsic to *cls2* in the regulation of *S. aureus* internalisation by DC, we next compared the capacity of DC to internalise A8819$_{Cls2\text{-}L52F}$ in comparison to the A9764 clinical isolate from which this mutation was derived (figure 5.11b). Of note, the A8819$_{Cls2\text{-}L52F}$ isolate was internalised more efficiently by all three splenic DC subsets than the A9764 isolate (figure 5.11); therefore clearly demonstrating that factors extrinsic to Cls2 contribute to internalisation of *S. aureus* by DC.

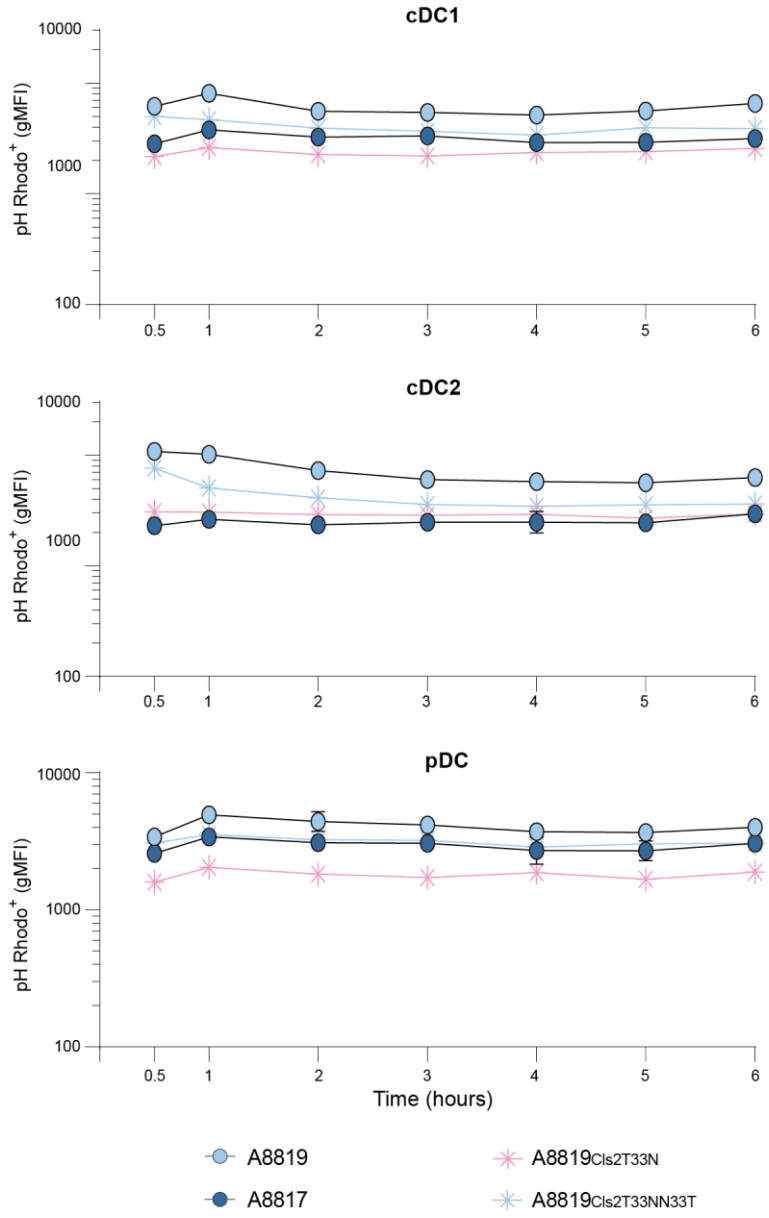

Figure 5.10 Time course showing pHrodo expression by splenic DC subsets following stimulation with DapS clinical A8819/A8817 pair and laboratory derived strains A8819$_{cls2T33N}$ and A8819$_{Cls2T33NN33T}$.

pHrodo geometric mean fluorescence intensity (gMFI) for cDC1, cDC2 and pDC, stimulated over 6 hours with pHrodo stained A8819 (DapS), and the lab strains A8819$_{cls2T33N}$ (DapR) and A8819$_{Cls2T33NN33T}$ (DapS) of MRSA. Splenic DC subsets were pre-stained with antibodies against key surface markers, and stimulated in bulk culture, allowing for discrimination of distinct DC subsets. Error bars (not visible as smaller than symbols) show the geometric mean and geometric SD of technical duplicates from one experiment, representative of trends from three independent experiments (n = 3).

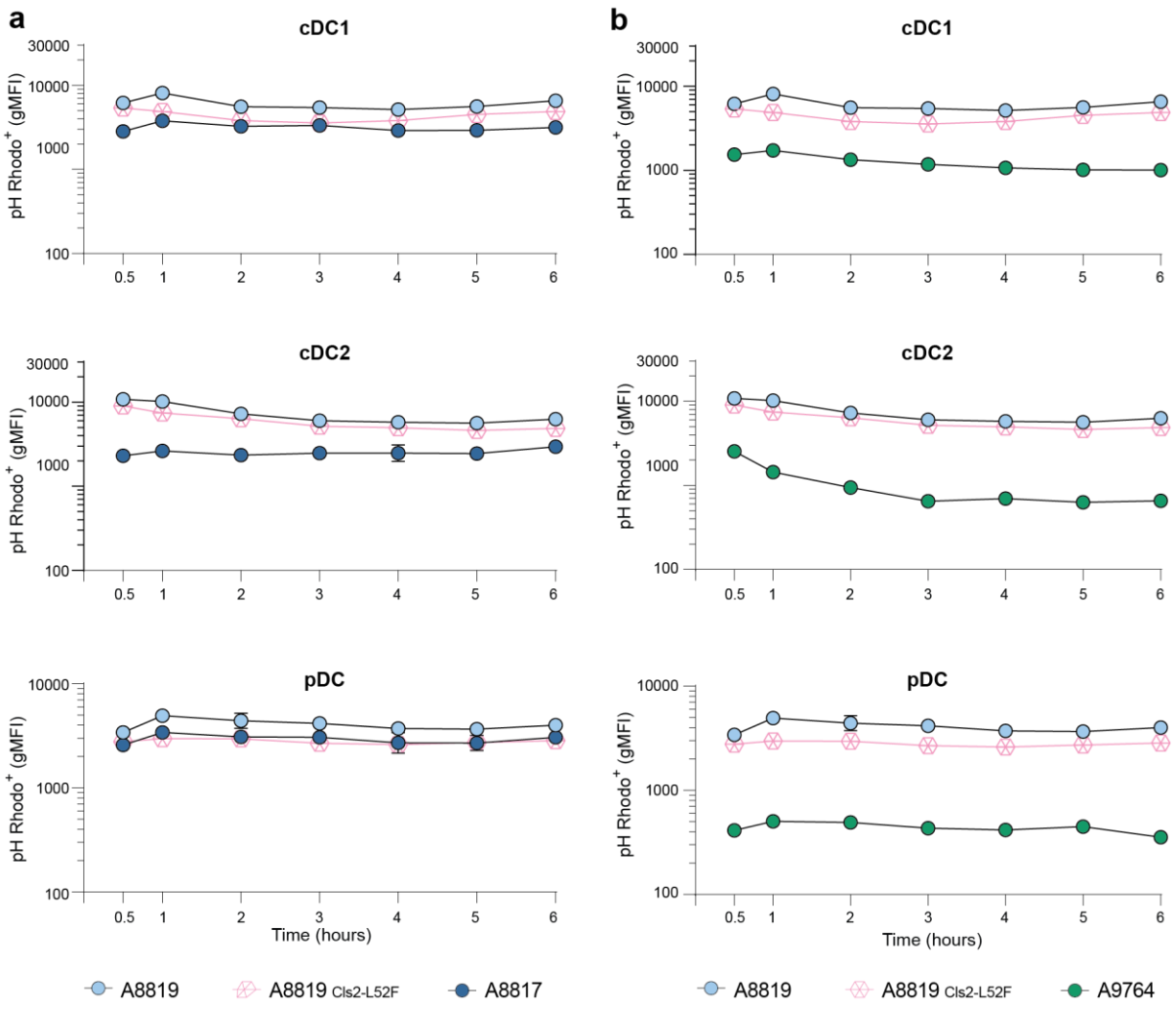

Figure 5.11 Time course showing pHrodo expression by splenic DC subsets following stimulation with DapS clinical isolates and laboratory derived strains A8819$_{cls2L52F}$.

pHrodo geometric mean fluorescence intensity (gMFI) for cDC1, cDC2 and pDC, stimulated over 6 hours with pHrodo stained DapS MRSA clinical isolate A8819 (light blue), the cls2 point mutant strain A8819$_{Cls2L52F}$ (pink) and DapR clinical isolates A8817 (a; dark blue) or A9764 (b; dark green). Splenic DC subsets were pre-stained with antibodies against key surface markers, and stimulated in bulk culture, allowing for discrimination of distinct DC subsets. Error bars (not visible for most samples, being smaller than graphed symbols) show the geometric mean and geometric SD of technical duplicates from one experiment, representative of trends from three independent experiments (n = 3).

5.3 Discussion

5.3.1 Systems for quantitation of *S. aureus* uptake by DC

Efficient bacterial internalisation by DC is critical in order to acquire sufficient antigen for presentation to elicit a potent T-cell response. Moreover, bacterial internalisation is also critical for DC stimulation and activation via the stimulation of internal innate PRRs such as cGAS, STING, TLR8, TLR9 and TLR13[5]. It is therefore useful to be able to easily and accurately quantify the relative amount of bacterial uptake by DC. Here we found that flow cytometry is a useful tool able to quantify relative differences in uptake of GFP recombinant *S. aureus* by DC. The use of this system provided a useful tool to quantify MRSA uptake by DC, and demonstrated DC internalisation of DapS A8819 is more efficient than that of the DapR A8817 daughter strain (figure 5.1c and d). These findings are consistent with our hypothesis that the activation of DC in response to these strains was related to their relative capacity for internalisation by DC.

Importantly, the use of GFP as model to quantify internalisation by DC presented two main issues: (i) that GFP is susceptible to degradation both by endosomal proteases and by the lowering of the pH[251]; and (ii) that in the absence of fluorescence microscopy, the acquisition of GFP expression by DC cannot reliably differentiate between bacterial internalisation and bacterial binding at the cell surface. In order to overcome these limitations, we optimised the pH sensitive dye pHrodo for flow analysis (figure 5.2). Indeed, the pHrodo system was found to be at least two times more sensitive than GFP; both in the estimation of number of DC internalising bacteria and the quantitation of relative uptake (figure 5.2). Importantly, pHrodo fluorescence was sufficiently sustained to identify positive DC over a 12 hour time course (figure 5.2b), following the initial fluorescent burst occurring in the first hour (figure 5.2).

While both pHrodo and GFP fluorescence decreased from as early as 4 hours post stimulus (figure 5.2c); the lower relative fluorescence of GFP led to an inability to distinguish DC which had internalised *S. aureus* (figure 5.2b). The poor performance of GFP under the acidified conditions of the endosomes are consistent with findings of Patterson *et. al.,* whereby GFP becomes highly unstable at pH below 6[251]. Of note, the degradation of GFP occurred more rapidly in cDC2 compared to cDC1; a finding consistent with the less acidic endosomes in cDC1, which are required for efficient cross-

presentation of antigen[252,253]. Indeed, the cDC2 exhibited a brighter pHrodo fluorescence than cDC1 over the time course (figure 5.2c), despite an equivalent GFP fluorescence (figure 5.2c), demonstrating a superior activation of the endosomal dye, as opposed to greater internalisation of bacteria. While the system can therefore provide accurate estimates of relative internalisation of various staphylococcal isolates by DC; we nonetheless suggest caution in the use of this system to directly compare internalisation between DC subsets or indeed multiple cell types.

Critically, the differential uptake of the A8819/A8817 clinical pair was evident across all three DC subsets, in both the GFP and pHrodo systems (figure 5.1d and 6.3 respectively). These findings were further validated through the use of TEM imaging to enumerate uptake in sections of cDC1 (figures 5.5 and 5.7), therefore validating that the differential in pHrodo fluorescence was indeed due to *bona fide* differences in bacterial internalisation, and not a differential endosomal acidification. Importantly, it was clear from the TEM that cDC1 were capable of internalising 2-fold more DapS A8819 than the DapR A8817 daughter strain (figure 5.7b), a finding that reached statistical significance. This trend was consistent throughout both the GFP and pHrodo experiments (figures 5.1, 5.2 and 5.3), therefore validating this approach to rapidly and accurately quantify bacterial internalisation. While both GFP and pHrodo labelled bacteria provided a useful tool for analysing bacterial internalisation by DC, the use of the pHrodo dye is superior for long term experiments, and is the only one of the two dyes capable of accurately distinguishing internalisation from surface binding without the use of microscopy.

5.3.2 Regulation of *S. aureus* internalisation by DC

Having demonstrated differential internalisation of the A8819/A8817 clinical pairs, with the DapS A8819 isolate being more efficiently internalised that the DapR A8817 isolate (table 5.1; figures 5.1, 5.5, 5.6 and 5.7); it seemed likely that the capacity for DC to internalise these strains would more broadly correlate with their subsequent activation. We therefore next considered the A9763/A9764 pair, given that the DapS A9763 isolate has previously been demonstrated to induce more potent inflammation than the A8819 DapS isolate (figure 5.10). Indeed, it was clear that the A9763 isolate was internalised up to four times more efficiently by cDC1 and cDC2 than the DapS A8819 isolate, especially at earlier time points (figure 5.8). Of note, despite differential internalisation of the DapS parent isolates, the two DapR daughter isolates, A8817 and A9764, were internalised by

cDC1 in equivalence (figure 5.8). Yet in contrast, while the DapR A9764 strain is less efficiently internalised by cDC2 than its DapS A9763 parent; this DapR isolate is internalised equally as efficiently as the unrelated DapS A8819 isolate (figure 5.8). These findings therefore suggest that other genetic differences between the two clinical isogenic pairs facilitate these differences in uptake.

In the previous chapter we identified that the acquisition of specific point mutations in both *mprF* and *cls2* are sufficient to impede DC activation (chapter 5, sections 5.2 and 5.3). We therefore theorised that these mutations would similarly impede bacterial internalisation by DC. Importantly, the individual recreation of the A8817 MprF-T345I mutation in A8819 ($A8819_{MprF\text{-}T345I}$), ***did not*** affect the internalisation of bacterial strains by DC (figure 5.9); despite both *cls2* and *mprF* mutations having been demonstrated to play a role in regulating differential activation of DC (chapter 5). Moreover, the individual recreation of two distinct *cls2* point mutations in A8819, were both sufficient to impede *S. aureus* internalisation by DC (figure 5.9 and 5.11); typically to levels approximately equivalent to that of the DapR A8817 isolate. Taken together, these findings explain why the recreation of these mutations in isolation were insufficient to recapitulate the activation phenotype of DC responding to DapR; in that while the *mprF* mutation marginally impedes DC activation by yet uncharacterised mechanisms, the mutation in *cls2* is required to reduce bacterial internalisation by DC, and likely therefore mediates a subsequent evasion of both endosomal and cytosolic sensors.

While the recreation of the *cls2* L52F and T33N mutations similarly impacted DC activation (figures 5.11, 5.12 and 5.17), we found that the recreation of the T33N point mutation had a more profound impact on bacterial internalisation in comparison to the L52F point mutation (figure 5.10 and 6.11). Importantly, the recreation of the L52F mutation in A8819 more closely modelled the level of internalisation of A8817, likely due to the similar closer positioning of the L52F to the F60S mutation arising in A8817 (figure 5.16)[158]. While the inability to recreate the F60S mutation in A8819 is a limitation of the current study, it is nonetheless clear that changes in *cls2* greatly regulate the capacity of DC to internalise clinical isolates of *S. aureus,* subsequently affecting the activation of these DC. It has recently been demonstrated that the *cls2*-T33N mutation impedes neutrophil recruitment to the site of soft tissue infection in zebrafish, as well as affecting human neutrophil migration *in vitro*[194]. The current data therefore suggest a model,

whereby the mutation in *cls2* impairs recognition and uptake by host DC, and likely other innate cells, leading to reduced secretion pro-inflammatory cytokines and importantly neutrophil chemo-attractants such as MIP-1α and MIP-1β.

Table 5.1 Summary of bacterial internalisation splenic DC subsets stimulated with the A8819/A8817 and A9763/A9764 clinical pairs.

	A8819 (DapS)	**A8817 (DapR)**	**A9763 (DapS)**	**A9764 (DapR)**
cDC1	++	+	+++	++
cDC2	+++	+	++++	+++
pDC	+	+	++	+

Chapter 6 – Molecular mechanisms regulating innate recognition of *S. aureus* by DC subsets

In this thesis we have identified novel differences in the capacity of distinct and paired clinical isolates of DC to induce activation of DC, both in terms of cytokine secretion and surface activation. We have further shown that these differences are further recapitulated at the level of internalisation, with poorly immunogenic strains being poorly internalised by DC relative to their more immunogenic parent strains. We therefore next sought to understand the molecular mechanisms by which these two concepts are linked. We hypothesised that a differential in the initial recognition of MRSA by DC may alter both activation and internalisation of these isolates; and further, that differences in internalisation may further impede activation, resultant from a decreased load of potential intracellular PRR ligands.

In this section we explore the role of the almost ubiquitous TLR signalling molecule MyD88 on the activation of DC in response to MRSA, and further consider the role of endosomal and intracellular PRRs in the recognition of these strains. We find that MyD88 is required for potent activation of DC in response to MRSA isolates, and demonstrate a partial dependence on TLR9. Moreover, we demonstrate in addition to the sensing of nucleic acid by TLR9, the cytosolic sensor cGAS is implicated in the sensing of these strains.

6.1 DC activation following MRSA stimuli is partly dependent on MyD88

Having demonstrated a differential in the internalisation of DapS and DapR clinical pairs by DC (chapter 6), it seemed likely that the subsequent differential in activation was due to a decreased pathogen load and availability of immunogenic PAMPs. We hypothesised that DC activation and bacterial internalisation were related, with reduced DC activation correlating reduced bacterial internalisation as a result of a decrease in pathogenic load. It seemed likely that these differences were regulated either via TLR2, regulating detection at the cell surface given the differences in the bacterial cell wall and membrane[158,194]; or via nucleic acid receptors such as TLR9, considering the differences in bacterial uptake and therefore subsequent reduction in nucleic acids for efficient

stimulation of DC. In order to further elucidate the role of these TLRs, we first considered the requirement for MyD88 signalling in the DC response to MRSA.

Given both our extensive phenotyping of FLDC presented in chapter 3, and the ability to culture FLDC in larger scale than directly purifying primary splenic DC, we next cultured FLDC from murine MyD88$^{-/-}$ bone marrow to examine the role of MyD88 signalling in the DC response to MRSA. We found that day 8 FLDC from MyD88 bone marrow were phenotypically similar to their WT counterparts (figure 6.1a), with each MyD88$^{-/-}$ subset differentiating in an approximately equivalent abundance to WT (figure 6.1a). We further compared the 18 hour survival of the DC in culture with and without stimuli with various TLR agonists and MRSA, and again found no substantive differences in cDC viability between the two strains (figure 6.1b). By contrast, MyD88$^{-/-}$ pDC viability tended to be lower than WT at 18 hours, both following stimuli, and with culture in media alone (figure 6.1b), indicating that MyD88 signalling may be required to sustain optimal pDC survival. As expected, we found that all MyD88$^{-/-}$ FLDC subsets were essentially unresponsive in terms of cytokine secretion following stimulation with the TLR9 and TLR2 agonists (CpG and PGN respectively), but not the TRIF dependent TLR3 agonist poly:IC (figure 6.3a and data not shown). Cumulatively, these data confirm functional KO of MyD88 in the DC examined, whilst validating the flt3-l induced DC culture system from MyD88$^{-/-}$progenitors.

6.1.1 DC surface maturation in response to MRSA is partially dependent on MyD88

Investigating the dependence of cDC1 on MyD88 signalling for cell surface activation of the DC revealed that they were partially dependent on MyD88 for activation, with co-stimulation markers reaching, on average, half that of their WT control (figure 6.2a). This was especially evident for the co-stimulatory markers CD40 and CD80, which averaged approximately 3-fold higher expression for WT than MyD88$^{-/-}$ following stimulation with the DapS A8819 isolate (figure 6.2a). Importantly, we found that the differential expression of CD80 in response to the A8819/A8817 clinical pair was conserved following stimuli of MyD88$^{-/-}$ cDC1- and indeed the cDC2 and pDC (figure 6.2). These data therefore demonstrate that the differences observed in CD80 expression following stimuli with these two strains occur independent of signalling through MyD88.

The expression of CD86, MHC-II and PD-L1 by MyD88$^{-/-}$ cDC2 following MRSA stimuli were approximately equivalent to that of the cDC1 (figure 6.2a and b), however MyD88$^{-/-}$ cDC2 upregulated both CD40 and CD80 co-stimulatory markers to levels higher than that of the KO cDC1 following stimuli with MRSA (figure 6.2a and b). This finding is consistent with the capacity of MyD88 deficient cDC2 to produce limited cytokines in response to these stimuli (figure 6.3b), and demonstrates that cDC2 are dependent on MyD88 signalling for activation in response to MRSA, -although less so than are cDC1. By contrast the surface profile of MyD88 deficient and WT pDC were comparable, suggesting that their activation in response to MRSA is independent of MyD88 signalling (figure 6.2c).

Importantly, the MyD88 deficiency suppressed the spontaneous upregulation of activation markers by cDC1, cDC2 and pDC typically observed following 18 hours culture in media alone (figure 6.2a, b and c respectively), indicating that this process was partially dependent on signalling via MyD88. However, this spontaneous activation was not however sufficient to account the difference between MyD88 deficient and WT FLDC stimulated with MRSA- with the difference in expression being in many cases greater than 2-fold (figure 6.2a and b).

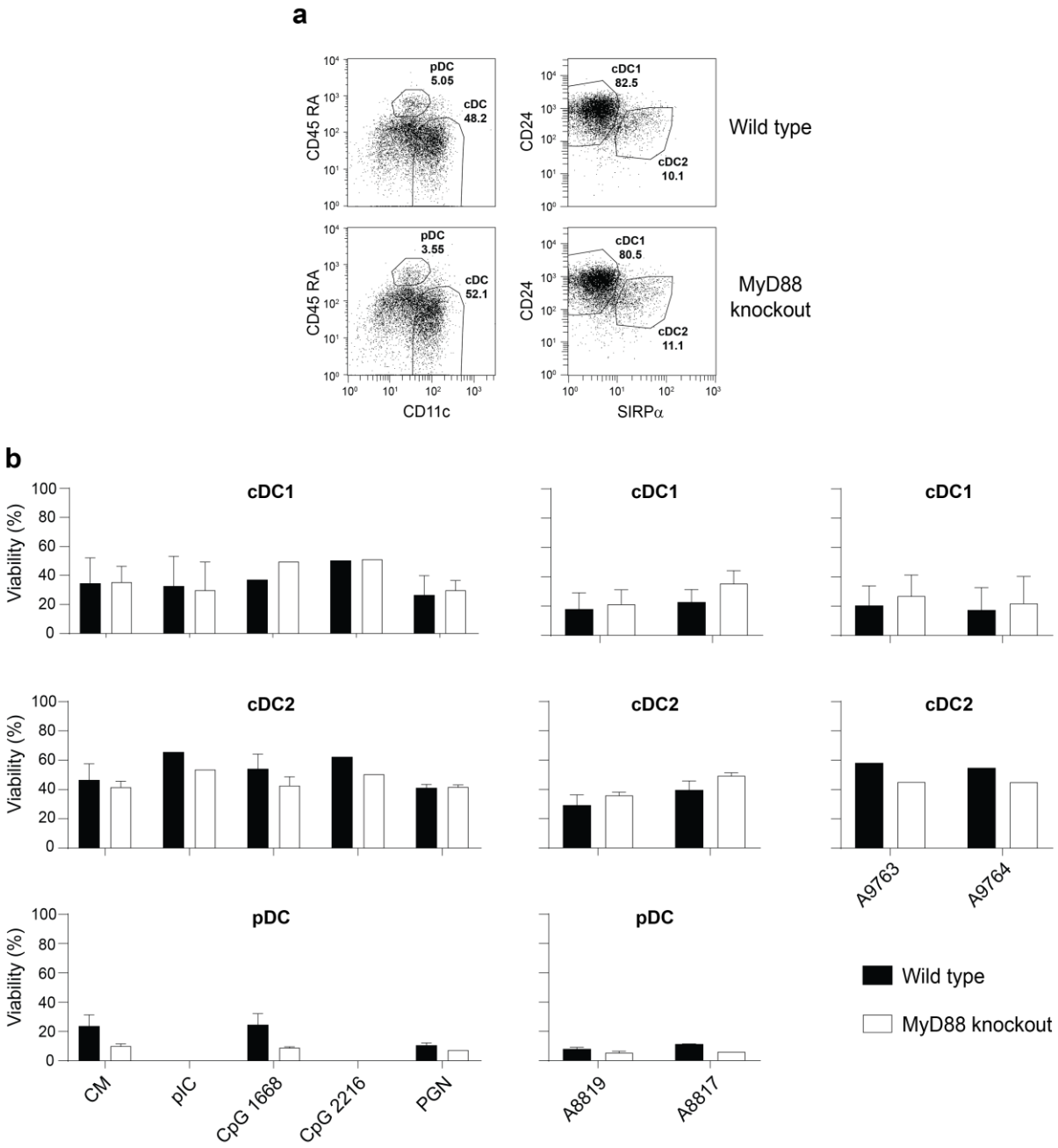

Figure 6.1 MyD88 FLDC differentiate equivalent to their wild-type counterparts.

(a) *Phenotype of unsorted day 8 wild-type (top) and MyD88 knockout (bottom) FLDC. FLDC were gated on cell sized events, and dead cells excluded via differential staining in propidium iodide (not shown). pDC and cDC were separated based on differential expression of CD11c (clone N418) and CD45RA (clone 14.8), with cDC1 and cDC2 subsequently separated based on their respective expression of CD24 (clone M1/69) and SIRPα (clone P84). Dot plots shown are from one experiment, representative of two independent experiments (n = 2).* ***(b)*** *Survival of FACS sorted MyD88 knockout (hollow bars) and wild-type (filled bars) FLDC, as determined via differential staining in propidium iodide. Survival was quantified via flow analysis at 18 hours post stimuli with pIC (100 µg/ml), CpG ODN 1668 and 2216 (0.5 µM), peptidoglycan (10 µg/ml), media alone and paired clinical isolates of daptomycin exposed MRSA A8819/A8817 and A9763/A9764 (MOI = 10). Error bars (where shown) indicate the range of viability from two independent experiments (n = 2).*

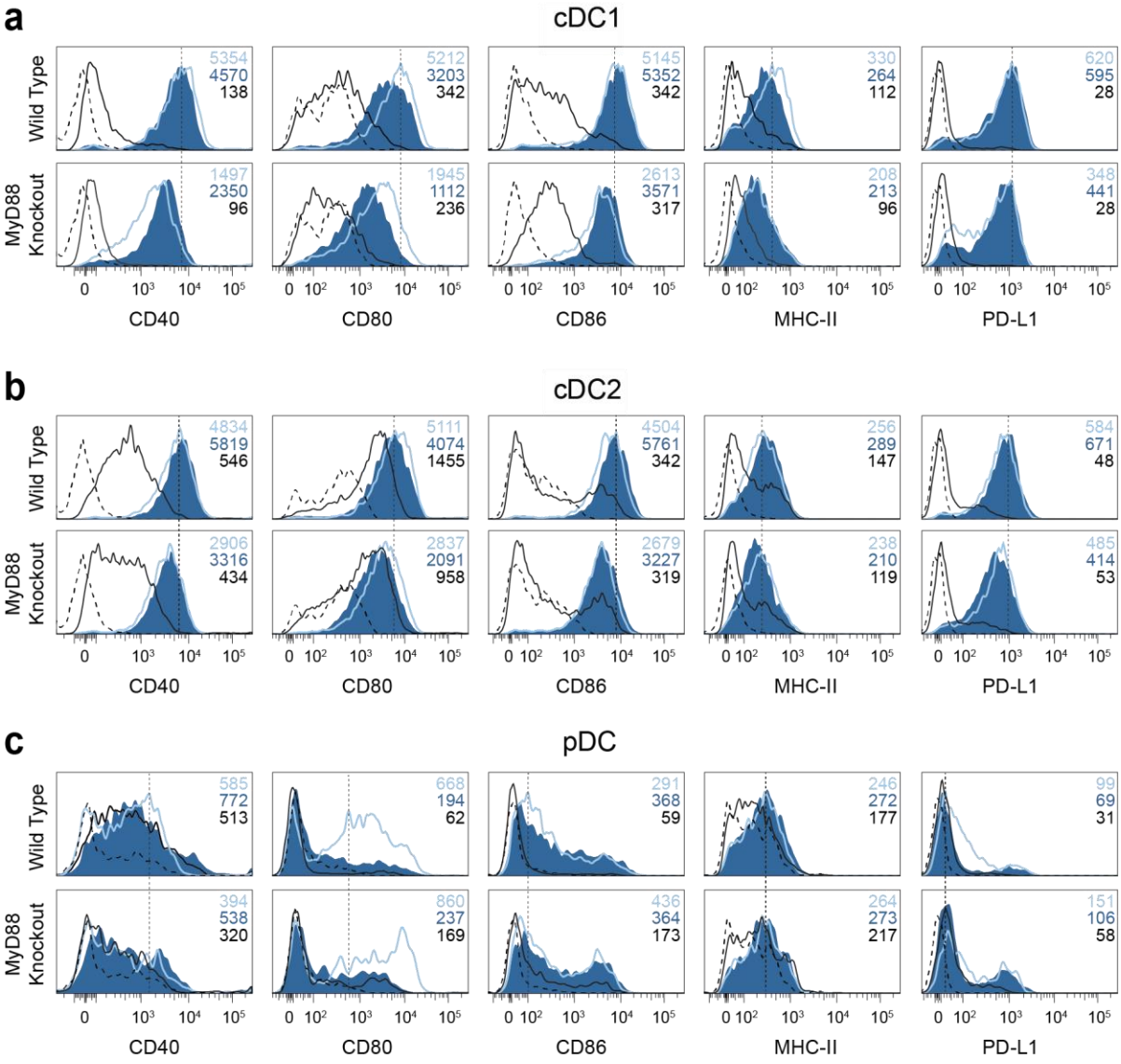

Figure 6.2 MyD88 knockout impedes but does not ablate surface activation of FACS sorted FLDC following MRSA stimuli.

Activation marker expression by FACS sorted cDC1 ***(a),*** *cDC2* ***(b)*** *and pDC* ***(c)*** *following 18 hour stimulation with A8819 DapS MRSA (light blue trace), A8817 DapR MRSA (dark blue shaded), or complete media (black solid line). Histograms showing CD40, CD80, CD86, MHC-II and PD-L1 expression with pooled FMO (dotted black line). Vertical dotted lines included on each panel from the mode of wild-type A8819 for each marker, to demonstrate peak shift in fluorescence between wild type and MyD88 knockout DC. Data shown from one experiment, without replicates for CD86 expression (CD86), but for all other markers representative of two independent experiments (n = 2).*

6.1.2 Cytokine secretion by DC in response to MRSA is dependent on MyD88

We therefore next compared the ability of MyD88$^{-/-}$ and WT FLDC subsets to respond to the daptomycin exposed A8817/A8819 and A9763/A9764 clinical pairs. We found that cDC1 were entirely dependent on MyD88 signalling to produce RANTES, MIP-1α, MIP-1β, IL-6, IL-10, IL-12p70 and TNF-α (figure 6.3a). The only cytokines tested that were produced by cDC1 independent of MyD88 in response to these stimuli were MDC and IFN–β, the latter of which can be induced in DC via the signalling of cytosolic DNA sensors[254]. Of particular note, MyD88$^{-/-}$ cDC1 produced more MDC in response to the A8819 DapS MRSA strain than they did the A8817 DapR strain- an *inverse* trend to which we have observed in all experiments thus far for this cytokine (figure 6.3a and chapter 3). These findings suggest that MDC is produced partly dependently and independently of MyD88. The higher production from cDC1 in response to the DapR strains though seems MyD88 *dependent*.

The cDC2 and pDC shared a similar dependence to cDC1 on MyD88 signalling for the production of all tested inflammatory mediators in response to MRSA stimuli, again with the exception of MDC and IFN-β (figure 6.3b). However, MyD88$^{-/-}$ cDC2 and pDC were not *entirely* dependent on MyD88 for production of detectable RANTES, MIP-1α, MIP-1β and TNF-α in response to MRSA stimuli (figure 6.3b), producing these cytokines to levels above the constitutive level observed following stimuli with media alone (data not shown) . These data therefore demonstrate that while both cDC2 and pDC are dependent on MyD88 signalling for activation in response to MRSA, they undergo partial activation mediated by a pathway independent of MyD88. Finally, as a validation step we examined the response of MyD88$^{-/-}$ and WT DC following stimuli with four other daptomycin exposed pairs (table 2.4), that reproduced these trends- clearly demonstrating dependence of DC on MyD88 for effective activation and cytokine production in response to MRSA (Appendix A5).

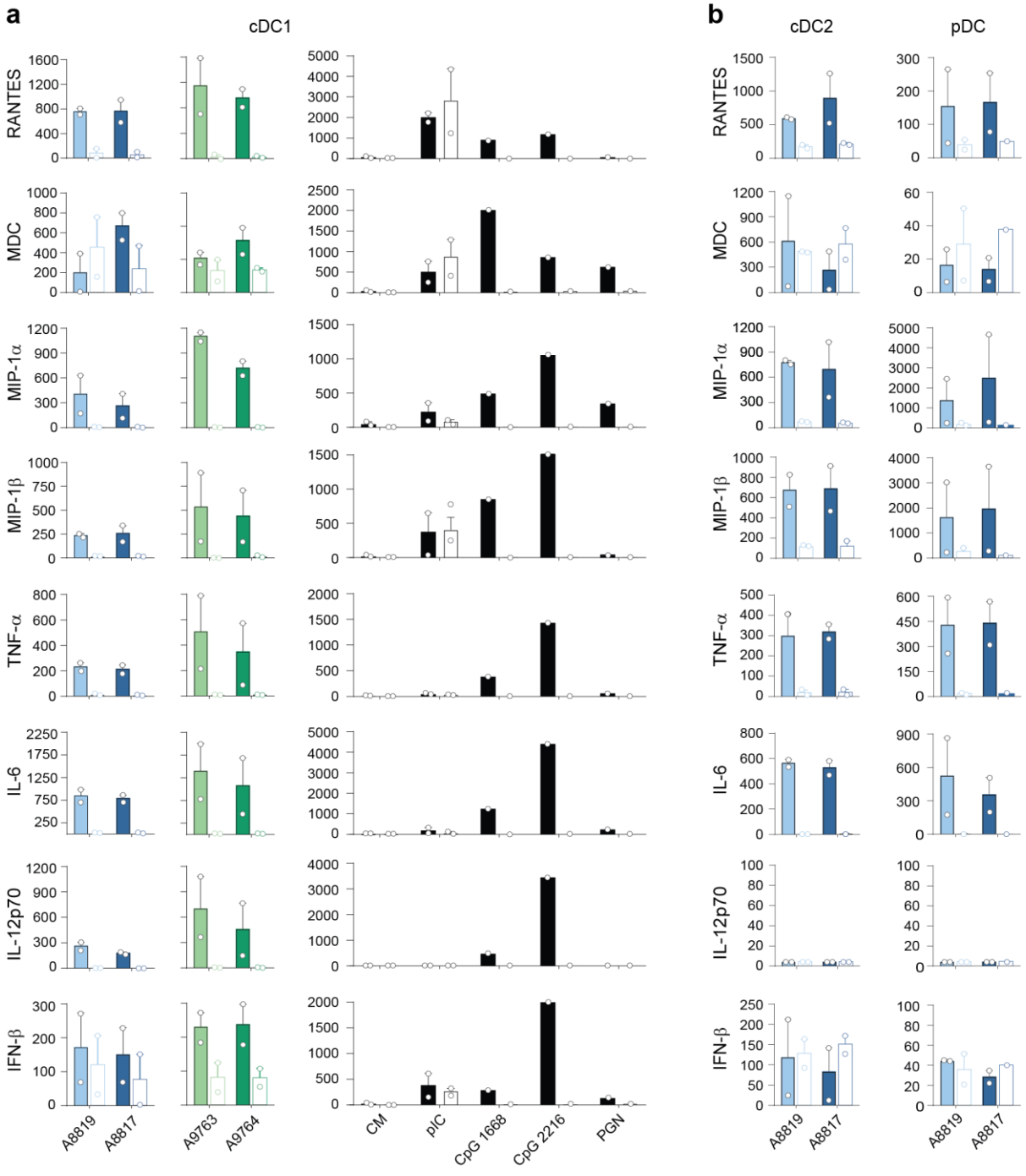

Figure 6.3 MyD88 signalling is required to produce inflammatory cytokines following MRSA stimuli. ***(a)*** *Cytokine production (pg/ml) by MyD88 knockout (hollow bars) and WT control (filled bars) FACS sorted cDC1 at 18 hour post stimulus with paired daptomycin exposed MRSA isolates (A8819/A8817; blue and A9763/A9764; green), complete media alone (CM), pIC (100 µg/ml), CpG ODN 1668 or 2216 (0.5 µM) and peptidoglycan (PGN, 10 µg/ml). Bars show the mean and range of replicates from two independent experiments (n = 2).* ***(b)*** *Cytokine production (pg/ml) by MyD88 knockout and WT control as in 'a', by FACS sorted cDC2 and pDC at 18 hour post stimulus with paired daptomycin exposed MRSA isolates (A8819/A8817; blue and A9763/A9764; green). Bars show the show the mean and range of replicates from two independent experiments (n = 2), except for the A8817 stimuli of pDC with one available replicate (n = 1).*

6.2 cDC1 cytokine production in response to MRSA is dependent on TLR9 and cGAS sensing of nucleic acids

6.2.1 TLR9 signalling affects surface activation, but not maturation or viability of splenic DC

Having demonstrated a clear dependence on MyD88 for inflammatory cytokine and chemokine production by all FLDC subsets in response to MRSA, we validated these findings in *ex vivo* splenic DC finding that the dependence on MyD88 was conserved (data not shown). We next considered the role of various TLRs in the response to *S. aureus.* Considering the reduction in uptake of DapR MRSA by DC described in chapter six, and that the MyD88 dependence was seen across the subsets, we therefore hypothesised that the differential recognition of MRSA was mediated by the endosomal sensor for bacterial DNA, TLR9, expressed by all subsets of FLDC.

We therefore next tested the effect of MRSA stimulation on *ex vivo* TLR9 knockout murine splenic DC. The phenotype of splenic DC subsets and their relative abundance were consistent between $TLR9^{-/-}$ and wild-type mice (figure 6.4a). Furthermore, the overall viability of DC subsets was relatively consistent between the two genotypes following overnight stimuli in media alone, pIC (TLR3 agonist), peptidoglycan (TLR2 agonist), and indeed the clinical isolates of *S. aureus* (figure 6.4b). Of note, despite equivalence in viability, the $TLR9^{-/-}$ cDC upregulated surface CD80, PD-1 and PD-L1 to levels up to 30% higher than WT following stimulation with A8819 (figure 6.5a and b). Similarly, upregulation of CD80, PD-1 and PD-L1 was impeded in $TLR9^{-/-}$ mice (figure 6.5c), although to a lesser extent than the cDC. Cumulatively, these findings suggest that TLR9 signalling negatively regulates the expression of CD80, PD-1 and PD-L1, ***but not*** MHC-II or PD-L2.

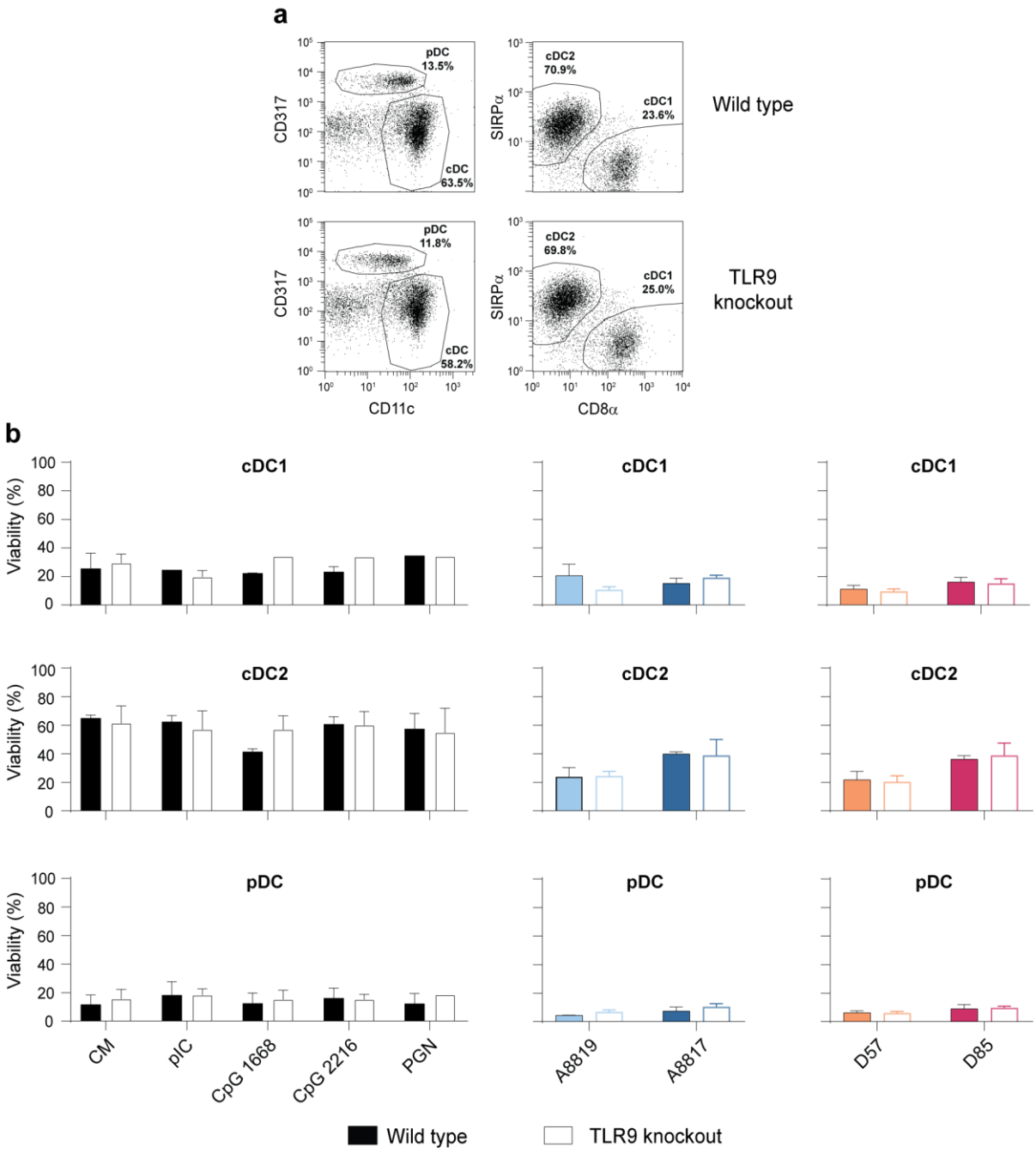

Figure 6.4 TLR9 knockout DC develop phenotypically equivalent to their wild-type counterparts in vivo. ***(a)*** *Phenotype ex vivo splenic DC from wild-type (top) and TLR9 knockout (bottom) mice. Splenic DC are gated on cell sized events, and dead cells subsequently excluded via differential staining in propidium iodide (PI, not shown). pDC and cDC are separated based on differential expression of CD11c (clone N418) and CD317 (clone 120.G8), with cDC1 and cDC2 subsequently separated based on respective expression of CD8α (clone 53-6.7) and SIRPα (clone P84). Dot plots shown from one experiment, representative of two independent experiments (n = 2).* ***(b)*** *Survival of FACS sorted TLR9 knockout (hollow bars) and wild-type (filled bars) ex vivo splenic DC, as determined via differential staining in PI, at 18 hours post stimuli with pIC (100 µg/ml), CpG ODN 1668 and 2216 (0.5 µM), peptidoglycan (10 µg/ml), media alone, paired clinical isolates of dap exposed MRSA A8819/A8817, MSSA isolates D57 and D85 (MOI = 10). Error bars (where shown) indicate the range of two independent experiments (n = 2).*

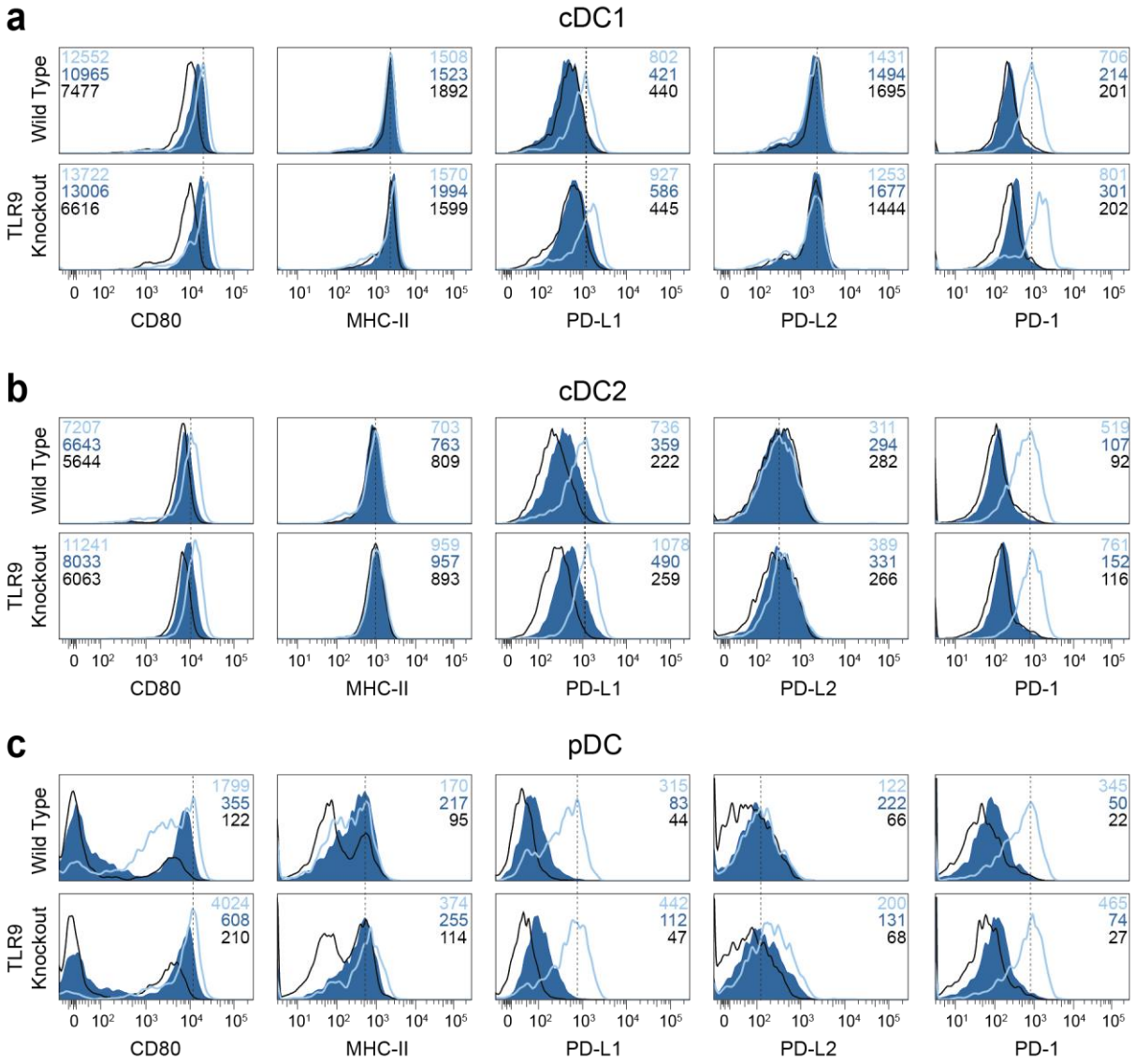

Figure 6.5 TLR9 knockout enhances surface activation of FACS sorted FLDC following MRSA stimuli. *Activation marker expression by FACS sorted cDC1* ***(a),*** *cDC2* ***(b)*** *and pDC* ***(c)*** *following 18 hour stimulation with A8819 DapS MRSA (light blue trace), A8817 DapR MRSA (dark blue shaded), or complete media (black solid line). Histograms showing CD40, CD80, CD86, MHC-II and PD-L1 expression with pooled FMO (dotted black line). Numerical values in each panel represent the gMFI of each marker for bacterial or mock CM stimuli as indicated. Vertical dotted lines included on each panel from the mode of wild-type A8819 for each marker, to demonstrate peak shift in fluorescence between wild type and TLR9 knockout DC. Data shown from one experiment, without replicates for CD86 expression (CD86), but for all other markers representative of two independent experiments (n = 2).*

6.2.2 Cytokine production by cDC1 but not cDC2 or pDC is dependent on TLR9 in response to *S. aureus* clinical isolates

Consistent with the MyD88$^{-/-}$ cDC1, we found that TLR9$^{-/-}$ splenic cDC1 were unable to produce appreciable MIP-1α in response to MRSA or MSSA isolates (figure 6.6); with the exception A9763/A9764 clinical pair, which elicited MIP-1α production to levels approximately half that of WT (figure 6.6). Further dependence on TLR9 was observed to produce TNF-α in response to both MRSA and MSSA, with the exception of one outlier for A8819 (figure 6.6). However, the production of MIP-1b appeared only partially dependent on TLR9 in response to MRSA, and to MSSA isolates (figure 6.6). Consistent with the MyD88$^{-/-}$ data, the production of MDC occurred entirely independently of TLR9 in response to both MRSA and MSSA isolates. (figure 6.6). Of note, MDC was the only inflammatory mediator detectable following stimulus of TLR9$^{-/-}$ cDC1 with CpG ODNs (figure 6.6), providing evidence that this chemokine may be regulated independently of the other inflammatory cytokines and chemokines in response to stimuli with *S. aureus*. The production of MDC in response CpG in TLR9$^{-/-}$ mice suggests detection by some other innate receptor able to detect ssDNA, subsequently inducing restricted cytokine production. This hypothesis may potentially explain the inverse trend of MDC production, relative to other cytokines, previously observed in response to the A8819/A8817 pair.

In stark contrast to splenic cDC1, neither cDC2 (figure 6.7) nor pDC (figure 6.8) were dependent on TLR9 for the production of MIP-1α, MIP-1b or TNF-α in response to the paired A8819/A8817 and A9763/A964 (where tested) MRSA clinical isolates. Independence of TLR9 was further observed for both cDC2 and pDC (figures 6.7 and 6.8 respectively) following stimulation with the unpaired MSSA clinical isolates D57 and D85, with the caveat of MIP-1α, which in one biological replicate was produced to far greater levels by wild-type cDC2 than TLR9$^{-/-}$ (figure 6.7).

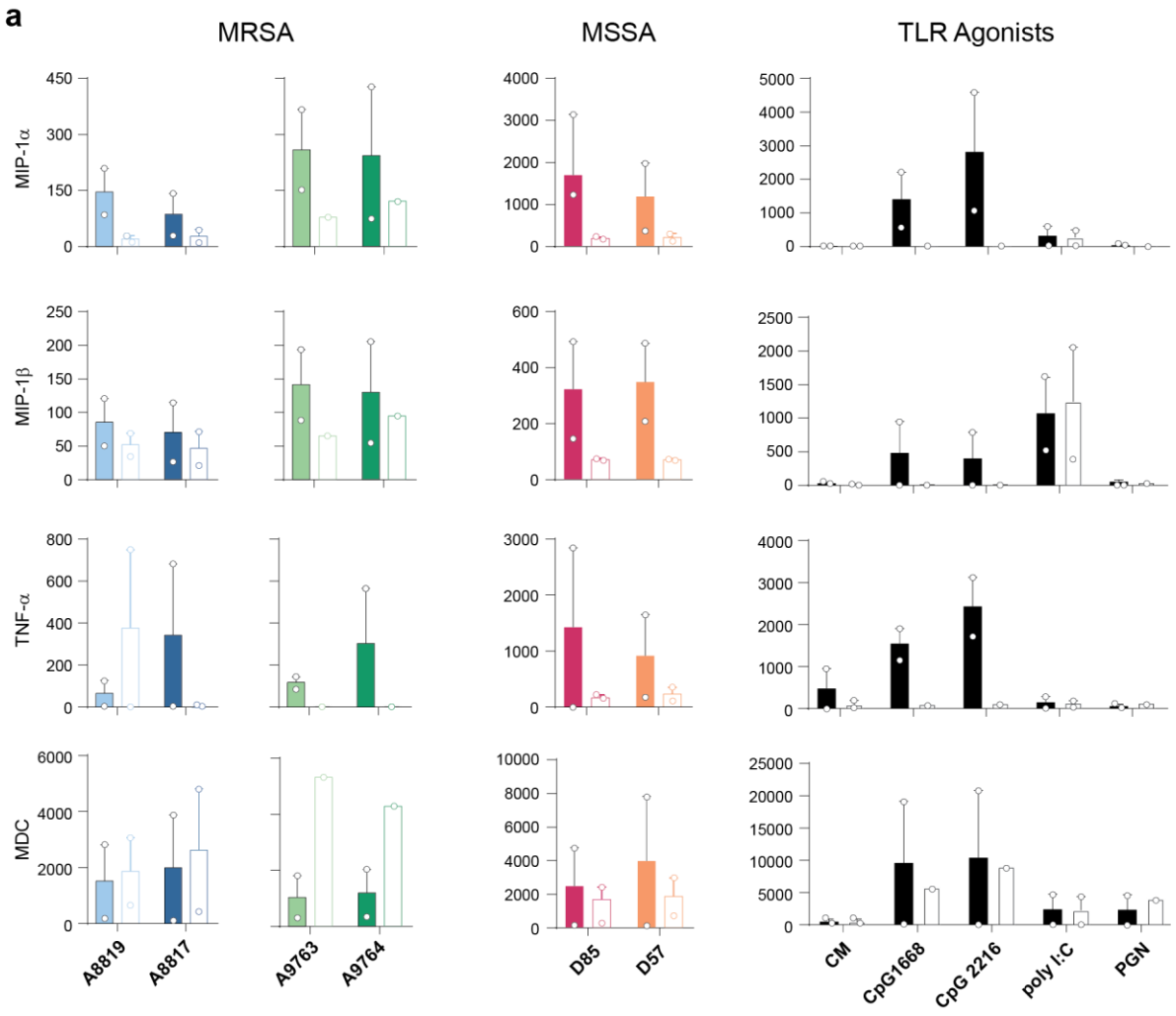

Figure 6.6 TLR9 is required by splenic cDC1 to induce strong TNF-a, MIP-1a and MIP-1b production in response to MRSA and MSSA clinical isolates.

(a) *Cytokine production (pg/ml) by wild-type (filled bars) and TLR9 knockout (hollow bars) by FACS sorted cDC1 at 18 hour post stimulus with paired daptomycin exposed MRSA isolates (A8819/A8817 and A9763/A9764), two unrelated MSSA isolates (D57 and D85), complete media alone, CpG ODN 1668 or 2216 (0.5 µM), pIC (100 µg/ml) and peptidoglycan (10 µg/ml). Bars show the mean and range of replicates from two independent experiments (n = 2).*

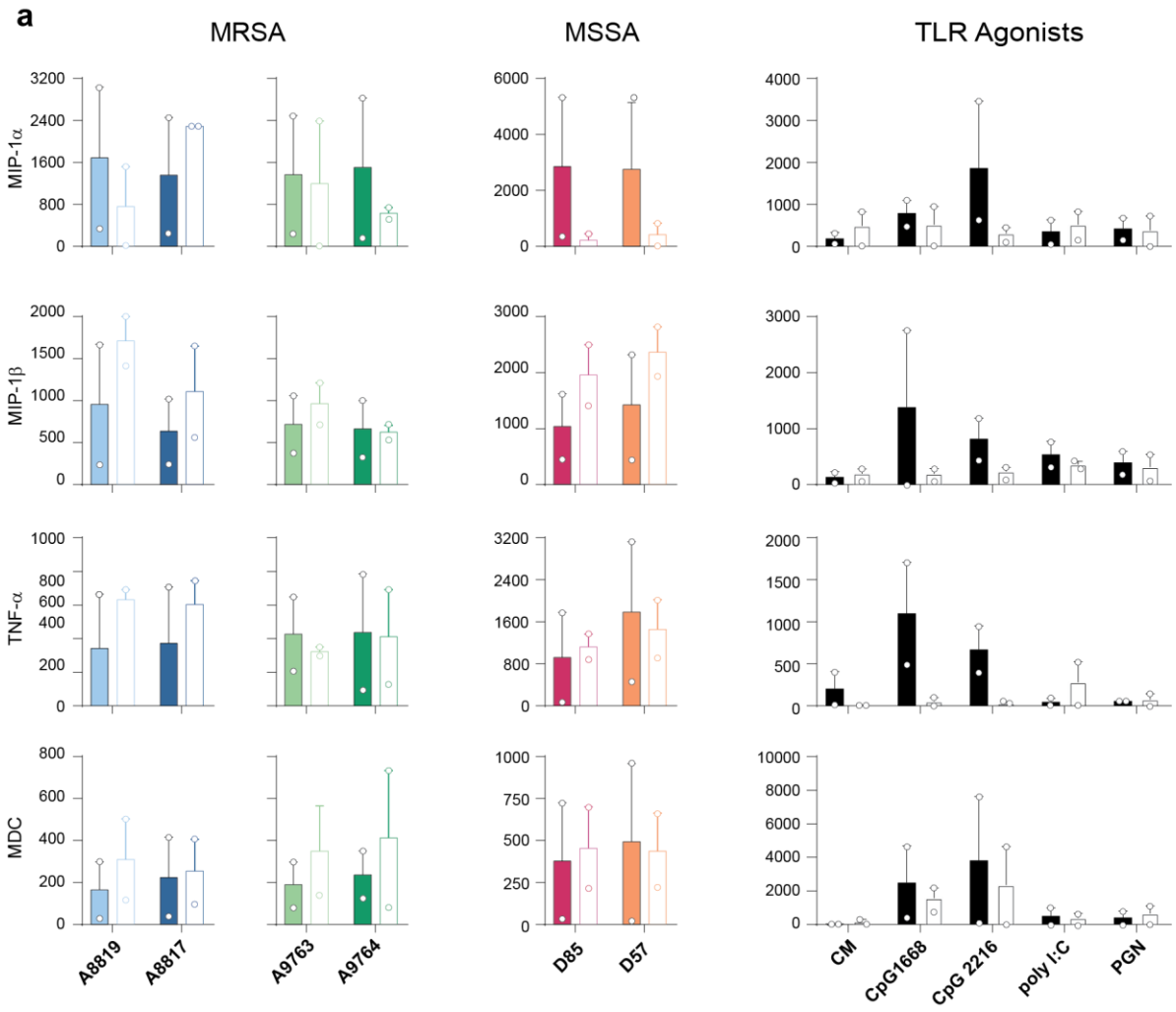

Figure 6.7 TLR9 is not required by splenic cDC2 to induce strong cytokine and chemokine production in response to MRSA and MSSA clinical isolates.

(a) *Cytokine production (pg/ml) by wild-type (filled bars) and TLR9 knockout (hollow bars) by FACS sorted cDC1 at 18 hour post stimulus with paired daptomycin exposed MRSA isolates (A8819/A8817 and A9763/A9764), two unrelated MSSA isolates (D57 and D85), complete media alone, CpG ODN 1668 or 2216 (0.5 µM), pIC (100 µg/ml) and peptidoglycan (10 µg/ml). Bars show the mean and range of replicates from two independent experiments (n = 2).*

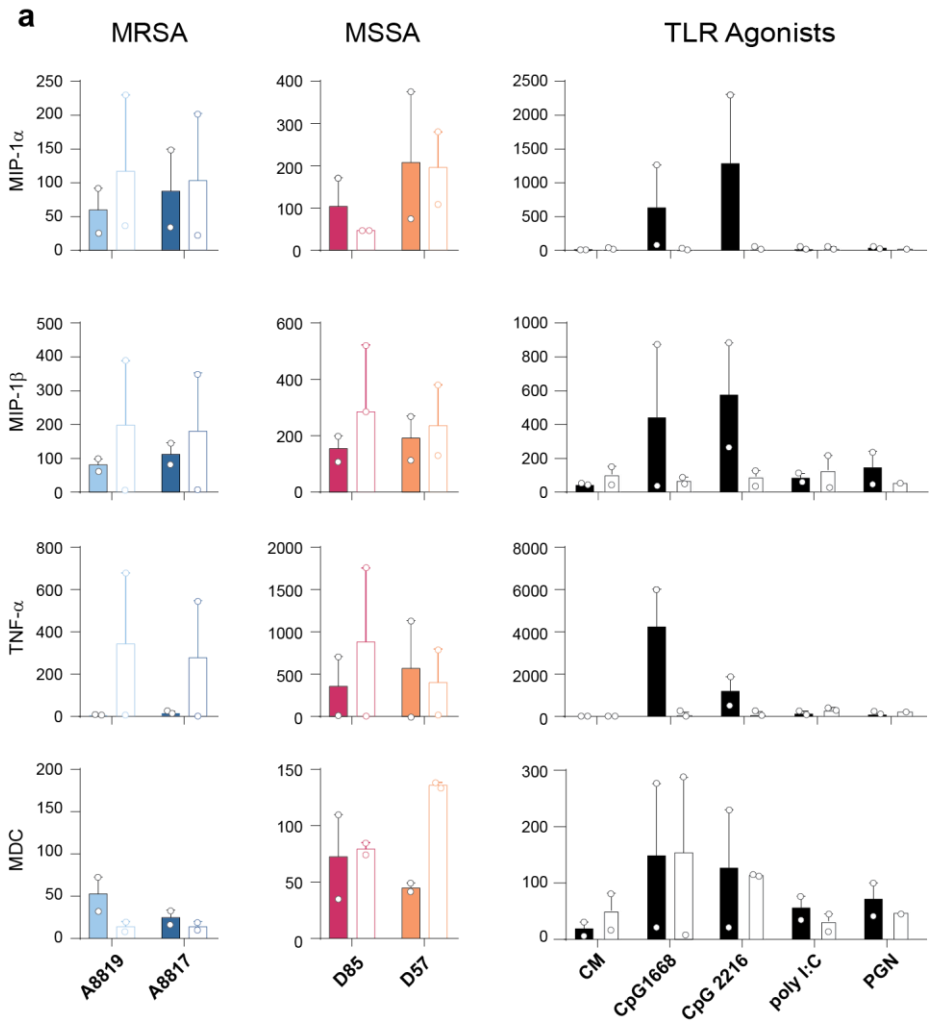

Figure 6.8 TLR9 is not required by splenic pDC to induce strong cytokine and chemokine production in response to MRSA and MSSA clinical isolates.

(a) Cytokine production (pg/ml) by wild-type (filled bars) and TLR9 knockout (hollow bars) by FACS sorted cDC1 at 18 hour post stimulus with paired daptomycin exposed MRSA isolates (A8819/A8817), two unrelated MSSA isolates (D57 and D85), complete media alone, CpG ODN 1668 or 2216 (0.5 µM), pIC (100 µg/ml) and peptidoglycan (10 µg/ml). Bars show the mean and range of replicates from two independent experiments (n = 2).

6.2.3 cGAS signalling does not affect maturation, viability or surface activation of splenic DC

Despite having observed a dependence of cDC1 on both MyD88 and TLR9 for the production of most inflammatory cytokines and chemokines, it remained to determine the regulatory pathways controlling the production of MDC and IFN-β in response to *S. aureus* isolates- which were produced independently of MyD88 signalling (figure 6.1). Given that IFN-β secretion following signalling of activated cytoplasmic nucleic acid sensors is well established[254], we sought to investigate the role of the well charactered PRR cyclic GAMP synthase (cGAS) in response to *S. aureus.*

We therefore next tested the effect of MRSA stimulation on *ex vivo* cGAS knockout murine splenic DC, in comparison to their wild-type counterparts. Importantly, we found that the both the phenotype of splenic DC subsets and their relative abundance within the spleen were consistent between the cGAS knockout mice and wild-type controls (figure 6.9a). Furthermore, the overall viability of DC subsets was consistent between the two genotypes following overnight stimuli in media alone, peptidoglycan (TLR2 agonist), pIC (TLR3 agonist), CpG ODNs 1668 and 2216 (TLR9 agonists) and indeed the daptomycin exposed clinical isolates of *S. aureus* (figure 6.9b). These findings therefore validate the functional equivalence of wild-type and cGAS$^{-/-}$ *ex vivo* murine splenic DC subsets for our studies regarding activation and immunogenicity in response to bacterial isolates.

The surface activation phenotype of cGAS$^{-/-}$ mice was unperturbed following stimulation with the A8819/A8817 clinical pair (figure 6.10), in contrast to the substantive difference observed for TLR9$^{-/-}$ mice (figure 6.5).

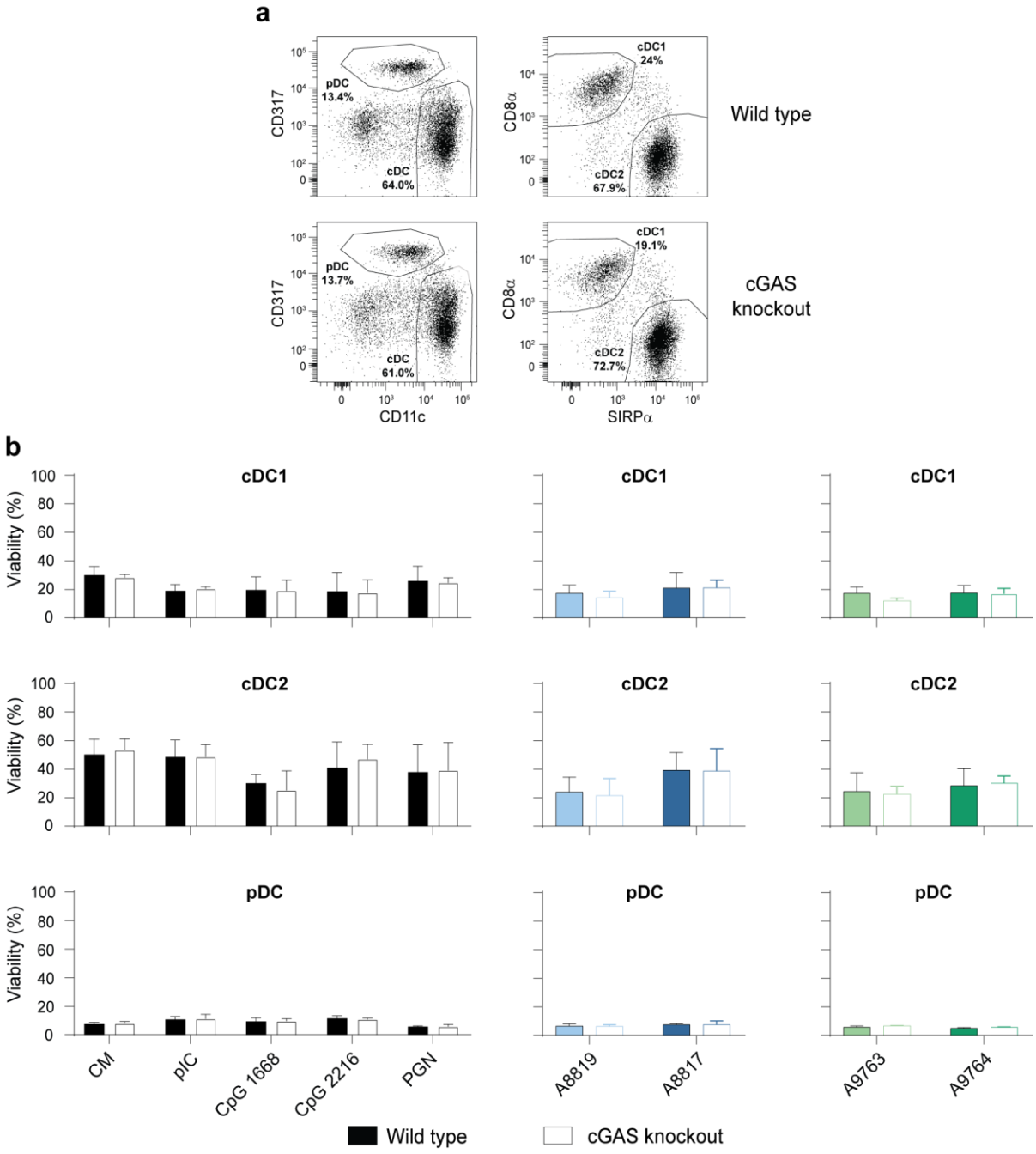

Figure 6.9 cGAS knockout DC develop phenotypically equivalent to their wild-type counterparts in vivo. ***(a)*** *Phenotype ex vivo splenic DC from wild-type (top) and cGAS knockout (bottom) mice. Splenic DC are gated on cell sized events, and dead cells subsequently excluded via differential staining in propidium iodide (PI, not shown). pDC and cDC are separated based on differential expression of CD11c (clone N418) and CD317 (clone 120.G8), with cDC1 and cDC2 subsequently separated based on respective expression of CD8α (clone 53-6.7) and SIRPα (clone P84). Dot plots shown from one experiment, representative of three independent experiments (n = 3).* ***(b)*** *Survival of FACS sorted cGAS knockout (hollow bars) and wild-type (filled bars) ex vivo splenic DC, as determined via differential staining in PI, at 18 hours post stimuli with pIC (100 µg/ml), CpG ODN 1668 and 2216 (0.5 µM), peptidoglycan (10 µg/ml), media alone, paired clinical isolates of dap exposed MRSA (A8819/A8817 and A9763/A9764)at a MOI of 10. Bars show the mean ± SEM from three independent experiments (n = 3).*

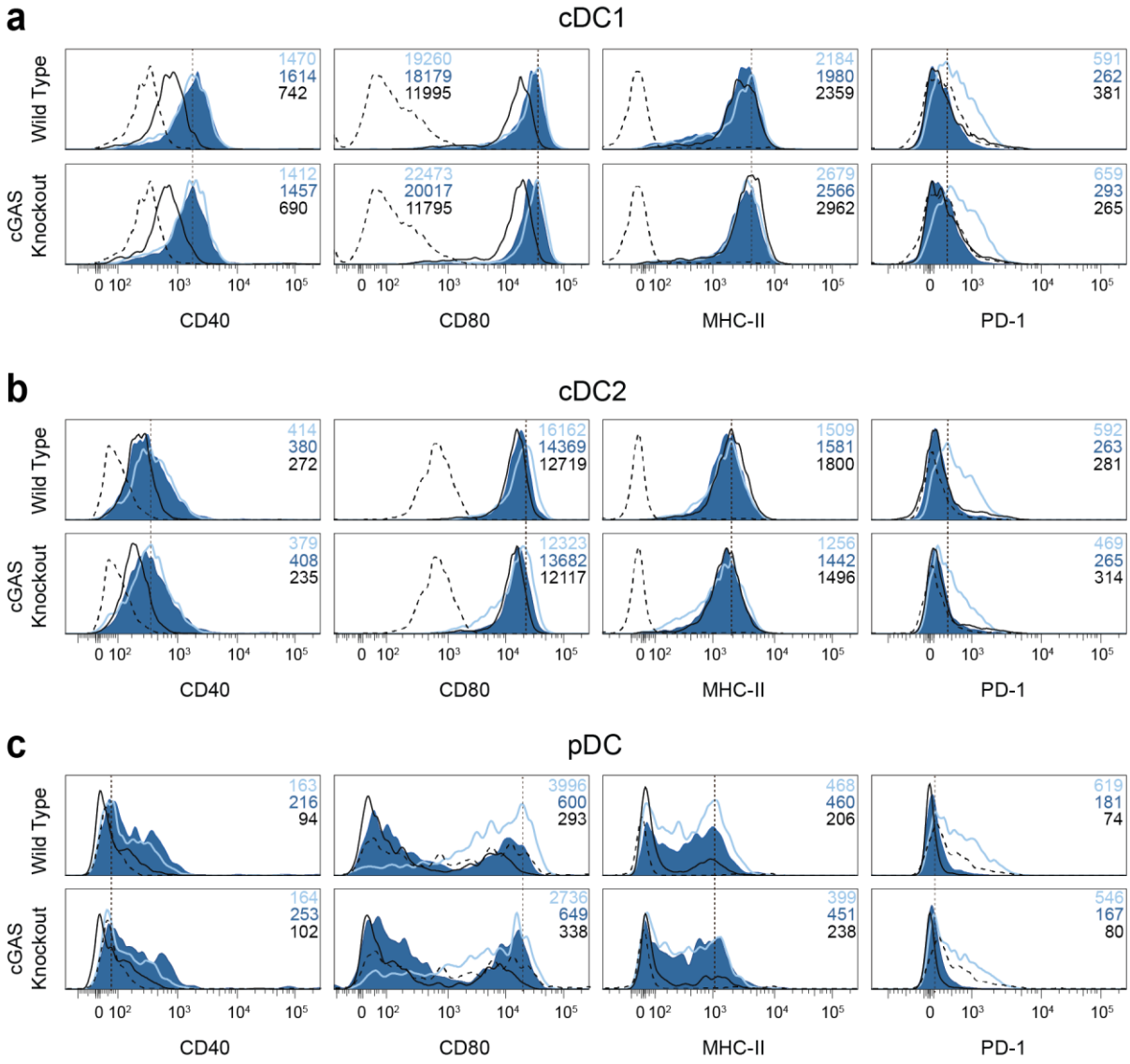

Figure 6.10 cGAS knockout impedes surface activation of FACS sorted pDC but not cDC following MRSA stimuli.

Activation marker expression by FACS sorted cDC1 (a), cDC2 (b) and pDC following 18 hour stimulation with A8819 DapS MRSA (light blue trace), A8817 DapR MRSA (dark blue shaded), or complete media (black solid line). Histograms showing CD40, CD80, MHC-II and PD-1 expression, with pooled FMO for each DC subset (dotted black line). Numerical values in each panel represent the gMFI of each marker for bacterial or mock CM stimuli as indicated. Vertical dotted lines included on each panel from the mode of wild-type A8819 for each marker, to demonstrate peak shift in fluorescence between wild type and cGAS knockout DC. Data shown from one experiment, without replicates for CD86 expression (CD86), but for all other markers representative of two independent experiments (n = 2).

6.2.4 Differential cytokine production in response to *S. aureus* clinical isolates by cDC1 is dependent on the cGAS/STING pathway

In stimulating cGAS$^{-/-}$ cDC1 with the DapS A8819 clinical isolate, we found that the production of TNF-α, IL-6, IL-12p70, and GROα was decreased overall in comparison to the WT control (figure 6.11a); suggesting that cDC1 may dependent on cGAS to produce these cytokines. In first considering the production of the aforementioned cytokines in response to stimulation with A8819/A8817 clinical pair (figure 6.11a), it is striking that stimulation of cGAS$^{-/-}$ cDC1 with the DapS A8819 isolate induces secretion approximately equivalent to stimulation of WT cDC1 with the DapR A8817 isolate (figure 6.11a). While statistical significance cannot be reliably ascertained due to the low sample size (n = 3), these trends were clearly replicated in two out of three independent experiments (figure 6.11a). In addition, there are no substantive differences in secretion of these cytokines between cGAS$^{-/-}$ and WT cDC1 following stimulation with the DapR A8817 (figure 6.11a). Based on these data we therefore hypothesise that the differential response of cDC1 following stimulation with the A8819/A8817 clinical pair, is due to a differential recognition of these strains by the cytoplasmic sensor cGAS.
Similarly, when considering the A9763/A9764 clinical pair (figure 6.12a), stimulation of cGAS$^{-/-}$ cDC1 with the A9763 DapS isolate induces lesser cytokine production on average than the WT control, but higher cytokine production than either genotype following stimuli with the DapR A9764 isolate (figure 6.12a). The intermediate phenotype suggests that while both clinical pairs may share a similar dependence on cGAS for recognition, there are distinct and currently unknown factor(s) regulating the differential recognition of the A9763/A9764 clinical pair. Importantly, these data are representative of either two or three independent experiments (as indicated), and future work should seek to validate these findings.

Of particular interest, variability in WT cDC1 cytokine responses to the DapS isolates (A8819 and A9763) between experimental replicates was consistently greater than observed for their DapR daughter strains (figure 6.11a and 6.12a), however when considering the cGAS$^{-/-}$ cDC1 responses from the same group of experiments the SEM was considerably smaller (figure 6.11a and 6.12a). These observations are consistent with the hypothesis that cGAS mediates the differential response of cDC1 to the DapS and DapR strains, and further suggest that the variability in responses between experiments

following stimulation with DapS isolates are – for not yet understood reasons – due to differential stimulation of cGAS.

In considering cDC2 and pDC, both subsets are clearly independent of cGAS signalling in the regulation of inflammation, with both WT and cGAS$^{-/-}$ DC producing all examined cytokines in approximate equivalence following stimulus with MRSA (figure 6.11b and 6.12b; figures 6.11c and 6.12c respectively). Consistent with these findings, the cDC2 and pDC cytokine response to the CpG ODNs 1668 and 2216 were similar between both WT and cGAS$^{-/-}$ (appendix A6), indicating that the recognition of the bacterial DNA mimics is indeed independent of cGAS. These findings are in stark contrast to those of the cDC1 whereby both the inflammatory cytokine response to CpG ODN 1668 and *S. aureus* were, in part, dependent on cGAS signalling, and therefore reduced in cGAS$^{-/-}$ (appendix A6). To our surprise, the production of IFN-β in response to MRSA, by cDC and pDC subsets, only exhibited a small dependence on cGAS (figure 6.11a and 6.12a). Having previously shown that the production of IFN-β was further independent of MyD88 signalling, it therefore remained to assess the contribution of other potential sensors. Despite the independence from cGAS in signalling it remained to consider STING, which signalling downstream of cGAS, is able to directly detect cyclic dinucleotides to elicit IFN production[106].

A role for STING in the recognition of MRSA by cDC1

In order to further investigate the dependence on the cGAS/STING signalling pathway for activation of cDC1 in response to MRSA, our lab is continuing to focus on both primary cDC1 and an equivalent in vitro culture model, the murine tumour (mutu)DC. Preliminary data, provided courtesy of Nazneen Jahan, supports our current hypothesis, showing that inhibition of STING with a small molecule inhibitor (H-151), ablates cytokine production by mutuDC in response to stimuli with DapS A8819 MRSA (figure 6.13). Similar to our observations for cGAS$^{-/-}$ cDC1 (figure 6.11a), this pilot data demonstrates that STING inhibition leads to reductions in secretion of TNF-α, IL-6 and IFN-λ in response to DapS A8819 with STING inhibition (figure 6.13). Importantly, and again similar to our observations for cGAS$^{-/-}$, the reduction in cytokine secretion in response to A8819 with STING inhibition is equivalent to that following stimulation with the DapR A8817 isolate alone (figure 6.13).

These findings are consistent with our current hypothesis, that the cGAS/STING signalling pathway plays a critical role in regulating the DC response to MRSA- and ***may*** be responsible for the differential in cytokine secretion by the cDC1 in response to the A8819/A8817 clinical pair. Importantly, given the small sample size these data are not statistically significant, and we have not yet attempted to replicate this very recent pilot data. The results described above are currently an area of current interest to our lab, and therefore of current and ongoing investigation. Further replication will shed greater light on the role and mechanisms by which MRSA is detected through this signalling pathway, which are current data suggest plays an important role in innate recognition by cDC1.

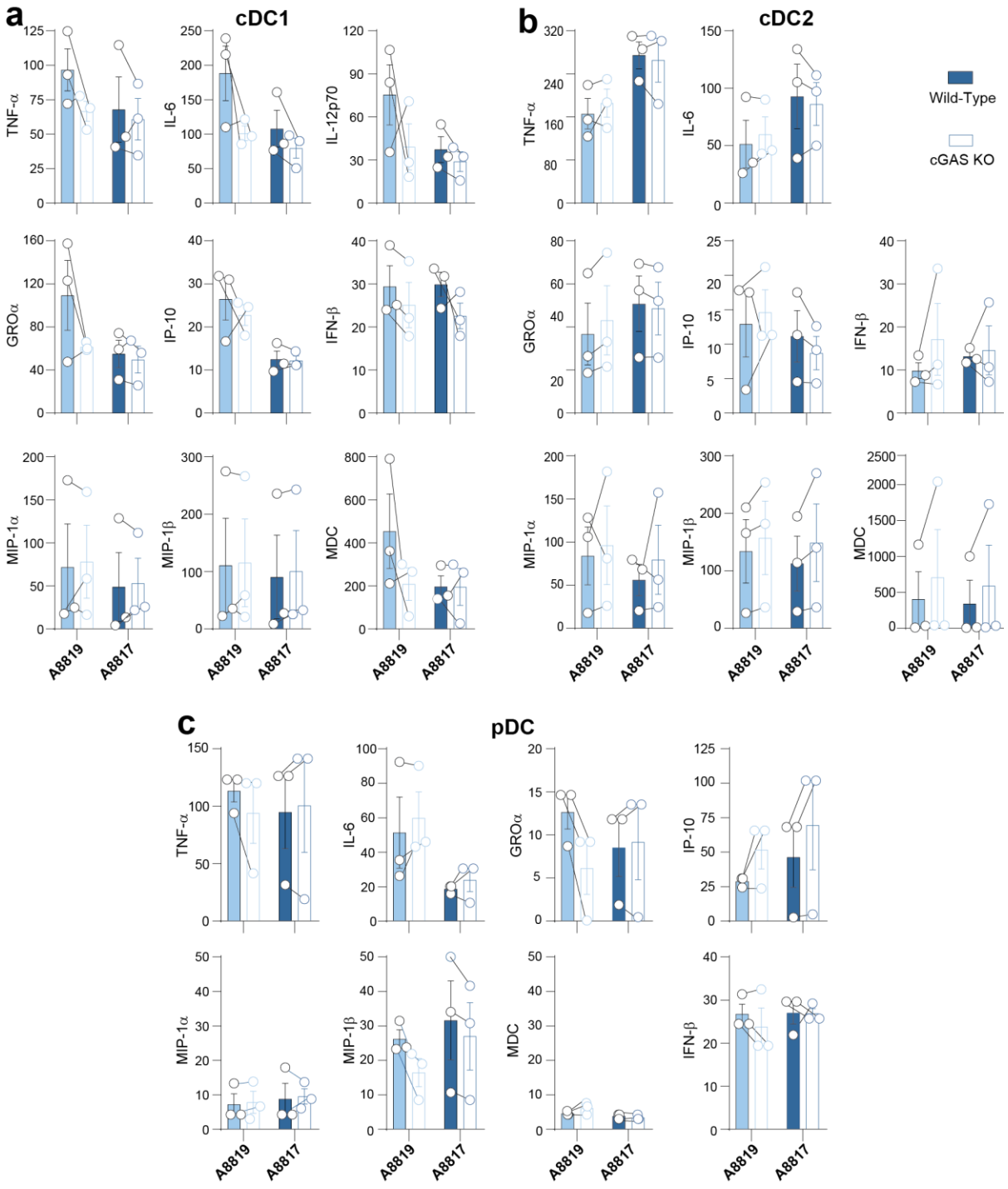

Figure 6.11 cGAS contributes to the production of inflammatory cytokine and chemokine, but not IFN, by cDC1 in response to the DapS A8819 isolate

Cytokine production (pg/ml) by wild-type (filled bars) and cGAS knockout (hollow bars) FACS sorted cDC1 ***(a),*** *cDC2* ***(b)*** *and pDC* ***(c)*** *at 18 hour post stimulus with paired daptomycin exposed MRSA isolates A8819 (DapS; light blue) and A8817 (DapR; dark blue). Each biological replicate (hollow circles) represents the average of technical duplicates of sorted splenic DC pooled from at least four mice. Bars show the mean and SEM of biological replicates from three independent experiments (n = 3).*

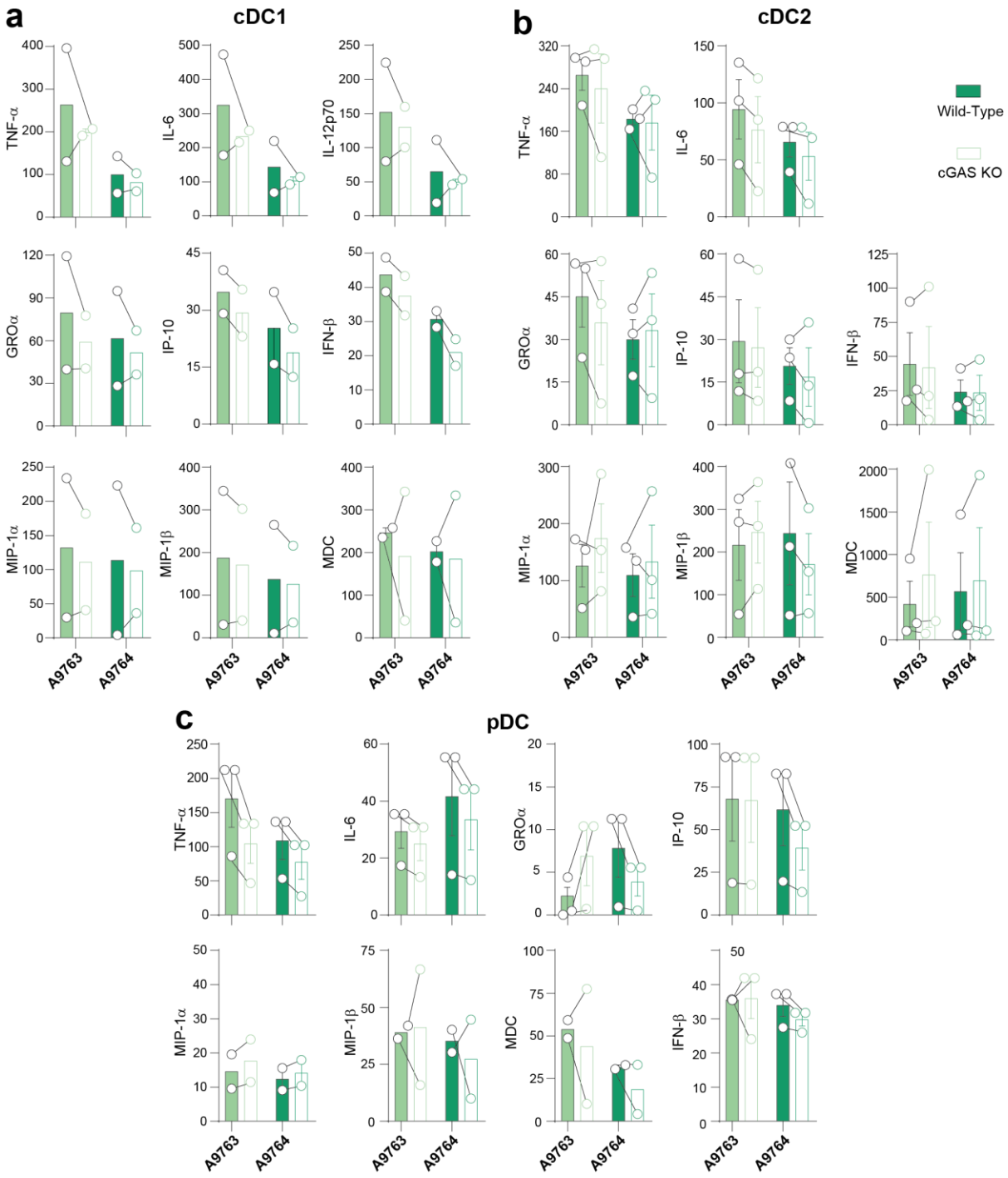

Figure 6.12 cGAS contributes to the production of inflammatory cytokine and chemokine, but not IFN, by all DC subsets in response to the DapS A9763 isolate

Cytokine production (pg/ml) by wild-type (filled bars) and cGAS knockout (hollow bars) FACS sorted cDC1 ***(a),*** *cDC2* ***(b)*** *and pDC* ***(c)*** *at 18 hour post stimulus with paired daptomycin exposed MRSA isolates A9763 (DapS; light green) and A9764 (DapR; dark green). Each biological replicate (hollow circles) represents the average of technical duplicates of sorted splenic DC pooled from at least four mice. Bars show the mean of biological replicates from two independent experiments for panel 'a' (n = 2). Bars show the mean and SEM (where applicable) of biological replicates pooled from two to three independent experiments for panels 'b' and 'c' (n ≥ 2).*

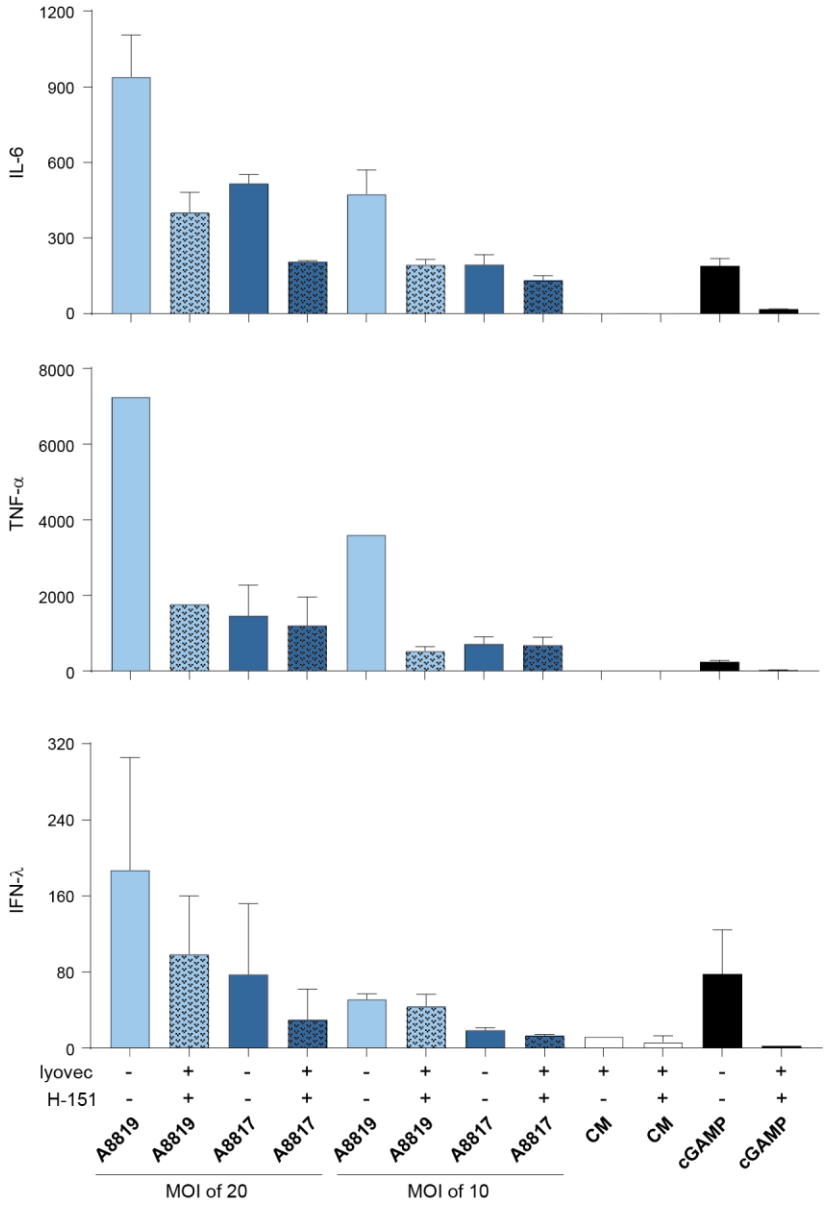

Figure 6.13 STING regulates inflammatory cytokine and IFN production by cDC1 in response to MRSA stimuli.

Cytokine production by mutuDC following overnight stimulation with DapS (A8819; light blue) and DapR (A8817; dark blue) MRSA (MOI of 10 or 20), 3'3' cGAMP (10 nmol) in LyoVec™ (10% $^{v}/_{v}$), media alone or media with LyoVec™. DC were pre-treated for 1 hour at 37°C with STING inhibitor H-151 (500 ng/ml) in LyoVec™ (dot filled bars), or LyoVec™ alone (plain filled bars). Bars indicate the mean, and range (where shown) of technical duplicates from a single experiment (n = 1). Samples without error bars indicate data whereby 1 technical replicate was excluded being greater than the assays limit of detection. These data have been kindly provided courtesy of Nazneen Jahan, whom performed the experiment described above.

6.3 Discussion

6.3.1 DC activation in response to *S. aureus* is dependent on MyD88 signalling

Consistent with previous studies using heat inactivated bacteria[71], we have shown that the production of most inflammatory cytokines and chemokines by DC subsets in response to live bacteria are dependent on signalling via MyD88 (figure 6.3). The exception to this being the production of both MDC and IFN-β by DC subsets, which was observed to be completely independent of MyD88 signalling (figure 6.3). The later of these observations contradict the earlier work of Kaplan and colleagues in finding that IFN-β production by DC is dependent on MyD88, but independent on cytosolic RNA sensors MDA-5 and RIG-I[234]. The discrepancies between the current study and that of Kaplan *et. al.,* may be explained by their use of a degradation sensitive laboratory strain of *S. aureus*, and/or their GM-CSF inducible DC model[234], of which may not fully recapitulate the molecular interactions occurring between primary *ex vivo* DC and fully antibiotic resistant clinical isolates of bacteria.

Further to impaired cytokine, the upregulation of MHC and co-stimulatory markers CD40, CD80 and CD86 by all DC subsets in response to MRSA isolates is also clearly impaired, but not ablated, in the absence of MyD88 signalling (figure 6.3). Importantly, the expression of these markers remains relatively high following MRSA stimulation of $MyD88^{-/-}$ DC in comparison to unstimulated controls (figure 6.3). There is therefore a clear differential dependence on MyD88 signalling for the induction of cytokine secretion by DC in comparison to the stimulation of surface activation- with the latter being regulated largely independently of MyD88. While signalling via MyD88 plays an integral role in the activation of all splenic DC subsets in response to MRSA, the results of this chapter make clear that the pathways regulating the activation of splenic DC subsets remain distinct.

Having demonstrated a differential in the internalisation of DapS and DapR clinical pairs by DC (chapter 6), it seemed likely that the subsequent differential in activation was due to a decreased bacterial load and availability of immunogenic PAMPs. We therefore hypothesised that the differential recognition of MRSA was mediated by the endosomal sensor for bacterial DNA, TLR9, or the cytosolic sensor cGAS.

Given that TLR9 and cGAS are expressed by all human and murine DC subsets[5], these receptors seemed likely candidates to regulate the differential activation of each DC subset- as their capacity to induce DC activation would be impaired with decreased bacterial internalisation.

6.3.2 Unique dependence on TLR9 and cGAS for efficient activation of cDC1

Despite a shared dependence on MyD88 signalling by DC subsets for potent cytokine production in response to MRSA, we found that the cDC1 are unique in their dependence on TLR9 (figures 6.6, 6.7 and 6.8). Indeed, while TLR9$^{-/-}$ cDC1 unable to produce appreciable MIP-1α or TNF-α in response to clinical isolates of MRSA, they were only partially restricted in their capacity to secrete MIP-1β (figure 6.6). Nonetheless, the capacity of cDC1 to produce MIP-1α, MIP-1β and TNF-α in response to clinical isolates of MSSA, D57 and D85, was almost entirely ablated in the absence of TLR9 (figure 6.6). In contrast to cDC1, neither cDC2 nor pDC were reliant on TLR9 signalling for activation in response to MRSA or MSSA isolates (figures 6.7 and 6.8 respectively); yet given their dependence on MyD88 for activation we hypothesise that the most likely candidate receptor regulating their activation is TLR2.

Having found that the endosomal sensor TLR9 is essential for the efficient production of cytokine and chemokine in response to MRSA and MSSA isolates, we next considered the contribution played by the cytosolic DNA sensor cGAS. We found cGAS deficient cDC1 were able to produce relatively abundant cytokine and chemokine in response to MRSA (figures 6.11a and 6.12a). Importantly, cGAS deficiency impaired the recognition of the DapS isolate A8819, but not the resistant daughter strain A8817 (figure 6.11a). Moreover, cGAS deficient DC were unable to produce cytokine in response to the A8819 DapS isolate to a greater level than wild-type DC sensing the DapR A8817 daughter (figure 6.11a); therefore indicating that cGAS sensing of *S. aureus* regulates the differential activation of cDC1 in response to the A8819/A8817 clinical pair. These findings are supported in the stimulation of DC with the A9763/A9764 clinical pair, whereby cGAS$^{-/-}$ DC are less efficiently activated by both isolates (figure 6.12a). Importantly, inhibition of STING signalling in mutuDC similarly impeded cytokine secretion (figure 6.13), further implicating this pathway in the recognition of MRSA.

Despite having established a critical role for TLR9 and cGAS signalling in cDC1, alongside a dependence on MyD88 signalling for cDC2 following stimuli with clinical isolates of MRSA, several questions remained unanswered. The first being how IFN-β production is regulated in response to *S. aureus* isolates. It has previously been shown that IFN-β production by human monocytes and macrophages in response to *S. aureus* ribosomal RNA is regulated via a TLR8-IRF signalling pathway[255], yet genetic differences between human and murine TLR8 render the latter unable to respond to RNA oligonucleotides[256]. The more likely candidate receptor is TLR13, which has been demonstrated to recognise 23S ribosomal RNA of *S. aureus* in mice – however our results clearly demonstrate that the production of IFN-β is occurring independent of MyD88 (figure 6.3). Our results also clearly indicate that the production of IFN-β is also independent of the cytosolic sensor cGAS (figure 6.11 and 6.12), and we therefore suggest that the production of IFN-β may be regulated downstream of cGAS with bacterial cyclic dinucleotides acting directly on STING. This hypothesis merits further investigation, as our current data cannot exclude the potential for redundancy between TLR9 and cGAS in the regulation of IFN-β to *S. aureus.*

6.3.3 Conclusions and future directions

Future work should further consider the role of TLR2 in the initial sensing and internalisation of these *S. aureus* isolates, as such sensing may explain the differential sensing of the A9763/A9764 clinical pair by cDC2 and pDC, which is occurring independently of both TLR9 and cGAS (figure 6.7, 6.12b and 6.12c). Moreover, a role for TLR2 in the internalisation of *S. aureus* would further fit the model for decreased activation of cDC1, as despite the differences in the internal sensing of bacteria, we have as of yet not established a mechanism regulating this uptake. TLR2 has previously been implicated in the phagocytosis of *S. aureus* in the RAW264.7 cell line[257], although further work is merited on DC. Importantly, while TLR2 mediates MyD88 dependent activation of DC, and bacterial internalisation[257], it may not necessarily regulate the differential between clinical isolates. It has been shown that efficient signalling via TLR2/6 heterodimers in response to *S. aureus* are further dependent on the scavenger receptor CD36, which is further required for efficient phagocytosis of *S. aureus* by macrophages[258]. The CD36 receptor recognises lipoteichoic acid[258], of which increased production has previously been associated with daptomycin resistance through a thickening of the cell

wall[259]. Therefore, given their shared dependence on cell wall ligands for bacterial recognition and internalisation, and their co-dependence for efficient response to *S. aureus*, both TLR2 and CD36 should be further investigated for their role in regulating the differential internalisation and activation of all DC subsets in response to clinical strains.

The precise mechanism as to how these mutations affect the bacterial isolates in such a way as to modulate the capacity of DC to sense and internalise these strains is of clear importance. Furthering this understanding these mechanisms will be essential to elucidate the underlying causes of differential activation of the DC in response to these isolates. It currently remains likely that the differential activation of DC is a result of altered bacterial internalisation, and therefore subsequent differences in signalling of endosomal TLRs and cytosolic PRR. However, it remains unclear whether the differential activation of DC is affected by the signalling of the initial recognition event inducing the internalisation of the bacteria, and the identification of the receptor responsible for initiating this process should be the focus of future research.

Final Discussion

In this thesis we have explored the innate recognition of live clinical isolates of *S. aureus* by DC, finding incredible diversity in the immunogenic potential these isolates. Indeed, these findings highlight the requirement to investigate primary isolates of *S. aureus*, as opposed to lab strains of the bacteria, in order to better appreciate immunopathogenesis. Importantly, this thesis has characterised in depth, the relationship between immunogenicity of *S. aureus* clinical isolates, and resistance to the last line antibiotic daptomycin.

It has previously been shown that increased levels of resistance to another last line antibiotic, vancomycin, in *S. aureus* clinical isolates are associated with poor clinical prognosis; noticeably even so in cases where vancomycin is not used as a therapeutic choice for treatment[260]. Indeed, the authors of this study, and others, have hypothesised that the vancomycin minimum inhibitory concentration (MIC) represents an as yet unidentified marker, of either host or organism factors, which hold significant sway on treatment outcome[260-262]. The data described in this thesis support this hypothesis, providing novel evidence that the acquisition of resistance to daptomycin – a last line antibiotic similar to vancomycin – simultaneously impedes innate immune recognition of clinical bacterial isolates by DC. Importantly, we observed that many isolates of broadly antibiotic resistant MRSA were poorly immunogenic toward DC, even prior to the acquisition of daptomycin resistance (figure 4.1 and 4.2). While the link between a bacterial isolates level of resistance to a given antibiotic and the innate immune perception of that bacteria are not immediately obvious, we contend that two are inextricably linked; given that the alterations to the bacterial cell wall and membrane required to achieve resistance to certain antibiotics, has in turn, consequences on the recognition of these isolates by PRR.

Nguyen and colleagues have recently shown various species of staphylococci differentially induce immune inflammation, with poor cytokine responses induced by lab strains of commensal *S. epidermis* and *S. aureus* in comparison to a non-commensal lab strain of *Staphylococcus carnosus*[219]. While novel, the work of Nguyen and colleagues utilised both laboratory strains of staphylococci and a human monocytic cell line, MM6. Therefore, the body of work described in this thesis remains the first to extensively

characterise the responses of primary DC subsets in response to various primary isolates of bacteria of the same species (*S. aureus)*, demonstrating a clear differential in DC activation. Moreover, we have further demonstrated that single amino acid point mutations occurring in isolates of *S. aureus* during clinical infection have the capacity to drastically alter immune recognition by DC – impeding both bacterial internalisation and the subsequent activation process of DC. These findings highlight the need for a greater understanding into the differences that occur between various isolates of infectious bacteria – not just at the species level – in order to better understand the immunopathogenesis of clinical infections, with the hope of developing novel therapeutics and treatment strategies.

The differential immunogenicity between staphylococcal species has been shown to be dependent on TLR2, and directly mediated by differences in the chemical composition of cell membrane lipoproteins[219]. The alterations occurring in the bacterial cell membrane and wall as a result of the *cls2* mutation occurring in the DapR strains modelled in this thesis have only very recently been characterised[194]. It is now known that the T33N, L52F and A23V occurring in the *cls2* gene of DapR isolates, confer a gain-of-function, leading to an increase in both the thickness and cardiolipin content of the cell membrane, alongside a simultaneous decrease in the cardiolipin precursor phosphatidyl glycerol[194]. Importantly, phosphatidyl glycerol is a known precursor of immunogenic staphylococcal lipoproteins (agonists of TLR2)[219,263]. In addition, these mutations further results in a significant thickening of the bacterial cell well[158], a common phenomenon in DapR strains, thought to be due to an alerted composition and increased abundance of wall teichoic acid[259] – an agonist of both TLR2[264] and Macrophage Inducible C-Type Lectin[265] (MINCLE). Cumulatively, these findings suggest a role for TLR2 in the differential recognition and internalisation of these *S. aureus* isolates by DC.

Indeed, while not directly investigated, our findings are consistent with this observation; given that *S. aureus* isolates are unable to elicit cytokine secretion by MyD88 KO DC (figure 6.3), and that the daptomycin exposed clinical pairs are differentially internalised by all DC subsets (figures 5.7 and 5.8). We therefore suggest that TLR2 may play a role in the internalisation of these isolates, and therefore affect the subsequent activation of DC. Importantly, we have further shown that cytokine secretion by cDC1 is partially dependent on TLR9 (figure 6.6); and that therefore the activation of DC through this

pathway is compromised in response to poorly internalised isolates, such as the DapR daughter isolates in the A8819/A8817 and A9763/A9764 clinical pairs (figure 7.1). Moreover, while TLR9 contributed to the activation and subsequent cytokine secretion of cDC1 (figure 6.6), we further demonstrated that a cytosolic DNA sensor cGAS mediated the differential recognition between the A8819/A8817 daptomycin exposed pair, and greatly contributed to the differential recognition of the A9763/A9764 clinical pair (figure 6.11 and 6.12). Moreover, preliminary data further implicates a role for STING in the sensing of these isolates (figure 6.13), although it remains unclear if this is entirely mediated via cGAS, or contributed to via sensing of bacterial CDN. Nonetheless, we hypothesise that in our model of cDC1 activation, some difference between the daptomycin exposed clinical pairs impedes the export or escape of DapR *S. aureus* DNA in to the cytoplasm, preventing innate recognition and signalling via cGAS/STING pathway.

While this work has provided a model for the innate recognition of *S. aureus* isolates by cDC1, it remains unclear as to the how cDC2 and pDC activation are regulated. Importantly, our work suggests a differential handling of the bacteria between DC subsets, and indeed between distinct clinical isolates. In example, while cDC1 were dependent on TLR9 for potent cytokine secretion (figure 6.6), the cDC2 and pDC were not (figures 6.7 and 6.8). Moreover, each of the A8819/A8817 and the A9763/A9764 clinical pairs were differentially internalised by DC subsets; yet only the A9763/A9764 clinical pair induced differential cytokine secretion by all three DC subsets (figure ref). We hypothesise that this differential in uptake may be mediated TLR2, but the extent of signalling and its contribution to overall activation is different between each DC subset. Further understanding the role of TLR2 in the innate detection of diverse *S. aureus* isolates would be of merit, as TLR2, unlike TLR9, is ubiquitously expressed across both human and murine cDC subsets[5]. Given TLR9 is not expressed by human cDC[5], yet is required for potent murine cDC1 activation, further work is therefore required to validate the role of human cDC1 in response to *S. aureus*; which may exhibit a stronger dependence on cGAS and STING signalling in the absence of TLR9 stimulation.

Further work should focus on elucidating the role of TLR2 in the activation of DC subsets and the internalisation of bacteria. In gaining a fuller understanding of how the internalisation of these isolates is differentially regulated we can seek to design novel

immunotherapeutic to overcome the impaired innate recognition of these bacteria, by DC and indeed other cells of the innate immune system. Finally, future work should focus on the translation of these research findings into human models of primary DC, as we have clearly shown differential handling of bacteria between DC subsets- and it is therefore likely that there will be differences between the two, despite the high level of conservation between human and murine DC.

Finally, research must seek to better understand the immunopathogenesis of *S. aureus* in humans, to further the potential for the design of novel immunotherapeutics, in the face of rising levels of broad antibiotic resistance. In understanding how *S. aureus* isolates are differentially recognised by the innate immune system new adjuvants can be developed or adapted to target poorly immunogenic isolates, thus restoring their immunogenic potential and allowing recognition and clearance. not just by DC, but indeed neutrophils, macrophages and other innate cells. We contend that further understanding the mechanisms of innate immunomodulation and immunoevasion employed by *S. aureus* will be critical to the development of such novel immunotherapies; and that such treatments have the potential to act as a front-line defence into the future in which we face ever increasing levels of broad resistance to our last line antibiotics.

References

1 Steinman, R. Dendritic cells are the principal stimulators of the primary mixed leukocyte reaction in mice. *J Exp Med* **157**, 613-627, doi:10.1084/jem.157.2.613 (1983).

2 Heath, W. R. & Carbone, F. R. Dendritic cell subsets in primary and secondary T cell responses at body surfaces. *Nat Immunol* **10**, 1237-1244, doi:10.1038/ni.1822 (2009).

3 Collin, M., McGovern, N. & Haniffa, M. Human dendritic cell subsets. *Immunology* **140**, 22-30, doi:10.1111/imm.12117 (2013).

4 Vu Manh, T. P., Bertho, N., Hosmalin, A., Schwartz-Cornil, I. & Dalod, M. Investigating Evolutionary Conservation of Dendritic Cell Subset Identity and Functions. *Front Immunol* **6**, 260, doi:10.3389/fimmu.2015.00260 (2015).

5 Macri, C., Pang, E. S., Patton, T. & O'Keeffe, M. Dendritic cell subsets. *Semin Cell Dev Biol* **84**, 11-21, doi:10.1016/j.semcdb.2017.12.009 (2018).

6 Sichien, D., Lambrecht, B. N., Guilliams, M. & Scott, C. L. Development of conventional dendritic cells: from common bone marrow progenitors to multiple subsets in peripheral tissues. *Mucosal Immunol* **10**, 831-844, doi:10.1038/mi.2017.8 (2017).

7 Gurka, S., Hartung, E., Becker, M. & Kroczek, R. A. Mouse Conventional Dendritic Cells Can be Universally Classified Based on the Mutually Exclusive Expression of XCR1 and SIRPalpha. *Front Immunol* **6**, 35, doi:10.3389/fimmu.2015.00035 (2015).

8 Guilliams, M. *et al.* Dendritic cells, monocytes and macrophages: a unified nomenclature based on ontogeny. *Nat Rev Immunol* **14**, 571-578, doi:10.1038/nri3712 (2014).

9 Hespel, C. & Moser, M. Role of inflammatory dendritic cells in innate and adaptive immunity. *Eur J Immunol* **42**, 2535-2543, doi:10.1002/eji.201242480 (2012).

10 Haniffa, M., Bigley, V. & Collin, M. Human mononuclear phagocyte system reunited. *Semin Cell Dev Biol* **41**, 59-69, doi:10.1016/j.semcdb.2015.05.004 (2015).

11 Vremec, D. & Shortman, K. What's in a Name? Some Early and Current Issues in Dendritic Cell Nomenclature. *Front Immunol* **6**, 267, doi:10.3389/fimmu.2015.00267 (2015).

12 Segura, E. & Amigorena, S. Inflammatory dendritic cells in mice and humans. *Trends Immunol* **34**, 440-445, doi:10.1016/j.it.2013.06.001 (2013).

13 Sancho, D. *et al.* Tumor therapy in mice via antigen targeting to a novel, DC-restricted C-type lectin. *J Clin Invest* **118**, 2098-2110, doi:10.1172/JCI34584 (2008).

14 Askew, D. & Harding, C. V. Antigen processing and CD24 expression determine antigen presentation by splenic CD4+ and CD8+ dendritic cells. *Immunology* **123**, 447-455, doi:10.1111/j.1365-2567.2007.02711.x (2008).

15 Galibert, L. *et al.* Nectin-like protein 2 defines a subset of T-cell zone dendritic cells and is a ligand for class-I-restricted T-cell-associated molecule. *J Biol Chem* **280**, 21955-21964, doi:10.1074/jbc.M502095200 (2005).

16 Uematsu, S. *et al.* Regulation of humoral and cellular gut immunity by lamina propria dendritic cells expressing Toll-like receptor 5. *Nat Immunol* **9**, 769-776, doi:10.1038/ni.1622 (2008).
17 Caminschi, I. *et al.* The dendritic cell subtype-restricted C-type lectin Clec9A is a target for vaccine enhancement. *Blood* **112**, 3264-3273, doi:10.1182/blood-2008-05-155176 (2008).
18 Guilliams, M. *et al.* Unsupervised High-Dimensional Analysis Aligns Dendritic Cells across Tissues and Species. *Immunity* **45**, 669-684, doi:10.1016/j.immuni.2016.08.015 (2016).
19 Heng, T. S., Painter, M. W. & Immunological Genome Project, C. The Immunological Genome Project: networks of gene expression in immune cells. *Nat Immunol* **9**, 1091-1094, doi:10.1038/ni1008-1091 (2008).
20 Dorner, B. G. *et al.* Selective expression of the chemokine receptor XCR1 on cross-presenting dendritic cells determines cooperation with CD8+ T cells. *Immunity* **31**, 823-833, doi:10.1016/j.immuni.2009.08.027 (2009).
21 Michea, P. *et al.* Epithelial control of the human pDC response to extracellular bacteria. *Eur J Immunol* **43**, 1264-1273, doi:10.1002/eji.201242990 (2013).
22 Chiang, M.-C. *et al.* Differential uptake and cross-presentation of soluble and necrotic cell antigen by human DC subsets. *Eur J Immunol* **46**, 329-339, doi:10.1002/eji.201546023 (2016).
23 Pooley, J. L., Heath, W. R. & Shortman, K. Cutting Edge: Intravenous Soluble Antigen Is Presented to CD4 T Cells by CD8- Dendritic Cells, but Cross-Presented to CD8 T Cells by CD8+ Dendritic Cells. *J Immunol* **166**, 5327-5330, doi:10.4049/jimmunol.166.9.5327 (2001).
24 Iyoda, T. *et al.* The CD8+Dendritic Cell Subset Selectively Endocytoses Dying Cells in Culture and In Vivo. *J Exp Med* **195**, 1289-1302, doi:10.1084/jem.20020161 (2002).
25 Bosnjak, L. *et al.* Herpes Simplex Virus Infection of Human Dendritic Cells Induces Apoptosis and Allows Cross-Presentation via Uninfected Dendritic Cells. *J Immunol* **174**, 2220-2227, doi:10.4049/jimmunol.174.4.2220 (2005).
26 Allan, R. S. *et al.* Epidermal viral immunity induced by CD8alpha+ dendritic cells but not by Langerhans cells. *Science* **301**, 1925-1928, doi:10.1126/science.1087576 (2003).
27 Zhao, X. *et al.* Vaginal Submucosal Dendritic Cells, but Not Langerhans Cells, Induce Protective Th1 Responses to Herpes Simplex Virus-2. *The Journal of Experimental Medicine* **197**, 153-162, doi:10.1084/jem.20021109 (2003).
28 Bursch, L. S. *et al.* Identification of a novel population of Langerin+ dendritic cells. *J Exp Med* **204**, 3147-3156, doi:10.1084/jem.20071966 (2007).
29 Poulin, L. F. *et al.* The dermis contains langerin+ dendritic cells that develop and function independently of epidermal Langerhans cells. *J Exp Med* **204**, 3119-3131, doi:10.1084/jem.20071724 (2007).
30 Ginhoux, F. *et al.* Blood-derived dermal langerin+ dendritic cells survey the skin in the steady state. *J Exp Med* **204**, 3133-3146, doi:10.1084/jem.20071733 (2007).
31 Bedoui, S. *et al.* Cross-presentation of viral and self antigens by skin-derived CD103+ dendritic cells. *Nat Immunol* **10**, 488-495, doi:10.1038/ni.1724 (2009).
32 Belz, G. T. *et al.* Distinct migrating and nonmigrating dendritic cell populations are involved in MHC class I-restricted antigen presentation after lung infection

with virus. *Proc Natl Acad Sci U S A* **101**, 8670-8675, doi:10.1073/pnas.0402644101 (2004).
33 GeurtsvanKessel, C. H. *et al.* Clearance of influenza virus from the lung depends on migratory langerin+CD11b- but not plasmacytoid dendritic cells. *J Exp Med* **205**, 1621-1634, doi:10.1084/jem.20071365 (2008).
34 Lukens, M. V., Kruijsen, D., Coenjaerts, F. E., Kimpen, J. L. & van Bleek, G. M. Respiratory syncytial virus-induced activation and migration of respiratory dendritic cells and subsequent antigen presentation in the lung-draining lymph node. *J Virol* **83**, 7235-7243, doi:10.1128/JVI.00452-09 (2009).
35 Kim, T. S. & Braciale, T. J. Respiratory dendritic cell subsets differ in their capacity to support the induction of virus-specific cytotoxic CD8+ T cell responses. *PLoS One* **4**, e4204, doi:10.1371/journal.pone.0004204 (2009).
36 Desch, A. N. *et al.* Dendritic cell subsets require cis-activation for cytotoxic CD8 T-cell induction. *Nat Commun* **5**, 4674, doi:10.1038/ncomms5674 (2014).
37 Hochrein, H. & O'Keeffe, M. Dendritic cell subsets and toll-like receptors. *Handb Exp Pharmacol*, 153-179, doi:10.1007/978-3-540-72167-3_8 (2008).
38 Villadangos, J. A. & Young, L. Antigen-presentation properties of plasmacytoid dendritic cells. *Immunity* **29**, 352-361, doi:10.1016/j.immuni.2008.09.002 (2008).
39 Reizis, B., Bunin, A., Ghosh, H. S., Lewis, K. L. & Sisirak, V. Plasmacytoid dendritic cells: recent progress and open questions. *Annu Rev Immunol* **29**, 163-183, doi:10.1146/annurev-immunol-031210-101345 (2011).
40 Dzionek, A. *et al.* BDCA-2, a Novel Plasmacytoid Dendritic Cell–specific Type II C-type Lectin, Mediates Antigen Capture and Is a Potent Inhibitor of Interferon α/β Induction. *J Exp Med* **194**, 1823-1834, doi:10.1084/jem.194.12.1823 (2001).
41 Fitzgerald-Bocarsly, P., Dai, J. & Singh, S. Plasmacytoid dendritic cells and type I IFN: 50 years of convergent history. *Cytokine Growth Factor Rev* **19**, 3-19, doi:10.1016/j.cytogfr.2007.10.006 (2008).
42 Honda, K. *et al.* Spatiotemporal regulation of MyD88-IRF-7 signalling for robust type-I interferon induction. *Nature* **434**, 1035-1040, doi:10.1038/nature03547 (2005).
43 Krug, A. *et al.* Interferon-producing cells fail to induce proliferation of naive T cells but can promote expansion and T helper 1 differentiation of antigen-experienced unpolarized T cells. *J Exp Med* **197**, 899-906, doi:10.1084/jem.20021091 (2003).
44 Young, L. J. *et al.* Differential MHC class II synthesis and ubiquitination confers distinct antigen-presenting properties on conventional and plasmacytoid dendritic cells. *Nat Immunol* **9**, 1244-1252, doi:10.1038/ni.1665 (2008).
45 Salio, M., Palmowski, M. J., Atzberger, A., Hermans, I. F. & Cerundolo, V. CpG-matured murine plasmacytoid dendritic cells are capable of in vivo priming of functional CD8 T cell responses to endogenous but not exogenous antigens. *J Exp Med* **199**, 567-579, doi:10.1084/jem.20031059 (2004).
46 Fonteneau, J. F. *et al.* Activation of influenza virus-specific CD4+ and CD8+ T cells: a new role for plasmacytoid dendritic cells in adaptive immunity. *Blood* **101**, 3520-3526, doi:10.1182/blood-2002-10-3063 (2003).
47 Schlecht, G. *et al.* Murine plasmacytoid dendritic cells induce effector/memory CD8+ T-cell responses in vivo after viral stimulation. *Blood* **104**, 1808-1815, doi:10.1182/blood-2004-02-0426 (2004).

48 Lauvau, G., Chorro, L., Spaulding, E. & Soudja, S. M. Inflammatory monocyte effector mechanisms. *Cell Immunol* **291**, 32-40, doi:10.1016/j.cellimm.2014.07.007 (2014).
49 Xiong, H. & Pamer, E. G. Monocytes and infection: modulator, messenger and effector. *Immunobiology* **220**, 210-214, doi:10.1016/j.imbio.2014.08.007 (2015).
50 Schakel, K. *et al.* 6-Sulfo LacNAc, a novel carbohydrate modification of PSGL-1, defines an inflammatory type of human dendritic cells. *Immunity* **17**, 289-301 (2002).
51 Döbel, T. & Schäkel, K. The role of human 6-sulfo LacNAc dendritic cells (slanDCs) in autoimmunity and tumor diseases. *JDDG: Journal der Deutschen Dermatologischen Gesellschaft* **12**, 874-879, doi:10.1111/ddg.12439 (2014).
52 Serbina, N. V., Salazar-Mather, T. P., Biron, C. A., Kuziel, W. A. & Pamer, E. G. TNF/iNOS-Producing Dendritic Cells Mediate Innate Immune Defense against Bacterial Infection. *Immunity* **19**, 59-70, doi:10.1016/s1074-7613(03)00171-7 (2003).
53 Guilliams, M. *et al.* IL-10 dampens TNF/inducible nitric oxide synthase-producing dendritic cell-mediated pathogenicity during parasitic infection. *J Immunol* **182**, 1107-1118, doi:10.4049/jimmunol.182.2.1107 (2009).
54 Macagno, A., Napolitani, G., Lanzavecchia, A. & Sallusto, F. Duration, combination and timing: the signal integration model of dendritic cell activation. *Trends Immunol* **28**, 227-233, doi:10.1016/j.it.2007.03.008 (2007).
55 Granucci, F., Vizzardelli, C., Virzi, E., Rescigno, M. & Ricciardi-Castagnoli, P. Transcriptional reprogramming of dendritic cells by differentiation stimuli. *Eur J Immunol* **31**, 2539-2546, doi:10.1002/1521-4141(200109)31:9<2539::AID-IMMU2539>3.0.CO;2-9 (2001).
56 Hashimoto, S. *et al.* Identification of genes specifically expressed in human activated and mature dendritic cells through serial analysis of gene expression. *Blood* **96**, 2206-2214 (2000).
57 Joffre, O., Nolte, M. A., Sporri, R. & Reis e Sousa, C. Inflammatory signals in dendritic cell activation and the induction of adaptive immunity. *Immunol Rev* **227**, 234-247, doi:10.1111/j.1600-065X.2008.00718.x (2009).
58 West, M. A. *et al.* Enhanced dendritic cell antigen capture via toll-like receptor-induced actin remodeling. *Science* **305**, 1153-1157, doi:10.1126/science.1099153 (2004).
59 Dalod, M., Chelbi, R., Malissen, B. & Lawrence, T. Dendritic cell maturation: functional specialization through signaling specificity and transcriptional programming. *EMBO J* **33**, 1104-1116, doi:10.1002/embj.201488027 (2014).
60 Kawai, T. & Akira, S. The role of pattern-recognition receptors in innate immunity: update on Toll-like receptors. *Nat Immunol* **11**, 373-384, doi:10.1038/ni.1863 (2010).
61 Lauterbach, H. *et al.* Mouse CD8alpha+ DCs and human BDCA3+ DCs are major producers of IFN-lambda in response to poly IC. *J Exp Med* **207**, 2703-2717, doi:10.1084/jem.20092720 (2010).
62 Akira, S. & Takeda, K. Toll-like receptor signalling. *Nat Rev Immunol* **4**, 499-511, doi:10.1038/nri1391 (2004).
63 van Egmond, M., Vidarsson, G. & Bakema, J. E. Cross-talk between pathogen recognizing Toll-like receptors and immunoglobulin Fc receptors in immunity. *Immunol Rev* **268**, 311-327, doi:10.1111/imr.12333 (2015).

64 Jongbloed, S. L. *et al.* Human CD141+ (BDCA-3)+ dendritic cells (DCs) represent a unique myeloid DC subset that cross-presents necrotic cell antigens. *J Exp Med* **207**, 1247-1260, doi:10.1084/jem.20092140 (2010).
65 Muzio, M. *et al.* Differential Expression and Regulation of Toll-Like Receptors (TLR) in Human Leukocytes: Selective Expression of TLR3 in Dendritic Cells. *J Immunol* **164**, 5998-6004, doi:10.4049/jimmunol.164.11.5998 (2000).
66 Edwards, A. D. *et al.* Toll-like receptor expression in murine DC subsets: lack of TLR7 expression by CD8 alpha+ DC correlates with unresponsiveness to imidazoquinolines. *Eur J Immunol* **33**, 827-833, doi:10.1002/eji.200323797 (2003).
67 Hornung, V. *et al.* Quantitative Expression of Toll-Like Receptor 1-10 mRNA in Cellular Subsets of Human Peripheral Blood Mononuclear Cells and Sensitivity to CpG Oligodeoxynucleotides. *J Immunol* **168**, 4531-4537, doi:10.4049/jimmunol.168.9.4531 (2002).
68 Gantner, B. N., Simmons, R. M., Canavera, S. J., Akira, S. & Underhill, D. M. Collaborative induction of inflammatory responses by dectin-1 and Toll-like receptor 2. *J Exp Med* **197**, 1107-1117, doi:10.1084/jem.20021787 (2003).
69 Plattner, F. *et al.* Toxoplasma profilin is essential for host cell invasion and TLR11-dependent induction of an interleukin-12 response. *Cell Host Microbe* **3**, 77-87, doi:10.1016/j.chom.2008.01.001 (2008).
70 Chattopadhyay, S. & Sen, G. C. Tyrosine phosphorylation in Toll-like receptor signaling. *Cytokine Growth Factor Rev* **25**, 533-541, doi:10.1016/j.cytogfr.2014.06.002 (2014).
71 Oldenburg, M. *et al.* TLR13 recognizes bacterial 23S rRNA devoid of erythromycin resistance-forming modification. *Science* **337**, 1111-1115, doi:10.1126/science.1220363 (2012).
72 Hoving, J. C., Wilson, G. J. & Brown, G. D. Signalling C-type lectin receptors, microbial recognition and immunity. *Cell Microbiol* **16**, 185-194, doi:10.1111/cmi.12249 (2014).
73 Geijtenbeek, T. B. & Gringhuis, S. I. Signalling through C-type lectin receptors: shaping immune responses. *Nat Rev Immunol* **9**, 465-479, doi:10.1038/nri2569 (2009).
74 Lahoud, M. H. *et al.* DEC-205 is a cell surface receptor for CpG oligonucleotides. *Proc Natl Acad Sci U S A* **109**, 16270-16275, doi:10.1073/pnas.1208796109 (2012).
75 Ahrens, S. *et al.* F-actin is an evolutionarily conserved damage-associated molecular pattern recognized by DNGR-1, a receptor for dead cells. *Immunity* **36**, 635-645, doi:10.1016/j.immuni.2012.03.008 (2012).
76 Hanč, P. *et al.* in *C-Type Lectin Receptors in Immunity* (ed S. Yamasaki) Ch. Chapter 5, 65-81 (Springer, 2016).
77 Zelenay, S. *et al.* The dendritic cell receptor DNGR-1 controls endocytic handling of necrotic cell antigens to favor cross-priming of CTLs in virus-infected mice. *J Clin Invest* **122**, 1615-1627, doi:10.1172/JCI60644 (2012).
78 Gringhuis, S. I. *et al.* Dectin-1 directs T helper cell differentiation by controlling noncanonical NF-kappaB activation through Raf-1 and Syk. *Nat Immunol* **10**, 203-213, doi:10.1038/ni.1692 (2009).
79 An, H. *et al.* Phosphatase SHP-1 promotes TLR- and RIG-I-activated production of type I interferon by inhibiting the kinase IRAK1. *Nat Immunol* **9**, 542-550, doi:10.1038/ni.1604 (2008).

80 Kim, E. J., Suk, K. & Lee, W. H. SHPS-1 and a synthetic peptide representing its ITIM inhibit the MyD88, but not TRIF, pathway of TLR signaling through activation of SHP and PI3K in THP-1 cells. *Inflamm Res* **62**, 377-386, doi:10.1007/s00011-013-0589-0 (2013).
81 Raulf, M. K. *et al.* The C-type Lectin Receptor CLEC12A Recognizes Plasmodial Hemozoin and Contributes to Cerebral Malaria Development. *Cell Rep* **28**, 30-38 e35, doi:10.1016/j.celrep.2019.06.015 (2019).
82 Neumann, K. *et al.* Clec12a is an inhibitory receptor for uric acid crystals that regulates inflammation in response to cell death. *Immunity* **40**, 389-399, doi:10.1016/j.immuni.2013.12.015 (2014).
83 Heath, W. R. *et al.* Cross-presentation, dendritic cell subsets, and the generation of immunity to cellular antigens. *Immunol Rev* **199**, 9-26, doi:10.1111/j.0105-2896.2004.00142.x (2004).
84 Cao, L., Chang, H., Shi, X., Peng, C. & He, Y. Keratin mediates the recognition of apoptotic and necrotic cells through dendritic cell receptor DEC205/CD205. *Proc Natl Acad Sci U S A* **113**, 13438-13443, doi:10.1073/pnas.1609331113 (2016).
85 McGreal, E. P., Miller, J. L. & Gordon, S. Ligand recognition by antigen-presenting cell C-type lectin receptors. *Curr Opin Immunol* **17**, 18-24, doi:10.1016/j.coi.2004.12.001 (2005).
86 Schetters, S. T. T. *et al.* Mouse DC-SIGN/CD209a as Target for Antigen Delivery and Adaptive Immunity. *Front Immunol* **9**, 990, doi:10.3389/fimmu.2018.00990 (2018).
87 McKenzie, E. J. *et al.* Mannose receptor expression and function define a new population of murine dendritic cells. *J Immunol* **178**, 4975-4983, doi:10.4049/jimmunol.178.8.4975 (2007).
88 Segura, E. Review of Mouse and Human Dendritic Cell Subsets. *Methods Mol Biol* **1423**, 3-15, doi:10.1007/978-1-4939-3606-9_1 (2016).
89 Zimara, N. *et al.* Dectin-1 Positive Dendritic Cells Expand after Infection with Leishmania major Parasites and Represent Promising Targets for Vaccine Development. *Front Immunol* **9**, 263, doi:10.3389/fimmu.2018.00263 (2018).
90 Margolis, S. R., Wilson, S. C. & Vance, R. E. Evolutionary Origins of cGAS-STING Signaling. *Trends in Immunology* **38**, 733-743, doi:10.1016/j.it.2017.03.004 (2017).
91 Chen, Q., Sun, L. & Chen, Z. J. Regulation and function of the cGAS–STING pathway of cytosolic DNA sensing. *Nature Immunology* **17**, 1142-1149, doi:10.1038/ni.3558 (2016).
92 Menu, P. & Vince, J. E. The NLRP3 inflammasome in health and disease: the good, the bad and the ugly. *Clin Exp Immunol* **166**, 1-15, doi:10.1111/j.1365-2249.2011.04440.x (2011).
93 Poyet, J.-L. *et al.* Identification of Ipaf, a Human Caspase-1-activating Protein Related to Apaf-1. *J Biol Chem* **276**, 28309-28313, doi:10.1074/jbc.C100250200 (2001).
94 Franchi, L., Eigenbrod, T., Muñoz-Planillo, R. & Nuñez, G. The inflammasome: a caspase-1-activation platform that regulates immune responses and disease pathogenesis. *Nat Immunol* **10**, 241-247, doi:10.1038/ni.1703 (2009).
95 Fernandes-Alnemri, T. *et al.* The AIM2 inflammasome is critical for innate immunity to Francisella tularensis. *Nat Immunol* **11**, 385-393, doi:10.1038/ni.1859 (2010).

96 Rathinam, V. A. K. *et al.* The AIM2 inflammasome is essential for host defense against cytosolic bacteria and DNA viruses. *Nat Immunol* **11**, 395-402, doi:10.1038/ni.1864 (2010).
97 Kawai, T. & Akira, S. Toll-like Receptor and RIG-1-like Receptor Signaling. *Ann NY Acad Sci* **1143**, 1-20, doi:10.1196/annals.1443.020 (2008).
98 Yoneyama, M. & Fujita, T. RNA recognition and signal transduction by RIG-I-like receptors. *Immunol Rev* **227**, 54-65, doi:10.1111/j.1600-065X.2008.00727.x (2009).
99 Ablasser, A. *et al.* cGAS produces a 2′-5′-linked cyclic dinucleotide second messenger that activates STING. *Nature* **498**, 380-384, doi:10.1038/nature12306 (2013).
100 Marinho, F. V., Benmerzoug, S., Oliveira, S. C., Ryffel, B. & Quesniaux, V. F. J. The Emerging Roles of STING in Bacterial Infections. *Trends in Microbiology* **25**, 906-918, doi:10.1016/j.tim.2017.05.008 (2017).
101 Andrade, Warrison A. *et al.* Type I Interferon Induction by Neisseria gonorrhoeae: Dual Requirement of Cyclic GMP-AMP Synthase and Toll-like Receptor 4. *Cell Reports* **15**, 2438-2448, doi:10.1016/j.celrep.2016.05.030 (2016).
102 Hansen, K. *et al.* Listeria monocytogenes induces IFN β expression through an IFI16-, cGAS- and STING-dependent pathway. *EMBO J* **33**, 1654-1666, doi:10.15252/embj.201488029 (2014).
103 Andrade, Warrison A. *et al.* Group B Streptococcus Degrades Cyclic-di-AMP to Modulate STING-Dependent Type I Interferon Production. *Cell Host & Microbe* **20**, 49-59, doi:10.1016/j.chom.2016.06.003 (2016).
104 Collins, Angela C. *et al.* Cyclic GMP-AMP Synthase Is an Innate Immune DNA Sensor for Mycobacterium tuberculosis. *Cell Host & Microbe* **17**, 820-828, doi:10.1016/j.chom.2015.05.005 (2015).
105 Prince, A. *et al.* Opposing roles of Toll-like receptor and cytosolic DNA-STING signaling pathways for Staphylococcus aureus cutaneous host defense. *PLOS Pathogens* **13**, doi:10.1371/journal.ppat.1006496 (2017).
106 Rueckert, C. *et al.* Cyclic dinucleotides modulate induced type I IFN responses in innate immune cells by degradation of STING. *FASEB J* **31**, 3107-3115, doi:10.1096/fj.201601093R (2017).
107 Cao, X. New DNA-sensing pathway feeds RIG-I with RNA. *Nat Immunol* **10**, 1049-1051, doi:10.1038/ni1009-1049 (2009).
108 Schroder, K., Muruve, D. A. & Tschopp, J. Innate immunity: cytoplasmic DNA sensing by the AIM2 inflammasome. *Curr Biol* **19**, R262-265, doi:10.1016/j.cub.2009.02.011 (2009).
109 Andersson, L. I., Hellman, P. & Eriksson, H. Receptor-mediated endocytosis of particles by peripheral dendritic cells. *Hum Immunol* **69**, 625-633, doi:10.1016/j.humimm.2008.07.010 (2008).
110 Rogers, N. C. *et al.* Syk-dependent cytokine induction by Dectin-1 reveals a novel pattern recognition pathway for C type lectins. *Immunity* **22**, 507-517, doi:10.1016/j.immuni.2005.03.004 (2005).
111 Le Bon, A. *et al.* Cross-priming of CD8+ T cells stimulated by virus-induced type I interferon. *Nat Immunol* **4**, 1009-1015, doi:10.1038/ni978 (2003).
112 Nizzoli, G. *et al.* Human CD1c+ dendritic cells secrete high levels of IL-12 and potently prime cytotoxic T-cell responses. *Blood* **122**, 932-942, doi:10.1182/blood-2013-04-495424 (2013).

113 Geginat, J. *et al.* Immunity to Pathogens Taught by Specialized Human Dendritic Cell Subsets. *Front Immunol* **6**, 527, doi:10.3389/fimmu.2015.00527 (2015).
114 Nizzoli, G. *et al.* IL-10 promotes homeostatic proliferation of human CD8(+) memory T cells and, when produced by CD1c(+) DCs, shapes naive CD8(+) T-cell priming. *Eur J Immunol* **46**, 1622-1632, doi:10.1002/eji.201546136 (2016).
115 Yu, C. I. *et al.* Human CD1c+ dendritic cells drive the differentiation of CD103+ CD8+ mucosal effector T cells via the cytokine TGF-beta. *Immunity* **38**, 818-830, doi:10.1016/j.immuni.2013.03.004 (2013).
116 Acosta-Rodriguez, E. V., Napolitani, G., Lanzavecchia, A. & Sallusto, F. Interleukins 1beta and 6 but not transforming growth factor-beta are essential for the differentiation of interleukin 17-producing human T helper cells. *Nat Immunol* **8**, 942-949, doi:10.1038/ni1496 (2007).
117 Megjugorac, N. J., Gallagher, G. E. & Gallagher, G. IL-4 enhances IFN-lambda1 (IL-29) production by plasmacytoid DCs via monocyte secretion of IL-1Ra. *Blood* **115**, 4185-4190, doi:10.1182/blood-2009-09-246157 (2010).
118 Luber, C. A. *et al.* Quantitative proteomics reveals subset-specific viral recognition in dendritic cells. *Immunity* **32**, 279-289, doi:10.1016/j.immuni.2010.01.013 (2010).
119 Proietto, A. I. *et al.* Differential production of inflammatory chemokines by murine dendritic cell subsets. *Immunobiology* **209**, 163-172, doi:10.1016/j.imbio.2004.03.002 (2004).
120 Williams, R. E. O. Healthy carriage of *Staphylococcus aureus:* its prevalence and importance. *Bacteriol Rev* **27**, 56-71 (1963).
121 Wertheim, H. F. L. *et al.* Risk and outcome of nosocomial Staphylococcus aureus bacteraemia in nasal carriers versus non-carriers. *The Lancet* **364**, 703-705, doi:10.1016/s0140-6736(04)16897-9 (2004).
122 Nouwen, J. Predicting the Staphylococcus aureus Nasal Carrier State: Derivation and Validation of a "Culture Rule". *Clin Infect Dis* **39**, 806-811 (2004).
123 Mitchell, B. G., Collignon, P. J., McCann, R., Wilkinson, I. J. & Wells, A. A major reduction in hospital-onset Staphylococcus aureus bacteremia in Australia-12 years of progress: an observational study. *Clin Infect Dis* **59**, 969-975, doi:10.1093/cid/ciu508 (2014).
124 Turnidge, J. D. *et al.* Staphylococcus aureus bacteraemia: a major cause of mortality in Australia and New Zealand. *Med J Aust* **191**, 368-373 (2009).
125 Blot, S. I., Vandewoude, K. H., Hoste, E. A. & Colardyn, F. A. Outcome and Attributable Mortality in Critically Ill Patients With Bacteremia Involving Methicillin-Susceptible and Methicillin-Resistant Staphylococcus aureus. *Archives of Internal Medicine* **162**, doi:10.1001/archinte.162.19.2229 (2002).
126 Bergin, S. P., Holland, T. L., Fowler, V. G., Jr. & Tong, S. Y. C. Bacteremia, Sepsis, and Infective Endocarditis Associated with Staphylococcus aureus. *Curr Top Microbiol Immunol* **409**, 263-296, doi:10.1007/82_2015_5001 (2017).
127 Verkaik, N. J. *et al.* Anti-staphylococcal humoral immune response in persistent nasal carriers and noncarriers of Staphylococcus aureus. *J Infect Dis* **199**, 625-632, doi:10.1086/596743 (2009).
128 Chang, F. Y. *et al.* Staphylococcus aureus bacteremia: recurrence and the impact of antibiotic treatment in a prospective multicenter study. *Medicine (Baltimore)* **82**, 333-339, doi:10.1097/01.md.0000091184.93122.09 (2003).
129 Kreisel, K., Boyd, K., Langenberg, P. & Roghmann, M. C. Risk factors for recurrence in patients with Staphylococcus aureus infections complicated by

bacteremia. *Diagn Microbiol Infect Dis* **55**, 179-184, doi:10.1016/j.diagmicrobio.2006.01.021 (2006).
130 Udo, E., Pearman, J. & W., G. Genetic analysis of community isolates of methicillin-resistant Staphylococcus aureus in Western Australia. *Journal of Hospital Infection* **25**, 97-108, doi:10.1016/0195-6701(93)90100-e (1993).
131 Boyle-Vavra, S., Yin, S., Jo, D. S., Montgomery, C. P. & Daum, R. S. VraT/YvqF is required for methicillin resistance and activation of the VraSR regulon in Staphylococcus aureus. *Antimicrob Agents Chemother* **57**, 83-95, doi:10.1128/AAC.01651-12 (2013).
132 Miller, L. G. *et al.* Necrotizing fasciitis caused by community-associated methicillin-resistant Staphylococcus aureus in Los Angeles. *N Engl J Med* **352**, 1445-1453, doi:10.1056/NEJMoa042683 (2005).
133 Graves, S. F., Kobayashi, S. D. & DeLeo, F. R. Community-associated methicillin-resistant Staphylococcus aureus immune evasion and virulence. *J Mol Med (Berl)* **88**, 109-114, doi:10.1007/s00109-009-0573-x (2010).
134 Nimmo, G. R. *et al.* Replacement of healthcare-associated MRSA by community-associated MRSA in Queensland: confirmation by genotyping. *J Infect* **67**, 439-447, doi:10.1016/j.jinf.2013.07.020 (2013).
135 Grayczyk, J. P., Harvey, C. J., Laczkovich, I. & Alonzo, F., 3rd. A Lipoylated Metabolic Protein Released by Staphylococcus aureus Suppresses Macrophage Activation. *Cell Host Microbe* **22**, 678-687 e679, doi:10.1016/j.chom.2017.09.004 (2017).
136 Parker, D. & Prince, A. Staphylococcus aureus induces type I IFN signaling in dendritic cells via TLR9. *J Immunol* **189**, 4040-4046, doi:10.4049/jimmunol.1201055 (2012).
137 Planet, P. J. *et al.* Lambda Interferon Restructures the Nasal Microbiome and Increases Susceptibility to Staphylococcus aureus Superinfection. *MBio* **7**, e01939-01915, doi:10.1128/mBio.01939-15 (2016).
138 Uebele, J. *et al.* Antigen delivery to dendritic cells shapes human CD4+ and CD8+ T cell memory responses to Staphylococcus aureus. *PLoS Pathog* **13**, e1006387, doi:10.1371/journal.ppat.1006387 (2017).
139 Parcina, M. *et al.* Pathogen-triggered activation of plasmacytoid dendritic cells induces IL-10-producing B cells in response to Staphylococcus aureus. *J Immunol* **190**, 1591-1602, doi:10.4049/jimmunol.1201222 (2013).
140 Warnking, K. *et al.* Super-infection with Staphylococcus aureus inhibits influenza virus-induced type I IFN signalling through impaired STAT1-STAT2 dimerization. *Cell Microbiol* **17**, 303-317, doi:10.1111/cmi.12375 (2015).
141 Jin, J. O., Zhang, W., Du, J. Y. & Yu, Q. BDCA1-positive dendritic cells (DCs) represent a unique human myeloid DC subset that induces innate and adaptive immune responses to Staphylococcus aureus Infection. *Infect Immun* **82**, 4466-4476, doi:10.1128/IAI.01851-14 (2014).
142 O'Keeffe, K. M. *et al.* Manipulation of Autophagy in Phagocytes Facilitates Staphylococcus aureus Bloodstream Infection. *Infect Immun* **83**, 3445-3457, doi:10.1128/IAI.00358-15 (2015).
143 Schindler, D. *et al.* Dendritic cells are central coordinators of the host immune response to Staphylococcus aureus bloodstream infection. *Am J Pathol* **181**, 1327-1337, doi:10.1016/j.ajpath.2012.06.039 (2012).

144 Fux, C. A., Shirtliff, M., Stoodley, P. & Costerton, J. W. Can laboratory reference strains mirror "real-world" pathogenesis? *Trends Microbiol* **13**, 58-63, doi:10.1016/j.tim.2004.11.001 (2005).
145 Darisipudi, M. N., Nordengrun, M., Broker, B. M. & Peton, V. Messing with the Sentinels-The Interaction of Staphylococcus aureus with Dendritic Cells. *Microorganisms* **6**, doi:10.3390/microorganisms6030087 (2018).
146 Parcina, M. *et al. Staphylococcus aureus*-induced plasmacytoid dendritic cell activation is based on an IgG-mediated memory response. *J Immunol* **181**, 3823-3833, doi:10.4049/jimmunol.181.6.3823 (2008).
147 Neves, P. *et al.* Signaling via the MyD88 adaptor protein in B cells suppresses protective immunity during Salmonella typhimurium infection. *Immunity* **33**, 777-790, doi:10.1016/j.immuni.2010.10.016 (2010).
148 Martin, A. W. in *Diagnostic Immunohistochemistry* 156-188 (2011).
149 Darkwah, S. *et al.* Differential Roles of Dendritic Cells in Expanding CD4 T Cells in Sepsis. *Biomedicines* **7**, doi:10.3390/biomedicines7030052 (2019).
150 Richardson, J. R. *et al.* PSM Peptides From Community-Associated Methicillin-Resistant Staphylococcus aureus Impair the Adaptive Immune Response via Modulation of Dendritic Cell Subsets in vivo. *Front Immunol* **10**, 995, doi:10.3389/fimmu.2019.00995 (2019).
151 Berends, E. T. M. *et al.* Staphylococcus aureus Impairs the Function of and Kills Human Dendritic Cells via the LukAB Toxin. *mBio* **10**, doi:10.1128/mBio.01918-18 (2019).
152 Pinchuk, I. V., Beswick, E. J. & Reyes, V. E. Staphylococcal enterotoxins. *Toxins (Basel)* **2**, 2177-2197, doi:10.3390/toxins2082177 (2010).
153 Krakauer, T. Induction of CC chemokines in human peripheral blood mononuclear cells by staphylococcal exotoxins and its prevention by pentoxifylline. *J Leukoc Biol* **66**, 158-164, doi:10.1002/jlb.66.1.158 (1999).
154 Fraser, J. D. & Proft, T. The bacterial superantigen and superantigen-like proteins. *Immunol Rev* **225**, 226-243, doi:10.1111/j.1600-065X.2008.00681.x (2008).
155 Wilson, G. J. *et al.* Bovine Staphylococcus aureus Superantigens Stimulate the Entire T Cell Repertoire of Cattle. *Infect Immun* **86**, doi:10.1128/IAI.00505-18 (2018).
156 Thomas, D. *et al.* Staphylococcus aureus superantigens elicit redundant and extensive human Vbeta patterns. *Infect Immun* **77**, 2043-2050, doi:10.1128/IAI.01388-08 (2009).
157 Holmes, N. E. *et al.* Morbidity from in-hospital complications is greater than treatment failure in patients with Staphylococcus aureus bacteraemia. *BMC Infect Dis* **18**, 107, doi:10.1186/s12879-018-3011-2 (2018).
158 Peleg, A. Y. *et al.* Whole genome characterization of the mechanisms of daptomycin resistance in clinical and laboratory derived isolates of Staphylococcus aureus. *PLoS One* **7**, e28316, doi:10.1371/journal.pone.0028316 (2012).
159 Krakauer, T., Pradhan, K. & Stiles, B. G. Staphylococcal Superantigens Spark Host-Mediated Danger Signals. *Front Immunol* **7**, 23, doi:10.3389/fimmu.2016.00023 (2016).
160 Miethke, T., Wahl, C., Holzmann, B., Heeg, K. & Wagner, H. Bacterial superantigens induce rapid and T cell receptor V beta-selective down-regulation of L-selectin (gp90Mel-14) in vivo. *J Immunol* **151**, 6777-6782 (1993).

161 Niedergang, F. *et al.* The Staphylococcus aureus enterotoxin B superantigen induces specific T cell receptor down-regulation by increasing its internalization. *J Biol Chem* **270**, 12839-12845, doi:10.1074/jbc.270.21.12839 (1995).
162 MacDonald, H. R., Lees, R. K., Baschieri, S., Herrmann, T. & Lussow, A. R. Peripheral T-cell reactivity to bacterial superantigens in vivo: the response/anergy paradox. *Immunol Rev* **133**, 105-117, doi:10.1111/j.1600-065x.1993.tb01512.x (1993).
163 Frodermann, V. *et al.* A modulatory interleukin-10 response to staphylococcal peptidoglycan prevents Th1/Th17 adaptive immunity to Staphylococcus aureus. *J Infect Dis* **204**, 253-262, doi:10.1093/infdis/jir276 (2011).
164 Lin, L. *et al.* Th1-Th17 Cells Mediate Protective Adaptive Immunity against Staphylococcus aureus and Candida albicans Infection in Mice. *PLoS Pathogens* **5**, doi:10.1371/journal.ppat.1000703 (2009).
165 Brown, A. F. *et al.* Memory Th1 Cells Are Protective in Invasive Staphylococcus aureus Infection. *PLOS Pathogens* **11**, doi:10.1371/journal.ppat.1005226 (2015).
166 Cho, J. S. *et al.* IL-17 is essential for host defense against cutaneous Staphylococcus aureus infection in mice. *J Clin Invest* **120**, 1762-1773, doi:10.1172/jci40891 (2010).
167 Chau, T. A. *et al.* Toll-like receptor 2 ligands on the staphylococcal cell wall downregulate superantigen-induced T cell activation and prevent toxic shock syndrome. *Nat Med* **15**, 641-648, doi:10.1038/nm.1965 (2009).
168 Li, Z., Levast, B. & Madrenas, J. Staphylococcus aureus downregulates IP-10 production and prevents Th1 cell recruitment. *J Immunol* **198**, 1865-1874, doi:10.4049/jimmunol.1601336 (2017).
169 Pauli, N. T. *et al.* Staphylococcus aureus infection induces protein A-mediated immune evasion in humans. *J Exp Med* **211**, 2331-2339, doi:10.1084/jem.20141404 (2014).
170 Falugi, F., Kim, H. K., Missiakas, D. M. & Schneewind, O. Role of protein A in the evasion of host adaptive immune responses by Staphylococcus aureus. *MBio* **4**, e00575-00513, doi:10.1128/mBio.00575-13 (2013).
171 Bjork, I., Petersson, B.-A. & Sjoquist, J. Some Physicochemical Properties of Protein A from Staphylococcus aureus. *European Journal of Biochemistry* **29**, 579-584, doi:10.1111/j.1432-1033.1972.tb02024.x (1972).
172 Potter, K. N., Li, Y. & Capra, J. D. Staphylococcal protein A simultaneously interacts with framework region 1, complementarity-determining region 2, and framework region 3 on human VH3-encoded Igs. *J Immunol* **157**, 2982-2988 (1996).
173 Graille, M. *et al.* Crystal structure of a Staphylococcus aureus protein A domain complexed with the Fab fragment of a human IgM antibody: Structural basis for recognition of B-cell receptors and superantigen activity. *Proc Natl Acad Sci U S A* **97**, 5399-5404, doi:10.1073/pnas.97.10.5399 (2000).
174 Cook, G. P. & Tomlinson, I. M. The human immunoglobulin VH repertoire. *Immunology Today* **16**, 237-242, doi:10.1016/0167-5699(95)80166-9 (1995).
175 Forsgren, A. & Quie, P. G. Effects of staphylococcal protein A on heat labile opsonins. *J Immunol* **112**, 1177-1180 (1974).
176 Goodyear, C. S. & Silverman, G. J. Death by a B cell superantigen: In vivo VH-targeted apoptotic supraclonal B cell deletion by a Staphylococcal Toxin. *J Exp Med* **197**, 1125-1139, doi:10.1084/jem.20020552 (2003).

177 Silverman, G. J., Sasano, M. & Wormsley, S. B. Age-associated changes in binding of human B lymphocytes to a VH3-restricted unconventional bacterial antigen. *J Immunol* **151**, 5840-5855 (1993).
178 Li, G. M. *et al.* Pandemic H1N1 influenza vaccine induces a recall response in humans that favors broadly cross-reactive memory B cells. *Proc Natl Acad Sci U S A* **109**, 9047-9052, doi:10.1073/pnas.1118979109 (2012).
179 Wrammert, J. *et al.* Rapid cloning of high-affinity human monoclonal antibodies against influenza virus. *Nature* **453**, 667-671, doi:10.1038/nature06890 (2008).
180 Kim, H. K., Cheng, A. G., Kim, H.-Y., Missiakas, D. M. & Schneewind, O. Nontoxigenic protein A vaccine for methicillin-resistantStaphylococcus aureusinfections in mice. *J Exp Med* **207**, 1863-1870, doi:10.1084/jem.20092514 (2010).
181 Barber, M. Sensitisation of Penicillin-Resistant Staphylococci. *The Lancet* **251**, doi:10.1016/s0140-6736(48)90428-0 (1948).
182 Rolinson, G. N. "Celbenin" - resistant Staphylococci. *Bmj* **1**, 125-126, doi:10.1136/bmj.1.5219.125 (1961).
183 Knox, R. A new penicillin (BRL 1241) active against penicillin-resistant Staphylococci. *Br Med J* **2**, 690-693 (1961).
184 Barber, M. Methicillin-resistant staphylococci. *J Clin Pathol* **14**, 385-393 (1961).
185 Friedman, L., Alder, J. D. & Silverman, J. A. Genetic changes that correlate with reduced susceptibility to daptomycin in Staphylococcus aureus. *Antimicrob Agents Chemother* **50**, 2137-2145, doi:10.1128/AAC.00039-06 (2006).
186 Howden, B. P. *et al.* Evolution of multidrug resistance during Staphylococcus aureus infection involves mutation of the essential two component regulator WalKR. *PLoS Pathog* **7**, e1002359, doi:10.1371/journal.ppat.1002359 (2011).
187 Fowler, V. G., Jr. *et al.* Daptomycin versus standard therapy for bacteremia and endocarditis caused by Staphylococcus aureus. *N Engl J Med* **355**, 653-665, doi:10.1056/NEJMoa053783 (2006).
188 Jiang, J. H. & Peleg, A. Y. Daptomycin-Nonsusceptible Staphylococcus aureus: The Role of Combination Therapy with Daptomycin and Gentamicin. *Genes (Basel)* **6**, 1256-1267, doi:10.3390/genes6041256 (2015).
189 Cameron, D. R. *et al.* Serine/threonine phosphatase Stp1 contributes to reduced susceptibility to vancomycin and virulence in Staphylococcus aureus. *J Infect Dis* **205**, 1677-1687, doi:10.1093/infdis/jis252 (2012).
190 Cui, L., Tominaga, E., Neoh, H. M. & Hiramatsu, K. Correlation between Reduced Daptomycin Susceptibility and Vancomycin Resistance in Vancomycin-Intermediate Staphylococcus aureus. *Antimicrob Agents Chemother* **50**, 1079-1082, doi:10.1128/AAC.50.3.1079-1082.2006 (2006).
191 Chambers, H. F. & Deleo, F. R. Waves of resistance: Staphylococcus aureus in the antibiotic era. *Nat Rev Microbiol* **7**, 629-641, doi:10.1038/nrmicro2200 (2009).
192 Cameron, D. R. *et al.* Impact of daptomycin resistance on Staphylococcus aureus virulence. *Virulence* **6**, 127-131, doi:10.1080/21505594.2015.1011532 (2015).
193 Yang, S. J. *et al.* Cell Wall Thickening Is Not a Universal Accompaniment of the Daptomycin Nonsusceptibility Phenotype in Staphylococcus aureus: Evidence for Multiple Resistance Mechanisms. *Antimicrob Agents Chemother* **54**, 3079-3085, doi:10.1128/aac.00122-10 (2010).
194 Jiang, J. H. *et al.* Antibiotic resistance and host immune evasion in Staphylococcus aureus mediated by a metabolic adaptation. *Proc Natl Acad Sci U S A* **116**, 3722-3727, doi:10.1073/pnas.1812066116 (2019).

195 Ernst, C. M. *et al.* The bacterial defensin resistance protein MprF consists of separable domains for lipid lysinylation and antimicrobial peptide repulsion. *PLoS Pathog* **5**, e1000660, doi:10.1371/journal.ppat.1000660 (2009).
196 Peschel, A. & Sahl, H.-G. The co-evolution of host cationic antimicrobial peptides and microbial resistance. *Nat Rev Immunol* **4**, 529-536, doi:10.1038/nrmicro1441 (2006).
197 Zasloff, M. Antimicrobial peptides of multicellular organisms. *Nature* **415**, 389-395, doi:10.1038/415389a (2002).
198 Hancock, R. E. W. & Sahl, H.-G. Antimicrobial and host-defense peptides as new anti-infective therapeutic strategies. *Nature Biotechnology* **24**, 1551-1557, doi:10.1038/nbt1267 (2006).
199 Yeaman, M. R. & Yount, N. Y. Unifying themes in host defence effector polypeptides. *Nat Rev Microbiol* **5**, 727-740, doi:10.1038/nrmicro1744 (2007).
200 Mishra, N. N. *et al.* In vitro cross-resistance to daptomycin and host defense cationic antimicrobial peptides in clinical methicillin-resistant Staphylococcus aureus isolates. *Antimicrob Agents Chemother* **55**, 4012-4018, doi:10.1128/AAC.00223-11 (2011).
201 Patton, T. *et al.* Daptomycin resistant Staphylococcus aureus clinical isolates are poorly sensed by dendritic cells. *Immunol Cell Biol*, doi:10.1111/imcb.12295 (2019).
202 Naik, S. H. *et al.* Cutting edge: generation of splenic CD8+ and CD8- dendritic cell equivalents in Fms-like tyrosine kinase 3 ligand bone marrow cultures. *J Immunol* **174**, 6592-6597 (2005).
203 Adachi, O. *et al.* Targeted Disruption of the MyD88 Gene Results in Loss of IL-1- and IL-18-Mediated Function. *Immunity* **9**, 143-150, doi:10.1016/s1074-7613(00)80596-8 (1998).
204 Martino, M. M. *et al.* Inhibition of IL-1R1/MyD88 signalling promotes mesenchymal stem cell-driven tissue regeneration. *Nat Commun* **7**, 11051, doi:10.1038/ncomms11051 (2016).
205 Hemmi, H. *et al.* A Toll-like receptor recognizes bacterial DNA. *Nature* **408**, 740-745, doi:10.1038/35047123 (2000).
206 Schoggins, J. W. *et al.* Pan-viral specificity of IFN-induced genes reveals new roles for cGAS in innate immunity. *Nature* **505**, 691-695, doi:10.1038/nature12862 (2014).
207 O'Keeffe, M. *et al.* Mouse plasmacytoid cells: long-lived cells, heterogeneous in surface phenotype and function, that differentiate into CD8(+) dendritic cells only after microbial stimulus. *J Exp Med* **196**, 1307-1319, doi:10.1084/jem.20021031 (2002).
208 Vremec, D., Pooley, J., Hochrein, H., Wu, L. & Shortman, K. CD4 and CD8 expression by dendritic cell subtypes in mouse thymus and spleen. *J Immunol* **164**, 2978-2986, doi:10.4049/jimmunol.164.6.2978 (2000).
209 Fuertes Marraco, S. A. *et al.* Novel murine dendritic cell lines: a powerful auxiliary tool for dendritic cell research. *Front Immunol* **3**, 331, doi:10.3389/fimmu.2012.00331 (2012).
210 Mwangi, M. M. *et al.* Tracking the in vivo evolution of multidrug resistance in Staphylococcus aureus by whole-genome sequencing. *Proc Natl Acad Sci U S A* **104**, 9451-9456, doi:10.1073/pnas.0609839104 (2007).
211 Bateman, B. T., Donegan, N. P., Jarry, T. M., Palma, M. & Cheung, A. L. Evaluation of a tetracycline-inducible promoter in Staphylococcus aureus in vitro and in vivo

and its application in demonstrating the role of sigB in microcolony formation. *Infect Immun* **69**, 7851-7857, doi:10.1128/IAI.69.12.7851-7857.2001 (2001).
212 O'Keeffe, M., Mok, W. H. & Radford, K. J. Human dendritic cell subsets and function in health and disease. *Cell Mol Life Sci* **72**, 4309-4325, doi:10.1007/s00018-015-2005-0 (2015).
213 Merad, M., Sathe, P., Helft, J., Miller, J. & Mortha, A. The dendritic cell lineage: ontogeny and function of dendritic cells and their subsets in the steady state and the inflamed setting. *Annu Rev Immunol* **31**, 563-604, doi:10.1146/annurev-immunol-020711-074950 (2013).
214 Kapsenberg, M. L. Dendritic-cell control of pathogen-driven T-cell polarization. *Nat Rev Immunol* **3**, 984-993, doi:10.1038/nri1246 (2003).
215 Yamazaki, T. *et al.* Expression of Programmed Death 1 Ligands by Murine T Cells and APC. *The Journal of Immunology* **169**, 5538-5545, doi:10.4049/jimmunol.169.10.5538 (2002).
216 Kuipers, H. *et al.* Contribution of the PD-1 ligands/PD-1 signaling pathway to dendritic cell-mediated CD4+ T cell activation. *Eur J Immunol* **36**, 2472-2482, doi:10.1002/eji.200635978 (2006).
217 Yao, S. *et al.* PD-1 on dendritic cells impedes innate immunity against bacterial infection. *Blood* **113**, 5811-5818, doi:10.1182/blood-2009-02-203141 (2009).
218 Nishat, S., Wuescher, L. M. & Worth, R. G. Platelets enhance dendritic cell responses against S. aureus through CD40-CD40L interactions. *Infect Immun*, doi:10.1128/IAI.00186-18 (2018).
219 Nguyen, M. T. *et al.* Lipid moieties on lipoproteins of commensal and non-commensal staphylococci induce differential immune responses. *Nat Commun* **8**, 2246, doi:10.1038/s41467-017-02234-4 (2017).
220 Naik, S. H., O'Keeffe, M., Proietto, A., Shortman, H. H. & Wu, L. CD8+, CD8-, and plasmacytoid dendritic cell generation in vitro using flt3 ligand. *Methods Mol Biol* **595**, 167-176, doi:10.1007/978-1-60761-421-0_10 (2010).
221 Hochrein, H. *et al.* Herpes simplex virus type-1 induces IFN-alpha production via Toll-like receptor 9-dependent and -independent pathways. *Proc Natl Acad Sci U S A* **101**, 11416-11421, doi:10.1073/pnas.0403555101 (2004).
222 Driesen, J., Popov, A. & Schultze, J. L. CD25 as an immune regulatory molecule expressed on myeloid dendritic cells. *Immunobiology* **213**, 849-858, doi:10.1016/j.imbio.2008.07.026 (2008).
223 Cella, M., Facchetti, F., Lanzavecchia, A. & Colonna, M. Plasmacytoid dendritic cells activated by influenza virus and CD40L drive a potent TH1 polarization. *Nat Immunol* **1**, 305-310, doi:10.1038/79747 (2000).
224 Ziegler, S. F. *et al.* The mouse CD69 gene. Structure, expression, and mapping to the NK gene complex. *J Immunol* **152**, 1228-1236 (1994).
225 Ziegler, S. F., Ramsdell, F. & Alderson, M. R. The activation antigen CD69. *Stem Cells* **12**, 456-465, doi:10.1002/stem.5530120502 (1994).
226 Alari-Pahissa, E. *et al.* CD69 does not affect the extent of T cell priming. *PLoS One* **7**, e48593, doi:10.1371/journal.pone.0048593 (2012).
227 Parker, D., Planet, P. J., Soong, G., Narechania, A. & Prince, A. Induction of type I interferon signaling determines the relative pathogenicity of Staphylococcus aureus strains. *PLoS Pathog* **10**, e1003951, doi:10.1371/journal.ppat.1003951 (2014).

228 Guilliams, M. & Malissen, B. A Death Notice for In-Vitro-Generated GM-CSF Dendritic Cells? *Immunity* **42**, 988-990, doi:10.1016/j.immuni.2015.05.020 (2015).
229 Lutz, M. B., Inaba, K., Schuler, G. & Romani, N. Still Alive and Kicking: In-Vitro-Generated GM-CSF Dendritic Cells! *Immunity* **44**, 1-2, doi:10.1016/j.immuni.2015.12.013 (2016).
230 Helft, J. *et al.* Alive but confused: heterogeneity of CD11c^{+} MHC Class II^{+} cells in GM-CSF mouse bone marrow cultures. *Immunity* **44**, 3-4, doi:10.1016/j.immuni.2015.12.014 (2016).
231 Haller, D., Bode, C. & Hammes, W. P. Cytokine Secretion by Stimulated Monocytes Depends on the Growth Phase and Heat Treatment of Bacteria. *Microbiology and Immunology* **43**, 925-935, doi:10.1111/j.1348-0421.1999.tb03353.x (1999).
232 Miettinen, M., Vuopio-Varkila, J. & Varkila, K. Production of human tumor necrosis factor alpha, interleukin-6, and interleukin-10 is induced by lactic acid bacteria. *Infect Immun* **64**, 5403-5405 (1996).
233 Braat, H. *et al.* Dichotomy between Lactobacillus rhamnosus and Klebsiella pneumoniae on dendritic cell phenotype and function. *J Mol Med (Berl)* **82**, 197-205, doi:10.1007/s00109-003-0509-9 (2004).
234 Kaplan, A. *et al.* Failure to induce IFN-beta production during Staphylococcus aureus infection contributes to pathogenicity. *J Immunol* **189**, 4537-4545, doi:10.4049/jimmunol.1201111 (2012).
235 Fitzgerald-Bocarsly, P. & Feng, D. The role of type I interferon production by dendritic cells in host defense. *Biochimie* **89**, 843-855, doi:10.1016/j.biochi.2007.04.018 (2007).
236 Honda, K., Yanai, H., Takaoka, A. & Taniguchi, T. Regulation of the type I IFN induction: a current view. *Int Immunol* **17**, 1367-1378, doi:10.1093/intimm/dxh318 (2005).
237 Marie, I., Durbin, J. E. & Levy, D. E. Differential viral induction of distinct interferon-alpha genes by positive feedback through interferon regulatory factor-7. *EMBO J* **17**, 6660-6669, doi:10.1093/emboj/17.22.6660 (1998).
238 Sato, M. *et al.* Positive feedback regulation of type I IFN genes by the IFN-inducible transcription factor IRF-7. *FEBS Letters* **441**, 106-110, doi:10.1016/s0014-5793(98)01514-2 (1998).
239 Sieradzki, K., Leski, T., Dick, J., Borio, L. & Tomasz, A. Evolution of a vancomycin-intermediate Staphylococcus aureus strain in vivo: multiple changes in the antibiotic resistance phenotypes of a single lineage of methicillin-resistant S. aureus under the impact of antibiotics administered for chemotherapy. *J Clin Microbiol* **41**, 1687-1693, doi:10.1128/jcm.41.4.1687-1693.2003 (2003).
240 Holmes, N. E., Tong, S. Y., Davis, J. S. & van Hal, S. J. Treatment of methicillin-resistant Staphylococcus aureus: vancomycin and beyond. *Semin Respir Crit Care Med* **36**, 17-30, doi:10.1055/s-0034-1397040 (2015).
241 Casanova, N. G., Ruiz, M. S. & Bellido, M. Mechanisms of resistance to daptomycin in *Staphylococcus aureus*. *Rev Esp Quimioter* **30**, 391-396 (2017).
242 Allen, N. E., Alborn, W. E., Jr. & Hobbs, J. N., Jr. Inhibition of membrane potential-dependent amino acid transport by daptomycin. *Antimicrob Agents Chemother* **35**, 2639-2642, doi:10.1128/aac.35.12.2639 (1991).
243 Alborn, W. E., Jr., Allen, N. E. & Preston, D. A. Daptomycin disrupts membrane potential in growing Staphylococcus aureus. *Antimicrob Agents Chemother* **35**, 2282-2287, doi:10.1128/aac.35.11.2282 (1991).

244 Silverman, J. A., Perlmutter, N. G. & Shapiro, H. M. Correlation of daptomycin bactericidal activity and membrane depolarization in Staphylococcus aureus. *Antimicrob Agents Chemother* **47**, 2538-2544, doi:10.1128/aac.47.8.2538-2544.2003 (2003).
245 Watanakunakorn, C. Mode of action and in-vitro activity of vancomycin. *J Antimicrob Chemother* **14 Suppl D**, 7-18, doi:10.1093/jac/14.suppl_d.7 (1984).
246 Peschel, A. *et al.* Staphylococcus aureus resistance to human defensins and evasion of neutrophil killing via the novel virulence factor MprF is based on modification of membrane lipids with l-lysine. *J Exp Med* **193**, 1067-1076, doi:10.1084/jem.193.9.1067 (2001).
247 Koprivnjak, T. *et al.* Characterization of Staphylococcus aureus cardiolipin synthases 1 and 2 and their contribution to accumulation of cardiolipin in stationary phase and within phagocytes. *J Bacteriol* **193**, 4134-4142, doi:10.1128/JB.00288-11 (2011).
248 Tsai, M. *et al.* Staphylococcus aureus requires cardiolipin for survival under conditions of high salinity. *BMC Microbiol* **11**, 13, doi:10.1186/1471-2180-11-13 (2011).
249 Fabbrini, M. *et al.* A new flow-cytometry-based opsonophagocytosis assay for the rapid measurement of functional antibody levels against Group B Streptococcus. *J Immunol Methods* **378**, 11-19, doi:10.1016/j.jim.2012.01.011 (2012).
250 Mintern, J. D. *et al.* Differential use of autophagy by primary dendritic cells specialized in cross-presentation. *Autophagy* **11**, 906-917, doi:10.1080/15548627.2015.1045178 (2015).
251 Patterson, G. H., Knobel, S. M., Sharif, W. D., Kain, S. R. & Piston, D. W. Use of the green fluorescent protein and its mutants in quantitative fluorescence microscopy. *Biophys J* **73**, 2782-2790, doi:10.1016/s0006-3495(97)78307-3 (1997).
252 Savina, A. *et al.* NOX2 controls phagosomal pH to regulate antigen processing during crosspresentation by dendritic cells. *Cell* **126**, 205-218, doi:10.1016/j.cell.2006.05.035 (2006).
253 Savina, A. *et al.* The small GTPase Rac2 controls phagosomal alkalinization and antigen crosspresentation selectively in CD8(+) dendritic cells. *Immunity* **30**, 544-555, doi:10.1016/j.immuni.2009.01.013 (2009).
254 Bode, C. *et al.* Human plasmacytoid dentritic cells elicit a Type I Interferon response by sensing DNA via the cGAS-STING signaling pathway. *Eur J Immunol* **46**, 1615-1621, doi:10.1002/eji.201546113 (2016).
255 Bergstrom, B. *et al.* TLR8 Senses Staphylococcus aureus RNA in Human Primary Monocytes and Macrophages and Induces IFN-beta Production via a TAK1-IKKbeta-IRF5 Signaling Pathway. *J Immunol* **195**, 1100-1111, doi:10.4049/jimmunol.1403176 (2015).
256 Liu, J. *et al.* A five-amino-acid motif in the undefined region of the TLR8 ectodomain is required for species-specific ligand recognition. *Mol Immunol* **47**, 1083-1090, doi:10.1016/j.molimm.2009.11.003 (2010).
257 Fang, L., Wu, H. M., Ding, P. S. & Liu, R. Y. TLR2 mediates phagocytosis and autophagy through JNK signaling pathway in Staphylococcus aureus-stimulated RAW264.7 cells. *Cell Signal* **26**, 806-814, doi:10.1016/j.cellsig.2013.12.016 (2014).

258 Stuart, L. M. *et al.* Response to Staphylococcus aureus requires CD36-mediated phagocytosis triggered by the COOH-terminal cytoplasmic domain. *J Cell Biol* **170**, 477-485, doi:10.1083/jcb.200501113 (2005).
259 Bertsche, U. *et al.* Correlation of daptomycin resistance in a clinical Staphylococcus aureus strain with increased cell wall teichoic acid production and D-alanylation. *Antimicrob Agents Chemother* **55**, 3922-3928, doi:10.1128/AAC.01226-10 (2011).
260 Holmes, N. E. *et al.* Antibiotic choice may not explain poorer outcomes in patients with Staphylococcus aureus bacteremia and high vancomycin minimum inhibitory concentrations. *J Infect Dis* **204**, 340-347, doi:10.1093/infdis/jir270 (2011).
261 Holland, T. L. & Fowler, V. G., Jr. Vancomycin minimum inhibitory concentration and outcome in patients with Staphylococcus aureus bacteremia: pearl or pellet? *J Infect Dis* **204**, 329-331, doi:10.1093/infdis/jir275 (2011).
262 Han, J. H., Mascitti, K. B., Edelstein, P. H., Bilker, W. B. & Lautenbach, E. Effect of reduced vancomycin susceptibility on clinical and economic outcomes in Staphylococcus aureus bacteremia. *Antimicrob Agents Chemother* **56**, 5164-5170, doi:10.1128/AAC.00757-12 (2012).
263 Nguyen, M. T. & Gotz, F. Lipoproteins of Gram-Positive Bacteria: Key Players in the Immune Response and Virulence. *Microbiol Mol Biol Rev* **80**, 891-903, doi:10.1128/MMBR.00028-16 (2016).
264 Schwandner, R., Dziarski, R., Wesche, H., Rothe, M. & Kirschning, C. J. Peptidoglycan- and lipoteichoic acid-induced cell activation is mediated by toll-like receptor 2. *J Biol Chem* **274**, 17406-17409, doi:10.1074/jbc.274.25.17406 (1999).
265 Imai, T. *et al.* Lipoteichoic acid anchor triggers Mincle to drive protective immunity against invasive group A Streptococcus infection. *Proc Natl Acad Sci U S A* **115**, E10662-E10671, doi:10.1073/pnas.1809100115 (2018).
266 Toledo, A. M. & Benach, J. L. in *Virulence mechanisms of bacterial pathogens* (eds I. Kudva *et al.*) Ch. Hijacking and use of host lipids by intracellular pathogens, (American Society for Microbiology, 2016).
267 Crowley, J. T. *et al.* Lipid exchange between Borrelia burgdorferi and host cells. *PLoS Pathog* **9**, e1003109, doi:10.1371/journal.ppat.1003109 (2013).
268 Boyle, M. D. P. in *Bacterial Immunoglobulin-binding Proteins* 17-28 (1990).
269 Lindmark, R., Thorén-Tolling, K. & Sjöquist, J. Binding of immunoglobulins to protein A and immunoglobulin levels in mammalian sera. *J Immunol Methods* **62**, 1-13, doi:10.1016/0022-1759(83)90104-7 (1983).
270 Coe, J. E., Coe, P. R. & Ross, M. J. Staphylococcal protein a purification of rodent IgG1 and IgG2 with particular emphasis on Syrian hamsters. *Molecular Immunology* **18**, 1007-1012, doi:10.1016/0161-5890(81)90119-x (1981).
271 Lindmark, R., Movitz, J. & Sjoquist, J. Extracellular protein A from a methicillin-resistant strain of Staphylococcus aureus. *Eur J Biochem* **74**, 623-628, doi:10.1111/j.1432-1033.1977.tb11431.x (1977).
272 Smith, E. J., Visai, L., Kerrigan, S. W., Speziale, P. & Foster, T. J. The Sbi protein is a multifunctional immune evasion factor of Staphylococcus aureus. *Infect Immun* **79**, 3801-3809, doi:10.1128/IAI.05075-11 (2011).

Appendices

Appendix A: Additional data and figures

A1: Optimisation of FLDC culture conditions

Cytokine and surface DC activation peaks at 18 hours post stimuli with live *S. aureus*

Having established an optimal MOI of 10 for DC activation, we next performed a time course to determine the optimal length of bacterial stimulation to accurately measure DC activation. Using heat inactivated isolates of MRSA, we therefore sought to address whether best to phenotype the early activation of the DC at 6 hours, or the end-point activation at 18 hours post stimulus. We found that similar to the TLR9 agonist CpG 2216, heat inactivated MRSA were incapable of inducing IL-6, MIP-1α, MIP-1β or MDC at appreciable levels within the first 6 hours of stimulus (figure A1.1a). Cytokine expression was rather found to peak at 18 hours regardless of stimuli (figure A1.1a), except for MIP-1β which only following stimuli with CpG 2216 peaked in secretion at 6 hours post stimulus (figure A1.1a). Surprising to us, and in spite of the complex mixture of PRR agonists, the heat inactivated MRSA stimuli typically resulted in cytokine secretion approximately 10-fold lower than that observed for CpG 2216 at 18 hours, with the exception of MDC which was produced in equivalence for both stimuli (figure A1.1a).

Given optimal secretion of cytokines by DC stimulated with bacteria requiring 18 hour stimulation, we next considered the kinetics of surface activation. Consistent with the cytokine data, we further observed a time dependence in the upregulation of all canonical surface activation markers except for CD69 and CD80; with the highest expression of CD40, CD86, MHC-I and MHC-II being observed at 18 hours post stimulus with DapS MRSA by both cDC1 and cDC2 (figure A1.1b). Similarly, the upregulation of PD-L2, GITR, CCR7 and CCR9 were highest at 18 hours post stimulus, requiring longer incubations with DapS MRSA to reach peak expression. By contrast, the upregulation of CD80 (figure A1.1b) and PD-L1 (figure A1.1c) were more rapid following MRSA stimuli, peaking and plateauing for both cDC1 and cDC2 at 6 hours post stimulus with DapS MRSA. Of note, expression of PD-1 peaked at 6 hours post stimulus, subsequently decreasing by 18 hours post stimulus with DapS MRSA (figure A1.1c). Overall, the longer 18 hour incubation was

required to induce potent DC activation in response to bacteria, with a vast majority of analysed soluble mediators and surface molecules upregulated to peak levels by 18 hours (figure A1.2a, A1.2b and A1.2c). We therefore selected this time point for all subsequent analysis.

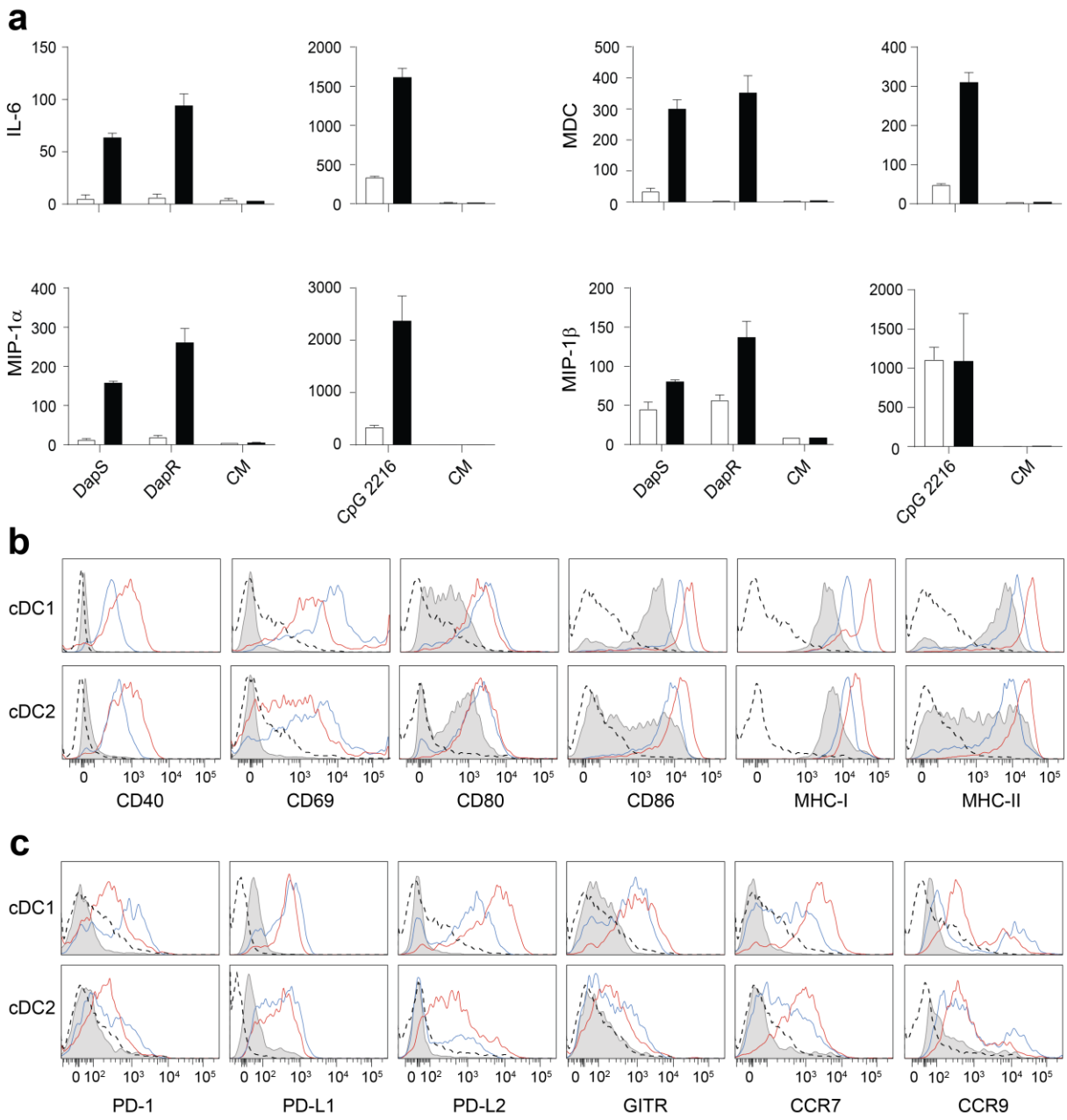

Figure A1-1 Time course assay of FLDC activation in response to a primary clinical isolate of MRSA. ***(a)*** *Secretion of IL-6, MDC, MIP-1α and MIP-1β (pg/ml) by FLDC at 6 hours (hollow bars) and 18 hours (filled bars) post stimulus with heat inactivated MRSA isolates. FLDC were stimulated with heat inactivated DapS and DapR MRSA isolates (A8819 and A8817 respectively, equivalent to MOI=10), CpG ODN 2216 (0.5 µM) or complete media (CM) alone. Bars show the mean and standard deviation of three technical replicates from a single experiment (n = 1).* ***(b)*** *Activation marker expression by FLDC stimulated with MRSA. Histograms showing CD40, CD69, CD80, CD86, MHC-I and MHC-II expression by cDC1 and cDC2 at 6 (blue line) and 18 hours (red line) post stimulus with heat inactivated A8819 DapS MRSA, media only mock stimuli at 6 hours (shaded grey) and 18 hour FMO control (dotted black line). Representative of two independent experiments (n = 2).* ***(c)*** *Chemokine receptor and inhibitory-type marker expression by FLDC stimulated with MRSA. Histograms overlays are as in 'a', showing PD-1, PD-L1, PD-L2, GITR, CCR7 and CCR9 expression. Representative of two independent experiments for all markers (n = 2), except for CCR7 and CCR9 plots which are shown from one experiment (n = 1).*

Penicillin and streptomycin are required to prevent bacterial overgrowth and DC death with live overnight stimulate of *S. aureus*

Having determined the optimal MOI and duration for stimulation of DC with bacteria, awe turned our attention to the composition of the culture medium- specifically the antibiotics. As a final optimisation step we sought to address the presence of both the penicillin and streptomycin in our DC culture medium. Given the experimental design of stimulating DC with live bacteria, we realised that the inclusion of these antibiotics could be advantageous inhibiting bacterial growth thus keeping our MOI consistent, yet simultaneously damaging to bacterial viability and function.

To evaluate the impact of our standard penicillin and streptomycin cocktail on the immunogenicity of MRSA isolates, we performed a side-by-side stimulation of DC with MRSA in the presence and absence of these antibiotics. We found that 18 hour culture of DC with these stimuli in the absence of antibiotics lead to overgrowth of the bacteria in culture media, including invasion of bacteria into neighbouring unstimulated wells showing mild bacterial growth visible via microscopic examination (data not shown). This bacterial growth was not evident for samples cultured in the presence of penicillin and streptomycin (data not shown). Further, we observed a disruption of pH as indicated by a colour change to orange in the HEPES buffered RPMI media base of samples stimulated in the absence of penicillin and streptomycin, likely due to increased metabolic activity in these samples (data not shown). Finally, bacterial stimuli in the absence of antibiotics resulted in complete death of the DC at 18 hours post stimuli with no DC visible by microscopic examination (data not shown).

Due to the overgrowth of bacteria and the safety risk posed by these clinical isolates at a higher concentration flow analysis of viability was not performed for these samples. Nonetheless, supernatants of these stimuli were able to be analysed to compare activation of the DC, and it was found that most inflammatory cytokines, chemokines and IFN were not produced in samples without penicillin and streptomycin (figure A1.2). Early phase cytokines including MDC and TNF-α were detected in the absence of penicillin and streptomycin (figure A1.2), suggesting that the DC only survived for the first few hours of stimulation. We further observed decreased expression of cytokines in response to positive and negative control stimuli in the absence of penicillin and

streptomycin, which we attributed to the invasion of these samples with bacteria which were incubated on the same 96-well plate. This is supported by the growth of bacteria observed in these wells via microscopic examination and the colour change in the media (data not shown). Subsequent tests of the penicillin and streptomycin negative media showed no bacterial growth over 7-days, confirming the media itself was free from contamination (data not shown).

We finally sought to examine the effect of our penicillin and streptomycin positive media on viability of the daptomycin exposed MRSA pair. To evaluate this, we cultured each of the DapS and DapR strains alone in the DC complete medium over 23 hours (table A1.1). We observed a sharp and rapid decline in MRSA viability in complete media, with a 3 log and 4 log decrease in CFU by 4.5 hours for the DapS and DapR strain respectively, and no viable bacteria detected by 23 hours (table A1.1).

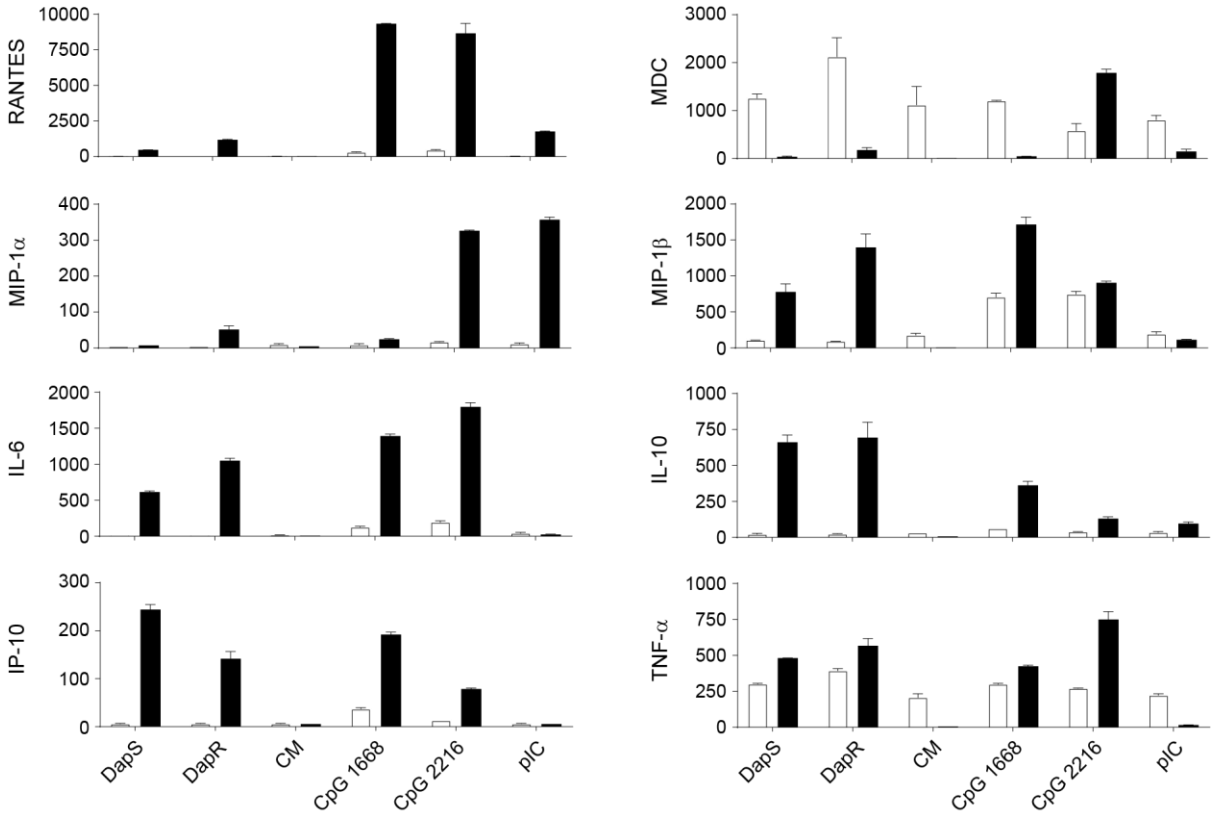

Figure A1-2 Comparison of DC activation following stimulus in the presence and absence of antibiotics. *Cytokine secretion (pg/ml) by FLDC at 18 hours following stimuli, in complete media with (black bars) and without (white bars) penicillin (10 U/ml) and streptomycin (10 µg/ml). Stimuli included paired strains of DapS (A8819) and DapR (A8817) MRSA (MOI=10), CpG 1668 and 2216 (0.5 µM), pIC (100 µg/ml) and media alone. Data shows the mean and range of two technical replicates from one experiment (n = 1).*

Table A1-1 Growth kinetics of Dap exposed MRSA clinical pairs in the DC complete medium

Time (hours)	A8819	A8817
0	7.9 x 10^6 CFU/ml	5.6 x 10^6 CFU/ml
4.5	3.8 x 10^3 CFU/ml	4.0 x 10^2 CFU/ml
23	<10 CFU/ml	<10 CFU/ml

Note: The bacterial growth at the 23 hour time point is lower than the detection limit, which is 10 CFU/ml.

A2: No IFN-α secretion by FLDC in response to bacterial stimuli

Having detected no secretion of IFN-α by DC in response to live bacterial isoaltes or heat inactivated bacteria, (chapter three; figures 3.2 and 3.7), we next sought to confirm that these differnces were not due the production of alternate IFN-α subtypes. We therefore tested FLDC for the secretion of all IFN–α subtypes in response to bacterial stimuli using the *PBL IFN-α Verikine* system, and found that none of the heat inactivated bacteria were able to induce the production of IFN-α (figure A2-1), consistent with the findings of chapter three.

Given the inability of heat inactivated bacteria to induce IFN-α production by DC, we next considered the ability of live bacterial isolates to stimulate IFN-α. We found that despite the potent production of IFN-α in response to CpG ODN 2216, neither the DapS or DapR paired isolates (A8819/A8817) were able to induce secretion by FLDC at 18 hours post stimulus (figure A2-2). Similarly, while both CpG ODNs 1668 and 2216 were able to induce secretion of IFN-α by purified splenic DC at 4, 8 and 24 hours post stimulus, the live bacterial strains were still unable to induce secretion of IFN-α at these time points (figure A2-2).

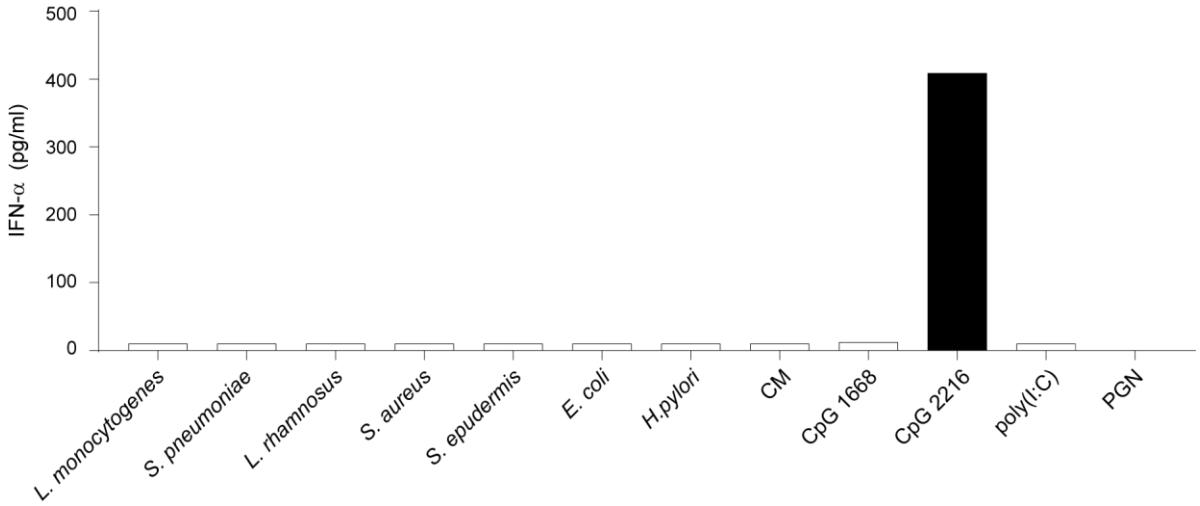

Figure A2-1 Quantitation of all IFN-α subtypes in supernatants of MRSA stimulated murine FLDC. ***(a)*** *Total IFN-α measured in supernatants of bulk FLDC stimulated for 18 hours with live paired daptomycin exposed MRSA isolates A8819 (DapS) and A8817 (DapR) at an MOI of 10, media alone (CM), CpG ODNs 1668 and 2216 (0.5 µM) and poly(I:C) (100 µg/ml). Data show the results of a single experiment, with a single data point for each stimuli (n = 1).*

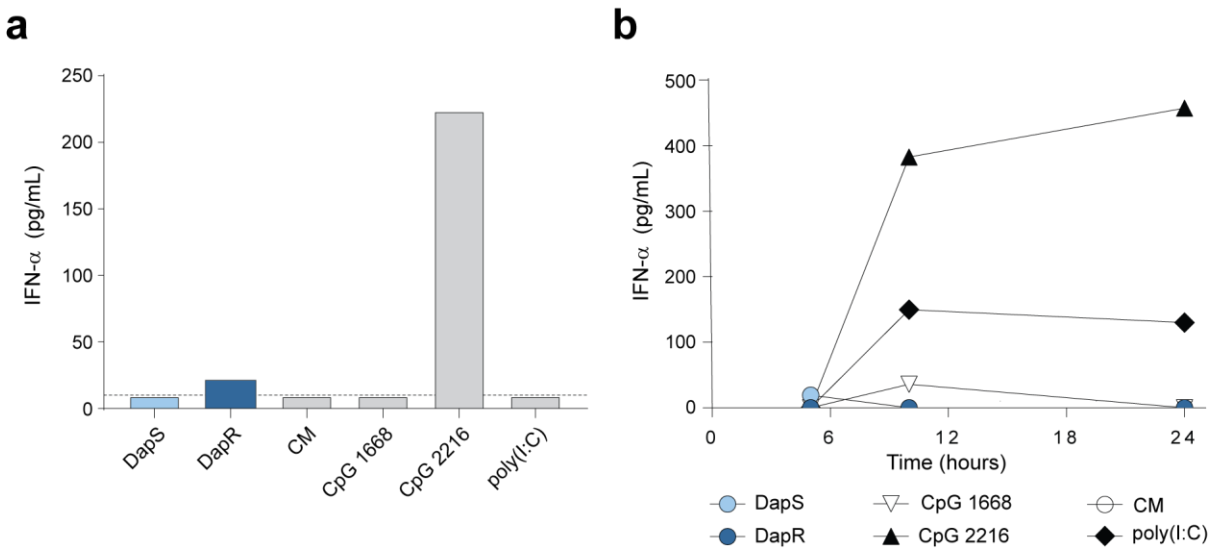

Figure A2-2 Quantitation of all IFN-α subtypes in supernatants of MRSA stimulated murine FLDC. ***(a)*** *Total IFN-α measured in supernatants of bulk FLDC stimulated for 18 hours with live paired daptomycin exposed MRSA isolates A8819 (DapS) and A8817 (DapR) at an MOI of 10, media alone (CM), CpG ODNs 1668 and 2216 (0.5 µM) and pIC (100 µg/ml). Data show the results of a single experiment, with a single data point for each stimuli (n = 1).* ***(b)*** *Total IFN-α measured in supernatants of bulk splenic DC stimulated for 4, 8 and 24 hours with live paired daptomycin exposed MRSA isolates A8819 (DapS) and A8817 (DapR) at an MOI of 10, media alone (CM), CpG ODNs 1668 and 2216 (0.5 µM) and pIC (100 µg/ml). Data show the results of a single experiment, with a single data point for each stimuli at each time point (n = 1).*

A3: Cytokine secretion by sorted FLDC in the absence of GM-CSF

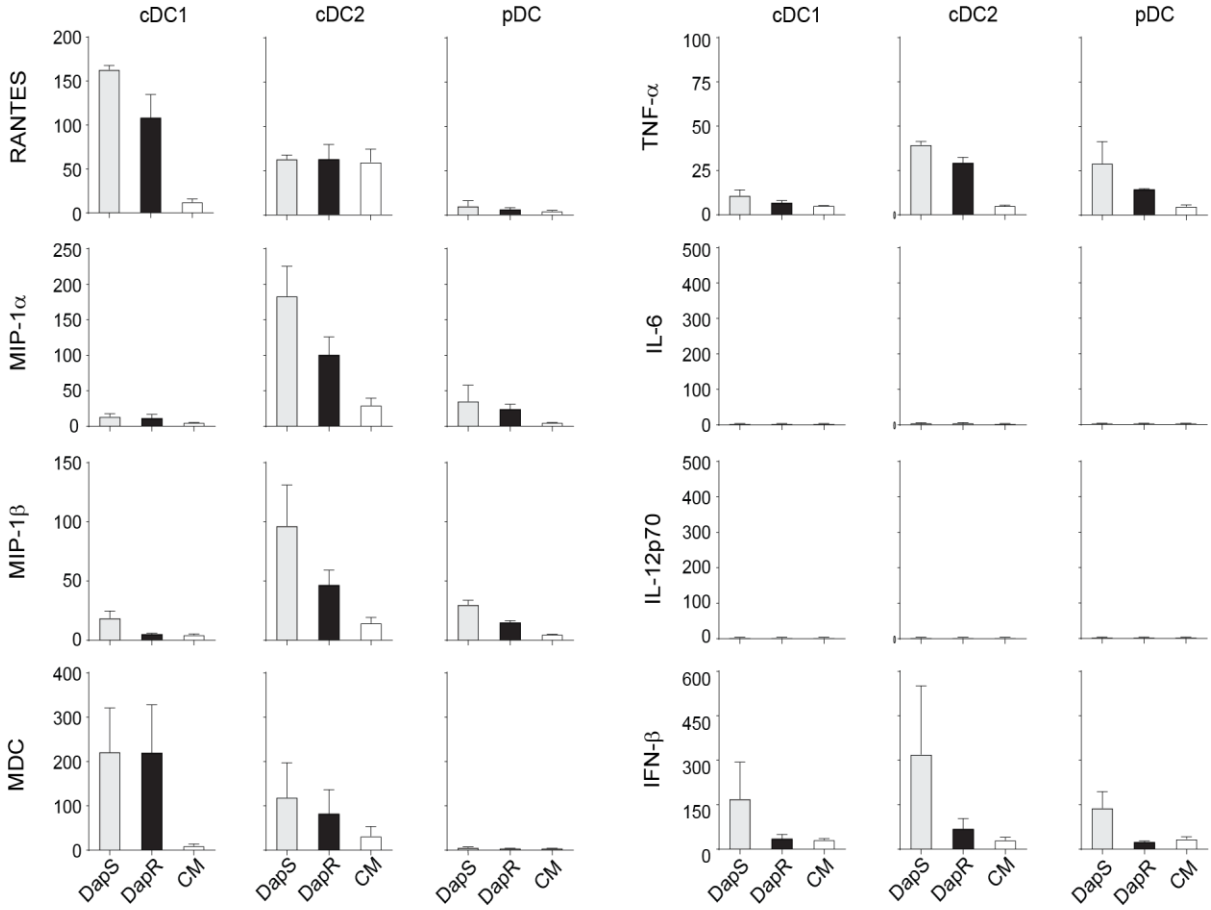

Figure A3-1 Cytokine secretion by FACS sorted FLDC exposed to paired clinical isolates of MRSA in the absence of GM-CSF. (a) *Cytokine production (pg/ml) by FACS sorted FLDC at 18 hour stimulus with A8819 (DapS) and A8817 (DapR) MRSA or complete media alone. Bars show the mean and standard error of the mean of biological replicates from 3 independent experiments (n = 3).* ***(b)*** *Viability of FACS sorted FLDC at 18 hour stimulus with A8819 (DapS) and A8817 (DapR) MRSA, media alone, CpG 1668 (0.5 µM) or pIC (100 µg/ml). Bars show the mean and standard error of the mean of replicates from 3 independent experiments (n = 3).*

A4: Cytokine secretion by sorted cDC1 following stimuli with cls2-T33N, *mprF*-T345I *and cls2*-T33NN33T point mutant strains of A8819

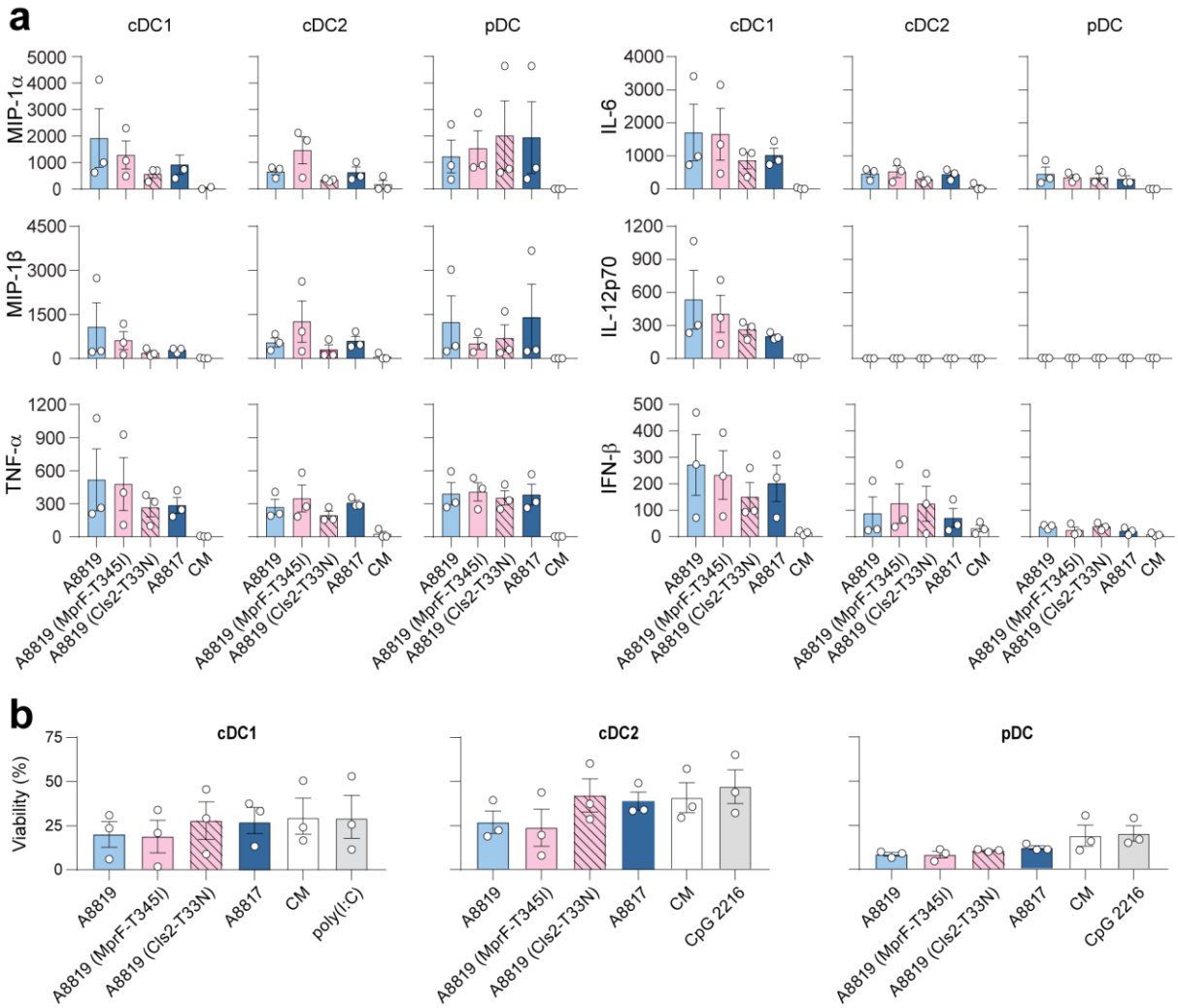

Appendix A4-1 Cls2-T33N mutation reduces cytokine secretion by FL-cDC1 (a) *Cytokine secretion (pg/mL) by FACS sorted FLDC subsets following 18 hour stimulus with A8819 and A8817 MRSA clinical isolates, and laboratory strains recreated for individual mutations in cls2 (A8819 Cls2-T33N) and mprF (A8819 MprF-T345I) at an MOI of 10. Data show the mean and SEM of replicates pooled from three independent experiments (n = 3).* ***(b)*** *Percentage viability of FACS sorted FLDC subsets stimulated as in 'a'. Viability quantified by flow cytometry via differential staining in propidium iodide at 18 hours post stimulus. Bars show the mean and SEM of replicates pooled from three independent experiments (n = 3).*

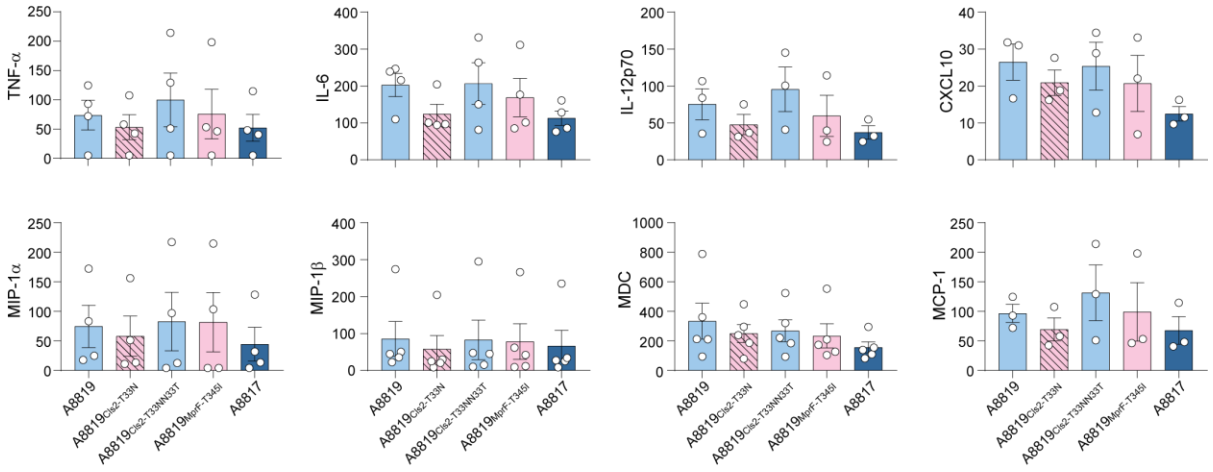

Appendix A4-2 Cytokine secretion by splenic cDC1 is impaired following stimulation with A8819 strain recreated for Cls2-T33N and MprF-T345I point mutations, and the response to A8819$_{Cls2\text{-}T33N}$ is rescued by reversion to Cls2-N33T. *Cytokine secretion (pg/mL) by splenic cDC1 following 18 hour stimulus with A8819 and A8817 MRSA clinical isolates, laboratory strains of A8819 recreated for the T345I point mutation in mprF (A8819$_{MprF\text{-}T345I}$), the T33N point mutation in cls2 (A8819$_{Cls2\text{-}T33N}$), and the A8819$_{Cls2\text{-}T33N}$ mutant strain restored to wild-type (A8819$_{Cls2\text{-}T33NN33T}$) at an MOI of 10. Data show the mean and SEM of biological replicates (hollow circles) pooled from between three and five independent experiments (n = 3).*

A5: Cytokine secretion by WT and MyD88$^{-/-}$ FL-cDC1 knockout in response to five daptomycin exposed clinical pairs

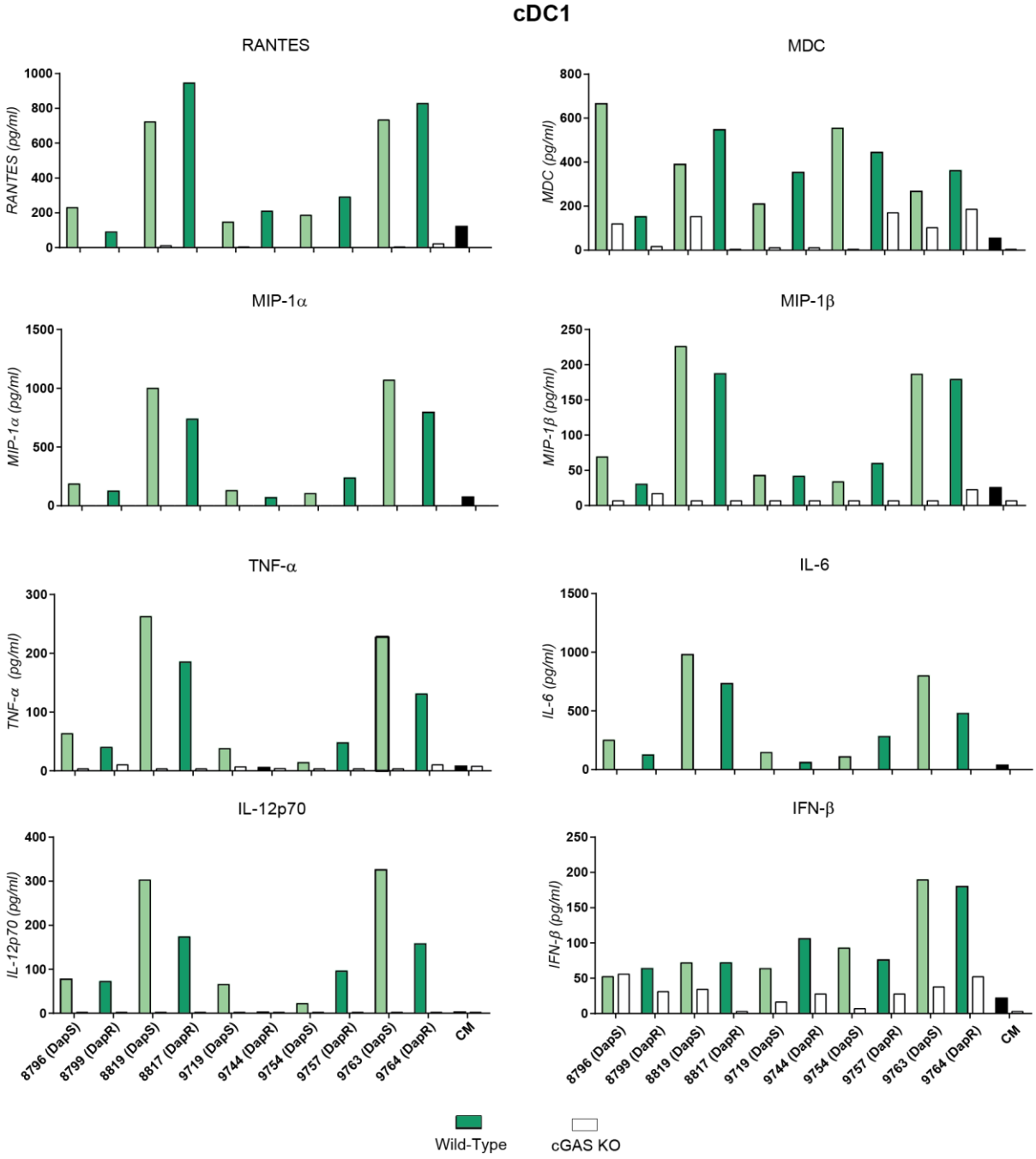

Appendix A5-1 MyD88 signalling is required by FLDC to produce pro-inflammatory cytokines following MRSA stimuli. *Cytokine production (pg/ml) by MyD88 knockout (hollow bars) and WT control (filled bars) FACS sorted cDC1 at 18 hour post stimulus with paired daptomycin exposed DapS (A8796, A8819, A9719, A975 and A9763; light green) and DapR (A8799, A8817, A9744, A9757 and A9764; dark green) MRSA isolates or complete media alone (CM). Bars show the cytokine secretion detected from a single replicate in a single experiment (n = 1).*

A6: Cytokine secretion by splenic cGAS knockout and wild-type DC in response to TLR agonists

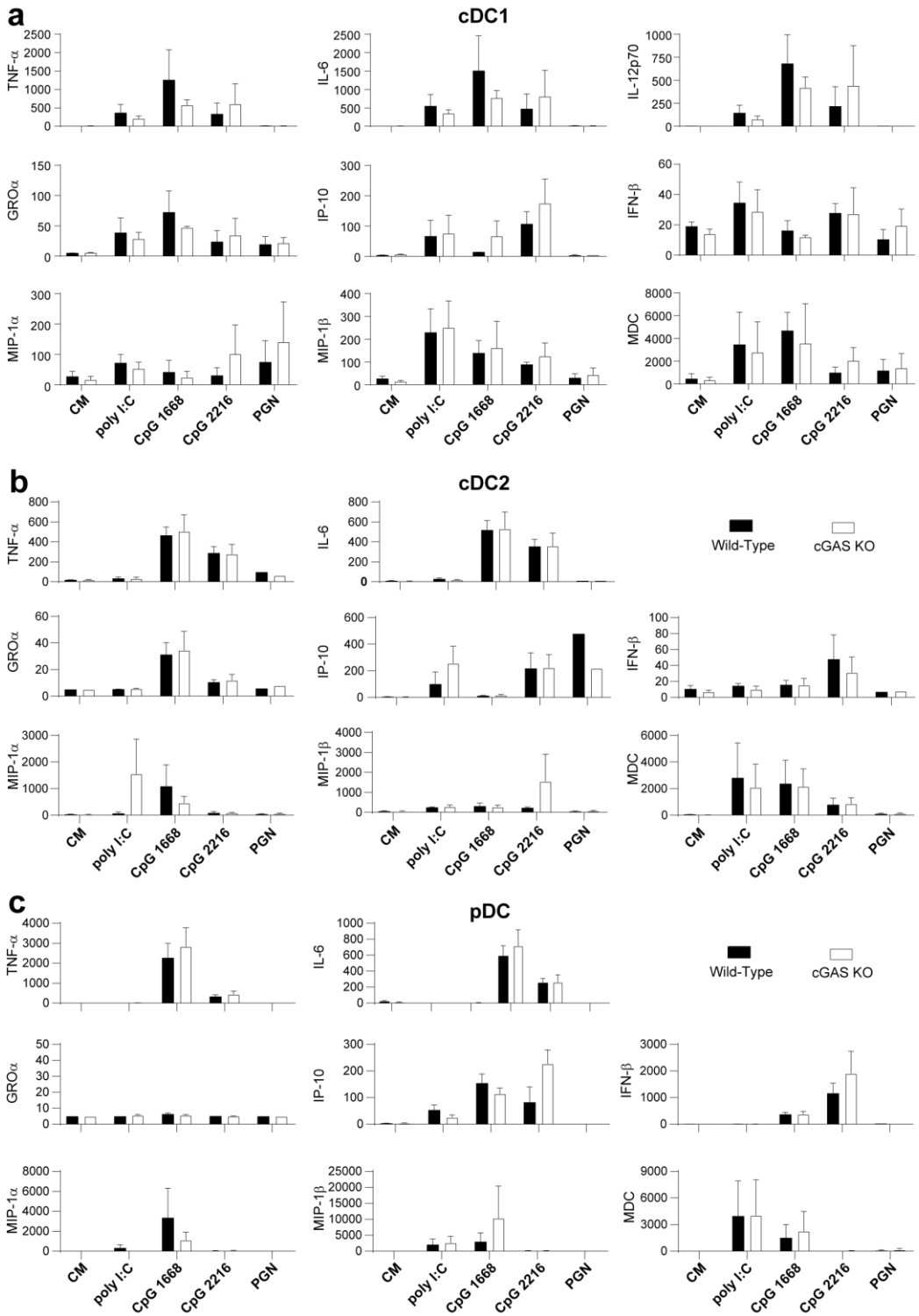

Figure A6-1 Cytokine production by FACS sorted splenic wildtype and cGAS knockout DC following stimulation with TLR agonists. *Cytokine production (pg/ml) by wild-type (filled bars) and cGAS knockout (hollow bars) FACS sorted cDC1* ***(a),*** *cDC2* ***(b),*** *and pDC* ***(c)*** *at 18 hour post stimulus with complete media alone (CM), CpG ODN 1668 or 2216 (0.5 µM), pIC (100 µg/ml) or peptidoglycan (10 µg/ml). Bars show the mean and SEM of biological replicates pooled from three independent experiments (n = 3).*

Appendix B: A novel antibody binding factor interferes with detection of CD69 on *S. aureus* stimulated DC

CD69 is also referred to as very early activation marker, given that it is rapidly upregulated on DC and a range of activated leukocytes[224-226]. Given its abundant expression on activated DC and T-cells, CD69 was initially hypothesised to play a role in T-cell activation; however more recently it has been shown that neither DC nor T-cell activation are impeded in CD69 knockout mice[226]. Indeed, unlike MHC-II and co-stimulatory markers, CD69 is typically most rapidly and potently upregulated on activated pDC as opposed to cDC[226], and is therefore not likely to play a role in antigen presentation or DC activation. The CD69 protein is itself a type II membrane glycoprotein belonging to the C-type lectin family[224], to date its ligand remains uncharacterised, and its role on DC upon activation is therefore yet to be elucidated.

In chapter three we detailed an in depth surface phenotype of both splenic DC and FLDC subsets in response to stimuli with paired clinical isolates of daptomycin exposed MRSA, corresponding to DapS (A8819) and DapR (A8817). Whilst finding subtle differences in the expression of activation markers and checkpoint inhibitors by each DC subset in response to these two clinical isolates, we found that DapS MRSA was capable of inducing up to 1,000 fold higher CD69 expression by splenic DC than the DapR daughter strain (figure 3.11). Further, we found that cDC subsets expressed levels of CD69 approximately equivalent to that of pDC- a surprising finding given that CD69 is associated with the early activation of pDC and typically expressed at considerably lower levels by activated cDC.

In this appendix we outline our current evidence that this binding of CD69 on cDC is representative of a novel and non-specific antibody binding interaction, unique to a specific subtype of hamster IgG. We demonstrate that this factor specifically binds hamster IgG1 and not IgG2, nor rat IgG, highlighting the specificity of this interaction. To date, we have not been able to elucidate the molecular nature of this antibody binding factor, or indeed the origin of this factor, being host or bacterial. Nonetheless, this short chapter reveals the novelty of a potentially new antibody binding factor, and briefly outlines our future plan to elucidate the molecular nature and origin of this factor.

B1: CD69 is potently and rapidly upregulated by DC subsets following bacterial stimulation

In order to address the molecular nature of the differential CD69 expression pattern following DapS/DapR MRSA stimuli, we first sought to clarify the typical phenotype of DC stimulated with a panel of other bacteria. Utilising the same commercial panel of heat inactivated (h.i) bacteria obtained from *Invivogen,* as outlined in chapter 3 (table 3.1), we examined CD69 expression by FL-cDC subsets in bulk culture at 18 hours post stimulus (figure B1-1a). As expected, each of the bacterial stimuli induced relatively low CD69 expression by cDC1 and cDC2, with none of the stimuli inducing expression equivalent to the CpG control (figure B1-1a). Of these heat inactivated stimuli, it was *E. coli* that induced the highest expression of CD69, notably more than the commercial lab strains of heat inactivated *S. aureus* and *S. epidermis* (figure B1-1a). By contrast, stimulation of cDC with the heat inactivated clinical isolate of DapS MRSA was able to promote potent CD69 expression- particularly by cDC1 which exhibited expression almost equivalent to that of the CpG control (figure B1-1a).

Being limited in our ability to gate out pDC from bulk FLDC cultures at 18 hours post stimulus with MRSA, we considered the surface phenotype of FACS sorted FLDC subsets following stimulation with the live DapS/DapR clinical pair. Consistent with our findings outlined for splenic DC (figure 3.11a), we found that cDC1, cDC2 and pDC all potently upregulated CD69 following stimuli with DapS MRSA (figure B1-1b), however both cDC subsets exhibited CD69 expression more than 10-fold higher than pDC (figure B1-1b)- a finding uncharacteristic of cDC.

Considering the uncharacteristically high expression of CD69 was not observed following stimuli with the heat inactivated commercial strain of MRSA (figure B1-1a), we next sought to consider whether these differences were unique to this particular daptomycin exposed clinical pair, or a broader feature prevalent in clinical MRSA isolates. We therefore further stimulated the sorted DC subsets with a second clinical pair of entirely distinct MRSA clinical isolates- a vancomycin exposed pair corresponding vancomycin susceptible *S. aureus* (VSSA) strain A8090, and vancomycin intermediate *S. aureus* (VISA). As with the daptomycin exposed pair, we found too that the vancomycin exposed MRSA induced uncharacteristically high expression of CD69 by cDC (figure B1-1b), and

exhibited a similar differential trend with higher CD69 expression observed when stimulated with the susceptible strain (figure B1-1b).

CD69 is typically upregulated to higher levels by pDC than cDC[226], a finding in stark contrast to our current results. Moreover, at the RNA level, CD69 expression typically peaks in the first 30-60 minutes post stimulus[224]. Given our novel differences in CD69 expression following stimuli with these paired clinical MRSA strains, and the uncharacteristically high expression of CD69 by cDC subsets, we next sought to examine the time kinetics of CD69 upregulation. To our surprise, we found that CD69 expression peaked on both cDC subsets as early as three hours post stimulus with MRSA (figure B1-1c); despite requiring at least six hours of stimulation with the CpG control to induce appreciable expression of CD69 by cDC (Figure B1-1c). Indeed, these findings are accentuated in the comparison of the CD69 expression profile of cDC following stimuli with the CpG control; whereby CD69 expression is almost 10,000 fold lower than elicited by stimulation with the DapS A8819 strain (figure B1-1c).

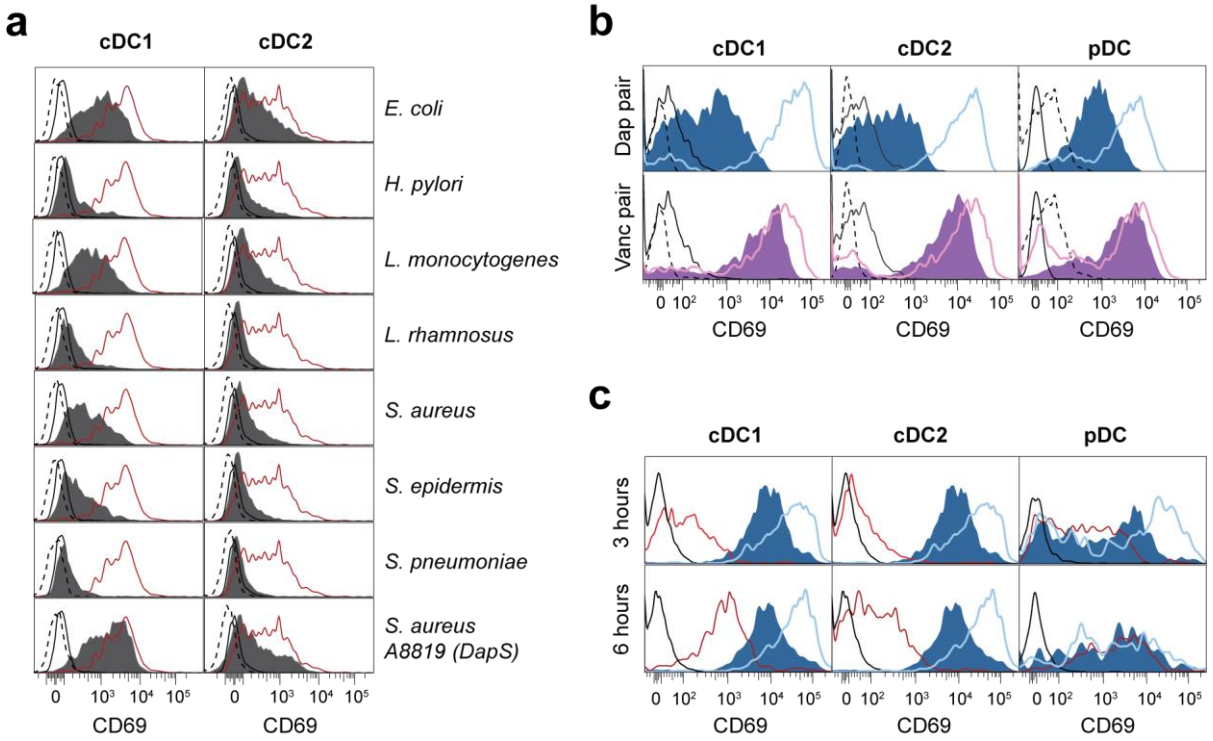

Figure B1-1 CD69 expression by murine primary splenic and FLDC exposed to bacterial stimuli including paired clinical isolates of MRSA. (a) *CD69 expression by conventional FLDC subsets (cDC1 and cDC2) following 18 hours stimuli with heat inactivated bacteria at an equivalent MOI of 10 (dark grey shaded), CpG 2216 at 0.5 µM (red trace), media alone (black trace) and FMO control (dashed black trace). Data shown from one experiment and representative of two independent experiments (n = 2).* ***(b)*** *CD69 expression by FACS sorted murine splenic DC following 18 hour stimulus with paired live clinical isolates of MRSA at an MOI of 10. Stimuli correspond DapS/DapR (A8819/A8817) isolates (light grey trace and dark grey shaded respectively), and VISA/VSSA (A8090/A8094) isolates (light grey trace and dark grey shaded respectively), media alone (black trace) and FMO control (dashed black trace). Data shown from 1 experiment representative of three independent experiments (n = 3).* ***(c)*** *CD69 expression by FLDC subsets stimulated for 3 and 6 hours with MRSA at an MOI of 10, corresponding to A8819 DapS (light grey trace) and A8817 DapR MRSA (dark grey shaded), CpG 2216 at 0.5 µM (red trace) and media alone (black trace). Data shown from 1 experiment (n = 1).*

B2: The binding of ⟨-CD69 following MRSA stimulation is non-specific

Having found such a drastic differential in the regulation of CD69 in response to paired clinical isolates of MRSA, and given the atypically high expression by cDC, we next sought to investigate the role of the protein in the DC response to *S. aureus*. We therefore next stimulated CD69 knockout and wild-type splenic DC subsets with the daptomycin exposed pair of MRSA.

As expected, we were able to detect expression of CD69 at baseline on all three wild-type DC subsets (figure B2-1a), and CD69 was further upregulated following 18 hour stimulation with CpG- most potently by the pDC subset (figure B2-1a). Confirming the functional knockout of CD69, there was no detectable expression above the FMO control for any KO DC subsets at baseline or following CpG stimuli (Figure B2-1a). However, to our surprise we observed substantial upregulation of CD69 by both WT and CD69 KO cDC following stimulation with DapS MRSA (figure B2-1b), with the WT expression peaking slightly higher the CD69 KO (figure B2-1b). Indeed, as measured by gMFI the CD69 detection in the CD69 knockout mice was almost half that of wild-type (figure B2-1b). These data therefore suggest that almost half of the CD69 expression previously observed is rather representative of non-specific antibody binding of our antibody to some yet uncharacterised factor, yet are still indicative of a differential in CD69 expression when corrected for non-specific binding. In support of the differential in *bona fide* CD69 expression by cDC, are the pDC. Indeed, the upregulation of CD69 was largely ablated in the KO pDC compared to WT (figure B2-1b). Cumulatively, these data suggest that while almost half of the CD69 expression previously observed in cDC is non-specific, the expression of CD69 by pDC is almost entirely representative of a genuine antibody-antigen interaction.

We next sought to phenotype the expression of CD69 by wild-type and knockout DC in response to entirely unrelated clinical strains; including the vancomycin exposed clinical pair A8090/A8094, and an MSSA clinical isolate, D57. Consistent with our observations for daptomycin exposed MRSA pair, we found that the vancomycin exposed pair similarly resulted in non-specific binding of α-CD69 by knockout DC (data not shown). However, in contrast the methicillin susceptible isolate, D57, was only subtly enhanced binding of CD69 in the knockout mice (figure 4.1c), indicating that a majority of the CD69 expression observed in response to these strains is genuine. WT and KO cDC subsets upregulated

CD69 to an equivalent level following stimuli with MSSA (figure B2-1c). Further, the MSSA strain was entirely incapable of inducing CD69 expression on knockout pDC (figure B2-1c), similar to the phenotype following DapS stimuli where the expression was largely ablated (figure B2-1b).

Finally, given the observed differential in CD69 expression after correcting for non-specific binding, we continued to examine cytokine expression by bulk splenic DC to determine if the molecule had any functional consequence on DC activation. Overall, CD69 KO splenic DC secreted more cytokine to MRSA stimuli than did WT DC (figure B2-2a), however this trend was further observed for most cytokines following stimuli with the CpG control (figure B2-2b). While it is unclear if this a result of CD69 either directly or indirectly enhancing DC activation, or merely an artefact of different mouse stocks-these results do not demonstrate any clear role for CD69 in the recognition or response to *S. aureus* by DC.

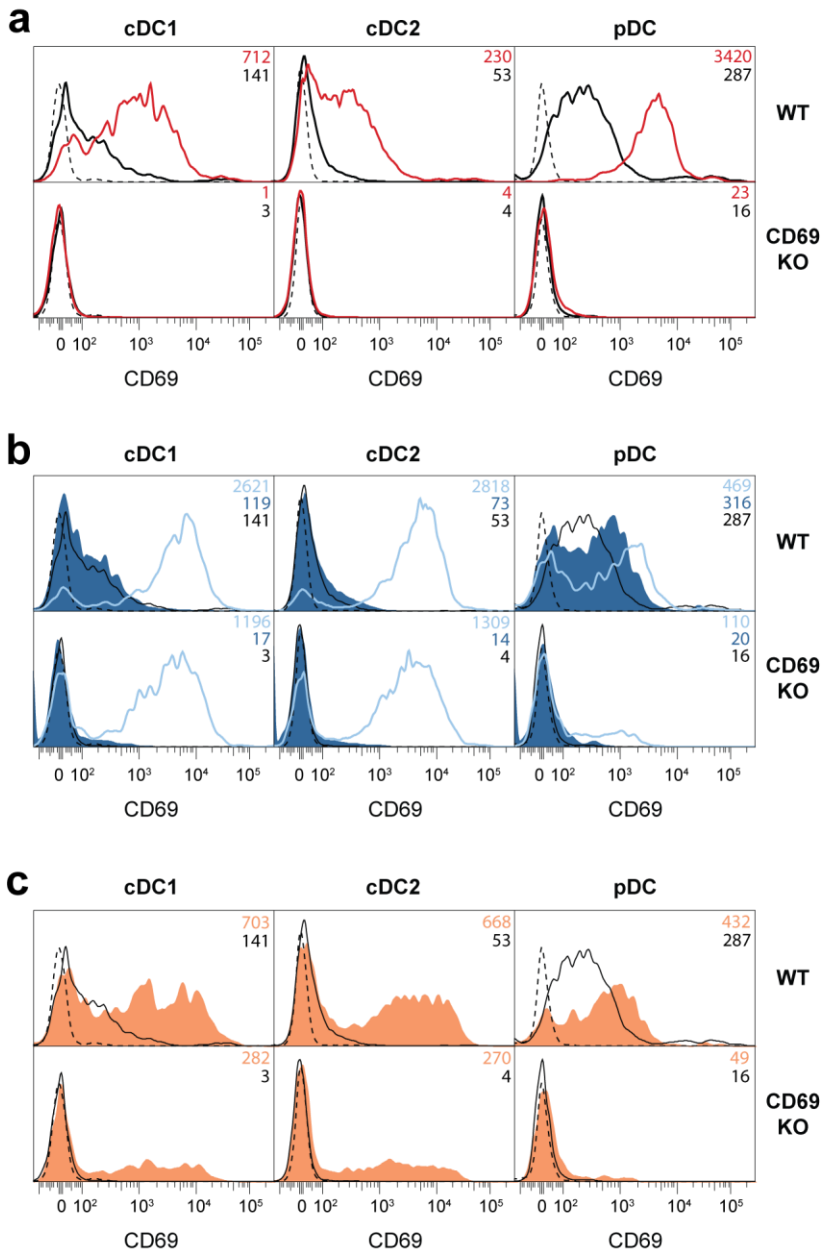

Figure B2-1 CD69 staining of wild type and CD69 knockout murine splenic DC exposed to bacterial stimuli including paired clinical isolates of MRSA. (a) *CD69 expression by wild type and CD69 knockout following 18 hours stimuli with 0.5 µM CpG 2216 (red trace), media alone (black trace), and FMO control (dashed black trace).* ***(b)*** *CD69 staining of murine splenic DC following 18 hour stimulus with paired live clinical isolates of MRSA at an MOI of 10. Stimuli correspond DapS A8819 (light blue trace) and DapR A8817 (dark blue shaded) isolates, media alone (black trace) and FMO control (dashed black trace).* ***(c)*** *CD69 staining of wild type and CD69 knockout murine splenic DC following 18 hours stimuli with MSSA isolate D57 (orange shaded), media alone (black trace), and FMO control (dashed black trace). Geometric mean fluorescence intensity indicated in top right corner of each histogram for all samples except FMO control. Data represent biological replicates of bulk splenic preparations from four individual mice (n = 4), with matched stimulated samples pooled after 18 hour stimulation for flow analysis.*

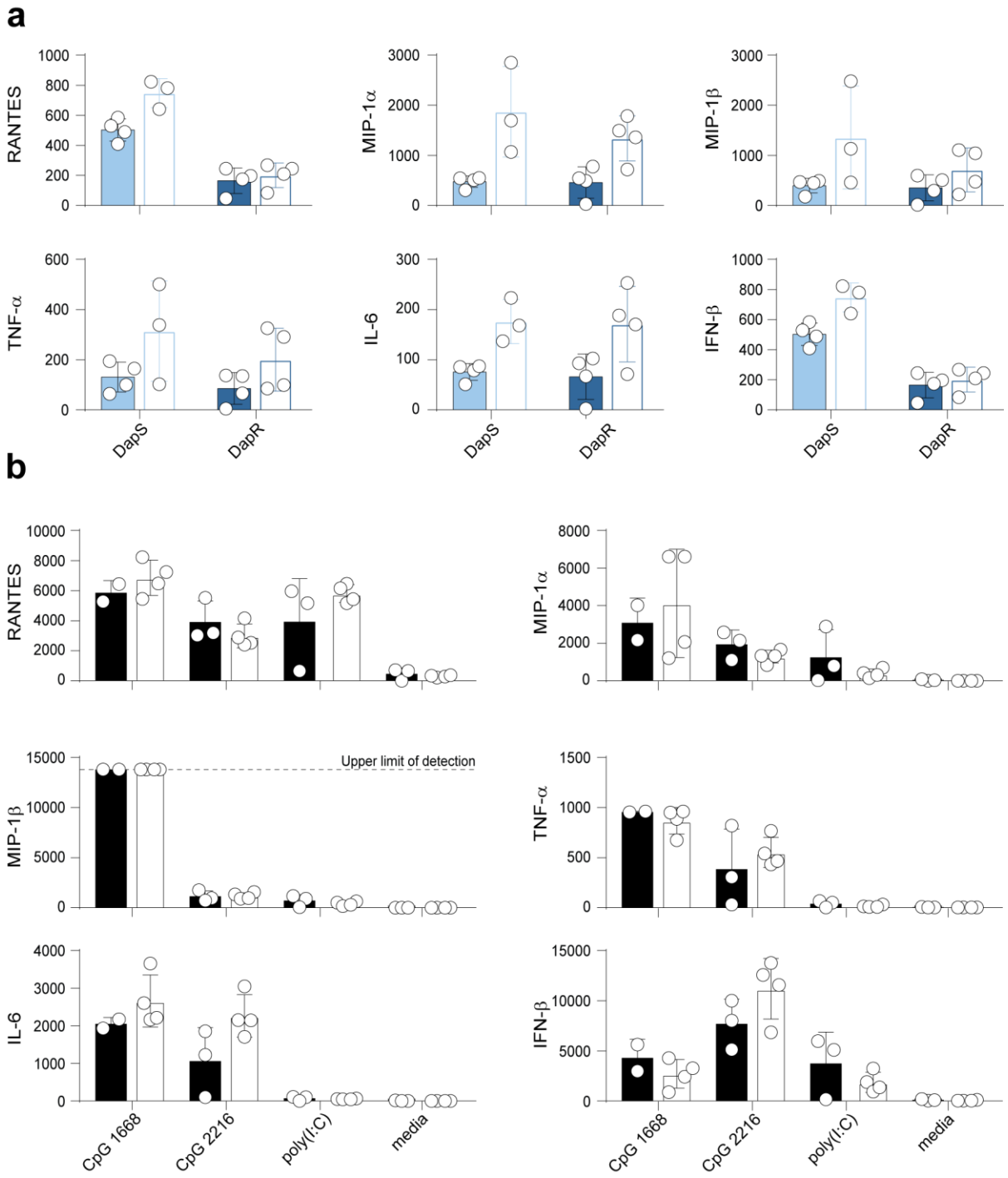

Figure B2-2 Cytokine secretion by wild type and CD69 knockout murine splenic DC exposed to bacterial stimuli including paired clinical isolates of MRSA. (a) *Cytokine secretion (pg/ml) by total wildtype (solid bars) and CD69 knockout (hollow bars) murine splenic DC following 18 hour stimuli with paired clinical isolates of DapS (A8819) and DapR (A8817) MRSA (MOI = 10).* ***(b)*** *Cytokine secretion (pg/ml) by total wildtype (solid bars) and CD69 knockout (hollow bars) murine splenic DC following 18 hour stimuli with 0.5 µM CpG 1668 or 2216, 100 µg/ml polyIC or media alone. Bars represent the mean and standard deviation of four biological replicates (n = 4), from one independent experiment (n = 1).*

B3: Hamster IgG1 λ3 light chain non-specifically binds DC following MRSA stimulation

The antibody used for the experiments thus far is a hamster α-mouse CD69 (clone H12.F3). As of the time of writing, H12.F3 remains the only commercially available clone manufactured by any major or reputable supplier, which has been validated for flow cytometry. Given our findings that the observed upregulation of CD69 was, in part, due to a non-specific binding interaction between the antibody and some yet uncharacterised factor, we had no alternative method to accurately quantify CD69 surface expression on murine DC. We therefore next sought to elucidate the molecular nature of this non-specific binding interaction.

Initially, we considered the staining profile of DC stimulated with MRSA and stained with the commercial isotype control. The antibody utilised for the experiments thus far is hamster α-murine CD69 (clone H12.F3), of an IgG1 isotype with a λ3 light chain. Indeed, this antibody is the only available clone available at the time of writing- and further the only commercially available isotype control was HTK88, a polyclonal preparation of affinity purified hamster immunoglobulin.

Despite these inadequacies of HTK888 as a true isotype control, we found that a concentration of the IgG polyclonal preparation equivalent to that used of the H12.F3 mAb was non-specifically bound by all three splenic DC subsets (figure B3-1a and B3-1b). Consistent with the CD69 knockout data, the isotype control similarly accounted for approximately half of the H12.F3 mAb staining observed for cDC, as measured by gMFI (figure B3-1a and B3-1b). Collectively these data demonstrate that the remainder is indeed representative of a genuine interaction of the mAb with surface expressed CD69, and that when correcting for non-specific binding, a differential expression of CD69 in response to the DapS/DapR clinical pair remains (figure B3-1a and B3-1b). It was again clear that there is only minimal non-specific binding of the isotype control to pDC at 24 hours post stimulation with MRSA (figure B3-1a and B3-1b), consistent with our observation of minimal binding of the CD69 mAb to pDC in CD69 knockout mice (Figure B2-1a and 4.2b). However, in contrast, we found that the isotype control non-specifically targeted pDC following stimuli with DapS MRSA only, at earlier time points of both 5 and 10 hours, but not the later time point of 24 hours (figure B3-1a and B3-1b). As a final validation that the isotype control was unable to bind CD69, we compared the staining

profile of splenic DC subsets stimulated with CpG 2216, and indeed found that the isotype and FMO controls exhibited identical stain profiles (figure B3-1c).

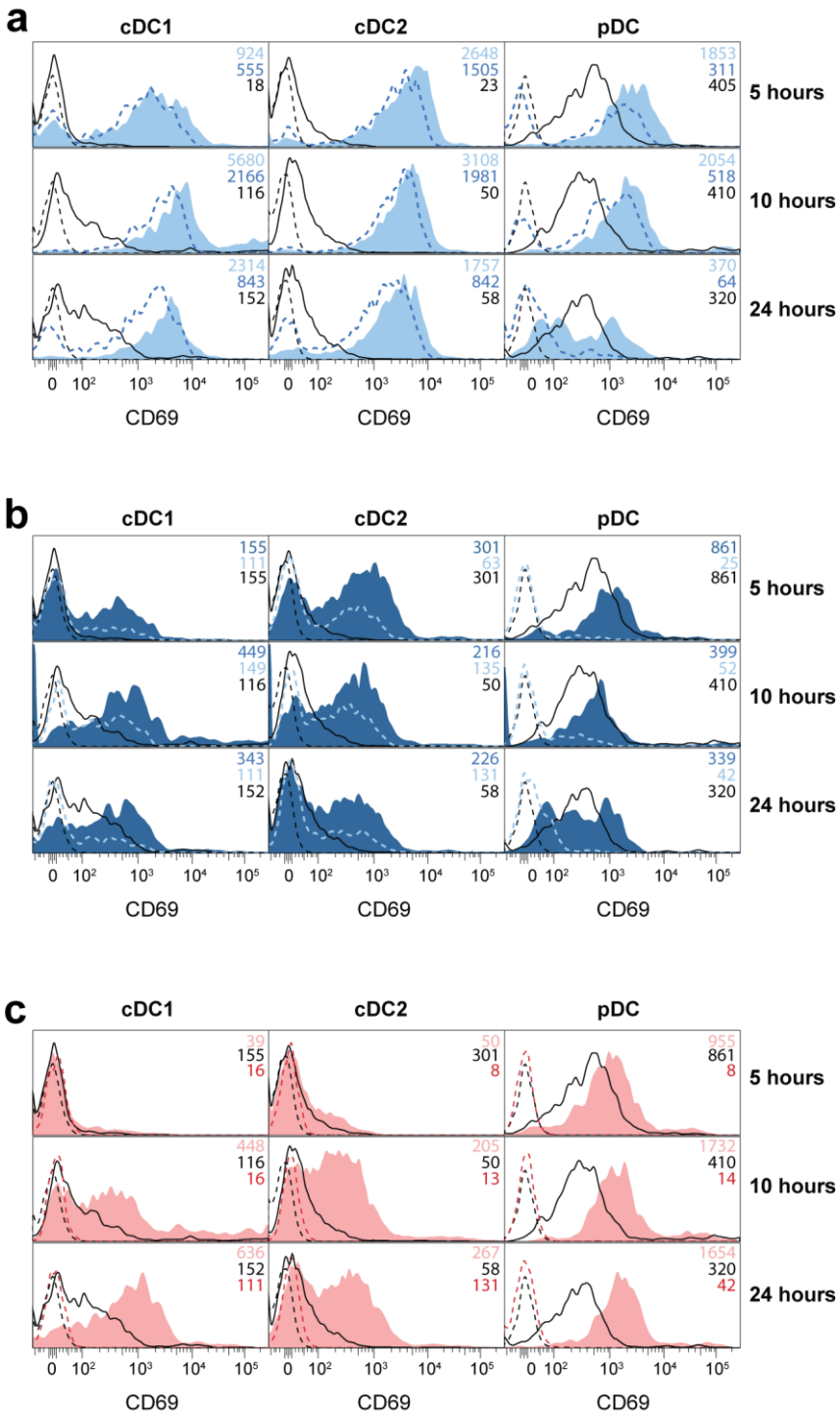

Figure B3-1 CD69 and isotype control staining of MRSA and CpG stimulated splenic DC over 24 hours. ***(a)*** *CD69 expression by splenic DC at 5, 10 and 24 hours post stimuli with DapS (A8819, MOI = 10) MRSA (light blue shaded), media alone (black trace), FMO control (dashed black trace) and isotype control (dashed blue trace).* ***(b)*** *As in 'a' following stimuli with DapR (A8817, MOI = 10) MRSA (dark blue shaded), media alone (black trace), FMO control (dashed black trace) and isotype control (dashed blue trace).* ***(c)*** *As in 'a' following stimuli with 0.5 μM CpG 2216 (red shaded), media alone (black trace), FMO control (dashed black trace) and isotype control (dashed red trace). All data* ***(a-c)*** *are shown from 1 experiment (n = 1).*

Having shown that both the hamster H12.F3 IgG1 λ3 mAb, and the polyclonal isotype control both non-specifically bind DC subsets following stimuli with MRSA (figures 4.2, and B3-1), we sought to determine if other hamster antibody isotypes in our flow panels were compromised and non-specifically binding DC stimulated with MRSA. Fortunately, only two other antibodies used in this research were derived from hamster, being α-CD11c (clone N418) and α-CD80 (clone 16-10A1), both of the isotype IgG2b with a κ light chain.

Given the use of CD11c as a population marker for FACS, and not having encountered issues in analysis of bulk cultures, we initially focussed on the antibody against CD80. When comparing the early CD80 expression with that of CD69, we observed a similar profile whereby all DC subsets upregulated CD80 to levels beyond that of CpG, following a short term five hour stimuli with MRSA (figure B3-2a). While these differences were only slight for cDC2, being the first to respond to CpG, the differences were more pronounced for cDC1 which did not upregulate CD80 relative to CM in the first five hours post stimulus with CpG (figure B3-2a). Similarly, there was no detectable CD80 expression above the FMO control for pDC following a five hour culture in media alone or with CpG, however there was relatively abundant CD80 detected following stimuli with MRSA (figure B3-2a).

Yet, these data do not conclusively show that the detected CD80 expression is an artefact of non-specific binding, so we next turned a rat clone of CD80 (clone 1G10). Unfortunately, while validated for flow cytometry, 1G10 did not perform well during titration (data not shown), however like α-CD69 H1.2F3 there were no other commercial clones available validated for flow from the major suppliers. We therefore compared the hamster α-mouse with the rat α-mouse side by side, only observing the staining differential between DapS and DapR MRSA when for cDC2 when staining with the rat clone (figure B3-2b). Nonetheless, given the poor performance of this clone in titration, we contend that these results are inconclusive.

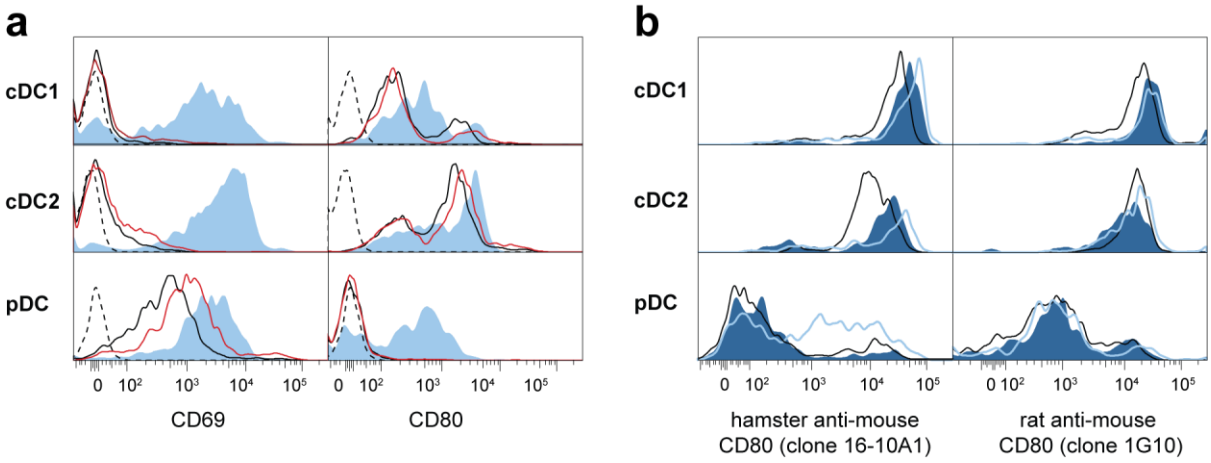

Figure B3-2 CD69 and CD80 staining at 5 hours post stimulus with MRSA and CpG. (a) *CD69 and CD80 staining on splenic DC at 5 hours post stimuli with DapS (A8819, MOI = 10) MRSA (light grey shaded), 0.5 µM CpG 2216 (red trace), media alone (black trace) and FMO control (dashed black trace).* ***(b)*** *Hamster and rat anti-CD80 staining on sorted splenic DC at 18 hours post stimulus with DapS (A8819, MOI = 10) MRSA (light grey trace), DapR (A8817, MOI = 10) MRSA (dark grey shaded), and media alone (black trace).*

To gain further insight into the non-specific binding of other hamster immunoglobulin subtypes we therefore considered blocking the interaction with Syrian hamster immunoglobulin. Indeed, increasing concentrations of hamster IgG inhibited binding of a-CD69 (figure B3-3a), although concentrations as high as 500 ug/ml were required to achieve potent blocking of this interaction. Validating these findings is the observation that the binding of the isotype control, HTK888, again required this higher concentration of polyclonal IgG to be potently blocked (figure B3-3a), although there was still detectable binding above the background. In contrast, the binding of CD11c and CD80 was only subtly perturbed when blocking with polyclonal hamster IgG, with a subtle peak shift observed with increasing concentrations of blocking Ig (figure B3-3a). While there were more obvious differences in α-CD80 and α-CD11c binding at the highest blocking concentration of 500 μg/ml, these differences were observed regardless of stimuli, and may rather represent a more general interference with antibody binding (figure B3-3a). Collectively, findings therefore suggest that there is some level of cross-reactivity in the non-specific binding of the hamster IgG1 and IgG2 isotypes, although the IgG1 isotype is more dominantly bound.

Importantly, the binding of the rat monoclonal α-CD24 (IgG2b, κ) was unable to be blocked by the polyclonal hamster IgG, thus demonstrating the sensitivity of this non-specific binding to hamster immunoglobulin. While the higher concentration of 500 μg/ml hamster IgG resulted in poorer staining of DC with α-CD24, this was again observed for both MRSA and CpG control stimulated cells (figure B3-3a), and therefore likely a result of more general interference with antibody binding.

Considering the subtle blocking of CD80 binding with polyclonal hamster IgG, it was therefore important to discern if this non-specific binding was the cause of the previously described differential in CD80 expression following stimulation with daptomycin exposed isolates of MRSA. We therefore compared the staining profiles of both cDC1 and cDC2 in the absence of blocking and with high concentration hamster Ig blocking (figure B3-3b). While this concentration of blocking agent was shown to efficiently block non-specific binding of IgG1 (figure B3-3a), and further inhibit antibody binding more generally as seen with CpG stimulated samples (figure B3-3a); a very subtle differential still remained between the DapS and DapR stimulated samples (figure B3-3b).

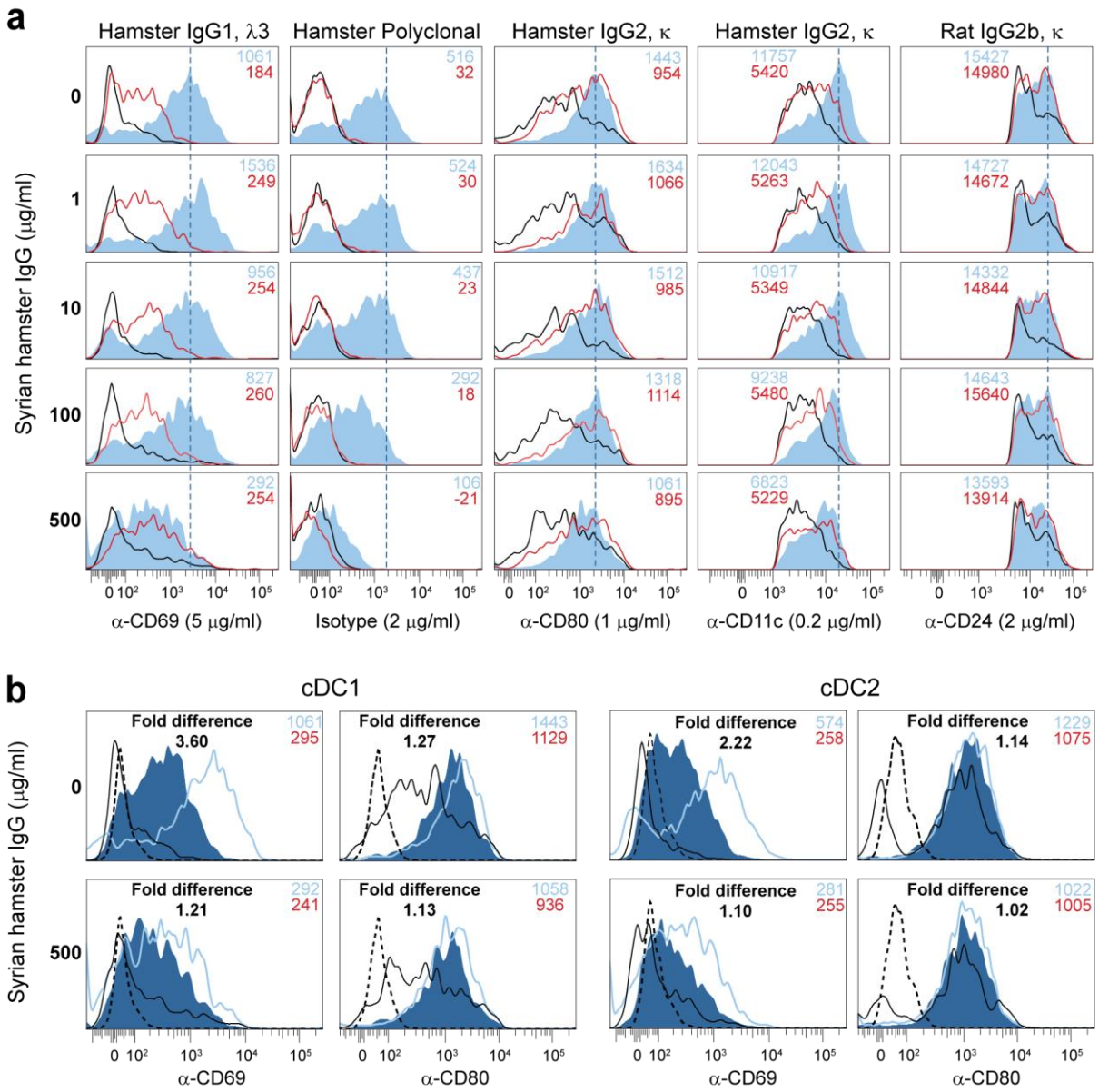

Figure B3-3 Blocking of non-specific binding of hamster IgG λ3 with polyclonal hamster immunoglobulin. ***(a)*** *FL-cDC1 were stimulated in bulk culture for 18 hours with DapS A8819 MRSA (MOI of 10; light blue shaded histogram,) CpG 2216 (0.5 μM; red trace) or media alone (black trace); subsequently blocked with increasing concentrations of Syrian hamster IgG (as indicated), and stained with antibodies against CD69 (H12.F3; hamster IgG1, λ3), KLH (polyclonal IgG isotype), CD80 (16-10A1; hamster IgG2, κ), CD11c (N418; hamster IgG2, κ) and CD24 (M1/69; Rat IgG2b, κ).* ***(b)*** *FL-cDC1 and FL-cDC2 were stimulated in bulk culture with A8819 (DapS; light blue trace) and A8818 (DapR; dark blue shaded) or media alone (black trace), and stained for CD69 and CD80 as in 'a'. Data in all panels are shown from 1 experiment (n = 1).*

B4: Hamster IgG1⌊3 can not reveal the non-specific binding agent in western blot

Having identified a novel binding interaction between hamster IgG1 and some factor present in samples containing cDC and DapS MRSA, it was therefore a priority to identify the molecular nature of this antibody binding factor. Indeed, it currently remain unclear whether this factor is of microbial or host origin. To gain an preliminary understanding as to the nature of this protein, we initially set out to determine whether this factor could be detected with purified hamster α-CD69 by western blot.

In running both DapS and DapR MRSA isolates on SDS-PAGE, and probing in western blot with hamster α-CD69, we were able to resolve two bands at 50 and 60 kDa respectively (figure B4-1a). However, these bands were resultant from the non-specific binding of our goat α-hamster IgG secondary, being resolved on blots in the absence of the hamster primary (figure B4-1b). While the identity of these bands remains unclear, it was apparent that the goat α-hamster secondary was not ideal given a non-specific binding interaction with some staphylococcal antibody binding protein. We therefore next considered a more direct approach in developing gels with streptavidin-HRP following probing with an α-CD69 biotin conjugate (figure B4-2).

In the direct detection with the biotinylated antibody we were able to resolve a band common to all DC regardless of stimuli, on both reducing and non-reducing gels at 98 kDa and kDa respectively (figure B4-2a). Moreover, we were able were able to resolve an additional band, unique to DC stimulated with MRSA on both reduced and non-reduced gels. This additional band was resolved to 138 kDa under reducing conditions, but above the 250 kDa standard under non-reducing conditions (figure B4-2b). Importantly, all of the resolved bands were present in the absence of the primary antibody (figure B4-2a and B4-2b), indicating that these proteins were recognised directly by either the streptavidin-HRP or StrepTacin, and not the hamster IgG1 λ3 antibody clone. It is therefore clear that despite the intensity of non-specific binding observed in flow cytometry, this clone is incompatible with western blot. We are therefore planning to utilise this antibody in future experiments to pull-down the antigen of interest using affinity chromatography, and identify the molecular identity through peptide sequencing.

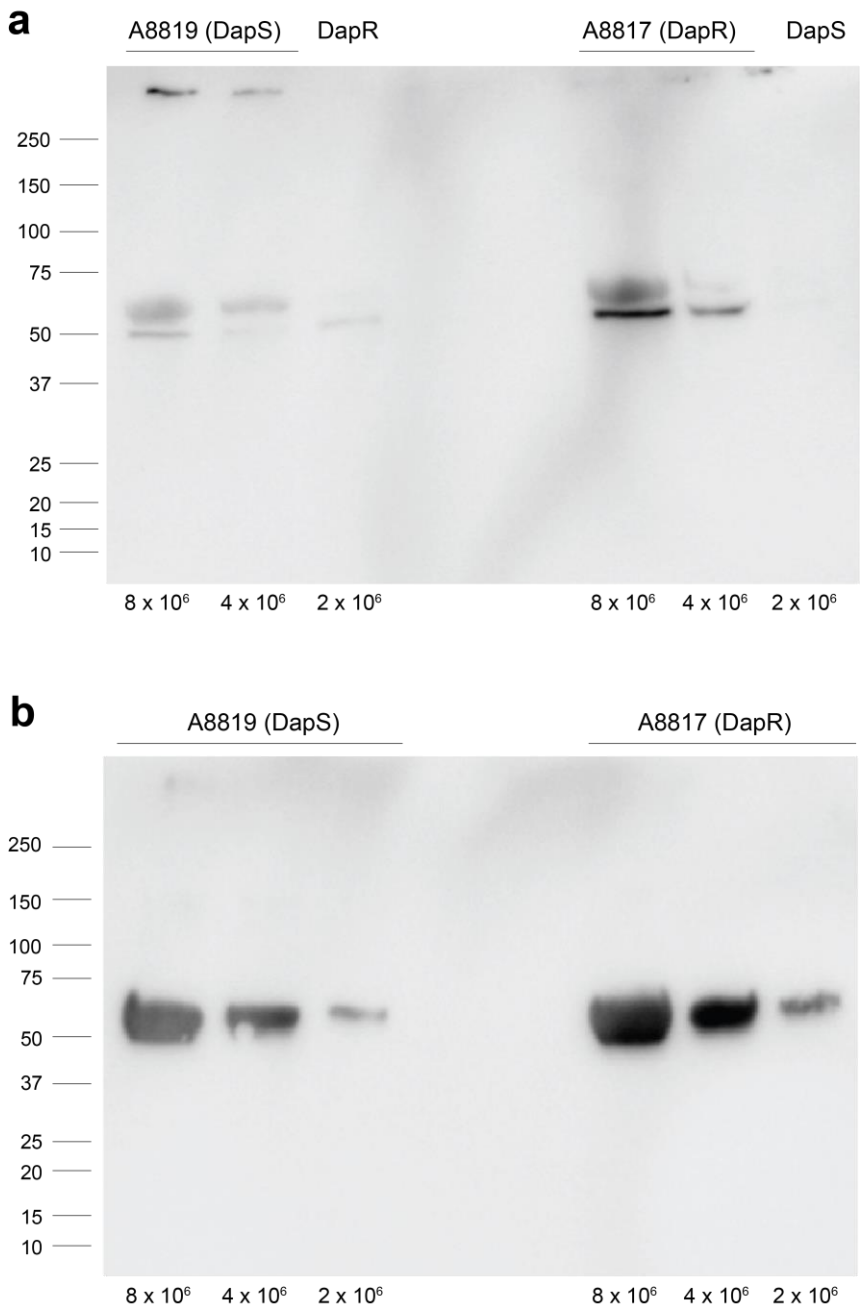

Figure B4-1 Non-specific detection of MRSA protein with hamster and goat IgG in western immunoblot. *Western blot of DapS and DapR MRSA titrated from paired DapS and DapR (A8819 and A8817) MRSA separated by SDS-PAGE under reducing conditions with 8, 4 and 2 x 10^6 cfu per lane.* ***(a)*** *Blot showing bands apparent at ~50 kDa and ~60 kDa, following two hour probe with purified hamster anti-mouse CD69 (clone H1.2F3, 1:3,000), and detection with goat anti-hamster Ig-HRPO (clone , 1:100,000).* ***(b)*** *Blot showing band apparent at ~60 kDa, stained as in 'a', substituting hamster anti-murine CD69 for a mock BSA control (PBS with 1% [$^{w}/_{v}$] BSA, 0.05% [$^{v}/_{v}$] Tween).*

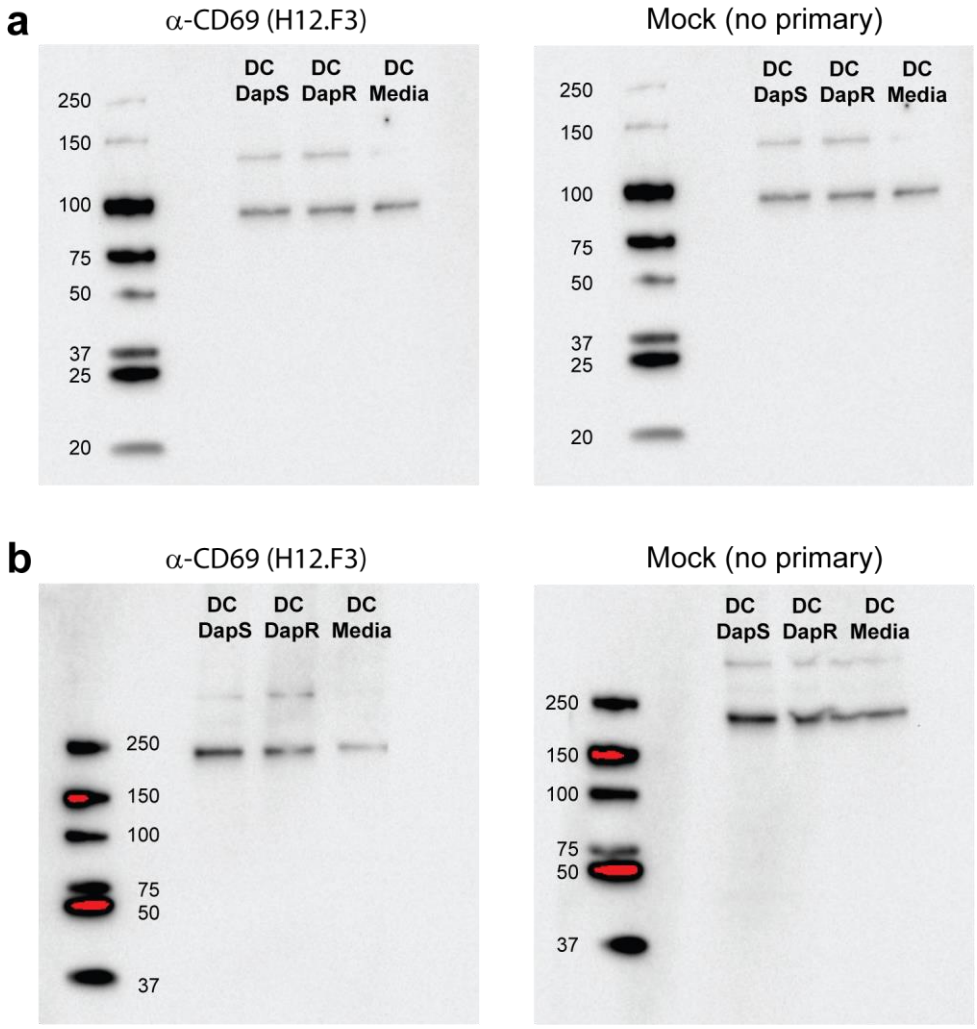

Figure B4-2 Non-specific detection of DC proteins with streptavidin-HRP in western immunoblot. Western blot of bulk FLDC at 18 hour post-stimulation with DapS (A8819; MOI 10), DapR (A8817; MOI 10) or media alone. *Samples were separated via SDS-PAGE under both reducing* ***(a),*** *and non-reducing conditions* ***(b),*** *with 1 X 10^6 DC loaded per lane. Both reducing and non-reducing gels were blocked with 10% BSA, and probed in the presence or absence either biotinylated α-CD69 H12.F3 (1:2,000), as indicated. Red regions of bands represent oversaturation of the standards. Data representative of two experiments for the α-CD69 stain (n = 2), and shown from one experiment for the mock stain (n = 1).*

B5: Discussion

Regulation of *bona fide* CD69 expression by DC subsets in response to MRSA

In this chapter we have identified some novel antibody binding factor, highly specific for hamster IgG1, but not IgG2 or rat IgG (figure B3-3a). This finding resolves the unusually high CD69 expression profile we have previously shown for cDC subsets following stimulation with DapS MRSA (figures 3.11, B1-1b and B1-1c). Despite the non-specific binding of the hamster immunoglobulin used to detect CD69, it was nonetheless clear that CD69 was indeed upregulated in response to MRSA. These findings are best demonstrated through the impaired staining profile of CD69 knockout DC; which while still able to non-specifically bind hamster IgG1, were less efficient than wild-type in binding the α-CD69 mAb (figure B2-1b). Importantly, these experiments indirectly suggest a true differential in CD69 expression following stimulation of cDC with the daptomycin exposed clinical pair of MRSA (figure B2-1b), as correcting for the non-specific binding observed in the CD69 knockouts does not fully account for the differences observed in response to this clinical pair in wild-type mice (Figure B2-1b).

Of particular interest, it was apparent that there was relatively low non-specific binding of α-CD69 to pDC following overnight stimuli with DapS MRSA (figure B2-1b), and none detectable following stimuli with the DapR daughter strain (figure B2-1b). These findings therefore suggest that the pDC CD69 expression profile is legitimate with only very mild interference from the yet unidentified hamster IgG1 binding factor. Moreover, the non-specific binding of the isotype control was evident on pDC stimulated with DapS MRSA at both 5 and 10 hours, but almost entirely ablated at 24 hours (figure B3-1a), despite a strong positive profile being maintained by cDC subsets. While potentially confounding, these data are in line with the CD69 KO data (figure B2-1a), suggesting that despite an initial non-specific binding event- the endpoint expression of CD69 by pDC at 24 hours post stimulus represents a genuine interaction of antibody binding to its target (in this case CD69).

Given the molecular origin of this hamster IgG1 binding factor remain unknown, either host or bacterial, these findings suggest one of two potential outcomes. Should this factor be of host origin, it is likely that the pDC transiently express the factor in response to DapS but not DapR MRSA, whereas the cDC upregulate and maintain the factor to substantially

higher levels. Although given the potent and rapid upregulation of this molecule by all DC subsets, as early as 3 hour post stimulus (figure 4.1c), we content that this scenario is unlikely. We hypothesise a more likely scenario whereby the factor is of bacterial origin, an indeed an antibody binding factor which is itself transferred or transported to the surface of the DC, and able to be cleared by pDC, but not cDC, within the first 24 hours (figure B5-1). Indeed, the 'theft' of host membrane components by pathogenic bacteria during infection has been reviewed[266], yet the mechanisms regulating these interactions are not well characterised. Importantly, Crowley *et. al.,* have previously demonstrated a bidirectional exchange of membrane lipids between *Borrelia burgdoferi* and host epithelial cells[267]. We therefore suggest a model in which a bacterial antibody binding protein, similar to protein A, is transferred to the surface of DC and able to non-specifically bind hamster γ-globulin.

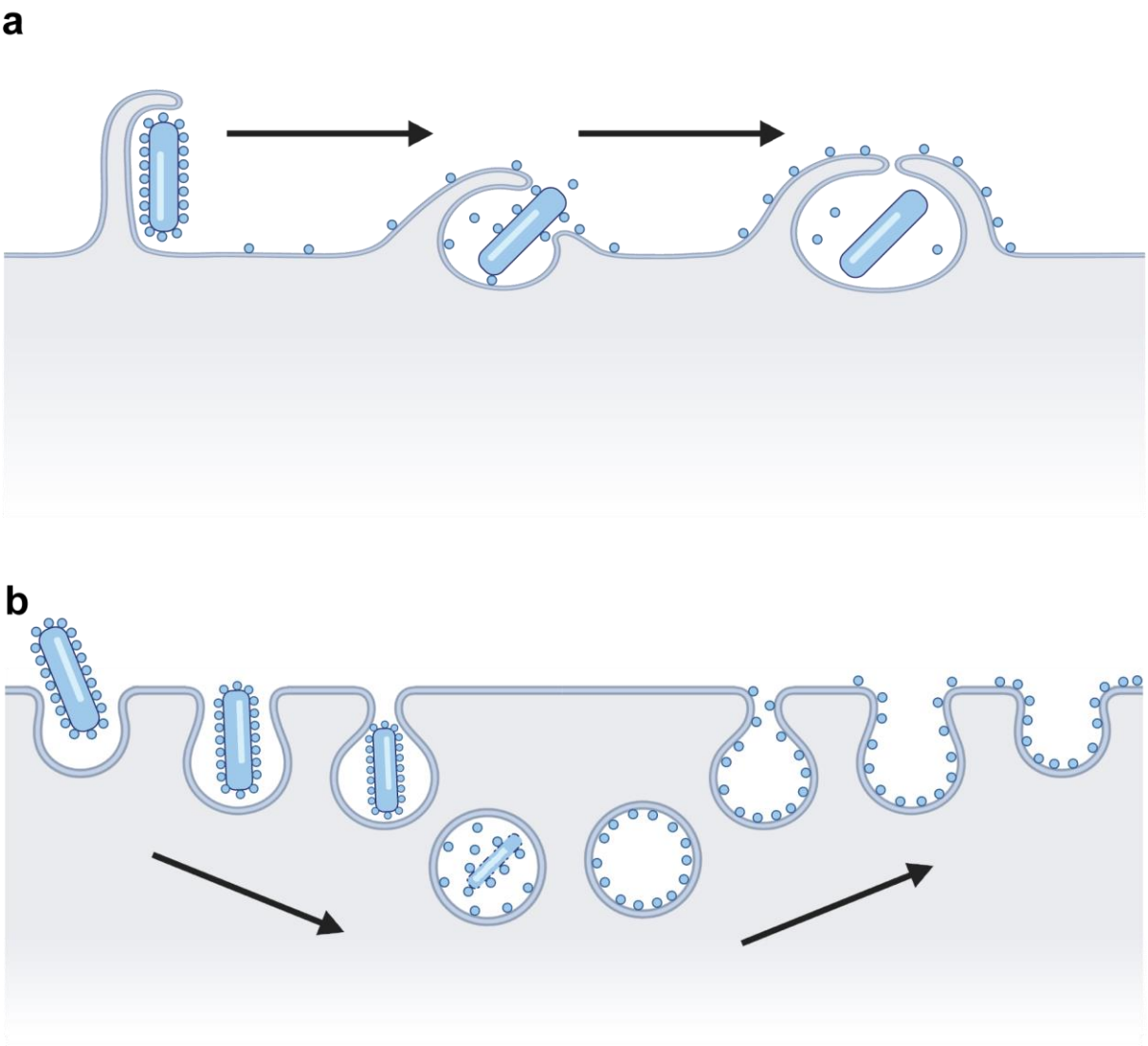

Figure B5-1 Hypothesised mechanisms for exchange of Staphylococcal immunoglobulin binding protein with dendritic cells. Isolates of S. aureus express cell wall and membrane associated antibody binding factors (Protein A or Sbi respectively), the latter of which may be exchanged between the S. aureus and host DC membrane during infection. (a) *During the phagocytic process, close interactions between the bacterial and host membrane result in the exchange of membrane phospholipids and proteins, facilitating the transfer of a bacterial immunoglobulin binding factor (blue studs) such as Sbi, at the cell surface.* ***(b)*** *Close membrane interactions occurring during the phagocytic process result in the exchange of membrane phospholipids and proteins, facilitating the transfer of a bacterial immunoglobulin binding factor (blue studs) such as Sbi, in the endosomes. These proteins are subsequently transported to the cell surface in the ordinary endosomal vesicles operating in the exogenous antigen processing pathway.*

Non-specific binding of hamster IgG1 by DC: A case for Protein A and Second Immunoglobulin Binding Protein

Given the non-specific binding of immunoglobulin following the stimulation with *S. aureus*, the most logical conclusion would be that it is the result of non-specific antibody binding by staphylococcal Protein A. Staphylococcal Protein A is well known to bind a diverse range of mammalian IgG, having the highest affinity for human, rabbit and pig γ-globulin[268,269]. Importantly Protein A has previously been demonstrated not to bind rat IgG, despite a strong affinity for Syrian hamster IgG_1 and IgG_2[270]. Therefore, Protein A interference with our experimental readouts would fit the current data; whereby our cytokine assays and flow cytometric analysis relying on rat Ig are unperturbed, yet the analysis of CD69 with hamster IgG_1 is impeded by non-specific binding interactions.

Despite the non-specific binding of a-CD69 IgG_1, we found only moderate interference with CD11c and CD80 of the IgG_2 isotype (figure 4.6a). Indeed, these findings are consistent with the early studies of Coe *et. al.,* whereby in the first purification of hamster IgG subtypes they found that IgG_1 and IgG_2 were eluted from protein A column at pH 5 and 6 respectively[270]; thereby indicating a stronger affinity of hamster IgG_1 for Protein A. Indeed, there is precedent for differential in the capacity of Protein A to differentially bind IgG subtypes within the same species, with other studies reporting that Protein A recognises human IgG_2 and IgG_3 with approximately 10-fold lower affinity than IgG_1[268]; and despite moderate binding of IgG_3 κ, Protein A is unable to bind IgG_3 λ[268] {Βοψλε, 1990 #480}. The preference of this yet uncharacterised factor to sequester IgG_1, is therefore reminiscent of the biochemical properties of Protein A.

It has also been shown that diverse clinical isolates of *S. aureus* secrete variable amounts of Protein A culture *in vitro*; and that the level of secreted protein A is directly related to its level of surface expression[268]. Given the mutations arising in the A8819 DapR isolate affecting cell membrane biosynthesis[158], and increasing cell wall teichoic acid[194], they therefore provide a potential mechanism for altered Protein A expression by the clinical pair. This could therefore potentially be attributed to the differential in in hamster Ig binding by DC stimulated with this clinical pair, regardless of the mechanism by which this factor is ends up on the cell surface. Fitting with this hypothesis, Lindmark *et. al.,* have previously demonstrated that a particular MRSA isolate, A676, secretes higher levels of protein A than does the MSSA cowan strain[271]. While this research only

considered a single MRSA isolate, should the trend hold across a broader panel of strains, these findings would be consistent with the lesser non-specific binding of hamster IgG_1 to DC observed in response to our MSSA isolate, D57 (Figure B2-1c).

Despite the body of evidence suggesting the IgG binding factor is Protein A, our western immunoblots are inconclusive given the resolution of reduced protein bands at 50 and 60 kDa respectively (figure B4-2). Given the molecular weight of Protein A is approximately 43 kDa, we therefore suggest that both the slightly larger band at 50 kDa, and indeed the appearance of the second larger band leaves the possibility that there is indeed some other immunoglobulin binding factor at play. The second immunoglobulin binding protein of *S. aureus* (Sbi) is known to co-localise with Protein A in electrophoresis, having a molecular weight of ~50 kDa[272]. Importantly, unlike Protein A, which is anchored to the bacterial cell wall, Sbi is localised only to the bacterial membrane[272]; and can therefore theoretically be exchanged between the bacterial and host membranes in line with our proposed model (figure B5-1). Further work is currently underway to pull down this factor from co-cultures of MRSA and DC to confirm the identity through mass spectrometry.

Concluding remarks

In this appendix we have explored the molecular interaction between hamster and IgG1 and a staphylococcal antibody binding protein. While we have not yet been able to definitively confirm the identity of this factor as Protein A, we have demonstrated that the expression of CD69 by DC subsets is differentially regulated in response to the A8819/A8817 clinical pair; despite non-specific binding. Importantly, we have shown that this factor interferes with antibody staining on cDC, but not pDC, at 18 hour post stimulus. Collectively, these findings validate the findings thus far on pDC, while suggesting some functional difference between cDC and pDC in their interaction with MRSA. As the cDC are far superior to pDC in the uptake and processing of antigen, it remains likely that the transfer of non-specific antibody binding protein to DC is, at least in part, dependent on phagocytic processes.

Appendix C: Technical Data Sheets

Appendix C1. Invivogen lumikine mIFN-α product information

LumiKine™ mIFN-α

Mouse IFN-alpha (multiple subtypes) bioluminescent ELISA kit

Catalog # lumi-mifna

http://www.invivogen.com/lumikine-mifna

For research use only

Version # 16L15-MM

PRODUCT INFORMATION

Contents (for five plates)

- 50 µg lyophilized mIFN-α Capture Antibody
- 5 µg lyophilized mIFN-α Biotinylated Antibody (detection antibody)
- 100 ng lyophilized mIFN-α Standard (HEK293-expressed cytokine)
- 2 pouches of QUANTI-Luc™
- 1 vial Streptavidin-Lucia
- 1 white flat-bottom MaxiSorp® 96-well plate with a plate sealer

Storage and stability

- Products are shipped at room temperature. Store at -20 °C. Lyophilized products are stable for 12 months when properly stored.
- Resuspended antibodies are stable for 1 month when stored at 4 °C or 12 months when aliquoted and stored at -20 °C.
- Resuspended cytokine is stable for 1 month when stored at 4 °C or 12 months when aliquoted and stored at -80 °C.
- Resuspended Streptavidin-Lucia is stable for 6 months when aliquoted and stored at -20 °C.
- Reconstituted QUANTI-Luc™ is stable for 1 week at 4 °C or 1 month at -20 °C. Prepare aliquots and protect from light.

Note: Avoid repeated freeze-thaw cycles for all products stored at -20 °C or -80 °C.

Quality control

- The sensitivity and specificity of this kit are validated for each lot.
- Rigorous quality control tests are performed to ensure lot-to-lot reproducibility and performance.

DESCRIPTION

LumiKine™ mIFN-α is a bioluminescent ELISA kit designed to quantify the levels of mouse interferon-alpha (mIFN-α) in cell culture supernatant, serum and plasma samples. This kit uses optimized matched pairs of monoclonal capture and detection antibodies to achieve sensitive and accurate measurement of the cytokine. The detection antibody is labeled with biotin to allow subsequent binding to streptavidin-Lucia, streptavidin conjugated to Lucia luciferase, a secreted reporter enzyme. Levels of mIFN-α are determined by measuring the luminescence produced by Lucia luciferase after hydrolysis of its substrate, coelenterazine. This substrate is provided in QUANTI-Luc™, a reagent that allows immediate reading of the luminescence.

Features

- **Target:** natural and recombinant murine IFN-α (multiple subtypes)
The following murine IFN subtypes are recognized by this kit; IFN-α1, IFN-α2, IFN-α4, IFN-α5, IFN-α6.
- **Standard:** HEK-expressed mouse IFN-α2
- **Format:** bioluminescent ELISA in white immuno 96-well plate
- **Measurement:** relative light units (RLUs)
- **Incubation Time:** 4.5 hours
- **Limit of detection:** 16 pg/ml (for calculation method, see reference 4)
- **Specificity:** no cross-reactivity with human IFN-α, human or mouse IFN-β
- **Sample size and type:** 100 µl of cell culture supernatant, serum and plasma

PRINCIPLE

The monoclonal mIFN-α Capture Antibody is coated onto the wells of a white immuno 96-well plate. Samples and the mIFN-α Standard are pipetted into these wells, followed by the addition of the monoclonal Biotinylated Antibody (detection antibody).

During the first incubation, the mIFN-α antigen binds to the immobilized mIFN-α Capture Antibody on one site, and during the second incubation, to the Biotinylated Antibody on a second site.

After removal of the excess detection antibody, Streptavidin-Lucia is added. This streptavidin conjugate binds to the Biotinylated Antibody. After a short third incubation and washing to remove all the unbound Lucia luciferase, QUANTI-Luc™, a solution that contains the substrate of Lucia luciferase, is added. No further incubation is required. The bioluminescent signal is emitted instantaneously and measured in Relative Light Units (RLU) by a luminometer. The intensity of this signal is directly proportional to the concentration of mIFN-α present in the samples.

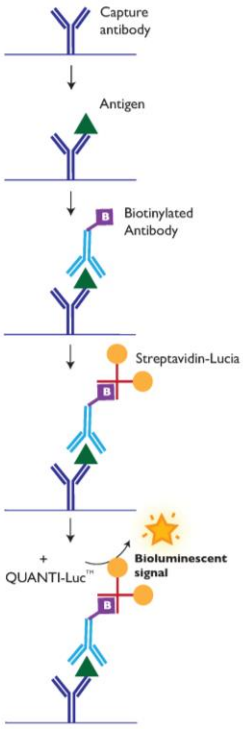

BACKGROUND

Interferon-alpha (IFN-α) is a type I interferon that has both anti-viral and immunomodulatory activities[1]. IFN-α is produced primarily by plasmacytoid dendritic cells[2]. Thirteen different IFN-α subtypes have been described. Although the reason for the multiple IFN-α subtypes is not fully understood, evidence suggests that they have distinct functions[3]. IFN-α binds to a ubiquitously expressed heterodimeric receptor composed of two chains (IFNAR1 and IFNAR2), resulting in the recruitment of JAK1 and TyK2. These kinases phosphorylate STAT1 and STAT2, leading to the formation of the IFN-stimulated gene factor 3 (ISGF3) complex, which binds to IFN-stimulated response elements (ISRE), thereby directly activating the transcription of IFN-stimulated genes (ISGs).

1. Trinchieri G., 2010. Type I interferon: friend or foe? JEM 207:2053 -2063. **2. Ivashkiv LB. & Donlin LT., 2014.** Regulation of type I interferon responses. Nat Rev Immunol. 14(1):36-49. **3. Gibbert K.et al., 2013.** IFN-α subtypes: distinct biological activities in anti-viral therapy. Br J Pharmacol. 168(5):1048-58. **4. Little TA., 2015.** Method Validation Essentials, Limit of Blank, Limit of Detection, and Limit of Quantitation. BioPharm International. 28:4.

TECHNICAL SUPPORT
InvivoGen USA (Toll-Free): 888-457-5873
InvivoGen USA (International): +1 (858) 457-5873
InvivoGen Europe: +33 (0) 5-62-71-69-39
InvivoGen Hong Kong: +852 3-622-34-80
E-mail: info@invivogen.com

InvivoGen
www.invivogen.com

OTHER SOLUTIONS & MATERIALS REQUIRED

- Coating Buffer: 0.2 M carbonate/bicarbonate buffer pH 9.4, 0.2 µm filtered

Note: Alternatively, you can use sterile PBS.

- Blocking buffer: PBS containing 2% BSA and 0.05% Tween 20, 0.2 µm filtered
- Wash buffer: PBS containing 0.05% Tween 20
- Reagent Diluent: PBS containing 1% BSA and 0.05% Tween 20, 0.2 µm filtered

- Luminometer
- Plate sealers
- Clean paper towels
- White flat-bottom 96-well ELISA plates (e.g. Nunc LumiNunc™ MaxiSorp® plates)

METHODS

Reagent Preparation

Bring all reagents to room temperature before use. Allow all components to sit for a minimum of 15 minutes with gentle agitation after initial reconstitution. Working dilutions should be prepared and used immediately.

Capture Antibody stock solution (100 µg/ml)

- Add 500 µl of sterile PBS and mix by pipetting up and down until completely dissolved.
- Use immediately or prepare aliquots and store at -20 °C.
- Dilute with Coating Buffer to a working concentration of 1 µg/ml.

Biotinylated Antibody stock solution (10 µg/ml)

- Add 500 µl of sterile PBS and mix by pipetting up and down until completely dissolved.
- Use immediately or prepare aliquots and store at -20 °C.
- Dilute with Reagent Diluent to a working concentration of 30 ng/ml.

Standard stock solution (100 ng/ml)

- Add 1 ml of Reagent diluent and mix by pipetting up and down until completely dissolved.
- Use immediately or prepare aliquots and store at -80 °C.

QUANTI-Luc™ assay solution

- Pour the pouch contents into a 50 ml screw cap tube.
- Add 25 ml of sterile water.
- Swirl product gently until powder is completely dissolved.
- Use QUANTI-Luc™ assay solution immediately or store at -20 °C.

Note: This product is photosensitive and must be protected from light.

Streptavidin-Lucia stock solution

- Reconstitute product by adding 500 µl H_2O to the content of each tube.
- Mix by vortexing.
- Use immediately or prepare aliquots and store at -20 °C.

General ELISA Protocol

Plate Preparation

1. Add 100 µl of Capture Antibody (diluted to 1 µg/ml in Coating Buffer) to each well of a white flat-bottom MaxiSorp® 96-well plate. Cover the plate with an adhesive seal and incubate overnight at room temperature.
2. Remove excess Capture Antibody by flicking the plate over a sink and patting it against clean paper towels to remove any remaining drops.
3. Add 200 µl of Blocking Buffer to each well and incubate for 2 hours at 37 °C.
4. Remove Blocking buffer by flicking the plate over a sink and patting it against clean paper towels. The plate is now ready for sample addition. Alternatively, the plate can be covered with an adhesive seal and stored at -20 °C for 3 months.

Assay Procedure

Note: We suggest to test standards and samples in triplicate.

1. Add 100 µl of sample or standard diluted in Reagent Diluent, or appropriate diluent, per well. Cover with an adhesive seal and incubate for 2 hours at 37 °C.

Notes:

- The Reagent Diluent selected for use can alter the performance of the immunoassay. Optimization of the Reagent Diluent for samples with complex matrices, such as serum and plasma, may improve the performance of the assay.
- We recommend to plot a seven point standard curve using a 2-fold serial dilution with the highest standard at 500 pg/ml.

2. Remove the liquid by flicking the plate over a sink. Fill each well with 200 µl of Wash Buffer. Repeat the washing process twice for a total of three washes. After the last wash, remove any remaining Wash buffer by patting the plate against clean paper towels.
3. Add 100 µl of Biotinylated Antibody (diluted to 30 ng/ml in Reagent Diluent). Cover with an adhesive seal and incubate for 2 hours at 37 °C.
4. Repeat the washing process as in step 2.
5. Add 100 µl of Streptavidin-Lucia diluted in reagent Diluent (1:1000). Cover with an adhesive seal and incubate for 30 min at 37 °C.
6. During this incubation time, prepare the QUANTI-Luc™ assay solution. If frozen bring to 15-25 °C.
7. Repeat the washing process as in step 2.
8. Set luminometer reading time to the minimum value (0.1-0.5 second).
9. Add 50 µl of QUANTI-Luc™ to each well and proceed IMMEDIATELY with the measurement.

CALCULATION OF RESULTS

Create a standard curve using a computer software capable of generating a four parameter logistic (4-PL) curve fit. As an alternative, construct a standard curve by plotting the mean absorbance for each standard on the y-axis against the concentration on the x-axis and draw a best fit curve through the points on the graph. The data may be linearlized by plotting the log of the cytokine concentrations versus the log of the relative light units (RLU) and the best fit line can be determined by regression analysis. This procedure will produce an adequate but less precise fit of the data.

TYPICAL DATA

This standard curve is only for demonstration purposes. A standard curve should be generated for each set of samples assayed. The dotted line represents the lower limit of detection.

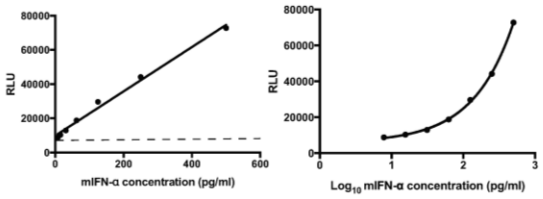

RELATED PRODUCTS

Product	Catalog Code
QUANTI-Luc™	rep-qlc1
LumiKine™ hIL-1β	lumi-hil1b
LumiKine™ Xpress hIL-1α	luex-hil1a
LumiKine™ Xpress mIL-1β	luex-mil1b

TECHNICAL SUPPORT
InvivoGen USA (Toll-Free): 888-457-5873
InvivoGen USA (International): +1 (858) 457-5873
InvivoGen Europe: +33 (0) 5-62-71-69-39
InvivoGen Hong Kong: +852 3-622-34-80
E-mail: info@invivogen.com

Appendix D: Personal communications

Letter D-1 Email communication with sales and technical support manager at Inivivogen,

re: preparation of heat inactivated bacterial strains

MONASH University

Tim Patton <timothy.patton@monash.edu>

Product enquiry - tlrl-hksa

Scott Vara <svara@invivogen.com>
To: Tim Patton <timothy.patton@monash.edu>

25 July 2019 at 01:24

Dear Tim Patton,

The strain of S. aureus that we sell as the HKSA is ATCC 6538. The preparation of the heat-killed S. aureus is as follows: Heat-Killed bacteria are prepared by autoclaving. After autoclaving (121 C for 15 minutes), the lack of viability is tested on both solid plates and liquid media for bulk preparation and again after final commercial vials are prepared. The bulk preparation is tested on 10 plates and in 10 vials of liquid media that are seeded with heat-killed suspension and placed at 37 C. Lack of growth is observed after 5 day incubation. After confirmation of no-growth, final commercial lots are prepared. From commercial lots, a suspension of heat-killed bacteria is tested on 5 plates and in 5 vials of liquid media for 5 days @ 37 C.

We do not fix the bacteria with formalin or do anything to specifically remove any other agonists. We do not regularly test this product on our TLR9 reporter cells, however we have tested heat-killed L. monocytogenes on our TLR9 reporter cells and do not see activity at concentrations as high as 10^8 cells/ml suggesting that there are not significant levels of CpG DNA present in the heat-killed bacterial preparations that would activate a TLR9 response.

Sincerely,

Scott R. Vara

Sales & Technical Support Manager

InvivoGen

10515 Vista Sorrento Pkwy.

San Diego, CA 92121

T: 858.457.5873 x112

[Quoted text hidden]

Appendix E: Complete recipe for media

E1: Complete formula for commercial preparation of RPMI 1640 GlutaMAX™

Components	Molecular Weight	Concentration (mg/L)	mM
Amino Acids			
Glycine	75	10	0.13
L-Alanyl-Glutamine	217	446	2.06
L-Arginine	174	200	1.15
L-Asparagine	132	50	0.38
L-Aspartic acid	133	20	0.15
L-Cystine	240	50	0.21
L-Glutamic Acid	147	20	0.14
L-Histidine	155	15	0.10
L-Hydroxyproline	131	20	0.15
L-Isoleucine	131	50	0.38
L-Leucine	131	50	0.38
L-Lysine hydrochloride	183	40	0.22
L-Methionine	149	15	0.10
L-Phenylalanine	165	15	0.09
L-Proline	115	20	0.17
L-Serine	105	30	0.29
L-Threonine	119	20	0.17
L-Tryptophan	204	5	0.02
L-Tyrosine	181	20	0.11
L-Valine	117	20	0.17
Vitamins			
Biotin	244	0.2	8.20E-04
Choline chloride	140	3	2.14E-02
D-Calcium pantothenate	477	0.25	5.24E-04
Folic Acid	441	1	2.27E-03
Niacinamide	122	1	8.20E-03
Para-Aminobenzoic Acid	137	1	7.30E-03
Pyridoxine hydrochloride	206	1	4.85E-03
Riboflavin	376	0.2	5.32E-04
Thiamine hydrochloride	337	1	2.97E-03
Vitamin B12	1355	0.005	3.69E-06
i-Inositol	180	35	1.94E-01
Inorganic Salts			
Calcium nitrate (Ca(NO3)2 4H2O)	236	100	0.42
Magnesium Sulfate (MgSO4-7H2O)	246	100	0.41
Potassium Chloride (KCl)	75	400	5.33
Sodium Bicarbonate (NaHCO3)	84	2000	23.81
Sodium Chloride (NaCl)	58	6000	103.45
Sodium Phosphate dibasic (Na2HPO4) anhydrous	142	800	5.63
Other Components			
D-Glucose (Dextrose)	180	2000	11.11
Glutathione (reduced)	307	1	0.00
Phenol Red	376.4	5	0.01

Cat 61870, RPMI 1640, GlutaMAX™

ThermoFisher at:
https://www.thermofisher.com/cn/en/home/technical-resources/media-formulation.122.html
on the 21st November 2019